# MODELLING OF A DIRECT OSMOTIC CONCENTRATION MEMBRANE SYSTEM

A thesis presented in partial fulfilment
of the requirements for the degree of

Doctor of Philosophy

in Food Engineering

at Massey University

Marie Wong

1997

# ABSTRACT

Direct osmotic concentration (DOC) is a novel continuous membrane process. Two co-current streams, separated by a semi-permeable membrane, are recycled through a DOC module. The turbulent-flow dilute juice stream is concentrated by osmotically extracting water across the membrane into a laminar-flow, concentrated osmotic agent (OA) stream. The semi-permeable membrane is asymmetric, with a non-porous active layer (15 μm) and a porous support layer (150 μm). Membrane solute rejection was greater than 99%. Normal operation orients the active layer towards the juice stream.

For this study, water (osmotic pressure = 0) was used in the juice channel. The relationship between water flux rate and the osmotic pressure of the bulk OA stream was asymptotic, reaching a maximum flux of $1.75 \times 10^{-3}$ kg m$^{-2}$ s$^{-1}$, when using fructose OA at 15 MPa osmotic pressure and 20°C.

Flux rates doubled when NaCl replaced fructose as OA. A doubling in temperature to 40°C resulted in a 50% increase in flux rate. OA solution properties, particularly viscosity and factors affecting diffusion coefficients had a strong influence on flux rates.

When the membrane was reversed, with the active layer facing the OA channel and the support layer filled only with water, flux rates were 40 to 60% higher than the normal orientation.

There were three resistances to water flow associated with: osmosis across the membrane active layer ($R_1$); diffusion and porous flow across the support layer ($R_2$), and; diffusion across the boundary layer in the OA channel ($R_3$). For fructose OA at 0.50 g (g solution)$^{-1}$ (osmotic pressure = 15 MPa), $R_1$ contributed 9% of the total resistance to water flux in the DOC module, $R_2$ contributed 64% and $R_3$ contributed 27%. For an iso-osmotic concentration of NaCl OA (0.15 g (g solution)$^{-1}$) the relative resistances were: $R_1$ = 17%, $R_2$ = 44% and $R_3$ = 39%. It was clear that the water flux from the dilute to concentrated stream was more strongly influenced by the support membrane and OA solution properties than the active semi-permeable membrane itself. This accounted for the asymptotic relationship between bulk OA stream properties and flux rate.

The mathematical model successfully incorporated these resistances and solution properties. Data calculated using this model agreed well with experimental results.

# ACKNOWLEDGEMENTS

I would like to express my sincere thanks and appreciation to all my supervisors Professors Ray Winger, Robert McKibbin and Ronald Wrolstad, for all their help, support and guidance throughout this research. Each supervisor helped me in very different ways towards completing this research and I have gained a lot from each.

I would like to thank Osmotek Inc. for supplying the DOC equipment and membranes. Thanks to Robert Salter, Keith Lampi, Dr Ed Beaudry, Dr Jack Herron and Carl Jochums for their help and generosity.

I would like to thank The Horticulture & Food Research Institute of NZ Ltd (HortResearch) for supporting me and providing financial assistance. I would also like to thank FRST for funding the programme through which this research was funded. I would like to thank Frucor Processors Ltd for supplying apple juice for trials.

Thanks to all members of the Food Science Group who were formally from the Food Science & Technology Group, HortResearch for their support. Special thanks to Jeff Keene for assistance on the HPLC.

Thanks to Paul Sutherland and Dr Ian Hallet for microscopy work. Thanks to the following people for letting me use their equipment: Dr Ron Wong, Crop & Food Research; Dr Don Stanton, ESR; Stephanie Parkes and Dr Ross Beever, LandCare.

Thanks to the Department of Food Science & Technology, Oregon State University (OSU), especially to those who helped me during my two visits to OSU and made the work more enjoyable and successful. Special thanks to Bob Durst and Ken Stewart.

I would like to thank John Maindonald, University of Newcastle (formally HortResearch), for his help and advice on the statistical analyses completed. I would also like to thank Dr Alan Easteal, University of Auckland, for his advice and discussions on diffusion coefficients.

Special thanks to Dr Ian Boag, Alicia Boag, Catriona Jenkinson, Dr Sam Peterson, Jane La Riviere and Jason Wallis who I am indebted to for their generosity and friendship. Special thanks to my parents for their continual support and encouragement.

Last but not least thanks to Phil for his patience, support and encouragement.

# TABLE OF CONTENTS

# LIST OF FIGURES

# LIST OF TABLES

# LIST OF ABBREVIATIONS

| | |
|---|---|
| am | - active membrane layer |
| bl | - boundary layer in OA channel |
| Case 1 | - active layer facing the juice circuit, support layer facing the OA circuit and a fully-developed velocity boundary layer in OA flow channel |
| Case 2 | - active layer facing the juice circuit, support layer facing the OA circuit, no velocity boundary layers in OA channel |
| Case 3 | - active layer facing the OA circuit, support layer facing the juice circuit and a fully-developed velocity boundary layer in OA flow channel |
| DOC | - direct osmotic concentration |
| ED | - electrodialysis |
| fdbl | - fully-developed boundary layer |
| Hg | - mercury |
| HPLC | - high performance liquid chromatography |
| GS | - gas separation |
| KCl | - potassium chloride |
| MD | - membrane distillation |
| MF | - microfiltration |
| NaCl | - sodium chloride |
| NF | - nanofiltration |
| NZ | - New Zealand |
| OA | - osmotic agent |
| $OA_{IN}$ | - flow rate of OA into module |
| $OA_{OUT}$ | - flow rate of OA out of module |
| OD | - osmotic distillation |
| p | - level of significance of a statistical test |
| PRO | - pressure retarded osmosis |
| PV | - pervaporation |
| PVC | - polyvinyl chloride |
| RO | - reverse osmosis |
| sm | - support membrane layer |
| UF | - ultrafiltration |
| USA | - United States of America |
| vs. | - versus |

# LIST OF NOMENCLATURE

$a_i$ - activity of solvent $i$ (always $\leq 1.0$)

$A_m$ - membrane area, $m^2$

$c_i$ - mass concentration of component $i$, kg $m^{-3}$

$C$ - membrane constant, kg $m^{-2}$ $s^{-1}$ $Pa^{-1}$

$d_a$ - thickness of membrane active layer, m

$d_s$ - thickness of membrane support layer, m

$D_{im}$ - diffusion coefficient of component $i$ within the membrane, $m^2$ $s^{-1}$

$D_{AA}$ - self diffusion coefficient, $m^2$ $s^{-1}$

$D_{A^*}$ - tracer diffusion coefficient, $m^2$ $s^{-1}$

$D_{AB}$ - binary diffusion coefficient of component $A$ in a mixture of $A$ and $B$, $m^2$ $s^{-1}$

$D^o_{AB}$ - binary diffusion coefficient of solute at infinite dilution at $T$ ° C, $m^2$ $s^{-1}$

$D_e(Y)$ - effective diffusion coefficient at concentration $Y$, $m^2$ $s^{-1}$

$D_H$ - equivalent hydraulic diameter, m

$df$ - degrees of freedom

$E_a$ - activation energy, J $mol^{-1}$

$E[x]$ - expected value of $x$-coefficient

$F$ - force, N

$F(Y)$ - integral function of $Y$

$g$ - gravitational acceleration, m $s^{-2}$

$G$ - Gibbs free energy, J

$G_p$ - pressure gradient in the $x$ direction, $dP/dx$

$h$ - equivalent flow channel height; distance between membrane and OA wall when fully deflected, m

$I$ - integral function describing velocity and concentration profiles across the OA channel

$I_R$ - correction factor for $I$

$J$ - molar diffusion flux, mol $m^{-2}$ $s^{-1}$

$k$ - mass transfer coefficient, m $s^{-1}$ [Section 2.4.2]

$k$ - Boltzmann constant, $1.38 \times 10^{-23}$ J $K^{-1}$

$k_p$ - permeability of porous media, $m^2$

$L$ - characteristic length, m

$L_a$ - length of membrane arc between two membrane support bars, m

$L_m$ - length of OA flow channel, m

$L'$ - entry length before fully-developed flow, m

$m$ - solution molality, mol (kg solvent)$^{-1}$

$m, n$ - number of periods in Fourier series

$m_i$ - mass diffusive flux of component $i$, kg m$^{-2}$ s$^{-1}$

$m_w$ - water mass flux rate, kg m$^{-2}$ s$^{-1}$

$m_w(x,y,z)$ - water mass flux rate at position $(x,y,z)$, kg m$^{-2}$ s$^{-1}$

$M$ - solution molarity, mol l$^{-1}$

$M_B$ - molecular weight of solvent, g mol$^{-1}$

$M_E$ - molecular weight of solute, g mol$^{-1}$

$n$ - number of samples for each mean

$n$ - number of horizontal flow channels in OA plate [Section 5.4.3]

$N_i$ - number of moles of component $i$ (normally the solvent)

$N_j$ - number of moles of component $j$ (normally the solute)

$Nu$ - Nusselt number

$p$ - pressure, Pa

$p_i^*$ - vapour pressure of pure solvent $i$, Pa

$p_i$ - partial vapour pressure of solvent, $i$, in solution, Pa

$\Delta p$ - hydraulic pressure difference, Pa

$p, q$ - number of periods in Fourier series

$q_{mw}$ - water mass flux rate per unit area along OA flow channel, kg m$^{-2}$ s$^{-1}$

$q_{mf}$ - fructose mass flux rate per unit area along OA flow channel, kg m$^{-2}$ s$^{-1}$

$Q_m$ - total mass flow along OA flow channel, kg s$^{-1}$

$Q_{mC}$ - total mass flow at channel entry, kg s$^{-1}$

$Q_{mf}$ - total mass flow of fructose along flow channel, kg s$^{-1}$

$r$ - pore radius, m

$R$ - gas constant, 8.314 J K$^{-1}$ mol$^{-1}$ ≡ 8.314 m$^3$ Pa K$^{-1}$ mol$^{-1}$

$R$ - resistance, m$^2$ s Pa kg$^{-1}$

$R_1$ - resistance in the active membrane layer, m$^2$ s Pa kg$^{-1}$

$R_2$ - resistance in the porous support layer, m$^2$ s Pa kg$^{-1}$

$R_3$ - resistance in the velocity boundary layer, m$^2$ s Pa kg$^{-1}$

$\%R$ - percentage rejection

$Re$ - Reynolds number

$RSE$ - residual standard error

$RSS$ - residual sum of squares

$s$ - pooled estimate of standard deviation

$S$ - osmosity, molar concentration of NaCl, mol l$^{-1}$

$Sc$ - Schmidt number

$sd$ - standard deviation

$SE$ - standard error

$SE[x]$ - standard error of $x$-coefficient

$SEM$ - standard error about the mean

$Sh$ - Sherwood number

$t$ - time, s

$T$ - absolute temperature, K

$u$ - velocity in the $x$ direction, m $s^{-1}$

$u(x,y,z)$ - velocity in the $x$ direction at position $(x,y,z)$, m $s^{-1}$

$U$ - bulk free-stream velocity in $x$ direction, m $s^{-1}$

$v$ - velocity in the $y$ direction, m $s^{-1}$

$\vec{v}$ - velocity vector

$\vec{v}_0$ - superficial or Darcy velocity, volume of flow through a unit cross-sectional area of the solid plus fluid, $m^3$ $m^{-2}$ $s^{-1}$

$V_w$ - volumetric water flux rate, $m^3$ $m^{-2}$ $s^{-1}$

$w$ - width between two adjacent membrane support bars, width of OA flow channel, m

$\omega$ - velocity in the $z$ direction, m $s^{-1}$

$x$ - horizontal distance parallel to the membrane, m

$x$ - coordinate

$x_A$ - mole fraction of component A

$y$ - distance perpendicular to the membrane (across membrane or away from the membrane), m

$y$ - coordinate

$Y$ - solute mass fraction, solute mass fraction in OA circuit, g (g solution)$^{-1}$

$Y(x,y,z)$ - solute mass fraction at position $(x,y,z)$, g (g solution)$^{-1}$

$z$ - coordinate

$\nabla$ - $\left( \frac{\partial}{\partial x}, \frac{\partial}{\partial y}, \frac{\partial}{\partial z} \right)$

vector differentiation operator

*Greek symbols*

$\alpha$ - power term for viscosity in relationship with diffusion coefficient

$\alpha$ - power term for velocity profile equation

$\gamma$ - activity coefficient

$\delta$ - velocity boundary layer thickness, m

$\delta(x)$ - velocity boundary layer thickness as a function of $x$, m

$\delta_c$ - concentration boundary layer thickness, m

$\Delta$ - membrane deflection between two membrane support bars, m

$\varepsilon$ - porosity

| | |
|---|---|
| $\kappa$ | - proportionality constant |
| $\lambda$ | - membrane thickness, m |
| $\mu_i$ | - chemical potential of component *i*, J $mol^{-1}$ |
| $\mu$ | - fluid or solution viscosity, kg $m^{-1}$ $s^{-1}$ |
| $\mu_0$ | - absolute viscosity of solvent at T °C, kg $m^{-1}$ $s^{-1}$ |
| $\mu(Y)$ | - viscosity of solution at concentration *Y*, kg $m^{-1}$ $s^{-1}$ |
| $\nu$ | - kinematic viscosity, $m^2$ $s^{-1}$ |
| $\pi$ | - osmotic pressure, MPa |
| $\pi_A$ | - osmotic pressure of solution *A*, MPa |
| $\pi(Y)$ | - osmotic pressure of solution at concentration *Y*, MPa |
| $\Delta\pi$ | - osmotic pressure difference, MPa |
| $\rho$ | - fluid or solution density, kg $m^{-3}$ |
| $\rho(Y)$ | - density of solution at concentration *Y*, kg $m^{-3}$ |
| $\tau$ | - tortuosity |
| $\upsilon_i$ | - partial molar volume of solvent *i*, $m^3$ $mol^{-1}$ |
| $\phi$ | - osmotic coefficient |
| $\psi$ | - water potential, J $kg^{-1}$ |

*Subscripts*

| | |
|---|---|
| 0 | - position at the interface between the support layer and the velocity boundary layer |
| 1 | - position at the surface of the active layer on OA side |
| *a* | - active layer |
| *C* | - bulk OA free-stream solution and bulk OA free-stream solution at flow channel entry |
| *f* | - fructose |
| *i* | - component in solution, normally the solvent |
| *J* | - juice circuit solution |
| *m* | - mass flow |
| *m* | - membrane |
| *m*, *n* | - number of periods in Fourier series [Equation (8.24)] |
| OA | - osmotic agent solution |
| *s* | - support layer |
| *w* | - water |

# CHAPTER 1
# INTRODUCTION

A membrane process uses a semi-permeable membrane to separate one or more components from a solution. The semi-permeable membrane acts as a selective barrier between solutions on either side of the membrane. The selectivity of the membrane is determined by the membrane characteristics, such as, type of membrane matrix, pore size, membrane charge or affinity towards the solution component. The properties and characteristics of a membrane are dependent on its polymer make-up and on the membrane manufacturing process used. Membranes are produced in a number of different forms (e.g. flat sheet, tubular, hollow fibre, spiral), designed for specific module housings which attempt to optimise the flow characteristics along the membrane. The membrane process system consists of a membrane and the appropriate module attached to a pump which moves the fluid past the membrane. In some membrane processes the pump is used to increase the pressure difference across the membrane and produce the driving force necessary for transfer of components across the membrane.

Major advances were made in the development of membrane processes for industrial use in the 1950's, when membranes were developed that were more robust and could withstand the high pressures required for reverse osmosis (RO). RO was studied for use in desalination of sea and brackish water. During this research important break-throughs were made in the field of membrane science and technology. RO is still being extensively used world-wide in the water and wastewater industries. Other membrane processes such as ultrafiltration, microfiltration and electrodialysis have been incorporated into the processing industries with RO. Over the last ten years the use of membrane processes has increased in the food and biotechnology industries (Cheryan, 1992).

The different membrane processes available are distinct from each other based on driving force, membrane characteristics and transport mechanism. New membrane processes are being developed or old processes are being re-developed as research into membrane science and technology expands. The main membrane processes used commercially today are RO, ultrafiltration (UF), microfiltration (MF), nanofiltration (NF), dialysis, electrodialysis (ED), pervaporation (PV) and gas separation (GS). Some of the newer or re-developed membrane processes are osmotic distillation (OD), membrane distillation (MD), liquid membranes and direct osmotic concentration (DOC).

In RO an high hydraulic pressure is exerted onto the feed solution causing the solvent to transfer across the membrane. This flow across the membrane is called the permeate flow. The hydraulic pressure exerted on the feed solution must be greater than the osmotic pressure of the solution forcing the solvent to move against the osmotic gradient. Membranes used for RO are described as non-porous and allow only the solvent (usually water) and some small solutes to pass through. The mechanism of transfer across the non-porous layer involves the dissolving of the transferring molecule into the membrane matrix, then its diffusion across the layer into the permeate stream (Cheryan, 1992).

MF, UF and NF all use porous membranes and separate components primarily based on size. NF retains the smallest molecules (0.5 - 5 nm). Larger components are retained by UF (1 - 100 nm) and MF (0.1 - 10 μm). The driving force for these three processes is an hydraulic pressure gradient across the membrane and the mechanism used to describe the transfer process is flow through pores or porous media (Strathmann, 1981; Lonsdale 1982; Mulder, 1993).

During PV a phase change from liquid to vapour takes place in the transfer process. The driving force for transfer is a partial pressure difference across the membrane and when the diffusing component reaches the permeate side of the membrane it evaporates. The selectivity of the membrane and the solubility of the compounds in the membrane influence the separation capabilities of PV (Rautenbach and Albrecht, 1989).

In dialysis the driving force for movement of low molecular weight compounds across the membrane is a concentration gradient. The membrane also excludes different components based on size. Electrodialysis uses anion and cation selective membranes and an electric field orthogonal to the membrane. Ions move across the membranes under the influence of the electric field. In liquid membrane processes, liquids such as hydrophobic solvents form selective barriers between the aqueous feed solution and the aqueous absorption phase. The driving force across the liquid membrane is a concentration gradient. The mechanisms involved are permeation and carrier transport (Rautenbach and Albrecht, 1989). Membrane gas separation processes can use porous or non-porous membranes. The mechanism for gas transfer is either based on kinetic gas principles for porous membranes or based on the solubility of the component in the membrane and diffusion for non-porous membranes. The driving force in gas separation is a pressure difference across the membrane (Rautenbach and Albrecht, 1989).

OD and MD both use hydrophobic (water hating) porous membranes. As the membranes are hydrophobic the components that pass through the membrane are in the vapour state and the membranes remain dry. The driving force for movement of solvent across the membrane in OD is a vapour pressure gradient which corresponds to the osmotic pressure difference between the two solutions on either side of the membrane. One solution is a highly concentrated solution exerting a high osmotic pressure. The solvent, in its vapour state, moves through the membrane into the concentrated solution on the other side (Lefebvre, 1988; Johnson et al., 1989; Sheng et al., 1991; Thompson, 1991, Mengual et al., 1993). In MD the driving force for transfer of components across the membrane is a large transmembrane temperature gradient which produces a water vapour pressure gradient across the membrane. The transfer mechanisms in OD and MD are based on molecular diffusion and flow through pores (Schneider et al., 1988; Gostoli and Sarti, 1989; Schofield et al., 1990).

DOC is a low hydraulic pressure separation process. DOC uses the same type of membranes as RO, though the driving force is the osmotic pressure difference across the membrane. A solution with a high osmotic pressure is placed on the opposite side of the membrane to a dilute solution to be concentrated. The water moving across the membrane is taken up by the concentrated solution. The mechanism of transfer was postulated to be the same as RO (Rautenbach and Albrecht, 1989).

The benefits of membrane processes are that they can operate at relatively low temperatures, therefore, reducing any heat damage to products. For many of the membrane processes a phase change is not required to separate a component from a solution. The energy requirement of RO for concentration is less than for evaporation (Pepper, 1990; Cheryan, 1992). Membrane processes provide the opportunity for industries to recover components present in small quantity or remove undesirable compounds relatively easily compared to other traditional separation methods.

The limitation of membrane processes is that they suffer from concentration polarisation and membrane fouling. Both these factors affect flux rates and operating practices which can influence the commercial acceptance of a membrane process. Rapid membrane fouling will result in longer down times for cleaning. Solutions cannot be taken to dryness with membrane processes. The main limiting factor for membrane processes is the maximum concentration level which can be achieved in concentration processes and the increase in viscosity in separation processes.

RO, DOC, OD, MD and PV are the membrane processes which are used for the removal of water from dilute solutions. RO is the main membrane concentration process used commercially. Concentration of fluids by RO is limited by the maximum hydraulic pressure that can be exerted on the membranes, 4 to 6 MPa (Cheryan, 1992). Juice concentration by RO is limited to a maximum of approximately 30% soluble solids. Reverse osmosis also suffers from membrane fouling because of the high hydraulic pressures used. To minimise the fouling problem, liquids to be concentrated are pre-filtered to remove insoluble materials prior to RO.

In comparison, DOC operates at relatively low hydraulic pressures and membrane fouling is less of a problem. Solutions with high insoluble solids content can also be concentrated without pre-filtering. The level of concentration achievable in DOC is dependent on the osmotic pressure of the concentrating agent but concentrations of greater than 30% soluble solids can be achieved. A fructose solution at 70% w/w (0.7 g (g solution)$^{-1}$) used as the concentrating agent has an osmotic pressure of approximately 30 MPa. The osmotic pressure of a single-strength fruit juice is approximately 1.5 MPa and once concentrated to 50% soluble solids its osmotic pressure is approximately 15 MPa. At this concentration level, assuming ideal conditions, there is still an osmotic pressure gradient available between the concentrating agent and the fruit juice concentrate.

To operate DOC high pressure pumps required for RO are not necessary, therefore, reducing the capital cost of the membrane system. But for DOC the concentrating agent is diluted by taking up the water transferring across the membrane and must be re-concentrated for continued use (Herron et al, 1995). The full cost of DOC will depend on the re-concentration method chosen.

A number of different researchers have investigated DOC for liquid concentration, sea water desalination and even power generation (Popper et al., 1966; Bolin and Salunkhe, 1971; Loeb and Bloch, 1973; Kravath and Davis, 1975; Lee et al., 1981, Beaudry and Lampi, 1990(a)). Fruit and vegetable juices, coffee and tea are examples of liquid foods concentrated by DOC. It has also been used to concentrate low grade grape juice before fermentation to wine and for dealcoholisation of grape wine (Herron et al., 1995).

DOC is not a well established commercial technique due to current limitations of low permeate flux rates. With recent developments in membrane manufacturing and module design, the process now has potential. New apparatus to carry out direct osmosis have been developed over the last eight years. Osmotek Inc., USA has developed a DOC

module using hydrophillic membranes, designed specifically for the concentration of dilute liquid foods. The DOC apparatus available from Osmotek Inc. was used in the research presented in this thesis.

Of the other membrane concentration techniques, OD can also concentrate to higher levels than RO. For increased permeate flux rates in OD it was recommended to pre-treat the feed solution with MD or UF, and pre-concentrate with RO (Canning et al., 1996). A group in Australia has developed an OD process using hydrophobic membranes. The system is still being tested at the pilot plant level (Thompson, 1991; Wilson, 1994). The requirement for a temperature gradient in MD means increased risk of heat damage and loss of flavours and aromas. MD has been studied for a number of different applications but commercial or pilot scale operations have not been reported (Sirkar, 1992). Pervaporation is used industrially to remove water from different process streams, such as the dehydration of ethanol and the removal of water from liquid organics. Pervaporation is used for separation of organic phases from aqueous phases in a variety of industrial processes (Flemming and Slater, 1992). It has been investigated for the concentration of aroma compounds from fruit juices (Bengtsson et al., 1992).

For high quality juice concentrates optimum volatile aroma retention and minimal colour change due to heat are desirable. Thus technologies to concentrate juices without heat have been sought and used throughout the world. Currently, the main commercial process is RO. DOC may provide an alternative means of concentrating juices while retaining good flavour and colour. DOC juice concentrates of high quality have been produced in factory pilot plant DOC units. When re-diluted back to single-strength they have a colour and flavour very similar to the original single strength juice (Wrolstad, 1993; Herron et al., 1995).

The DOC membrane process developed by Osmotek Inc. was studied in order to understand the mechanisms and constraints of DOC by modelling the process. RO has been extensively modelled and the exact transport mechanism is still argued and debated in the literature. DOC has not been extensively modelled, of the small number of models published, most are based on models proposed for RO. A membrane transport model for direct osmosis is necessary in order to relate the performance to the operating conditions and other measurable properties of the system (Cheryan and Nichols, 1992). The relationships between water flux, boundary concentration and resistances will be defined and the mass transfer characteristics of the system will be described in relation to the feed solution properties and the fluid mechanics in the system.

A complete understanding of the forces and mechanisms involved in DOC will assist with the future development of the membrane process and future operational procedures for maximum flux rates. Process modelling also results in a cost effective tool for experimental guidance, a means of testing new hypotheses, predicting design parameters and optimising and controlling the process. DOC has not been thoroughly modelled and tested with extensive experimental data from a commercial DOC system.

**The objectives of this research were to**

**1. Define the system parameters (channel geometry, fluid properties, membrane characteristics), operating and boundary conditions of a DOC module.**

**2. Determine the mass transfer properties of the membrane to solute and solvent.**

**3. Define the resistances in the system to solute and solvent flow.**

**4. Mathematically model the DOC process.**

# CHAPTER 2
# LITERATURE REVIEW

## 2.1. Osmosis

Osmosis is the tendency of a pure solvent (usually water) to diffuse across a semi-permeable membrane from a solution of high solvent concentration to one of low solvent concentration (Reid, 1966). Solvent flow continues until concentrations are equal on both sides of the membrane. In this context, a semi-permeable membrane ideally is a membrane that is selectively permeable to the solvent but excludes the passage of other molecules, especially solutes (Gove, 1966).

The driving force for the flow of solvent across the membrane is the difference in osmotic pressure between the two solutions. This osmotic pressure is a colligative property of the solution and is a fundamental physical property determined by temperature, pressure and solute concentrations (Atkins, 1982). Manipulation of any of these three parameters will have a profound effect on the solvent flow rate. For example, it is possible to impede the flow by exerting a hydrostatic pressure on the concentrated solution taking up the solvent. Increasing the solute concentration of the concentrated solution can increase the solvent flow rate.

In thermodynamic terms, the osmotic pressure is equal to the pressure required to increase the chemical potential of the concentrated solution to that of the dilute solution (usually the solvent) (Reid, 1966; Sourirajan, 1970). Colligative properties are experimental properties that are determined by the differences in chemical potential of solutions. The reduction in chemical potential of the solvent because of the presence of a solute is reflected in the lowering of the vapour pressure, elevation of the boiling point, depression of the freezing point and an increase in the osmotic pressure of the solution.

The chemical potential ($\mu_i$) of component $i$ (normally the solvent) in a solution is defined in terms of Gibbs free energy ($G$) by the relation

$$dG = -SdT + Vdp + \sum_i \mu_i dN_i \qquad (2.1)$$

therefore, at constant temperature and pressure,

$$\mu_i = \left( \frac{\partial G}{\partial N_i} \right)_{T,p,N_j} \tag{2.2}$$

$G$ - Gibbs free energy, J
$S$ - entropy, J $K^{-1}$
$T$ - absolute temperature, K
$V$ - volume, $m^3$
$p$ - pressure, Pa
$N_i$ - number of moles of component $i$ (normally the solvent)
$N_j$ - number of moles of component $j$ (normally the solute)
$\mu_i$ - chemical potential of component $i$, J $mol^{-1}$
(Reid, 1966; Katchalsky and Curran, 1967; Sourirajan, 1970).

At equilibrium the solvent's chemical potential must be the same on both sides of the membrane (Reid, 1966; Reid, 1972; Tombs and Peacocke, 1974). If we start with a pure solvent at pressure $p''$ on both sides of the membrane, the two phases will be in equilibrium having chemical potential $\mu_i^*$. If we now add solute to the solvent on one side, its chemical potential is reduced to that shown in the following equation:

$$\mu_i(p'') = \mu_i^*(p'') + RT \log_e a_i(p'') \tag{2.3}$$

$\mu_i^*(p'')$ - chemical potential of the pure solvent at pressure $p''$, J $mol^{-1}$
$\mu_i(p'')$ - chemical potential of solvent $i$ in the solution at pressure $p''$, J $mol^{-1}$
$a_i(p'')$ - activity of solvent in the solution $i$ at pressure p" (always $\leq 1.0$)
$p''$ - pressure, Pa
$T$ - absolute temperature, K
$R$ - gas constant, 8.314 J $K^{-1}$ $mol^{-1}$ $\equiv$ 8.314 $m^3$ Pa $K^{-1}$ $mol^{-1}$

The activity of the solvent ($a_i$) can be expressed in terms of the vapour pressures of the solution $p_i$ and of the pure solvent $p_i^*$ as

$$a_i \approx \frac{p_i}{p_i^*} \tag{2.4}$$

$p_i^*$ - vapour pressure of pure solvent, Pa
$p_i$ - partial vapour pressure of solvent in solution at the same pressure and temperature, Pa

From Equation (2.3) the following equation for osmotic pressure ($\pi$) can be derived

$$\pi \upsilon_i = RT \log_e a_i(p, T) \tag{2.5}$$

$\pi$ - osmotic pressure, Pa

$\upsilon_i$ - partial molar volume of the solvent $i$, $m^3\ mol^{-1}$

and therefore,

$$\pi \upsilon_i = RT \log_e \left( \frac{p_i}{p_i^*} \right) \tag{2.6}$$

Equation (2.6) gives values of osmotic pressure which are in good agreement with experimentally determined data (Reid, 1966; Cheryan, 1992). However, this equation holds true only for dilute solutions or for ideal solvents. Most solvents (including water) are not ideal and a new term is required which defines the solvent's deviation from ideality. The term is the osmotic coefficient, $\phi$, and is defined by:

$$\phi = \frac{\pi_{observed}}{\pi_{ideal}} \tag{2.7}$$

$\pi_{observed}$ - osmotic pressure experimentally measured

$\pi_{ideal}$ - osmotic pressure for an ideal solution of the same molal composition (Tombs and Peacocke, 1974).

Published data are available on osmotic coefficients for aqueous solutions (Lang, 1967; Robinson and Stokes, 1970; Lobo and Quaresma, 1989; James and Lord, 1992). The activity of water ($a_w$) can be determined from the osmotic coefficient using the following equation (Sourirajan, 1970):

$$\log_e a_w = - \frac{\Sigma_i m M_B}{1000} \phi \tag{2.8}$$

$\Sigma_i$ - total number of moles of ion given by one mole of solution ($\Sigma_i = 1$ for non-electrolyte solutions)

$m$ - solution molality, mol (kg solvent)$^{-1}$

$M_B$ - molecular weight of water (18 g mol$^{-1}$)

$\phi$ - osmotic coefficient of solution

Substituting Equation (2.8) into (2.5) for water as solvent, then,

$$\pi = \frac{\Sigma_i RTM_B}{1000 \upsilon_w} m \phi \tag{2.9}$$

$\upsilon_w$ - partial molar volume of water, $m^3\ mol^{-1}$

(Robinson and Stokes, 1970; Sourirajan, 1970).

Values for osmotic pressures of aqueous solutions, calculated using Equation (2.9) have been published (Sourirajan, 1970). The osmotic pressure of sugar solutions have been measured and these agree with values calculated using Equation (2.9) (Merson and Morgan, 1968; Sourirajan, 1970; Matsurra et al., 1973; Matsurra et al., 1974; Nabetani et al., 1992). Osmotic pressure data for concentrated binary solutions at different temperatures were also published by Timmermans (1960).

For dilute solutions only and using Raoults law, Equation (2.6) can be simplified to the following equation known as the van't Hoff equation:

$$\pi = MRT \tag{2.10}$$

$M$ - molar concentration of solute, mol $l^{-1}$

The van't Hoff equation for osmotic pressure only holds for dilute solutions (Tombs and Peacocke, 1974). For concentrated solutions (greater than 0.2 mol $l^{-1}$) this equation is not accurate as osmotic pressure increases exponentially with solute concentration (Cheryan, 1992; Nabetani et al., 1992).

Osmotic pressure can be estimated from other colligative properties. These measurements may include determining the vapour pressure (Lang, 1967; Sourirajan, 1970), or depression of freezing point of solutions using the following equation (Reid, 1966; Reid, 1972):

$$\pi \upsilon_i = \frac{\theta \Delta h_{fi}}{T_f T_f^*} T \tag{2.11}$$

$T_f^*$ - the freezing point of the pure solvent, K

$T_f$ - the freezing point of the solution under discussion, K

$\theta = T_f^* - T_f$ - the freezing point depression, K

$T$ - absolute temperature, K

$\Delta h_{fi}$ - the heat of fusion of the solvent $i$, J $mol^{-1}$

The water potential, $\psi$, of aqueous solutions is related to the vapour pressure of the water in the system,

$$\psi = -2RTm\phi \tag{2.12}$$

$\psi$ - water potential, J $kg^{-1}$

Data on experimental and calculated water potentials of sodium chloride solutions have been published (Lang, 1967).

In accord with fundamental thermodynamics, it is possible to impede the flow of solvent across the membrane by exerting hydrostatic pressure on the concentrated solution. If sufficient hydrostatic pressure is applied, the flow across the membrane will be stopped. The hydrostatic pressure required to stop the solvent flow is equivalent to the osmotic pressure of the concentrated solution (Reid, 1966). The osmotic pressure is the pressure of the solution relative to the pressure of the solvent. A further increase of the hydrostatic pressure will result in solvent moving against the osmotic gradient, from the concentrated solution to the dilute solution. This is the basis of reverse osmosis (Reid, 1966).

### 2.1.1. Equivalent osmotic pressure terms

The osmotic pressure of a dilute solution (less than 0.2 mol $l^{-1}$) can be expressed as a concentration term which gives a relative measure of the solute concentration that exerts the same osmotic pressure as an ideal solution. This is expressed as osmolality (molal concentration) or osmolarity (molar concentration). For example, a 0.2 Osmolal solution of sucrose has a different solute concentration (0.196 molal or 64.2 g $l^{-1}$), but equivalent osmotic pressure to a 0.2 Osmolal solution of sodium chloride (0.108 molal or 6.25 g $l^{-1}$). Osmolality (or osmolarity) provides an approximation of the number of osmotically active species per kg of solvent (or litre of solution). The ratio between the observed osmolality of the solution and the ideal osmolality is equal to the osmotic coefficient. However, the definition of osmolality (or osmolarity) is based on the van't Hoff equation and strictly holds true only for dilute solutions (Tombs and Peacocke, 1974).

For concentrated solutions the osmosity of the solution can be used. The osmotic pressure of a solution can be expressed in a relative sense by comparison of the solute concentration to that of a 'standard' sodium chloride solution. The osmosity of a solution is the molar concentration (mol $l^{-1}$) of a sodium chloride solution which gives the identical osmotic pressure to the experimental solution. The value is usually determined from the freezing point depression of the solution. Values for both osmolality and osmosity for aqueous solutions are published in literature (Tombs and Peacocke, 1974; Weast, et al. 1984, D272; Wolf et al., 1984).

For electrolytic solutions, if the salt dissociates into $\nu$ ions, the osmotic pressure should be $\nu$ times greater than a non-electrolytic solution of the same molal concentration. The ratio is usually between 1 and $\nu$, as partial dissociation usually occurs. For dilute solutions of strong electrolytes dissociation is assumed complete (Reid, 1966).

Osmotic pressure can also be measured directly using osmometers (Staverman, 1951; Tombs and Peacocke, 1974). There are two types of methods used: static and dynamic. The static osmometers usually have a concentrated solution on one side of a semi-permeable membrane, in a chamber connected to a manometer. The system is allowed to reach equilibrium and the hydraulic pressure head above the solution is measured on the manometer. The dynamic methods involve varying the hydraulic pressure on one side of the membrane and measuring the flow rate of solvent across the membrane. By interpolating the results the pressure at which there is no solvent flow can be identified as the equilibrium osmotic pressure (Merson and Morgan, 1968; Tombs and Peacocke, 1974; Nabetani et al., 1992). Tombs and Peacocke (1974) also describe a method to determine osmotic pressure by measuring the shrinkage or swelling of gels.

## 2.2. Membrane Processing

Membrane concentration processes are used to remove water from dilute feed liquids. The basis of a membrane process is a semi-permeable membrane and a driving force to transfer one or more components across the membrane. The driving force can be due to a difference in pressure, solute concentration or temperature. The performance of the membrane process is influenced by the selectivity of the membrane and the flow rate of components through it. Membrane concentration processes for liquid foods require a semi-permeable membrane that is ideally highly selective for water and impermeable to solutes.

Various membrane processes are available for the concentration of liquids and these have been outlined in the introduction. The most common membrane process used commercially is RO. DOC is operated at pilot plant scale in a commercial plant for the concentration of small volume speciality products. While the other membrane concentration processes are important they will not be discussed.

RO was initially investigated as a method for production of potable water from brackish or saline water. The first break-through for RO was the discovery of cellulose acetate membranes which could withstand high pressures and produce high flux rates with reasonable rejection (Reid and Breton, 1959). Flux rates were further improved by the development of asymmetric cellulose acetate membranes (Loeb and Sourirajan, 1962). Since these early developments RO has expanded to the chemical processing industry, and the food and biotechnology industries (Cheryan, 1992).

In RO the semi-permeable membrane separates the feed solution to be concentrated from the solvent. An hydraulic pressure is applied to the feed solution. Once the pressure

exceeds the osmotic pressure of the feed solution, water flows across the membrane into the solvent stream. The membranes used are impermeable to most solutes, therefore, there is little or no loss of solutes from the concentrated solution. Hydraulic pressures applied range from 2 to 5 MPa, dependent on the osmotic pressure of the concentrated solution (Cheryan, 1992). For example, a sucrose solution (0.3 g (g solution)$^{-1}$) at 25°C has an osmotic pressure of approximately 3.5 MPa and a sodium chloride solution (0.05 g (g solution)$^{-1}$) has an osmotic pressure of approximately 4 MPa.

The concepts, transport models and operation of RO have been well reviewed in the literature (Johnson et al., 1966; Merton, 1966; Sourirajan, 1970; Lonsdale, 1972; Belfort, 1977; Lonsdale, 1982; Belfort, 1984; Punzi and Muldowny, 1987; Rautenbach and Albrecht, 1989; Bhattacharyya and Williams, 1992; Cheryan, 1992; Cheryan and Nichols, 1992). The key features of RO defined in these references, which have lead to the success of RO have been: (1) The development of asymmetric membranes, membranes with improved selectivity and rejection properties, stronger membranes able to withstand higher pressures; (2) The development of membrane modules which provide more membrane area and improved fluid flow characteristics, such as hollow fibre and spiral wound modules; (3) The improved understanding of the mechanism of RO with a number of different but valid models which provide the transport equations for predicting the performance of RO systems. All these key developments have resulted in RO systems with acceptable flux rates and systems that are now relatively competitive with other de-watering processes. RO has a lower energy consumption than the other de-watering processes plus, with no thermal input liquid products sensitive to heat damage can be successfully concentrated (Pepper, 1990; Cheryan, 1992).

Although RO is used extensively commercially, there are still some limitations to its use in some applications in the food industry. These limitations include the relatively low water removal rates compared to evaporative processes; the limit to the level of concentration achievable (approximately 0.3 g (g solution)$^{-1}$ for fruit juices), limited by increased viscosity levels at high concentration (Merson and Ginnette, 1972; Howell, 1993); high fouling and concentration polarisation problems; cleaning problems; and the requirement of pre-filtered solutions containing low levels of insoluble material (Lonsdale, 1972; Cheryan, 1992).

In DOC the semi-permeable membrane separates the dilute feed solution to be concentrated from a highly concentrated solution which has an osmotic pressure much greater than the feed solution. Due to osmosis, water from the feed solution moves into the concentrated solution and the feed solution becomes more concentrated. The driving

force for DOC is the osmotic pressure difference across the membrane which is influenced by the relative solute concentrations in the two solutions. In comparison to RO, DOC does not require high hydraulic pressures to operate, but both processes are influenced by temperature and solute concentrations. The key features of DOC are its ability to concentrate at low temperatures, low hydraulic pressures and to concentrate solutions with high insoluble solids content (Beaudry and Lampi, 1990(a)).

The concentration of fruit juices by direct osmosis is not a new concept. Popper et al.(1966) was the first to report the development of a dialyser, set up like a plate and frame filter press, to concentrate fruit juices. They used a sodium chloride (NaCl) solution as the concentrating agent and cellulose acetate membranes which were found to retain sodium ions. With moderate stirring, they were able to concentrate grape juice from 16% to 60% soluble solids with a flux rate of $6.9 \times 10^{-7}$ $m^3$ $m^{-2}$ $s^{-1}$. They also tested tubular modules of denitrified cellulose nitrate membranes with invert sugar as the concentrating agent. With these membranes they observed the transfer of labelled $C^{14}$ glucose across the membrane from the concentrating agent into the juice.

A module of hollow fibre membranes was used to dewater orange juice with NaCl as the concentrating agent. The hollow fibre membranes were cellulose triacetate. Water flux rates were reported to be $2 \times 10^{-5}$ kg $m^{-2}$ $s^{-1}$ and it was claimed no loss of volatiles from the orange juice occurred (Thijssen and Middelberg, 1966). Tomato juice has also been concentrated with cellophane membranes and polyethyleneglycol as the concentrating agent (Thijssen and Middelberg, 1966; Thijssen, 1974).

DOC was used to concentrate apple, peach and cherry juices (Bolin and Salunkhe, 1971). The concentration process was found to be very slow and the loss of volatiles was observed in all the juices. DOC has also been used for concentrating orange and apple juices (Loeb and Bloch, 1973). Direct osmosis was used for desalination of sea or brackish water, for production of potable water (Popper et al., 1968; Osterle and Feng, 1974; Kravath and Davis, 1975; Kessler and Moody, 1976), and for de-watering concentrated solutions after reverse osmosis or evaporative processes (Loeb and Bloch, 1973; Loeb et al., 1973; Loeb et al., 1975). Direct osmosis has also been used for the production of power, called pressure-retarded osmosis (PRO). The flow of water across the membrane was harnessed and used to run a turbine generator (Loeb, 1975; Loeb, 1976; Lee et al., 1981; Loeb et al., 1990; Mulder, 1992). Models for determining the water flux rates and the amount of power generation were presented by Lee et al. (1981) and Honda and Barclay (1990).

More recently DOC has been used for concentrating red raspberry juice (Wrolstad et al., 1993; Rommel and Wrolstad, 1993) and other juices or dilute beverages such as orange juice, tomato juice, coffee, and for dealcoholisation of grape wines (Herron et al., 1994). During concentration of raspberry juice, the membranes excluded sugars from the concentrating agent and there were only minor differences in the composition of the juices before concentration and after re-dilution of the concentrate. There was insignificant alteration in the sensory characteristics comparing the original single-strength juices, DOC concentrates and evaporated concentrates (Wrolstad et al., 1993). Different membranes were found to have different retention of flavonol compounds after raspberry juice concentration (Rommel and Wrolstad, 1993). Pulpy cantaloupe juice concentrates concentrated by DOC and by evaporation were found to vary in chemical composition and in sensory characteristics (Galeb, 1994).

The water flux rates obtained with direct osmosis are relatively low compared to RO and other concentration processes. This is one of the main reasons which limits its full adoption commercially. The advantages of DOC over RO are: a higher degree of concentration can be achieved, low hydraulic pressures are used, there is little or no fouling and therefore, unfiltered liquid solutions can be concentrated successfully.

The application of DOC for low temperature concentration of liquid food streams was considered to be potentially economical if other auxiliary processes (such as the reconcentration of the concentrating agent) could be operated economically (Popper et al., 1966). Direct osmosis was not considered to be economical for the concentration of Dead Sea brine (Loeb et al., 1975) or for PRO for power generation (Lee et al., 1981) The main reason for this was related to the observed flux rates which were not as high as obtained in RO with the same membrane (Lee et al., 1981). Flux rates were not directly proportional to the osmotic pressure potential, from the bulk solutions, across the membrane. These problems were mainly attributed to concentration polarisation boundary layers on either side of the membrane and within the porous support layer of asymmetric membranes (Loeb et al., 1973; Loeb et al., 1975; Kessler and Moody, 1976; Moody and Kessler, 1976; Lee et al., 1981; Honda and Barclay, 1990). The concentration polarisation layer on the outside of the membrane could be reduced by mixing or stirring. The concentration boundary layer within the membrane could only be reduced by changing the structure of the porous support layer. The concentration polarisation layer in the porous support layer is not a problem in reverse osmosis (Lee et al., 1981).

The economics of removing the water from the concentrating solution is one of the major limitations of DOC. Depending on the concentrating agent this can be carried out by solar methods, RO or evaporation. The energy required to remove a kilogram of water using a triple effect evaporator is 400% more than required when using RO to reconcentrate the concentrating agent (Herron et al., 1995). Selection criteria for the concentrating agent and concentration method were outlined by Herron et al. (1995).

## 2.3. DOC apparatus designed by Osmotek Inc.

A DOC process primarily for liquid food concentration has been developed by Osmotek Inc. (Caro and Salter, 1988). The first module utilised tubular membranes with the dilute solution to be concentrated flowing down the centre of the tubular membrane and the concentrating solution (osmotic agent, OA) on the outside (Caro and Salter, 1988; Beaudry et al., 1989; Milleville, 1990). The flow in the two flow channels was turbulent. The first membrane modules consisted of 0.6 m to 3.0 m long membrane tubes, membrane thickness was 25 to 100 μm with a molecular weight cut off of 100 g $mol^{-1}$. The water flux rate through the membrane declined by 25% after 40 hours continuous operation and the fruit juice was concentrated to 40% soluble solids. Fouling or concentration polarisation was not considered to be a problem during concentration (Caro and Salter, 1988; Beaudry et al., 1989; Milleville, 1990). There was no movement of sugar from the osmotic agent into the dilute solution and less than 0.1% of the colour compounds were lost from the dilute solution into the OA (Beaudry et al., 1989; Milleville, 1990).

The DOC module was re-designed as a plate and frame apparatus using flat sheets of DOC membranes (Beaudry and Lampi, 1990(a); Beaudry and Lampi, 1990(b); Herron et al., 1994; Herron et al., 1995). The new module design was used for this study and will be describe in detail later. The new module design ensured turbulent flow in the flow channel containing the dilute solution to be concentrated (Herron et al., 1994). Membrane fouling was minimal and there was no transfer of sugars from the OA across the membrane (Beaudry and Lampi, 1990(a); Beaudry and Lampi, 1990(b); Wrolstad et al., 1993; Herron et al., 1995). The auxiliary equipment required to run the DOC apparatus for fruit juice concentration was described by Herron et al. (1995). Beaudry and Lampi (1990(a)) reported water flux rates of $1.1 \times 10^{-6}$ $m^3$ $m^{-2}$ $s^{-1}$ for a new membrane with a molecular cut-off of 100 g $mol^{-1}$.

A number of case studies are provided by Herron et al. (1995) to show the economics of a DOC system using RO to reconcentrate the OA. For the concentration of carrot juice using a DOC unit from Osmotek, the profit margin after concentration was

calculated to be US$ 1.45 (l conc)$^{-1}$ based on a premium concentrate market value of US$ 3.96 (l conc)$^{-1}$. The concentration of especially heat sensitive fruit purees would lead to savings in shipping costs. The quality of reconstituted DOC concentrates of tropical fruits was comparable to the single strength puree, so the economics of DOC was evaluated by comparing the cost to remove the water and to ship (Herron et al., 1995). For a system which concentrates 2,500 kg h$^{-1}$ mango puree, the savings in shipping costs was $US 0.385 (kg water removed)$^{-1}$. The cost to concentrate tomato puree with DOC was found to be US$ 0.033 (kg conc)$^{-1}$ more than by evaporation with a triple effect evaporator capable of 50,000 kg h$^{-1}$. The improvement in the quality of the fruit concentrates from DOC would command a premium price, off-setting the slightly higher production costs compared to evaporation (Le Friec, 1994; Herron et al., 1995).

## 2.4. Modelling direct osmotic concentration

The flux rate of water across a homogeneous non-porous membrane is proportional to the osmotic pressure driving force across the membrane (Moody and Kessler, 1976; Lee et al., 1981; Rautenbach and Albrecht, 1989). The mass flux rate of water across an ideal homogeneous membrane is defined by

$$m_w = C (\pi_{OA} - \pi_J) \qquad (2.13)$$

$m_w$ - mass flux rate of water, kg m$^{-2}$ s$^{-1}$

$\pi_J$ - osmotic pressure of dilute solution to be concentrated, juice circuit solution, Pa

$\pi_{OA}$ - osmotic pressure of concentrating solution, OA solution, Pa

$C$ - membrane constant, kg m$^{-2}$ Pa$^{-1}$ s$^{-1}$

When water is separated by an ideal semi-permeable membrane from a concentrated solution, in an ideal system the water flux rate due to osmosis across the membrane is directly proportional to the osmotic pressure driving force (Lonsdale, 1972; Strathmann, 1981; Cheryan and Nichols, 1992). This theoretical model holds for systems in which the membrane is ideal, there are no concentration polarisation boundary layers, the solution properties are favourable (high diffusivity) and flow conditions are ideal (Lonsdale, 1972; Lee et al., 1981; Cheryan, 1992).

There have been three different models proposed for DOC. The first model is for a counter-current DOC system (Moody and Kessler, 1976), the second model is based on the solution-diffusion model and determines mass transfer coefficients (Rautenbach and Albrecht, 1989) and the third model is a resistance model (Beaudry and Lampi, 1990(a)).

### 2.4.1. Model for a counter-current direct osmosis system

The first detailed analysis of the transport equations required to model direct osmosis was completed by Moody and Kessler (1976). They proposed three different mathematical models to describe the mass transport phenomena across an homogenous membrane in a counter-current direct osmosis module. Their third model was found to agree well with experimental results for extracting drinking water from sea water (Kessler and Moody, 1976). This model assumed two un-stirred films or concentration boundary layers of unknown thickness at the membrane. They assumed that the concentration of solute in the dilute solution side remained constant, that it was an infinite pool of dilute solution. Solute rejection by the membrane was assumed to be less than 100% but greater than 90%. Concentration polarisation occurred at the membrane surface on the dilute side and dilution of the solute concentration occurs on the concentrating solution (OA) side.

Equations were derived and solved by numerical integration to calculate the solute concentration in the boundary layers, the mass flow rates of the dilute and OA solutions in the flow channels, and the water flux rate across the membrane. The model contained the design characteristics for the direct osmosis unit based on the membrane transport properties, the diffusion coefficients of the two solutions and average values for the thicknesses of the concentration boundary layers. The equations solved to determined the membrane flux rate were:

$$q_m(x) = L\left(\pi_d(x)\, e^{-q_m(x)\delta_d/\bar{D}_d(x)} + \pi_{ds}(x) - \pi_s\, e^{q_m(x)\delta_s/D_s}\right) \tag{2.14}$$

$$\bar{D}_d(x) = \frac{\int_{c_{dw}(x)}^{c_d(x)} D_d(c_d')\, dc_d'}{c_d(x) - c_{dw}(x)} \tag{2.15}$$

$$\frac{dq_m}{ldx} = \frac{\left(\frac{c_d\delta_d q_m}{\bar{D}_d^2}\left(\frac{\partial\bar{D}_d}{\partial c_d}\frac{dc_d}{ldx} + \frac{\partial D_d}{\partial c_{dw}}\frac{\partial c_{dw}}{\partial c_{ds}}\frac{dc_{ds}}{ldx}\right) + \frac{dc_d}{ldx}\right)\alpha_d RTe^{-q_m\delta_d/\bar{D}_d} + \alpha_s RT\frac{dc_{ds}}{ldx}}{\frac{1}{L} + \alpha_d RT\frac{\delta_d}{\bar{D}_d}\left(1 - \frac{q_m}{\bar{D}_d}\frac{\partial\bar{D}_d}{\partial c_{dw}}\frac{\partial c_{dw}}{\partial q_m}\right)e^{-q_m\delta_d/\bar{D}_d} + \alpha_s RTc_s\frac{\delta_s}{D_s}e^{q_m\delta_s/D_s}} \tag{2.16}$$

$$\frac{dQ_d}{ldx} = q_m \tag{2.17}$$

$c_i$ - concentration of solute $i$, mol m$^{-3}$

$\bar{D}_d(x)$ - diffusion coefficient of the OA solute averaged in the $y$ direction, m$^2$ s$^{-1}$

$D$ - diffusion coefficient of the solute in the dilute solution, $m^2\ s^{-1}$

$h$ - height of membrane module, m

$l$ - width of membrane, m

$L$ - membrane water permeability coefficient, $m\ s^{-1}\ Pa^{-1}$

$q_m(x)$ - local membrane flux at $x$ distance along the membrane, $m\ s^{-1}$

$R$ - gas constant ($8.314\ J\ K^{-1}\ mol^{-1} \equiv 8.314\ m^3\ Pa\ K^{-1}\ mol^{-1}$)

$T$ - temperature, K

$x$ - distance along the membrane, $0 \leq x \leq h$, m

$\alpha_i$ - osmotic coefficient of solute $i$

$\pi_d$ - osmotic pressure of osmotic agent, Pa

$\pi_{ds}$ - osmotic pressure of dilute solution solute which has passed through the membrane, Pa

$\pi_s$ - osmotic pressure of the dilute solution, Pa

$\delta_d$ - boundary layer thickness of the concentration polarisation on OA side of the membrane, m

$\delta_s$ - boundary layer thickness of the concentration polarisation on dilute solution side of the membrane, m

Subscripts

$d$ - osmotic agent

$s$ - dilute solution

$dw$ - osmotic agent property at the membrane surface

$ds$ - dilute solution solute which has passed through the membrane

The derivative of Equation (2.16) yielded a linear equation for $dq_m(x)/ldx$. The equation was integrated to obtain $q_m(x)$ which was again integrated to yield $Q_d(x)$, the solvent counterflow for the osmotic agent ($m^3\ s^{-1}$). The change in OA concentration along the length of the membrane was determined as it took up the water. This model assumed a steady state situation and did not consider changes over time.

Kessler and Moody (1976) extracted drinking water from sea water and were able to predict the water flux rates using the model of Moody and Kessler (1976). They assumed the concentration of the dilute solution in the module did not change after one pass because the mass flow rate of the dilute solution was much larger than the water flux rate across the membrane.

The equations developed by Moody and Kessler (1976) were not specifically relevant to the DOC module developed by Osmotek Inc. The flow geometries were different and

Moody and Kessler made assumptions that there was an infinite volume of dilute solution and that the membrane was homogenous in structure.

### 2.4.2. Solution-diffusion model for asymmetric membranes

The Osmotek DOC membranes are asymmetric membranes produced using the phase inversion principle. An asymmetric membrane consists of two layers: one very thin active skin layer and a much thicker porous support layer. The procedure for manufacturing these membranes has been described (Strathmann, 1990; Mulder, 1992). The membrane's selectivity and rejection capabilities are affected by the polymer type, polymer concentration and by the conditions used during manufacturing. The amount of interaction (affinity, solubility) between the membrane polymer and the permeating species also influences the selectivity (Strathmann, 1990; Mulder, 1992; Mulder, 1993).

Rautenbach and Albrecht (1989) modelled direct osmosis taking into account an asymmetric membrane structure, and membrane and boundary layer resistances. They determined the effect of the porous support layer on the transport process in direct osmosis and the mass transport resistances in the boundary layers using the concept of mass transfer coefficients. Where the mass transfer coefficient through a concentration boundary layer was defined by:

$$k = \frac{D_{AB}}{\delta_c} \tag{2.18}$$

$k$ - mass transfer coefficient, m $s^{-1}$

$D_{AB}$ - diffusion coefficient of component A in a mixture of A and B, $m^2$ $s^{-1}$

$\delta_c$ - concentration boundary layer thickness, m

Transport resistances were identified in the two concentration boundary layers on both sides of the membrane and in the two membrane layers. The transport mechanism in the active skin layer obeyed the solution-diffusion model whereas in the porous support layer the convective flow through the pores was described by the pore model.

Rautenbach and Albrecht (1989) modelled direct osmosis under steady state conditions, therefore, water and solute flux were constant at any point in the four layer system (two concentration boundary layers and two membrane layers). Both fluxes were completely determined by the concentration difference across the membrane. A set of equations was derived using the solution-diffusion model and the pore model to calculate the osmotic fluxes taking into account the concentration boundary layers and the transport resistance of the porous support layer. The equations were derived for two membrane orientations: (1) With the active skin layer facing the dilute solution and the porous support layer

facing the OA; (2) With the active skin layer facing the OA and the porous support layer facing the dilute solution. The equations for the first orientation are presented in Figure 2.1. To solve this model, three mass transfer coefficients for the two concentration boundary layers and the porous support layer, and the membrane constants must be determined from experimental data.

Rautenbach and Albrecht (1989) observed that the effective osmotic pressure difference, determined by the concentration difference across the active skin layer, was considerably reduced by the transport resistance of the porous support layer. The concentration difference across the support layer had the most influence in determining the solvent flux. An increase in the overall concentration difference across the membrane for the two solutions ($c_{s2} - c_{s4}$) resulted in only a marginal increase in the effective driving force and hence in the osmotic flux. The size of the concentration boundary layers can be reduced by controlling the flow conditions in the two flow channels. They also observed that the orientation of the asymmetric membrane had an influence on solvent flux rates due to the significant influence of the porous support layer resistances. They modelled the process for the two possible membrane orientations and found greater fluxes would be obtained when the active skin layer was facing the concentrated OA solution. The model was used to produce theoretical results using data from RO experiments. The model was not tested with DOC experimental data.

**2.4.2.1. Mass transfer coefficients**

The resistance to mass transfer in diffusion processes can be described by mass transfer coefficients. For diffusive transfer from an interface, the constant which defines the relationship between the flux and the driving force for a particular system is the mass transfer coefficient, usually denoted as '$k$'. The mass transfer coefficients are considered to be analogous to heat transfer coefficients (Incropera and DeWitt, 1985; Lienhard, 1987).

Mass transfer coefficients can be determined by a set of dimensionless equations which are analogous to the heat transfer dimensionless groups. The Sherwood number ($Sh$) is equal to the dimensionless concentration gradient and is related to the concentration boundary layer as is the Nusselt number ($Nu$) to the thermal boundary layer (Incropera and DeWitt, 1985)

$$Sh = \frac{kL}{D_{AB}} \qquad (2.19)$$

$k$ - mass transfer coefficient, m $s^{-1}$

$L$ - characteristic length, m

**Figure 2.1. Solution-diffusion model for asymmetric membranes**
(Source: Rautenbach and Albrecht, 1989)

Membrane orientated with active skin layer facing the dilute solution and the porous support layer facing the OA solution

1. OA solution side concentration boundary layer

$$\frac{c_{s1} + \frac{B}{Ab}}{c_{s2} + \frac{B}{Ab}} \approx e^{\frac{V_w}{k_1}}$$

2. Porous support layer

$$\frac{c_{s2} + \frac{B}{Ab}}{c_{s3} + \frac{B}{Ab}} \approx e^{\frac{V_w}{k_p}}$$

2. Active membrane skin layer

$$V_w = \frac{m_w}{\rho_w} = Ab(c_{s3} - c_{s4})$$

$$m_s = B(c_{s3} - c_{s4})$$

4. Dilute solution side concentration boundary layer

$$\frac{c_{s4} + \frac{B}{Ab}}{c_{s5} + \frac{B}{Ab}} \approx e^{\frac{V_w}{k_2}}$$

Total volumetric water flux rate

$$V_w = Ab\left\{\left(c_{s1} + \frac{B}{Ab}\right) e^{\left[-V_w\left(\frac{1}{k_1} + \frac{1}{k_p}\right)\right]} - \left(c_{s5} + \frac{B}{Ab}\right) e^{\left(\frac{V_w}{k_2}\right)}\right\}$$

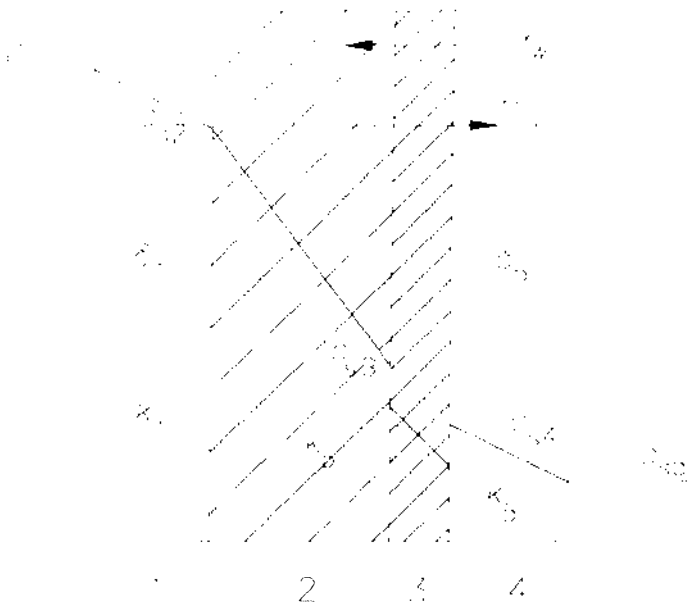

1 - OA solution side concentration boundary layer
2 - porous support layer of membrane
3 - active skin layer of membrane
4 - dilute solution side concentration boundary layer

$A$ - membrane permeability constant, m $s^{-1}$ $Pa^{-1}$
$B$ - solute permeation constant, m $s^{-1}$
$b$ - osmotic pressure coefficient, $m^3$ Pa $kg^{-1}$
$c_{sx}$ - solution concentration at position $x$, kg $m^{-3}$
$k_x$ - mass transfer coefficient at position $x$, m $s^{-1}$
$V_w$ - volumetric water flux, $m^3$ $m^{-2}$ $s^{-1}$
$\delta$ - thickness of concentration boundary layer, m

subscripts

$p$ - porous support layer
$s$ - solute
$w$ - water

The Reynolds number ($Re$) is the ratio of inertia to viscous forces.

$$Re = \frac{\rho u L}{\mu} \tag{2.20}$$

$u$ - mean fluid velocity, m $s^{-1}$

$\rho$ - fluid density, kg $m^{-3}$

$\mu$ - fluid viscosity, kg $m^{-1}$ $s^{-1}$

The Schmidt number ($Sc$) is a measure of the relative effectiveness of momentum and mass transport by diffusion in the velocity and concentration boundary layers.

$$Sc = \frac{\nu}{D_{AB}} \tag{2.21}$$

$\nu$ - kinematic viscosity, $m^2$ $s^{-1}$

For a set geometry, $Sh$ = function of {$Re$, $Sc$, geometry}. For different geometries the function for the Sherwood number has been defined, usually in the form of

$$Sh = c Re^{m} Sc^{n} \tag{2.22}$$

where $c$, $m$ and $n$ are constants. The exact form of the equation and the values of $c$, $m$ and $n$ can be derived theoretically from the boundary layer equations for a particular geometry or can be determined empirically from experimental data (Incropera and DeWitt, 1985; Lienhard, 1987; Rautenbach and Albrecht, 1989).

Rautenbach and Albrecht (1989) presented the dimensionless equations for mass transport in a tube or across a vertical wall in laminar and turbulent flow. They also describe the direct osmosis equipment used to determine the parameters required to solve the dimensionless equations and to determine the necessary mass transfer coefficients.

**2.4.2.2. Transport models for membrane processes**

The solution-diffusion model is one theory used to describe membrane transport through a non-porous barrier. This model assumes all transported molecular species dissolve in the membrane depending on the phase equilibrium present, then diffuse through the membrane by the same mechanism that governs diffusion through solids and liquids. The driving force for diffusion is a concentration or pressure gradient. The flux through the membrane is described in terms of the chemical potentials (Merton, 1966).

$$m_i = -\frac{D_{im} c_{im}}{RT}\left(\frac{\partial \mu_i}{\partial c_{im}}\frac{dc_{im}}{dy} + \upsilon_i \frac{dp}{dy}\right) \qquad (2.23)$$

$m_i$ - mass diffusive flux of component $i$, kg m$^{-2}$ s$^{-1}$

$D_{im}$ - diffusion coefficient of component $i$ within the membrane, m$^2$ s$^{-1}$

$c_{im}$ - mass concentration of component $i$ in the membrane, kg m$^{-3}$

$\mu_i$ - chemical potential of component $i$, J mol$^{-1}$

$\upsilon_i$ - partial molar volume of component $i$, m$^3$ mol$^{-1}$

$p$ - hydraulic pressure, Pa

$y$ - perpendicular distance across the membrane, m

For the solvent water, the flux rate depends on the pressure gradient driving force. Equation (2.23) was integrated to yield

$$m_w = -\frac{D_{wm} c_{wm} \upsilon_w}{RT\lambda}(\Delta p - \Delta\pi) \qquad (2.24)$$

$\Delta p$ - applied hydraulic pressure difference, Pa

$\Delta\pi$ - osmotic pressure difference, Pa

$\lambda$ - membrane thickness, m

$w$ - water

The solute flux across the membrane is dependent upon the concentration gradient. Equation (2.23) was integrated to yield

$$m_s = -\frac{D_{sm} K}{\lambda}\Delta c_{solution} \qquad (2.25)$$

$K$ - distribution coefficient of solute (concentration of solute in membrane/concentration of solute in solution)

$\Delta c_{solution}$ - difference in solute concentrations in solutions, kg m$^{-3}$

$s$ - solute

These equations for the solution-diffusion model are based on high membrane selectivity. The solution properties and membrane thickness are combined into the membrane constants, which must be determined experimentally. They are independent of the solution concentrations on either side of the membrane but are dependent on the type of solutions and the membrane (Rautenbach and Albrecht, 1989). Lonsdale (1972) reported that the effect of temperature on the permeability of cellulose acetate membranes to solutes was dependent on the annealing temperature used during

membrane manufacture. For cellulose acetate and other RO membranes solute transfer has been found to increase with increasing temperature and diffusion coefficients, and with decreasing solution viscosities (Sourirajan, 1970; Lonsdale, 1972; Rautenbach and Albrecht, 1989).

For convective flow though a porous membrane, the pore model can be used to determine the membrane flux. The membrane pores are assumed to be parallel capillaries. Transport within the pore fluid is determined by both viscous flow and diffusion. The total volumetric flow through a highly porous membrane can be described using Poiseuille's law (Merton, 1966; Cheryan and Nichols, 1992; Field, 1993), where the pore velocity is equivalent to the water flux:

$$V_w = \varepsilon v_w = \frac{\varepsilon r^2 \Delta p}{8 \mu_w \tau \lambda} \qquad (2.26)$$

$V_w$ - volumetric water flux, $m^3\ m^{-2}\ s^{-1}$

$v_w$ - pore velocity of water, $m\ s^{-1}$

$\mu_w$ - viscosity of water, $kg\ m^{-1}\ s^{-1}$

$r$ - pore radius, m

$\varepsilon$ - porosity of membrane

$\tau$ - tortuosity

$\lambda$ - membrane thickness, m

The tortuosity factor, $\tau$, accounts for twisting of the pores and increases in effective pore length. The solute flux is given by the combined viscous flow and diffusion in the pores.

$$m_s = c_{sm} v - D_{sw} \frac{dc_{sm}}{dy} \qquad (2.27)$$

$m_s$ - mass flux rate of solute within pores, $kg\ m^{-2}\ s^{-1}$

$c_{sm}$ - concentration of solute in the membrane, $kg\ m^{-3}$

$D_{sw}$ - diffusion coefficient of solute in aqueous solution, $m^2\ s^{-1}$

$v$ - velocity of fluid in the pores, $m\ s^{-1}$

(Merton, 1966)

### 2.4.3. Resistance model

Beaudry and Lampi (1990(a)) found that the rate of water removal in DOC was proportional to the difference in osmotic pressures of the OA and the dilute solution during juice concentration. The proportionality constant was approximated as the inverse of the sum of four resistances. Four resistances were encountered by the water as it

diffused from the dilute solution through a fouling layer at the membrane surface, across the membrane and into the OA.

$R_J$ is the resistance in the juice (dilute solution) for the water to diffuse to the fouling layer on the membrane.
$R_f$ is the resistance of any fouling layer to the permeation of water to the membrane.
$R_m$ is the resistance of the membrane to the permeation of water.
$R_{OA}$ is the resistance in the OA solution for the water to diffuse from the membrane (Beaudry and Lampi, 1990(a)).

The rate of water removal from the juice was expressed as :

$$V_w = \frac{(\pi_{OA} - \pi_J)}{(R_J + R_f + R_m + R_{OA})} \qquad (2.28)$$

$V_w$ - volumetric water flux rate, $m^3\ m^{-2}\ s^{-1}$
$\pi_{OA}$ - osmotic pressure of OA solution, Pa
$\pi_J$ - osmotic pressure of juice, Pa

Beaudry and Lampi (1990(a)) found it simpler to approximate the flux rate from the difference in the soluble solids concentration or °Brix , where

$$V_w = k\ (B_{OA} - B_J) \qquad (2.29)$$

$k$ - proportionality constant, $m\ s^{-1}\ (°Brix)^{-1}$
$B_{OA}$ - soluble solids concentration in the OA, °Brix
$B_J$ - soluble solids concentration in the juice, °Brix

Values for the proportionality constant $k$ were determined from experimental data when the concentration difference and operating conditions were kept constant (Beaudry et al., 1989; Beaudry and Lampi, 1990(a)). The main factors affecting the proportionality constant were temperature, solution concentrations, fluid velocities, membrane thickness and membrane molecular weight cut-off. Beaudry and Lampi (1990(a)) found that the first two factors influence viscosities and diffusion coefficients in the solutions. With constant operating conditions and concentration difference across the membrane Beaudry and Lampi (1990(a)) observed that the proportionality coefficient did not decline with time, concluding that fouling was not occurring and the resistance $R_f$ had a minimal effect. They found this model to agree with what they observed during juice concentration where flux rates decreased correspondingly with the reduction in the concentration difference between the OA and the juice.

## 2.5. Diffusion in liquids

Fundamental to the operation of a membrane concentration system is the diffusion of solutes and solvents across boundary layers. The first law of diffusion is Fick's law

$$\vec{J}_A = -cD_{AB} \nabla \vec{x}_A \qquad (2.30)$$

$J_A$ - molar diffusion flux of species $A$, mol $m^{-2}$ $s^{-1}$

$x_A$ - mole fraction of $A$

$D_{AB}$ - mass diffusivity of component $A$ in a mixture of $A$ and $B$ = diffusion coefficient of component $A$ in a mixture of $A$ and $B$, $m^2$ $s^{-1}$

$c$ - molar concentration of solution, mol $m^{-3}$

$\nabla$ - $\left( \frac{\partial}{\partial x}, \frac{\partial}{\partial y}, \frac{\partial}{\partial z} \right)$ vector differentiation operator

(Bird et al. 1960; Cussler, 1984)

In a binary mixture of $A$ and $B$, component $A$ will diffuse from a high to a low concentration of $A$ if a concentration gradient is present. In a binary system the diffusion coefficient $D_{AB} = D_{BA}$. Diffusion coefficients in liquids are strongly concentration dependent and generally increase with temperature (Bird et al., 1960; Cussler, 1984; Reid et al., 1987).

The diffusion coefficient is described in a variety of different ways:

$D_{AA}$ - self diffusion coefficient

$D_{A^*}$ - tracer diffusion coefficient

$D_{AB}$ - binary diffusion coefficient of $A$ in a mixture of $A$ and $B$ (inter and intra diffusion coefficients exist)

$D_{BA}$ - binary diffusion coefficient of $B$ in a mixture of $A$ and $B$

The self-diffusion coefficient, $D_{AA}$, represents the diffusion of a molecule of component $A$ in itself (Reid et al., 1987). The $D_{AA}$ for water at 25°C is 2.299 x $10^{-9}$ $m^2$ $s^{-1}$ (Easteal, 1990; Menting et al., 1970). A special case of $D_{A^*}$ is the tracer diffusion coefficient. This is the diffusion coefficient of a labelled molecule of component $A$ in a solution of unlabelled component $A$ (Reid et al., 1987). Tracer diffusion coefficients should not be compared to binary diffusion coefficients as the labelled or tagged molecule may diffuse differently to an unlabelled or un-tagged molecule (Cussler, 1984; Reid et al., 1987). A special case of $D_{AB}$ are the interdiffusion coefficients, when two solutions diffuse into each other. Intradiffusion coefficients arise when a solute is introduced to, and diffuses through a pure solution or a homogeneous mixture. The diffusion coefficient is

correlated to the size or molecular diameter of the diffusing particle and to the molecular size ratio between the solute and solvent molecules (Menting et al., 1970; Cussler, 1984).

Numerous methods have been developed to experimentally measure diffusion coefficients in binary systems (Cussler, 1984; Tyrrell and Harris 1984). To avoid measuring diffusion coefficients in every diffusion situation studied, two theories have been proposed for diffusion in liquids to calculate diffusion coefficients from solution data. One theory is based on absolute reaction rates (Glasstone et al., 1941) and the other based on hydrodynamic theory (Bird et al., 1960).

Under the reaction rate theory, diffusion in a liquid requires that one molecule in a liquid layer moves from one equilibrium position to another in the same layer. This usually involves a solute molecule slipping past a solvent molecule. A molecule moves from one equilibrium position to the next by overcoming the free energy of activation. Glasstone et al (1941) proposed the "hole" theory for diffusion, during which two forms of energy are required. Firstly energy is required to make one molecule jump to another position to make a hole. Secondly, energy is required for the diffusing molecule to jump into the hole formed. The total energy required for diffusion is dependent on the molecular size and polarity of the diffusing species. Molecular attractions (e.g. hydrogen bonding) also influence the diffusion rate. Solvents attracted to a diffusing solute molecule will result in more rapid diffusion of the solute through that solvent (Menting, 1970). With increasing temperature the activation energy required for diffusion reduces leading to more rapid diffusion. High diffusion coefficients imply a small activation energy. Described qualitatively, slow diffusing substances have to form relatively large holes for the molecule in the activated state, therefore, the activation energy is large (Glasstone et al., 1941).

When the solute molecule is larger than the solvent, the movement of the solvent molecule between equilibrium points in the solution determines the activation energy for diffusion (Glasstone et al., 1941). In aqueous solutions the transition of water molecules between equilibrium points is the rate determining factor in diffusion. At high water concentrations, the water molecules are bound with considerable hydration energy to the solute molecules. This hydration energy must be added to the normal activation energy for each water molecule to move from one position to the next (Gladden and Dole, 1953). The activation energy for diffusion increases linearly with mole fraction for sucrose and glucose solutions (Gladden and Dole, 1953).

Using the reaction rate theory the diffusion coefficient of a molecule, in an ideal solution of similar molecular sized species, can be determined using the following equation

$$D_{AB} = \frac{\lambda_1 kT}{\lambda_2 \lambda_3 \mu} \tag{2.31}$$

$D_{AB}$ - diffusion coefficient of molecule $A$ in a mixture of $A$ and $B$, $m^2\ s^{-1}$

$k$ - Boltzmann constant, $1.38 \times 10^{-23}$ J $K^{-1}$

$T$ - temperature, K

$\mu$ - solution viscosity, kg $m^{-1}\ s^{-1}$

$\lambda_1, \lambda_2, \lambda_3$ - distance between two equilibrium positions, subscript 1,2,3 - position in $x,y,z$ direction away from the equilibrium position

(Glasstone et al., 1941)

For non-ideal (concentrated) solutions, the following equation was derived for the diffusion coefficient. The diffusion coefficient in an ideal solution is represented by the self diffusion coefficient of that component ($D_{AA}$).

$$D_{AB} = D_{AA}\left(1 + \frac{\partial \ln \gamma_A}{\partial \ln x_A}\right) \tag{2.32}$$

$\gamma_A$ - activity coefficient of component $A$

$x_A$ - mole fraction of component $A$

$D_{AA}$ - self diffusion coefficient, is estimated by the geometric average of the two self diffusion coefficients of the individual components $A$ and $B$, $m^2\ s^{-1}$

(Glasstone et al., 1941; Cussler, 1984; Reid et al., 1987).

The hydrodynamic theory was originally derived from the Nernst-Einstein equation. The binary diffusion coefficient is:

$$D_{AB} = kT\frac{u_A}{F_A} \tag{2.33}$$

$k$ - Boltzmann constant, $1.38 \times 10^{-23}$ J $K^{-1}$

$T$ - temperature, K

$u_A/F_A$ - mobility of particle or solute $A$, the steady state velocity attained by the particle or solute under the action of a unit force, m $s^{-1}$ / N

(Bird et al., 1960)

The value of $F_A$ can be calculated using Stokes' law,

$$F_A = 6\pi\mu_B u_A R_A \tag{2.34}$$

$\mu_B$ - viscosity of solvent $B$, kg m$^{-1}$ s$^{-1}$

$u_A$ - velocity of particle or solute $A$, m s$^{-1}$

$R_A$ - radius of particle or solute $A$, m

$\pi$ - 3.14159

By substituting Equation (2.34) into Equation (2.33),

$$D_{AB} = \frac{kT}{6\pi\mu_B R_A} \tag{2.35}$$

This equation, called the Stokes-Einstein equation, holds for large spherical solutes diffusing in a continuum of small solvent molecules. If there is no tendency for the solvent to stick at the surface of the diffusing solute then the equation is modified from $6\pi$ to $4\pi$ on the denominator (Bird et al., 1960; Cussler, 1984). When the ratio between the molecular sizes of the solute and solvent is less than five Equation (2.35) is no longer valid. Errors are especially large also in high viscosity solutions (Cussler, 1984).

The Stokes-Einstein equation is the most commonly used method for determining diffusion coefficients. The Stokes-Einstein equation, has also been used as the basis for deriving empirical equations for calculating binary diffusion coefficients in organic solutions (Reid et al., 1987).

The Stokes-Einstein equation is the basis of the following simplified relationship between the diffusion coefficient and the viscosity of the solution,

$$\frac{D_{AB}}{T} \propto \mu^{\alpha} \qquad -1 \leq \alpha \leq -0.5 \tag{2.36}$$

$\alpha$ - power term for viscosity in relationship with diffusion coefficient, determined experimentally for each solution

$\mu$ - viscosity of solution, kg m$^{-1}$ s$^{-1}$

This equation has found to be valid for aqueous sugar solutions (Henrion, 1964; Chandrasekaran and Judson King, 1972; Hiss and Cussler, 1973, Oosting et al., 1985; Easteal, 1990). The proportionality constant required to solve Equation (2.36) does not necessarily equal the constants in Equation (2.35).

$D_{AB}$ is proportional to solution viscosity in binary systems, Oosting et al. (1985) and Reid et al. (1987) reported that $D_{AB} \propto \mu^{\alpha}$, where $-0.5 \leq \alpha \leq -1$. Others found $D_{AB} \propto \mu^{-2/3}$

(Hiss and Cussler, 1973; Frey and Judson King, 1982; Cussler, 1984; Easteal, 1990). For viscosities below $10^{-3}$ kg m$^{-1}$ s$^{-1}$, $\alpha = 1$ holds, and for viscosities from $5 \times 10^{-3}$ to 5 kg m$^{-1}$ s$^{-1}$, $\alpha = -^{2}/_{3}$. Oosting et al.(1985) rationalised the use of $\alpha = -^{2}/_{3}$ by using the theory of absolute reaction rates.

The binary diffusion coefficients of aqueous glucose or sucrose solutions at 25 and 35°C from very dilute (0.0075 g (g solution)$^{-1}$), to supersaturated (0.80 g (g solution)$^{-1}$) solutions have been published (English and Dole, 1950; Gladden and Dole, 1953; Henrion, 1964). Supersaturated sugar solutions are stable at these supersaturated concentrations and are resistant to crystallisation as long as the solutions have no crystallisation nuclei present. The diffusion coefficients reported were calculated from measurements of changes in interference fringes over time produced in a diffusion cell (English and Dole, 1950; Gladden and Dole, 1953). Chandrasekaran and Judson King (1972) considered the diffusion coefficients for fructose and water were the same as for glucose and water.

Tracer diffusion coefficients for water in sucrose solutions are presented by Easteal (1990). Tracer diffusion coefficients have been found to have the same relationship with viscosity as do binary diffusion coefficients (Easteal, 1990).

The binary diffusion coefficients of two similar solutes can be related by the following equation for glucose and fructose molecules in aqueous solutions at temperature $T$,

$$\frac{D_{AB\ fructose}}{D_{AB\ glucose}} = \left( \frac{\mu_{glucose}}{\mu_{fructose}} \right)^{\alpha} \qquad (2.37)$$

$D_{AB\ fructose}$ - binary diffusion coefficient of fructose aqueous solution at $T$ °C, m$^2$ s$^{-1}$

$D_{AB\ glucose}$ - mutual diffusion coefficient of glucose aqueous solution at $T$ °C, m$^2$ s$^{-1}$

$\mu_{fructose}$ - viscosity of fructose solution at $T$ °C, kg m$^{-1}$ s$^{-1}$

$\mu_{glucose}$ - viscosity of glucose solution at $T$ °C, kg m$^{-1}$ s$^{-1}$

$\alpha$ - power term for viscosity in relationship with diffusion coefficient

This equation was derived from Equation (2.36) (Easteal, 1996). As glucose and fructose molecules have the same molecular weight and have similar shapes it was assumed that the $\alpha$ term obtained for glucose could also be used for fructose to solve this equation. From published data on glucose solution viscosities and diffusion coefficients at 25°C (Gladden and Dole, 1953), a value for $\alpha$ was determined from the following linear relationship

$$\log_e\left(\frac{D_{AB}}{T}\right) = \beta - \alpha \log_e(\mu) \tag{2.38}$$

$\beta$ - intercept of the line on the y axis

$\text{Log}_e(D_{AB}/T)$ was plotted versus $\log_e(\mu)$ and from linear regression analysis, $\alpha$ was determined to be 0.47 (standard error for $\alpha$ was 0.01). From published solution property data for sucrose solutions at 25°C (English and Dole, 1950; Gladden and Dole, 1953; Henrion, 1964), $\alpha$ was determined to be 0.38 (standard error for $\alpha$ was 0.01). Oosting et al. (1985) reported $\alpha$ to be 0.50 for glucose solutions and 0.37 for sucrose solutions.

Diffusion coefficients are related to temperature by the Arrhenius equation (English and Dole, 1950; Gladden and Dole, 1953; Menting et al., 1970; Oosting et al., 1985). The diffusion coefficient data provided for glucose solutions at 25°C (Gladden and Dole, 1953) was used to calculate the diffusion coefficients for glucose solutions at 10, 20 and 40°C using the following Arrhenius relationship

$$\log_e(D_{AB}) = \log_e B - \frac{E_a}{RT} \tag{2.39}$$

Equation (2.39) can be modified to the following equation to calculate diffusion coefficients at different temperatures,

$$\log_e\left(\frac{D_{AB}}{D_{AB1}}\right) = \frac{E_a}{R}\left(\frac{1}{T_1} - \frac{1}{T}\right) \tag{2.40}$$

$D_{AB}$ - binary diffusion coefficient for $A$ in a mixture of $A$ and $B$, at temperature $T$, $m^2\ s^{-1}$

$D_{AB1}$ - binary diffusion coefficient for $A$ in a mixture of $A$ and $B$, at reference temperature $T_1$, $m^2\ s^{-1}$

$B$ - constant, determined from intercept of $\log_e(D_{AB})$ versus $1/T$

$E_a$ - activation energy, $J\ mol^{-1}$

$R$ - gas constant, 8.314 $J\ mol^{-1}\ K^{-1}$

$T$ - experimental temperature, K

$T_1$ - reference temperature, 298 K

The activation energy for diffusion in glucose and sucrose solutions was found by Gladden and Dole (1953) to be linearly related to mole fraction. The mole fraction of a solution can be calculated from the mass fraction using the following equation (Weast et al., 1984),

$$x = \frac{(Y/M_E)}{(Y/M_E) + (1 - Y)/M_B} \tag{2.41}$$

$x$ - mole fraction

$Y$ - solute mass fraction, g (g solution)$^{-1}$

$M_E$ - molecular weight of solute, g mol$^{-1}$

$M_B$ - molecular weight of solvent, g mol$^{-1}$

The following relationship for glucose, using data from Gladden and Dole, (1953), was found to hold

$$E_a\ (diffusion) = 16.9 + 120x_G \tag{2.42}$$

for $0 \leq x_G \leq 0.3$

$x_G$ - mole fraction for glucose solution

The following relationship was found to hold for sucrose solutions, using the data of Gladden and Dole (1953),

$$E_a\ (diffusion) = 17.9 + 156x_S \tag{2.43}$$

for $0 \leq x_S \leq 0.15$

$x_S$ - mole fraction for sucrose solution

Using Equations (2.40) and (2.42) the diffusion coefficients for glucose solutions at 10, 20 and 40°C were determined with published diffusion coefficients at 25°C (Gladden and Dole, 1953). These are presented in Figure 2.2(a). Using Equations (2.40) and (2.43) the diffusion coefficients for sucrose solutions at 20°C were determined from the published diffusion coefficients at 25°C (English and Dole, 1950; Gladden and Dole, 1953; Henrion, 1964). These are also presented in Figure 2.2(a)

The binary diffusion coefficient of component $A$ in an infinitely dilute solution of $A$ in $B$ ($D^o_{AB}$) can be extrapolated from the plot of binary diffusion coefficient and concentration (Gladden and Dole, 1953). The values of $D^o_{AB}$ for glucose and sucrose solutions are presented in Table 2.1. For sugar solutions, the logarithm of the diffusion coefficient ratio ($\log_e(D^o_{AB}/D_{AB})$) was found to be linearly related to mole fraction by Gladden and Dole (1953).

**Figure 2.2. Binary diffusion coefficients for aqueous solutions**

Binary diffusion coefficients ($D_{AB}$) from published data and calculated based on method outlined in Section 2.5.

(a) Glucose and sucrose solutions.

——— Glucose solutions 10, 20 and 40°C determined from published data using the Arrhenius relationship (Gladden and Dole, 1953).

— — Sucrose solutions at 20°C determined from published data using the Arrhenius relationship from published data (English and Dole, 1950; Gladden and Dole, 1953; Henrion, 1964).

(b) NaCl solutions, at 18, 25 and 35°C.

o NaCl solutions from published data (Vitagliano and Lyons, 1956; Lobo and Quaresma, 1984).

(a)

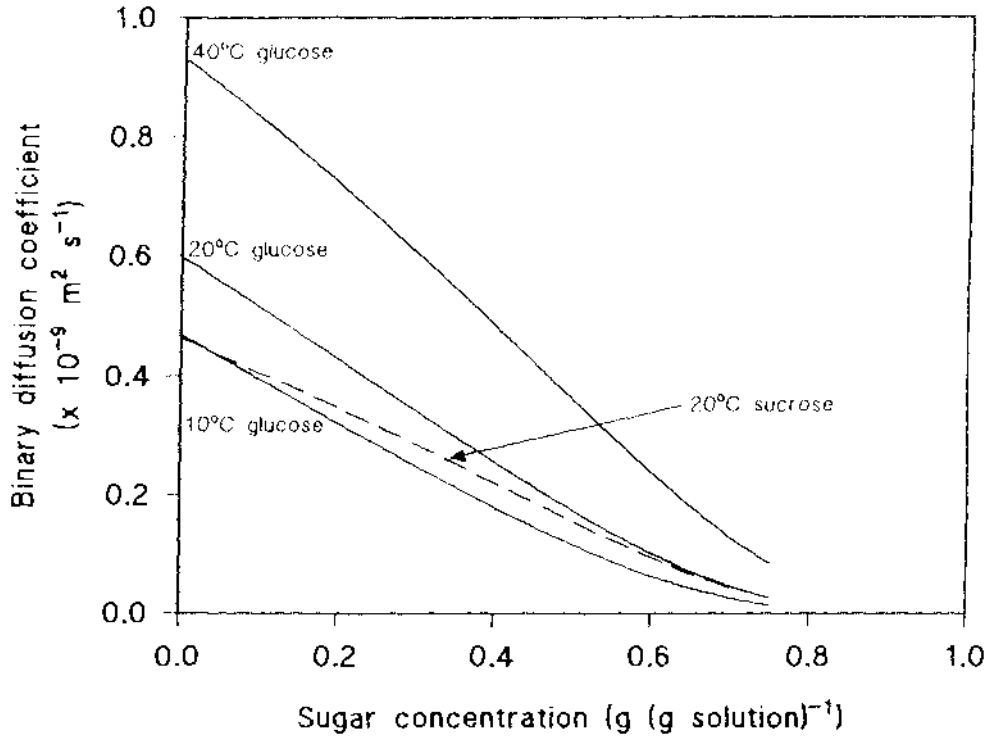
40°C glucose
20°C glucose
10°C glucose
20°C sucrose
Binary diffusion coefficient
(x 10⁻⁹ m² s⁻¹)
Sugar concentration (g (g solution)⁻¹)
0.0
0.2
0.4
0.6
0.8
1.0

(b)

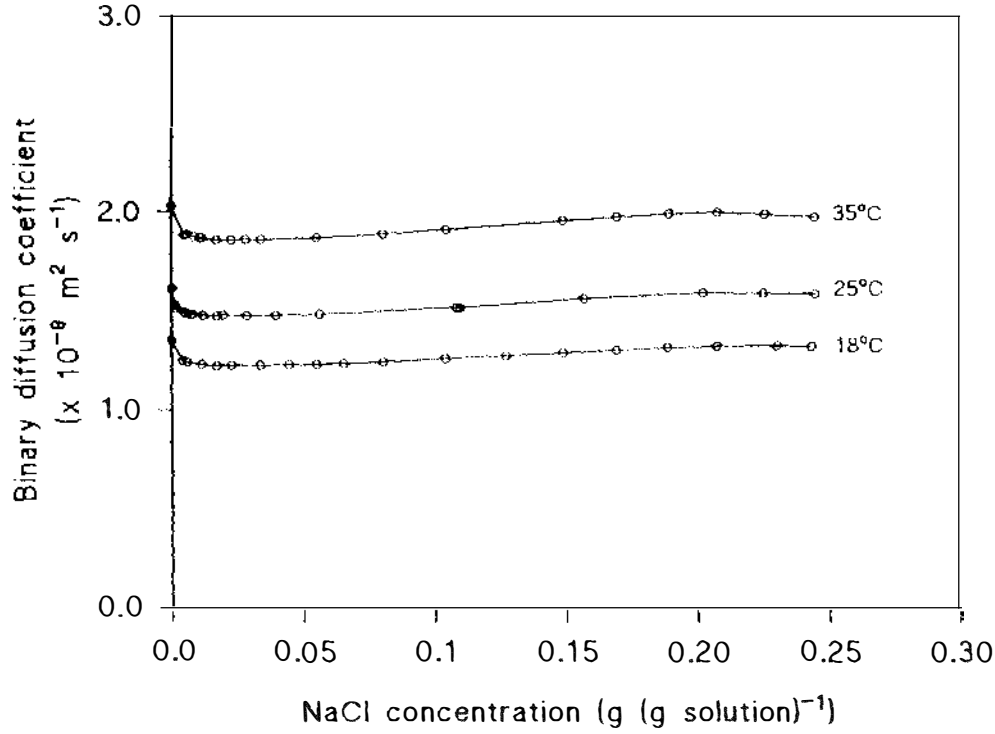
35°C
25°C
18°C
Binary diffusion coefficient
(x 10⁻⁸ m² s⁻¹)
NaCl concentration (g (g solution)⁻¹)
0.0
1.0
2.0
3.0
0.05
0.1
0.15
0.20
0.25
0.30

$$\log_e\left(\frac{D^{o}_{AB}}{D_{AB}}\right) = a\,x_A \qquad \text{at temperature } T\ ^{o}C \tag{2.44}$$

$D^{o}_{AB}$ - binary diffusion coefficient of solute at infinite dilution at $T$ ° C, $m^2\ s^{-1}$

$a$ - constant

The values of '$a$' which solve Equation (2.44) for glucose and sucrose solutions at different temperatures are presented in Table 2.1.

**Table 2.1. $D^{o}_{AB}$ and the relationship between $\log_e(D^{o}_{AB}/D_{AB})$ and mole fraction for sugar solutions**

| | Temperature | $D^{o}_{AB}$ ($\times 10^{-9} m^2\ s^{-1}$) | Constant '$a$' required to solve $\log_e(D^{o}_{AB}/D_{AB}) = a\,x^{d}$ (2.43) | Standard deviation of coefficient |
|---|---|---|---|---|
| Glucose | 10°C[b] | 0.47 | 15.4 | < 0.01 |
| | 20°C[b] | 0.60 | 13.7 | < 0.01 |
| | 25°C[a] | 0.67 | 12.9 | < 0.01 |
| | 40°C[b] | 0.93 | 10.5 | < 0.01 |
| Sucrose | 20°C[b] | 0.46 | 21.9 | 0.1 |
| | 25°C[c] | 0.52 | 20.7 | 0.1 |

a. Gladden and Dole (1953).

b. Determined from Arrhenius relationship [Equations (2.40), (2.42) and (2.43)].

c. English and Dole (1950); Gladden and Dole (1953); Henrion (1964).

d. Glucose $0 \le x \le 0.3$; sucrose $0 \le x \le 0.15$.

When a salt dissociates in solution, ions rather than molecules diffuse. In the absence of an electric potential, however, the diffusion of a single salt may be treated as molecular diffusion (Reid et al., 1987). The mutual diffusion coefficient for the salt ($D_{AB}$) will be approximately equal to that of water diffusing in the salt solution ($D_{BA}$). For dilute solutions of a single salt, the diffusion coefficient is given by the Nernst-Haskell equation:

$$D^{o}_{AB} = \frac{RT\,[(1/n_+) + (1/n_-)]}{F^2\,[(1/\lambda^{o}_+) + (1/\lambda^{o}_-)]} \qquad (2.45)$$

$\lambda^{o}_+$, $\lambda^{o}_-$ - limiting (zero concentration) ionic conductances, (A $m^{-2}$)(V $m^{-1}$) (mol $m^{-3}$) (Reid et al., 1987)

$n_+$, $n_-$ - valances of cation and anion, respectively

$F$ - Faraday constant, 96,486 C $mol^{-1}$

The Nernst-Hartley equation presented next was used by Vitagliano (1960) to determine the diffusion coefficients for NaCl,

$$D_{AB} = \frac{\nu_-\omega_+ + \nu_+\omega_-}{(\nu_+ + \nu_-)\omega_+\omega_-} RT\left(1 + \frac{d\ln y_\pm}{d\ln c}\right) = M_F\left(1 + \frac{d\ln y_\pm}{d\ln c}\right) \qquad (2.46)$$

$\nu_+$, $\nu_-$ - number of cations and anions dissociating from a molecule

$\omega_+$, $\omega_-$ - mobility of individual ions, $m^2\ s^{-1}\ J^{-1}\ K^{-1}$

$y_\pm$ - activity coefficient of the ionic medium

$c$ - molar concentration, mol $m^{-3}$

$M_F$ - mobility factor, $m^2\ s^{-1}$

Empirical relationships for electrolyte solutions have also been proposed (Reid et al., 1987).

Binary diffusion coefficients for NaCl solutions, at 25°C, have been reported by Stokes (1950), determined using a porous-diaphragm cell, and Vitagliano and Lyons (1956) reported diffusion coefficients determined using the Gouy interferometric optical technique. Binary diffusion coefficients for aqueous NaCl solutions at different temperatures have been calculated using the Nearnst-Hartley equation (Lobo and Quaresma, 1989). Lobo and Quaresma (1989) presented a collection of published data on binary diffusion coefficients at different temperatures. No data were found for binary diffusion coefficients in NaCl solutions at 20°C.

The diffusion coefficient for NaCl solutions does not vary greatly between 0 and 0.25 g (g solution)$^{-1}$) as shown in Figure 2.2(b), although there is a significant impact of temperature. The mean binary diffusion coefficients for water in NaCl solutions over the range 0 to 0.25 g (g solution)$^{-1}$, from published data, are presented in Table 2.2.

**Table 2.2. Mean binary diffusion coefficients for NaCl solutions between 18 and 35°C**

| Temperature | | Mean binary diffusion coefficient ($m^2\ s^{-1}$) | Standard deviation | n |
|---|---|---|---|---|
| K | °C | | | |
| 291 | 18 | $1.27 \times 10^{-9}$ | $4 \times 10^{-11}$ | 21 |
| 298 | 25 | $1.51 \times 10^{-9}$ | $5 \times 10^{-11}$ | 21 |
| 308 | 35 | $1.92 \times 10^{-9}$ | $6 \times 10^{-11}$ | 19 |

Source: Vitagliano and Lyons (1956) and Lobo and Quaresma (1989).

## 2.6. Viscosity of fluids

When looking at the flow of, or diffusion in liquid solutions, a key solution property is the viscosity. The viscosity of a solution is a measure of the fluid's resistance to flow or deformation (Perry et al., 1984; Toledo, 1991). Glasstone et al. (1941) describes viscosity as the measure of the force which must be applied to displace one layer of liquid parallel to a second layer, at a certain velocity. There is a difference in velocity (a velocity gradient) between adjacent layers of molecules and the resistance of a material to flow or deformation is known as stress. The shear stress ($\tau$) is the term given to the stress induced when molecule layers slip past one another along a defined plane. The velocity gradient ($du/dy$) is a measure of how fast one molecule is slipping past another and is also referred to as the rate of shear. Fluids which exhibit a linear increase in the shear stress with the rate of shear are called Newtonian fluids and can be described by the following relationship where $\mu$ is the absolute viscosity,

$$\tau = \mu \frac{du}{dy} \tag{2.47}$$

$\tau$ - shear stress, kg $m^{-1}$ $s^{-2}$

$\mu$ - absolute viscosity, kg $m^{-1}$ $s^{-1}$

$u$ - velocity horizontal to the plane, m $s^{-1}$

$y$ - distance between two molecule layers, m

(Vennard and Street, 1982; Perry et al., 1984; Toledo, 1991)

A number of references cover the theory and measurement of viscosity (Bourne, 1982; Vennard and Street, 1982; Perry et al., 1984; Reid et al., 1987; Toledo, 1991; Steffe, 1992).

Viscosity of solutions is often expressed as relative viscosity. This is the ratio between absolute viscosity of a solution and the absolute viscosity of the pure solvent at the same temperature,

$$relative\ viscosity = \left(\frac{\mu}{\mu_0}\right) \tag{2.48}$$

$\mu$ - absolute viscosity of test solution at $T$ °C, kg m$^{-1}$ s$^{-1}$

$\mu_0$ - absolute viscosity of pure solvent at $T$ °C, kg m$^{-1}$ s$^{-1}$

$\mu/\mu_0$ - relative viscosity; ratio of absolute viscosity of solution and the absolute viscosity of the pure solvent at $T$ °C.

As for diffusion coefficients, the temperature dependence of viscosity can be expressed in the following form of the Arrhenius equation (Toledo, 1994),

$$\log_e\left(\frac{\mu}{\mu_1}\right) = \frac{E_a}{R}\left\{\frac{1}{T} - \frac{1}{T_1}\right\} \tag{2.49}$$

$\mu$ - unknown viscosity at the experimental temperature ($T$), kg m$^{-1}$ s$^{-1}$

$\mu_1$ - known viscosity at reference temperature ($T_1$), kg m$^{-1}$ s$^{-1}$

$T$ - experimental temperature, K

$T_1$ - reference temperature, 298 K

$E_a$ - activation energy, J mol$^{-1}$

This can be simplified according to the Guzman-Andrade equation (Perry et al., 1984; Reid et al., 1987; Singh and Heldman, 1993; Toledo, 1994),

$$\log_e \mu = A + \frac{B}{T} \tag{2.50}$$

A plot of $\log_e(\mu)$ versus $1/T$ will have an intercept $A$ and slope $B$. The slope, $B$ is equal to $E_a/R$ in Equation (2.49).

Gladden and Dole (1953) also found that the activation energy for viscous flow in glucose solutions was related linearly to mole fraction. The following relationship was found to hold for their data,

$$E_a\ (viscous) = 16.3 + 151 x_G \tag{2.51}$$

for $0 \le x_G \le 0.3$

$E_a$(viscous) - activation energy of viscous flow, J mol$^{-1}$

Using viscosity data for glucose at 25°C (Gladden and Dole, 1953), and Equations (2.49) and (2.51) the viscosity of glucose solutions at 10, 20 and 40°C were determined and are presented in Figure 2.3.

Gladden and Dole (1953) also found for glucose and sucrose that there was a linear relationship between mole fraction and relative viscosity ($\mu/\mu_0$), where $b$ is a constant:

$$\log_e\left(\frac{\mu}{\mu_0}\right) = b\,x \qquad \textit{at temperature } T\ ^\circ C \tag{2.52}$$

The relationship between relative viscosity and mole fraction for glucose and sucrose solutions at different temperatures is presented in Table 2.3. The published data of Norris (1967) and Wolf et al. (1984) for glucose and sucrose solution viscosities at 20°C agreed with the values calculated.

**Table 2.3. Relationship between $\log_e(\mu/\mu_0)$ and mole fraction of sugar solutions at various temperatures**

| | Temperature | $\mu_0$[e] (kg m$^{-1}$ s$^{-1}$) | Constant '$b$' required to solve $\log_e(\mu/\mu_0) = b\,x$[f] (2.51) | Standard deviation of coefficient |
|---|---|---|---|---|
| Glucose | 10°C[b] | 0.001307 | 30.59 | < 0.01 |
| | 20°C[b] | 0.001002 | 28.40 | < 0.01 |
| | 25°C[a] | 0.000890 | 27.36 | 0.04 |
| | 35°C[a] | 0.000719 | 25.38 | 0.04 |
| | 40°C[b] | 0.000653 | 24.44 | < 0.01 |
| Sucrose | 20°C[c] | 0.001002 | 56.4 | 0.2 |
| | 25°C[d] | 0.000890 | 54.2 | 0.2 |

a. Gladden and Dole (1953).
b. Determined from Arrhenius relationship [Equations (2.49) and (2.51)].
c. Norris (1967) and Wolf et al. (1984).
d. Gladden and Dole (1953).
e. Weast et al. (1984).
f. Glucose $0 \le x \le 0.3$; sucrose $0 \le x \le 0.15$.

**Figure 2.3. Viscosity of glucose solutions at different temperatures**

Absolute viscosity of glucose solutions determined from published data (Gladden and Dole, 1953) and using the Arrhenius equation [Equation (2.49)].

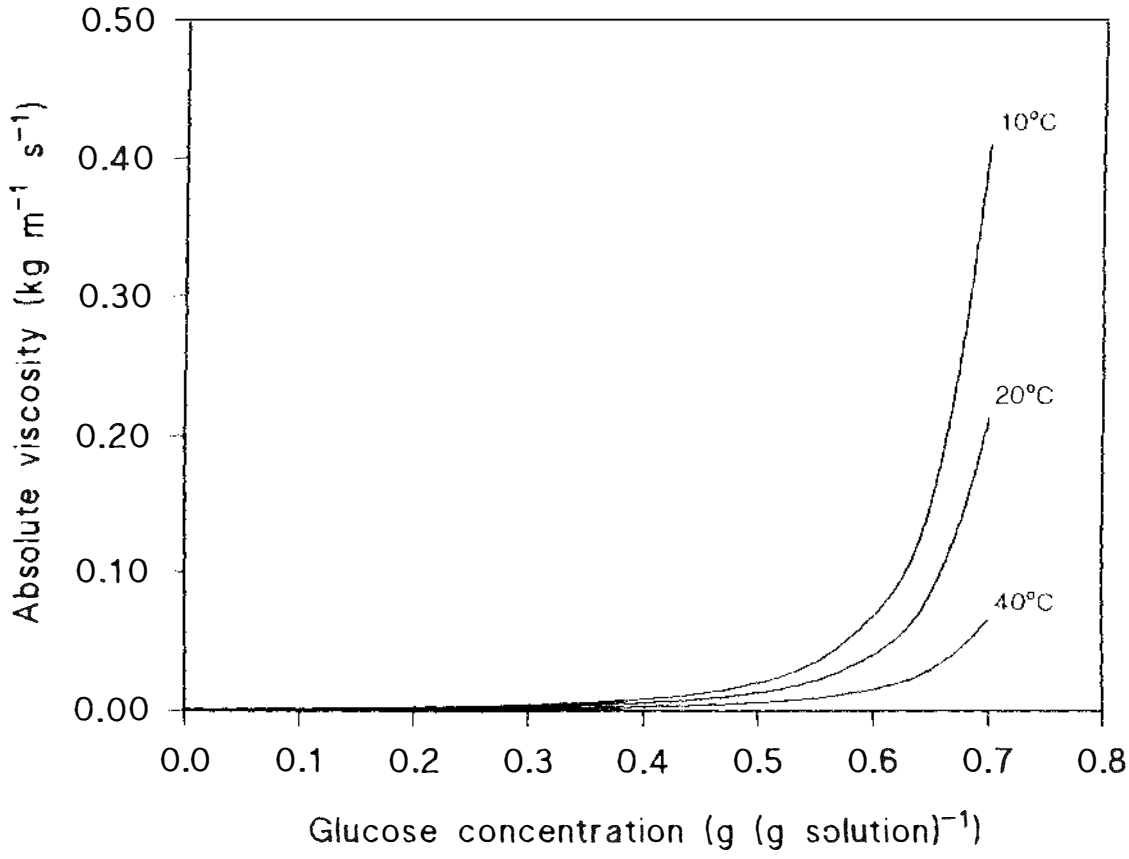
0.50
0.40
0.30
0.20
0.10
0.00
Absolute viscosity (kg m$^{-1}$ s$^{-1}$)
10°C
20°C
40°C
0.0
0.1
0.2
0.3
0.4
0.5
0.6
0.7
0.8
Glucose concentration (g (g solution)$^{-1}$)

## 2.7. Flow of real fluids

In a real fluid, viscosity provides resistance to motion by causing shear or friction forces between fluid particles and between the particles and boundary walls. For flow to take place work must be done against these resistance forces.

The flow of fluid in a pipe is laminar or turbulent depending on the velocity of the fluid, the fluid's density and viscosity and on the dimensions of the pipe. In laminar flow the fluid particles move in an ordered manner along parallel stream lines or layers. The agitation of the particles within the layers is only on the molecular level. The shear stress between adjacent layers is determined by the viscosity of the fluid. In turbulent flow, fluid particles move in a heterogeneous entirely haphazard manner. This results in the microscopic mixing of the flowing fluid (Foust et al., 1980; Vennard and Street, 1982; Incropera and DeWitt, 1985). Flow involves forces associated with viscosity and inertia. In laminar flow, viscous forces dominate. When the inertia forces are dominant, the flow is likely to be turbulent although both inertia and viscous forces are important in turbulent flow (Vennard and Street, 1982; Incropera and DeWitt, 1985).

The Reynolds number [Equation (2.20)] is used to characterise the nature of the flow in ducts and pipes (Foust, 1980; Vennard and Street, 1982; Perry et al., 1984; Incropera and DeWitt, 1985). The lower limit of turbulent flow, below which the flow will always be laminar, is defined by the lower critical Reynolds number (*Re*). This value is approximately 2,100 (Vennard and Street, 1982). The critical Reynolds number is a function of boundary geometry. Different critical *Re*'s are used for different geometries (Vennard and Street, 1982).

The characteristic linear dimension $L$, required to calculate the *Re*, is the diameter of circular pipes but for a non-cylindrical flow channel $L$ is represented by the equivalent hydraulic diameter $D_H$,

$$D_H = \frac{4 \times \textit{cross sectional area of flow}}{\textit{wetted perimeter}} \qquad (2.53)$$

Perry et al. (1984) presented various forms of Equation (2.53) for various cross-section shapes.

Fluids flowing past solid bodies adhere to them, so a region of variable velocity is built up between the body and the free fluid stream. This region is called a boundary layer. The development of a boundary layer is shown schematically in Figures 2.4(a) and (b). As a fluid flows into a pipe or channel entrance, fluid particles at the walls remain at

**Figure 2.4. Boundary layer formation in laminar flow conditions**

(a) Development of fully-developed laminar flow

(b) Formation of laminar boundary layer

Flow is parallel to the surface in the $x$-direction with velocity $u$. Any movement of particles perpendicular to the surface move with velocity $v$ in the $y$-direction. Boundary layer thickness, $\delta$, is perpendicular to the flat surface. The free-stream velocity, $U$, is outside of the boundary layer.

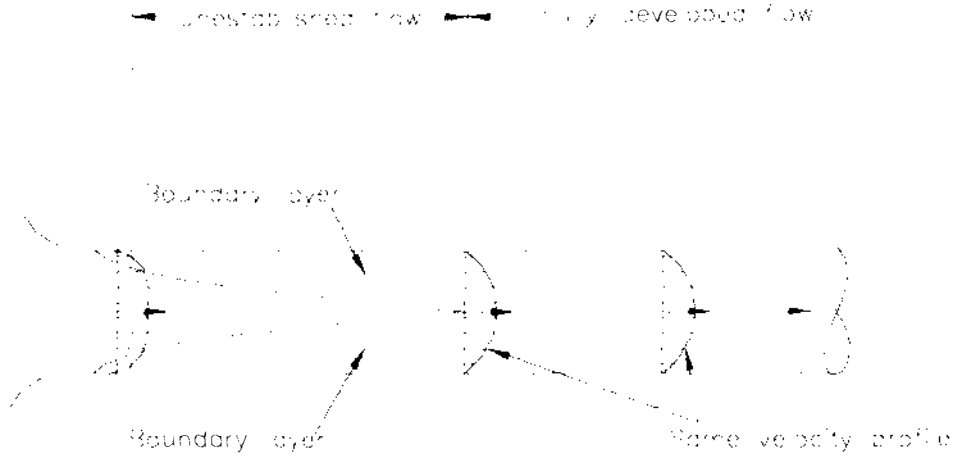
Boundary layer
Boundary layer
Same velocity profile

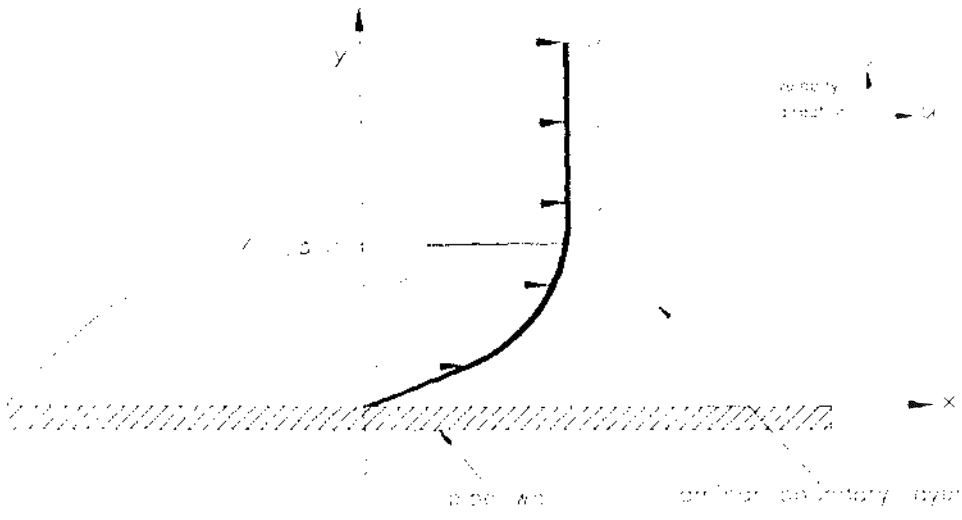
y
x

rest and a high velocity gradient is developed in the boundary layer. The high velocity gradients are associated with large frictional stresses in the boundary layer which cause the slowing down of the flow further downstream in the successive fluid elements. Thus the boundary layer steadily thickens downstream along the channel. The flow in the boundary layer can be either laminar or turbulent (Foust et al., 1980; Vennard and Street, 1984, Lienhard, 1987).

The Reynolds number is also used to characterise the flow in the boundary layer. The characteristic dimension used in Equation (2.20) is the boundary layer thickness ($\delta$) or the distance along the flow channel ($x$). Therefore, for the boundary layer the Re is written as,

$$Re = \frac{u\delta\rho}{\mu} \quad or \quad Re = \frac{ux\rho}{\mu} \tag{2.54}$$

The critical values for the $Re$ in the boundary layer is different to that for the free flowing fluid in the centre of the pipe, it is approximately 4,000 when $\delta$ is used and approximately 500,000 when $x$ is used. Below these critical values the boundary layer is laminar (Vennard and Street, 1984).

A schematic diagram of a boundary layer in laminar flow is shown in Figure 2.4(b). Typically the boundary layer thickness ($\delta$) is arbitrarily defined as the distance from the wall at which the flow velocity approaches to within 1% of the free-stream velocity ($U$) (Foust et al., 1980; Lienhard, 1987). In a laminar flow regime the boundary layer thickness can be estimated at a point $x$ along the channel using the following equation which uses $Re$ for the free flowing fluid in the centre of the pipe [$(Re)_x$] (Foust et al., 1980),

$$\frac{\delta}{x} = \frac{4.64}{(Re)_x^{0.5}} \tag{2.55}$$

This equation implies that if the velocity is high or the viscosity is low, when the $Re$ is large, then $\delta/x$ will be relatively small and the boundary layer will be thin. If the velocity is low the boundary layer will be relatively thick (Lienhard, 1987).

For flow in a pipe the boundary layers can steadily thicken until they meet in the middle and envelop the entire flow. At that point the flow is "established" or "fully-developed" and there is no further change in the velocity profile (Foust et al., 1980; Vennard and Street, 1984; Incropera and DeWitt, 1985). Fully-developed flow in a cylindrical pipe is shown in Figure 2.4(a). If the Reynolds number for fully-developed flow is less than

2,100, then it is inferred that the fully-developed flow has resulted from the growth of laminar flow boundary layers (Foust et al., 1980; Vennard and Street, 1984) .

The distance from the entry of a pipe before fully-developed laminar flow is given by the following equation, using *Re* for the entire flow channel:

$$\frac{L'}{D_H} \approx a\,Re \tag{2.56}$$

$L'$ - entry length, m

$a$ - constant ranging from 0.05 to 0.0575 for laminar flow

(Foust et al., 1980; Vennard and Street, 1984; Incropera and DeWitt, 1985).

These boundary layers are related to fluid velocity and are called velocity boundary layers. Thermal boundary layers ($\delta_t$) may also develop if the fluid free-stream and surface temperatures differ. Concentration boundary layers ($\delta_c$) may develop when the concentration at the surface (wall) differs from the concentration in the free-stream. It is the region of fluid in which concentration gradients exits and its thickness is defined by $\delta_c$ (Incropera and DeWitt, 1985). When the three boundary layers coexist, they rarely develop at the same rate and the values of $\delta$, $\delta_t$, $\delta_c$ at a given $x$ location are not usually the same.

For two-dimensional, steady-flow conditions, equations defining boundary layer conditions have been developed. A continuity equation for conservation of mass has been derived for a velocity boundary layer,

$$\frac{\partial(\rho u)}{\partial x} + \frac{\partial(\rho v)}{\partial y} = 0 \tag{2.57}$$

$u$ - velocity in the $x$ direction, m $s^{-1}$

$v$ - velocity in the $y$ direction, m $s^{-1}$

$\rho$ - density of fluid, kg $m^{-3}$

$x$ - distance along the solid surface, m

$y$ - distance perpendicular to the solid surface, m

Equating the rate of change in the $x$ momentum of the fluid to the sum of forces in the $x$ direction (Newton's second law of motion), the following equation was derived for momentum fluxes in the $x$ direction

$$\rho\left(u\frac{\partial u}{\partial x} + v\frac{\partial u}{\partial y}\right) = \frac{\partial}{\partial x}(\sigma_{XX} - p) + \frac{\partial \tau_{YX}}{\partial y} + X \tag{2.58}$$

and in the $y$ direction

$$\rho\left(u\frac{\partial v}{\partial x} + v\frac{\partial v}{\partial y}\right) = \frac{\partial \tau_{XY}}{\partial x} + \frac{\partial}{\partial y}(\sigma_{YY} - p) + Y \qquad (2.59)$$

The equations for the associated stresses are

$$\sigma_{XX} = 2\mu\frac{\partial u}{\partial x} - \frac{2}{3}\mu\left(\frac{\partial u}{\partial x} + \frac{\partial v}{\partial y}\right)$$

$$\sigma_{YY} = 2\mu\frac{\partial v}{\partial y} - \frac{2}{3}\mu\left(\frac{\partial u}{\partial x} + \frac{\partial v}{\partial y}\right) \qquad (2.60)$$

$$\tau_{XY} = \tau_{YX} = \mu\left(\frac{\partial u}{\partial x} + \frac{\partial v}{\partial y}\right)$$

$\sigma$ - normal stress, kg $m^{-1}$ $s^{-2}$

$\tau$ - shear stress, kg $m^{-1}$ $s^{-2}$

subscript - first subscript indicates the orientation, second subscript indicates the direction of the force

$X$, $Y$ - components of the body force per unit volume, N $m^{-3}$

(Incropera and DeWitt, 1985)

Equations (2.57) to (2.60) can be solved to determine the velocity field in the boundary layer for two dimensional flow.

In a thermal boundary layer the equation for conservation of energy is

$$\rho u\frac{\partial i}{\partial x} + \rho v\frac{\partial i}{\partial y} = \frac{\partial}{\partial x}\left(k\frac{\partial T}{\partial x}\right) + \frac{\partial}{\partial y}\left(k\frac{\partial T}{\partial y}\right) + \left(u\frac{\partial p}{\partial x} + v\frac{\partial p}{\partial y}\right) + \mu\Phi + \dot{q}_1) \qquad (2.6$$

where $i$ is the enthalpy per unit mass of mixture (J $kg^{-1}$), $i = e + p/\rho$. $\mu\Phi$ is the viscous dissipation, defined as

$$\mu\Phi = \mu\left\{\left(\frac{\partial u}{\partial y} + \frac{\partial v}{\partial x}\right)^2 + 2\left[\left(\frac{\partial u}{\partial x}\right)^2 + \left(\frac{\partial v}{\partial y}\right)^2\right] - \frac{2}{3}\left\{\frac{\partial u}{\partial x} + \frac{\partial v}{\partial y}\right\}^2\right\} \qquad (2.62)$$

$k$ - thermal conductivity, W $m^{-1}$ $K^{-1}$

$\dot{q}$ - rate of energy generation per unit volume, W $m^{-3}$

$e$ - thermal internal energy per unit mass, J $kg^{-1}$

$\Phi$ - viscous dissipation function, $s^{-2}$

For a binary mixture in which there are concentration gradients of each species, there will be relative transport of the species and conservation of species at each point in the concentration boundary layer. Species $A$ can be transported by advection and diffusion

(Fick's law) in each of the coordinate directions. By taking into account the advection and diffusion of a species into and out of a control volume the following equation was derived to determine conditions in the concentration boundary layer, where the total mass density, ρ, was assumed to be constant (Incropera and DeWitt, 1985):

$$u\frac{\partial \rho_A}{\partial x} + v\frac{\partial \rho_A}{\partial y} = \frac{\partial}{\partial x}\left(D_{AB}\frac{\partial \rho_A}{\partial x}\right) + \frac{\partial}{\partial y}\left(D_{AB}\frac{\partial \rho_A}{\partial y}\right) + \dot{n}_A \qquad (2.63)$$

$\rho_A$ - density of species $A$, kg m$^{-3}$

$\dot{n}_A$ - mass rate of increase of species $A$ per unit volume due to chemical reactions, kg s$^{-1}$ m$^{-3}$

The transfer of molecules in the concentration boundary layer is by bulk fluid motion and diffusion across a concentration gradient (Incropera and DeWitt, 1985). At the surface wall, where there is no fluid motion, i.e. at $y = 0$, transfer is by diffusion only.

The boundary layer thickness, concentration gradient, solution properties and convection mass transfer coefficients across the boundary layer will influence the diffusion rate of molecules into and out of the boundary layer (Jonsson and Boesen, 1984; Incropera and DeWitt, 1985; Lienhard, 1987; Rautenbach and Albrecht, 1989).

## 2.8. Flow through porous media

Many membrane processes involve the flow of fluid through porous media of uniform porosity. The equations of continuity and motion may be described by

*modified equation of continuity*

$$\varepsilon\frac{\partial \rho}{\partial t} = -\nabla \cdot (\rho v_0) \qquad (2.64)$$

*Darcy's law*

$$\vec{v}_0 = -\frac{k_p}{\mu}(\nabla p - \rho\vec{g}) \qquad (2.65)$$

$\varepsilon$ - porosity, ratio of pore volume to total volume

$\rho$ - fluid density, kg m$^{-3}$

$t$ - time, s

$\vec{v}_0$ - superficial or Darcy velocity, volume of flow through a unit cross-sectional area of the solid plus fluid, m$^3$ m$^{-2}$ s$^{-1}$

$k_p$ - permeability of porous media, m$^2$

$\mu$ - fluid viscosity, kg m$^{-1}$ s$^{-1}$

$p$ - hydraulic pressure, Pa

$\vec{g}$ - gravitational acceleration, m s$^{-2}$

(Bird et al., 1960)

These equations are for laminar flow conditions through a homogenous porous medium where the flow is viscosity dominated. The porous medium consists of a set of inter-connected pores that can pass a significant volume of fluid. Vennard and Street (1982) present the derivation of Darcy's law from the Bernoulli equation for one-dimensional flow of an incompressible fluid.

Convective flow through porous membranes is also been described using the Hagen-Poiseuille equation for the pressure drop across the membrane. This is the basis of the pore model which has been discussed earlier. The pore model assumes parallel symmetrical pores, whereas in porous membranes the pores are more likely follow tortuous paths and to have a range of dimensions. Field (1993) suggests the membranes are more like packed beds and that using the Carmen-Kozeny equation which calculates the pressure drop for laminar flow through packed beds will give a better approximation of the flux through a porous membrane. Using the Carmen-Kozeny equation (Foust et al., 1980) the following equation can be used to determine the convective flux,

$$V = \frac{\varepsilon^3 \Delta p}{K S^2 \mu \lambda} \tag{2.66}$$

$V$ - volumetric flux, $m^3\ m^{-2}\ s^{-1}$

$\varepsilon$ - porosity

$K$ - dimensionless constant

$S$ - surface area of particles per unit volume of the bed, $m^2\ m^{-3}$

$\lambda$ - membrane thickness, m

(Rautenbach and Albrecht, 1989; Field, 1993)

## 2.9. Conclusions

The concepts and thermodynamic principles of osmosis and osmotic pressure have been well documented for dilute solutions, but the information available on the practical measurement of osmotic pressure in concentrated solutions is limited. The main set of osmotic pressure data for concentrated solutions is for NaCl solutions. The osmotic pressure of the solution can be measured, or can be determined by a relative relationship between osmosity and osmotic pressure using data for NaCl solutions.

DOC has been investigated over a number of years as a possible membrane process for liquid concentration. It is able to concentrate dilute liquids at low temperature and low hydraulic pressure. It does not have the same limitations as RO in that liquids can be concentrated to a higher degree, even with insoluble solids, and fouling is minimal. The flux rates obtained in DOC at present limit its full commercial acceptance but if flux

flux rates obtained in DOC at present limit its full commercial acceptance but if flux rates can be improved, it can potentially compete with RO.

DOC has been modelled mathematically for three different systems for liquid concentration. Each model was found to have limited application to the DOC system used in this study. Therefore, none was suitable. DOC has not been modelled as extensively as RO.

In order to model the DOC process, knowledge of solution viscosity, diffusion coefficients and flow in pipe channels and porous media is required. The fundamental equations which define these solution processes or properties were described.

# CHAPTER 3
# MATERIALS AND METHODOLOGY

## 3.1. Materials and equipment

**Amaranth dye solution**

A 0.000165M (0.1 g $l^{-1}$) solution of amaranth dye (3-hydroxy-4-[(4-sulpho-1-naphthalenyl)azo]-2,7-naphthalenedisulphonic acid trisodium salt, BDH Chemicals, Poole, England) was prepared by dissolving the dye in either RO water or aqueous sugar solutions, depending on the usage.

**Ball valves**

PVC ball valves (Ashi, Japan).

**Calipers**

Metric calipers (Kanon, Japan or Mitutoyo, Japan) were used with maximum scale 150 mm, accuracy 0.05 mm.

**Chilled water (USA)**

Chilled water produced in a chilled water plant, custom built at Oregon State University, Oregon, USA .

**Conductivity meter (NZ)**

Radiometer Conductivity Meter CDM3 with Type CDC 314 Cell, nominal cell constant 0.316 cm (Radiometer, Copenhagen, Denmark).

**Conductivity meter (USA)**

Orion Conductivity Meter, Model 101 (Orion Research Inc., USA).

**Cooling coil**

A 5.5 m stainless steel tube (inside diameter = 4 mm, outside diameter = 7 mm) formed into a coil with an outside diameter of 110 mm. Propylene glycol (Mobil Oil, NZ) was circulated within the coil in NZ and chilled water in USA.

**Density meter**

PAAR Calculating Density Meter DMA 55 (Anton Paar K.G., Graz, Austria). Density meter operated at 20 ± 0.1°C.

**Desiccator**

Glass desiccator containing silica gel desiccant, blue indicating (Aldrich Chemicals, Wisconsin, USA).

**Disposable membrane filters**

Millex-HA 0.45μm filters (Millipore Corporation, Massachusetts, USA).

**DOC module**

Small laboratory and pilot plant DOC modules supplied by Osmotek Inc, Oregon, USA.

**DOC membranes**

Osmotek Type B membranes supplied by Osmotek Inc, Oregon, USA. Two batches, Batches 1 and 2. Rolled sheets of membrane were stored at 4°C with water containing P3-Oxonia active sanitiser (0.05% v/v) inside sealed plastic bags.

**Dye feed vessel**

One litre plastic bottle, with an outlet at the base fitted with a nylon barbed hose connector (Tefen, Israel).

**Evaporator (NZ)**

Centri-therm CT1B-2 (Alfa Laval, Lund, Sweden).

**Evaporator (USA)**

Centri-therm CT1B-1 (Alfa Laval, Lund, Sweden).

**Fructose osmotic agent**

The fructose osmotic agent was made with food grade crystalline fructose (99.9% purity) (In NZ: Cornsweet crystalline fructose, ADM Corn Processing, Iowa, USA. In USA. Krystar crystalline fructose, A.E Staley MFG Co , Illonois, USA.) RO water was used in NZ and in the USA tap water (103 μmhos $cm^{-1}$) was used instead as RO water was not available in the pilot plant.

The osmotic agent was made up in 50 or 100 litre batches. The required weight of sugar was weighed on an electronic balance (Sartorius F150S-*D2, Sartorius GMBH, Germany) in NZ or the OA balance in the USA, then made up to the final weight with RO or tap water. The solutions were mixed with a paddle stirrer until the solute was completely dissolved. The osmotic agent solutions were stored at 2°C for up to four days

prior to use. These solutions were stored at -20°C if they were not used within four to five days.

**Glass sample vials**

Four millilitre glass Sunvial vials with fitted polyethylene caps (Sun International Trading Ltd, North Carolina, USA).

**Glucose osmotic agent**

The glucose osmotic agent was made up as described for the fructose osmotic agent with food grade glucose:dextrose monohydrate (dextrose equivalent 99.0%) (Prasertchai Co. Ltd, Thailand via APS Chemicals Ltd., Auckland, NZ).

**Helium gas**

Helium UHP, purity 99.999% (BOC Gases, Auckland, NZ).

**High pressure liquid chromatography (HPLC) (NZ)**

Shimadzu LC10A Series HPLC System (Shimadzu Corporation, Japan) comprised of a Shimadzu CBM-10A communication bus module, Shimadzu LC-10AD liquid chromatograph solvent delivery system and Shimadzu SIL-10A auto injection system.

**HPLC (USA)**

HPLC system consisted of a Varian 5000 liquid chromatograph solvent delivery system (Varian, USA), Perkin Elmer LC1100 laboratory computing integrator (Perkin Elmer, USA) and a Beckman 501 auto sampler (Beckman Instruments, USA).

**HPLC column (NZ)**

Zorbax-$NH_2$ column (4.6 x 250 cm) (Rocklands Technologies Inc, USA), used as a reverse-phase column.

**HPLC column (USA)**

Aminex CHO HPX-87C column (7.8 x 300 cm) (BioRad Laboratories, California, USA), used as a reverse-phase column.

**HPLC detector (NZ)**

A Waters Model R401 refractive index detector (Waters Associates, USA).

**HPLC detector (USA)**

A Varian refractive index detector (Varian, USA).

**HPLC mobile phase (NZ)**

Eighty percent by volume acetonitrile (Chrom AR HPLC grade, Mallinckrodt Chemicals, Kentucky, USA) and 20% by volume ultra pure water were combined and filtered under vacuum through one membrane filter (Milli-HA 0.45 filters, 47 mm diameter, Millipore Corporation, Massachusetts, USA). The mobile phase was stored at 20°C.

**HPLC mobile phase (USA)**

Ultra pure water containing 200 mg $l^{-1}$ calcium nitrate ($Ca(NO_3)_2$) (Merck Chemicals, USA). The $Ca(NO_3)_2$ was included in the mobile phase to ensure Ca, the counter ion on the column, was maintained. The mobile phase was stored at 20°C.

**HPLC sugar standards**

D(-) fructose (Sigma Chemicals, Montana, USA or Aldrich Chemicals, Wisconsin, USA), D(+) glucose and sucrose (Sigma Ultra grade, Sigma Chemicals, Montana, USA) were dried in a vacuum oven at 75°C and a vacuum of 760 mm Hg for approximately 24 hours. They were placed in a desiccator and cooled prior to weighing out. Weight by weight standards were made up and diluted with ultra pure water.

**Juice circuit feed vessel**

Plastic one litre graduated measuring cylinder (Azlon, UK), with an outlet at the base fitted with a nylon barbed hose connector (Tefen, Israel).

**Juice circuit pump (NZ)**

A Masterflex 7019 peristaltic pump head (Cole-Parmer, Illonois, USA), driven by a DC motor (Leeson DC motor 180W, 1750 rpm, Leeson Electric Corporation, Wisconsin, USA). The pump motor was controlled with a variable speed controller (Electropar DC Speed Controller 240 VAC input/180 VDC output, Electropar, Auckland, NZ). Flow rates could be controlled from $3.4 \times 10^{-6}$ to $1.5 \times 10^{-4}$ $m^3$ $s^{-1}$

**Juice circuit pump (USA)**

Centrifugal pump (Little Giant 115V, 60Hz, USA) for both small and large DOC modules. The flow rate in the juice circuit was controlled with a ball valve placed in line after the juice pump.

**Mercury calibration thermometer**

Calibrated mercury thermometer (Institute of Environmental Science and Research Ltd (ESR), Auckland).

**Nylon fittings**

Nylon 66 fittings from Tefen, Israel (barbed hose connectors, tee junctions etc., with BSP sizing).

**Osmotic agent (OA) balance (NZ)**

Precisa Model 8000D-24000G electronic balance (PAG Oerlikon Ag, Zurich, Switzerland). Dual range balance, capacity 24 kg, readability 0.0001 kg up to 8 kg and 0.001 kg up to 24 kg.

**OA balance (USA)**

AND Model PV-60K electronic balance (A & D Mercury, USA). Capacity 60 kg, readability 0.02 kg.

**OA circuit pump (NZ)**

A Masterflex 7019 peristaltic pump head (Cole-Parmer, Illonois, USA), driven by a DC motor (Leeson DC motor 180W, 1750 rpm, Leeson Electric Corporation, Wisconsin, USA). The pump motor was controlled with a variable speed controller (Electropar DC Speed Controller 240 VAC input/180 VDC output, Electropar, Auckland, NZ). Flow rates could be controlled from $6 \times 10^{-6}$ to $1.8 \times 10^{-4}$ $m^3$ $s^{-1}$.

**OA circuit pump (USA)**

A Masterflex 7021-21 peristaltic pump (Cole-Parmer, Illonois, USA), controlled with a Masterflex variable speed controller (Cole-Parmer, Illonois, USA). Flow rate range $7 \times 10^{-6}$ to $5 \times 10^{-5}$ $m^3$ $s^{-1}$.

**OA reservoir (NZ)**

A 25 litre plastic tub (Payless Plastics, Auckland, NZ).

**OA reservoir (USA)**

A 30 and a 50 litre plastic tub (Rubbermaid, USA) were used for the small and large laboratory DOC modules, respectively.

**OA stirrer (NZ)**

Stainless steel axial impeller (85 mm diameter) was attached to a stainless steel shaft to form the mixing propeller. The propeller was attached to a IKA-Labortechnik RE16 variable speed motor (Janke and Kunkel GMBH & Co., Germany).

**OA stirrer (USA)**

The same propeller as used with the OA stirrer (NZ) was attached to a variable speed drill.

**P3-Oxonia active**

P3-Oxonia active, peroxyacetic acid sanitiser (Klenzade, Ecolab, Minnesota, USA).

**Pasteuriser**

Stainless steel tubular heat exchanger built by HortResearch, Auckland, NZ, with a Honeywell controller (Honeywell, Pennsylvania, USA) and Watson-Marlow 603U0 peristaltic pump with a Watson-Marlow 501T controller (Watson-Marlow Ltd, Cornwall, England).

**Potassium chloride solution**

Potassium chloride (KCl) (AnalaR grade, BDH Chemicals, Poole, England), 0.7456 g, was dissolved and made up to 1000 ml with ultra pure water at 25°C. This standard reference solution has a conductivity of 1413 μmhos $cm^{-1}$ at 25°C (Clesceri et al., 1989).

**Plastic bucket**

Ten and 20 litre Polypail plastic buckets (Nexus CPI Containers, Auckland, NZ)

**Pressure gauges**

Haenni pressure gauges with 63 mm dial and liquid filled (Haenni, Switzerland), pressure range of 0 - 100 kPa. Pressure gauges were fitted to diaphragm seals (3000 Nitrile, filled system) inside stainless steel housings (Applied Instruments, Auckland, NZ).

**PVC tubing**

Polyvinyl chloride (PVC) non-toxic clear tubing (10 mm internal diameter, 14 mm outside diameter) (Paykel Engineering, Auckland, NZ).

**Refractometer (NZ)**

Atago ABBE Refractometer Type 302 and Atago Illuminator (Atago, Japan). Temperature of prism determined with thermometer fitted to refractometer.

**Refractometer (USA)**

Reichert Auto Abbe Automatic Refractometer (Reichert Scientific Instruments, New York, USA). Automatic temperature compensation.

**Reverse osmosis water (RO water)**

RO water obtained from a Milli-RO 20 Reverse Osmosis Water System (Millipore, Massachusetts, USA). The specific conductance of the water was < 300 μmhos $cm^{-1}$.

**Rheometer**

Bohlin VOR Rheometer (Bohlin Reologi AB, Sweden), with the C25 measuring system (concentric cylinders, cup and bob) and 4.62 g $cm^{-1}$ torque bar.

**Silicone tubing**

Silicone tubing (3.5 mm internal diameter, 6 mm outside diameter) (Biolab Scientific, Auckland, NZ).

**Sodium chloride osmotic agent**

The sodium chloride (NaCl) osmotic agent was made up as described for the fructose osmotic agent with food grade crystalline sodium chloride (purity 99.8%) containing no added free flowing agent or iodine (In NZ: James Crisp NZ Ltd (NZ Salt), Auckland, NZ. In USA: Cargill Top Flo Evaporated Salt, Cargill International, Michigan, USA.).

**Sodium chloride standards**

Sodium chloride (NaCl) (AnalaR grade, BDH Chemicals, Poole, England) was dried in a vacuum oven at 75°C and a vacuum of 760 mm Hg for 24 hours. It was cooled and placed in a desiccator for two weeks prior to weighing out. Weight by weight standards were made up and diluted with ultra pure water. The concentration of the standards was checked by measuring their specific conductance with a conductivity meter.

**Sucrose osmotic agent**

The sucrose osmotic agent was made up as described for the fructose osmotic agent with food grade crystalline sucrose (purity 99.9%) (NZ Sugar Company, Auckland, NZ).

**Temperature probe and display unit**

Digi-Temper TDS temperature probe (Tsuruga Electric Works Ltd., Japan), with an accuracy of 0.1°C.

**Tubing clamp**

Polycarbonate tubing clamps (Biolab Scientific, Auckland, NZ).

**Ultra pure water**

Ultra pure water obtained from a Milli-Q Plus Ultra Pure Water System (Millipore, Massachusetts, USA). The specific conductance of the water was 0.42 ± 0.04 μmhos $cm^{-1}$.

**Ultrasil 53**

Ultrasil 53 enzymatic detergent (Klenzade, Ecolab, Minnesota, USA).

**Vacuum oven**

Thermostat vacuum oven (Townson & Mercer Ltd, Croydon, England).

**Video camera**

Sony Handycam 8 mm video recorder (Sony Corporation, Japan).

**Water bath heater (NZ)**

Techne Tempette Junior TE-8J water bath heater, circulator and controller (Techne Ltd, Cambridge, UK).

**Water bath heater (USA)**

Brinkmann Model IC-2 water bath heater, circulator and controller (Brinkmann, USA)

## 3.2. Methodology

### 3.2.1. Density

Three millilitres of sample was injected into the density meter, temperature controlled at 20.0 ± 0.1°C. The cell was allowed to stabilise before readings were taken. After each sample the cell was twice flushed with glass distilled water.

The meter was calibrated with glass distilled water, for which the density reading was 997.15 kg $m^{-3}$ at 20°C. Readings from the meter were uncorrected density values. The densities were corrected for the buoyant effect errors which are the errors due to the difference between the volume and density of the unknown and the volume and density of the weights used as standards (Kenner and O'Brien, 1971). Measured densities were corrected as follows

$$corrected\ \rho_{sample,20°C} = uncorrected\ \rho_{sample,20°C} \times \frac{corrected\ \rho_{water,20°C}}{uncorrected\ \rho_{water,20°C}} \quad (3.1)$$

$$corrected\ \rho_{sample,20°C} = uncorrected\ \rho_{sample,20°C} \times \frac{998.20}{997.15} \quad (3.2)$$

### 3.2.2. Refractive index

The refractive index of samples were determined with a refractometer (NZ or USA). The refractometers were calibrated with ultra pure water. The refractive index and prism temperature were recorded for each reading. The refractive index was corrected to 20°C using Table 3.1. Each sample was measured three times and the mean value determined.

### 3.2.3. Viscosity

A rheometer was used to determine the absolute viscosity of various solutions at controlled temperatures. The shear number range 44 - 56 was covered, the torque range was greater than 1% over this range for all samples. The absolute viscosity value (kg $m^{-1}$ $s^{-1}$) was taken from the viscosity reading given at a shear rate of 2.91 × $10^2$ $s^{-1}$, shear number 53. Approximately 13 ml of sample was poured into the cup into which the bob was lowered. The temperature of the cup was equilibrated to the desired temperature (10, 20 or 40°C) before the measurement was carried out. For each solution the absolute viscosity was the average of duplicate samples measured.

### 3.2.4. Specific conductance

Specific conductance was determined with manual temperature compensation (at 20°C), with the conductivity meters used. The meter was checked and calibrated with ultra pure water (specific conductance less than 1 μmhos $cm^{-1}$) and with 0.01M KCl at 25°C.

For the conductivity meter (NZ), the samples, equilibrated to 20°C, were drawn up into the conductance cell and the value of the conductance read from the analog scale. For the conductivity meter (USA), the conductivity electrode was immersed into the sample and the conductance was read off the digital read out. Each sample was measured three times and the average value determined.

### 3.2.5. Storage and re-concentration of osmotic agents

At the end of a day's processing the sugar solutions were pasteurised, at 95°C for 30 seconds, cooled to 72 °C, then stored at 2°C.

**Table 3.1. Mean values of the refractive index and the dispersion varied according to the temperature of distilled water**

| Temperature (°C) | Refractive index (nD) | Mean Dispersion (nF - nC) | Temperature (°C) | Refractive index (nD) | Mean Dispersion (nF - nC) |
|---|---|---|---|---|---|
| 10 | 1.33369 | 0.00600 | 26 | 1.33240 | 0.00596 |
| 11 | 1.33364 | 0.00600 | 27 | 1.33229 | 0.00595 |
| 12 | 1.33358 | 0.00599 | 28 | 1.33217 | 0.00595 |
| 13 | 1.33352 | 0.00596 | 29 | 1.33206 | 0.00594 |
| 14 | 1.33346 | 0.00599 | 30 | 1.33194 | 0.00594 |
| 15 | 1.33339 | 0.00599 | 31 | 1.33182 | 0.00594 |
| 16 | 1.33331 | 0.00598 | 32 | 1.33170 | 0.00593 |
| 17 | 1.33324 | 0.00598 | 33 | 1.33157 | 0.00593 |
| 18 | 1.33316 | 0.00598 | 34 | 1.33144 | 0.00593 |
| 19 | 1.33307 | 0.00597 | 35 | 1.33131 | 0.00592 |
| 20 | 1.33299 | 0.00597 | 36 | 1.33117 | 0.00592 |
| 21 | 1.33290 | 0.00597 | 37 | 1.33104 | 0.00591 |
| 22 | 1.33280 | 0.00597 | 38 | 1.33090 | 0.00591 |
| 23 | 1.33271 | 0.00596 | 39 | 1.33075 | 0.00591 |
| 24 | 1.33261 | 0.00596 | 40 | 1.33061 | 0.00590 |
| 25 | 1.33250 | 0.00596 | | | |

Source: Table 1, Instructions of Atago Abbe Refractometer Improved Type No. 302.

The sugar osmotic agents were reconcentrated in the evaporators (NZ and USA). In the evaporator (NZ), the evaporation temperature was 70°C and the solutions were concentrated by recirculating the solution ($1.42 \times 10^{-5}$ $m^3$ $s^{-1}$) until the desired concentration was obtained. The vacuum in the evaporating chamber was maintained at -9000 to -8000 kg $m^{-2}$ and in the steam chamber -5500 kg $m^{-2}$.

In the evaporator (USA), the evaporation temperature was 80°C and the solutions were concentrated by recirculating the solution (approximately $5 \times 10^{-6}$ $m^3$ $s^{-1}$) until the desired concentration was obtained. The vacuum in the evaporating chamber was maintained at -8000 to -7000 kg $m^{-2}$.

NaCl solutions were not re-concentrated. The concentration of diluted NaCl solution was increased by addition of crystalline NaCl.

### 3.2.6. Determining the concentration of the sugar OA solutions

The refractive index was the standard method for measuring sugar concentrations during a DOC experimental run. Calibration curves relating refractive index to concentration were obtained from literature and verified using HPLC analysis of prepared standards.

For verification of the published data, fructose, glucose and sucrose standards were made up with fructose, glucose and sucrose analytical grade and ultra pure water as described for HPLC sugar standards. For each sugar the highest concentration required for the calibration curve was made up with the exact weight of the sugar, weighed (± 0.001 g) into a glass test tube (with ground glass stopper) then dissolved and made up to exact weight with ultra pure water. The remaining concentrations for the standards were diluted from this standard.

The refractive index, density and concentration by HPLC was determined for each solution.

### 3.2.7. Determining the concentration of sodium chloride OA solutions

As for the sugar solutions, the refractive index was the standard method for measuring NaCl concentrations during a DOC run. Calibration curves relating refractive index to concentration were obtained from literature and verified by measuring the specific conductance of prepared standards [see 3.2.4].

## 3.2.8. HPLC analysis of sugars

### Sample and standards preparation

Calibration samples were made using HPLC sugar standards as follows:

- fructose 0.001, 0.005, 0.01, 0.015 and 0.02 g (g solution)$^{-1}$ (0.006, 0.03, 0.06, 0.08, 0.11 molal),
- glucose 0.020, 0.050, 0.070 and 0.10 g (g solution)$^{-1}$ (0.11, 0.29, 0.42, 0.62 molal),
- sucrose 0.01, 0.02, 0.04 and 0.06 g (g solution)$^{-1}$ (0.03, 0.06, 0.12, 0.19 molal).

Ultra pure water was used as the blank. Total peak areas were used to prepare calibration curves. Calibration curves were determined for each set of samples analysed Also the standards were analysed randomly amongst the unknown samples.

The standards and samples were filtered through one disposable membrane filter directly into clean glass sample vials ready for HPLC injection. Where appropriate, experimental samples were diluted with ultra pure water to ensure the sugar concentration fell within the range of the calibration curves.

### HPLC procedure

Procedures were different in NZ and the USA.

In both NZ and the USA the mobile phase was degassed with helium gas at a flow rate of $6.7 \times 10^{-7}$ m$^3$ s$^{-2}$, for five minutes prior to introduction into the HPLC column.

An isocratic gradient was maintained with the mobile phases. The HPLC mobile phase (NZ) was pumped at a flow rate of $2.5 \times 10^{-8}$ m$^3$ s$^{-1}$ through the HPLC column (NZ) and the column temperature was maintained at 40°C. The HPLC mobile phase (USA) was pumped at a flow rate of $1.17 \times 10^{-8}$ m$^3$ s$^{-1}$ through the HPLC column (USA) and the column temperature was maintained at 85°C.

During sample injection and detection, helium gas was continually sparged into the mobile phase at $1 \times 10^{-7}$ m$^3$ s$^{-1}$. Each standard or experimental sample was injected twice and determined in duplicate (duplicates analysed randomly). The injection volume was 20 µl. Detection of the sugar peaks was by refractive index. The experimental samples' concentrations were obtained by comparing peak areas to the calibration curves.

### 3.2.9. DOC apparatus and operation

The DOC equipment and technology used during this research was patented by Osmotek Inc., Corvallis, Oregon, USA (Herron et al., 1994). The DOC module is described in detail in Chapter 5. The small laboratory DOC module was used in NZ and the USA. The pilot plant DOC module was used in the USA only. The dilute solution to be concentrated flows through the juice circuit which consists of the flow channel in the DOC module, the adjoining tubing and the juice pump. The concentrating agent, the OA, flows through the OA circuit which consists of the flow channels in the DOC module, the adjoining tubing and the OA pump. A schematic diagram showing the arrangement of the DOC system is shown in Figure 3.1.

The juice circuit setup was the same for both NZ and the USA. The juice circuit feed vessel [1] outlet was connected with PVC tubing into the recycle loop of the juice circuit [8], before the juice circuit pump [2]. The dilute solution was recirculated around the juice circuit with the juice circuit pump which was connected to the DOC module [5] and feed vessel with PVC tubing and nylon fittings. Ball valves were used to stop the flow in the juice circuit, if required. Pressure gauges [4,6] were placed in the juice circuit tubing immediately prior to the inlet and immediately after the outlet of the module. A "bleed valve" [7] was placed at the top of the juice circuit, using silicone tubing and a tubing clamp. A sample port [3], with a silicone rubber seal, was placed in the juice circuit allowing the solution in the circuit to be sampled during operation.

The juice feed vessel ensured a constant volume was maintained in the juice circuit. Thus the reduction in volume in the juice circuit feed vessel over time was recorded as the loss of water from the juice circuit. Water loss was assumed to be only due to water transfer across the membrane as no leaks in the juice circuit were observed.

The OA circuit setup was also the same for both NZ and the USA. The same type of PVC tubing, nylon fittings and ball valves were used in the OA circuit [9] as in the juice circuit. The OA was drawn from the OA reservoir [10], pumped through the DOC module [5] and returned back into the reservoir with the OA circuit pump [11]. PVC tubing was connected to a nylon fitting tee junction placed prior to the entry to the module to allow the OA to be drained quickly from the module at the end of each run. The outlet to the OA drain tube was kept closed during operation with a ball valve. A pressure gauge [12] was placed in the PVC tubing, at the inlet to the DOC module and a ball valve was placed after the OA pump to stop the flow in the OA circuit, if required.

**Figure 3.1. DOC unit flow diagram**



juice circuit



OA circuit

1. Juice circuit feed vessel
2. Juice circuit pump
3. Sampling port for juice circuit, rubber septum
4. Pressure gauge, juice circuit inlet to module
5. DOC module
6. Pressure gauge, juice circuit outlet from module
7. Bleed valve for juice circuit
8. Juice circuit
9. OA circuit
10. OA reservoir
11. OA circuit pump
12. Pressure gauge, OA circuit inlet to module
13. OA balance
14. Cooling coil
15. OA stirrer
16. Water bath heater

Not drawn to scale

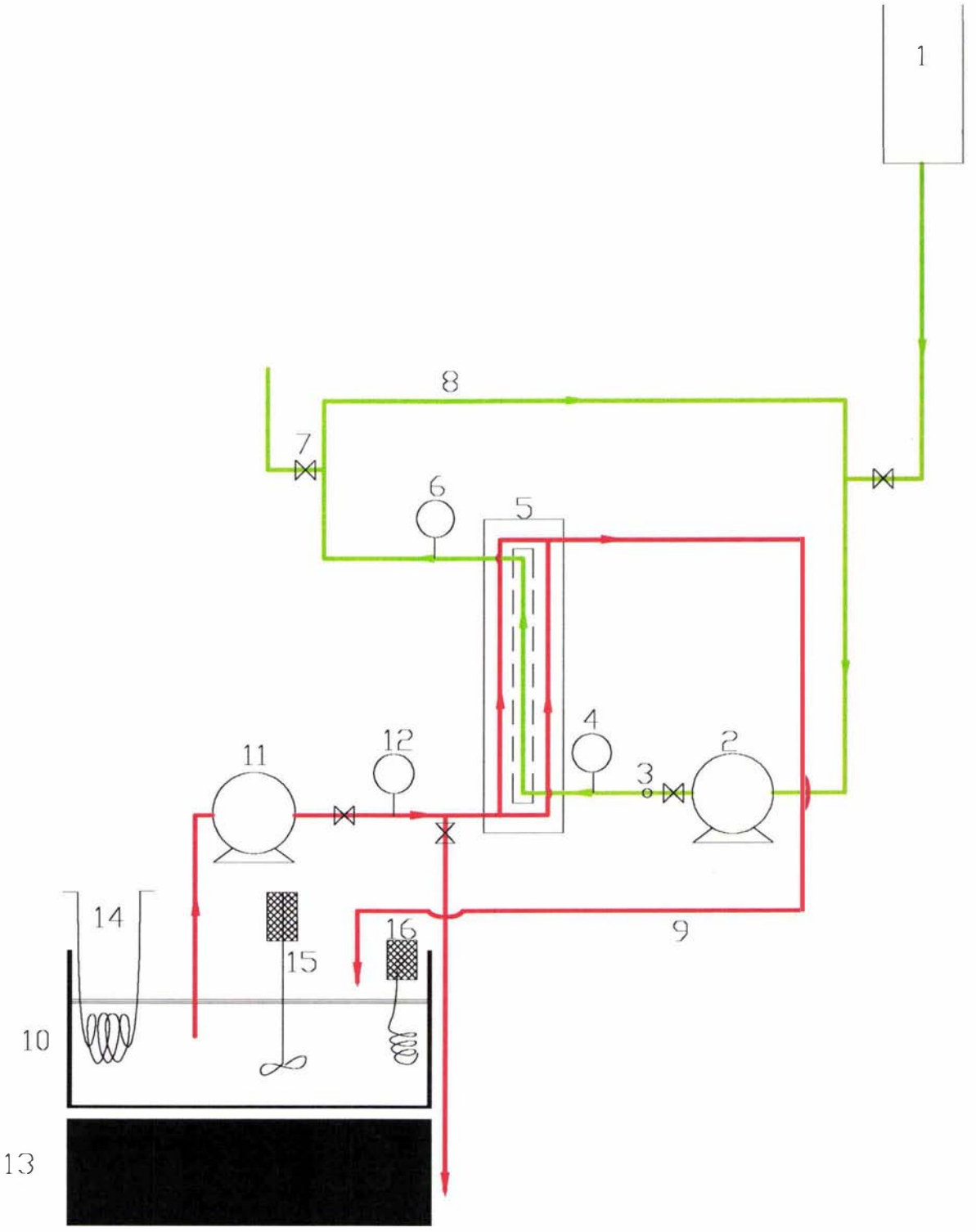
1
8
7
6
5
4
2
3
12
11
14
16
15
9
10
13

The OA reservoir was placed on the OA balance [13] in order to measure the changes in OA solution weight. The inlet and outlet tubes for the OA were secured over the OA reservoir with clamps so they did not touch the reservoir. The OA solution in the OA reservoir was kept well mixed with the OA stirrer [15] and the circulator on the water bath heater [16]. The temperature in the OA reservoir was controlled by cooling with propylene glycol (−5 to −2°C) (chilled water in USA) circulated in the cooling coil [14] at a constant flow rate and by heating from the water bath heater. The temperature in the water bath was maintained at ± 0.1°C. The temperature of the OA was monitored with a temperature probe attached to a display unit. The temperature probe was calibrated with a mercury calibration thermometer.

A constant volume was maintained in the OA circuit, excluding the OA reservoir which acted as a buffer tank. Water crossing the membranes and taken up in the OA circuit resulted in an increase in the total weight of OA in the reservoir. This was measured on the OA balance.

### 3.2.10. Standard operation start up procedure of DOC apparatus

At start up, the juice circuit was first filled with RO water, at the desired operating temperature, from the juice circuit feed vessel. Any air in the lines was released at the bleed valve. The juice circuit was flushed out with five litres of fresh RO water, then the RO water was continuously recirculated. The feed vessel maintained a constant head of 540 mm above the base of the DOC module. The volume of water in the juice circuit feed vessel was maintained between 500 and 1000 millilitres. The volumetric water flow rate in the juice circuit was set and maintained at $4 \times 10^{-5}$ $m^3$ $s^{-1}$, except when the effect of juice circuit flow rate was investigated. The flow rate was set in the pilot plant DOC module to obtain the same Reynolds number as obtained in the small module in the juice circuit. The flow rate was checked using a calibrated measuring cylinder before recycling operation. The hydraulic pressure in the juice circuit was 14 - 17 kPa at the module inlet and 5 - 7 kPa at the module outlet.

The juice circuit was established before any OA solution was circulated. The OA was then slowly pumped into the OA circuit and air bubbles removed by tilting the DOC module from side to side. The flow rate of the OA was constant at $7 \times 10^{-6}$ $m^3$ $s^{-1}$ for all experiments. The flow rate was checked using a calibrated measuring cylinder. The hydraulic pressure in the OA circuit was 0 - 5 kPa at the inlet to the DOC module and atmospheric at the outlet.

### 3.2.11. Equilibration of DOC module

It was necessary to equilibrate the module and membranes before collection of data. The following equilibration operation was carried out after standard operation start up and prior to any data collection.

Firstly the juice and OA circuits were flushed out for 10 minutes in the small laboratory module, with RO water or intended OA, respectively. Then the OA inlet hose was transferred to a new bucket containing about 15 kg of fresh OA ensuring no air was introduced to the OA circuit. The OA was recycled for one hour to allow the membranes to equilibrate. No attempt was made to maintain the OA concentration during this time.

The same equilibration procedure was used for the pilot plant DOC module. However, the OA circuit was initially flushed for 20 minutes and the membranes were equilibrated for 90 minutes with 25 - 30 kg of OA.

### 3.2.12. Experimental operation of DOC apparatus

After the equilibration process the inlet hose of the OA circuit was transferred into a new OA solution in the OA reservoir, at the desired concentration and temperature. For the next 10 minutes of operation, the OA exiting the module was discarded (20 minutes for the pilot plant module) before the outlet hose was clamped over the OA reservoir allowing OA to recycle. At the same time the juice circuit was flushed with fresh RO water. The OA was left to circulate for five minutes before the initial weight of OA was recorded as "zero time". For the small or pilot plant DOC module the OA reservoir contained approximately 25 or 56 kg of OA, respectively. The mass of OA used ensured the OA concentration did not change by more than 5% over the data collection period.

Experimental trials looking at the effect of operating temperature were carried out randomly with respect to temperature. Between each trial the juice and OA circuits were equilibrated to the next desired operating temperature.

### 3.2.13. Determination of water flux rate

The weight of the OA in the reservoir and the volume of water in the juice circuit feed vessel were recorded at 5 minute intervals for 45 minutes. The OA temperature, OA circuit inlet hydraulic pressure, juice circuit inlet and outlet hydraulic pressures were also recorded at the same time. The temperature of the juice circuit at the beginning and at the end of the run was recorded. There was no temperature control in the juice circuit, as the volume in the juice circuit was small (approximately $3.18 \times 10^{-4}$ $m^3$) compared

to the OA circuit and reservoir (approximately 0.02 $m^3$). Polystyrene foam sheets were placed around the module to provide insulation.

Samples of the juice and OA circuits before and after each experimental run were collected. The refractive index of these samples was measured and the concentrations determined from calibration curves. These samples were frozen and stored at -20°C for further analyses (e.g. HPLC).

### 3.2.14. Data analysis for flux rate

The water flux rate across the membrane was determined after linear regression analysis of the OA weight versus time data (MINITAB Release 9.2, Minitab Inc. Pennsylvania, USA). The gradient of the regression line obtained was the mass flow rate of water across the membrane (kg $s^{-1}$). Except where stated, trials were carried out in triplicate.

### 3.2.15. Cleaning of DOC module and membranes

After each day the OA was drained while the RO water was still circulating in the juice circuit. Both the juice and OA circuits were flushed first with warm water (35 - 40°C) for 30 minutes, followed by cold water (15 - 20°C) for a further 20 minutes. Each circuit was then rinsed with five litres of 0.1% v/v P3-oxonia active sanitiser. After sanitisation, both circuits were rinsed with RO water for 15 minutes. The OA circuit was drained first then the juice circuit. Moisture was left in the juice circuit to keep the membranes moist. In the pilot plant DOC module all washing times were extended by 10 minutes.

When the membranes were considered to be "dirty", they were washed with a 10 g $l^{-1}$ solution of Ultrasil 53 enzyme detergent. Five litres were circulated in the juice and OA circuits for 20 minutes after the first rinse. The circuits were then rinsed again with cold water (10 minutes) before sanitisation with P3-oxonia active.

### 3.2.16. Membrane replacement

Membranes were replaced when they had measurable leaks. The asymmetric membranes were cut to the correct shape placed on each OA plate of the module, with the active layer of the membrane facing the required direction and kept taut with masking tape. The two OA plates were then clamped together securing the membranes in place. Screws and bolts around the edge were tightened until the membranes were sealed between the seals and there were no water leaks from the module. The masking tape was then removed.

Water was circulated in the juice circuit (OA circuit empty) and the amount of water lost through the membrane after one hour was determined. The normal loss was 10 - 15 ml. If more than 15 ml of water was lost the membranes were inspected and replaced. Water leakage from the juice circuit at the base of the module was less than 1 ml $hour^{-1}$. In most cases there was no water loss from the juice circuit from the base of the module.

Each new set of membranes was tested also for salt permeability to establish that the new set had similar mass transfer properties to previous sets. Following membrane replacement the juice circuit was drained and flushed with 1 litre of 0.10 g (g solution)$^{-1}$ fructose solution and then drained again. Two kilograms of 0.10 g (g solution)$^{-1}$ fructose solution were then introduced to and circulated in the juice circuit while two kilograms of 0.15 g (g solution)$^{-1}$ NaCl solution were circulated in the OA circuit. After three hours, typically about 1 kg of water was lost from the juice circuit into the OA circuit. The fructose solution in the juice circuit was collected quantitatively then re-diluted back to its original concentration. The specific conductances of the initial and final fructose solutions were measured to determine the amount of NaCl which had passed through the membrane into the juice circuit.

### 3.2.17. Determining the time required to flush the OA circuit

The DOC apparatus was set up as outlined for standard operation [see 3.2.10]. RO water was circulated in the juice circuit and fructose solutions (0.1, 0.3, 0.5 and 0.7 g (g solution)$^{-1}$) were used as the OA. Following the set up of flow in the juice circuit, osmotic agent was introduced to the module and the refractive index of the exiting OA was measured every minute for the first 10 minutes. It was then measured approximately every 5 minutes for the next 80 minutes. The time required to flush all the water out of the OA circuit and to obtain a steady-state concentration of OA exiting the module was determined for each concentration of OA, in at least duplicate trials. For 0.1 and 0.7 g (g solution)$^{-1}$ fructose solutions experiments were carried out in triplicate.

### 3.2.18. Determining the time required for equilibration of membranes

The DOC apparatus was set up as outlined for standard operation [see 3.2.10]. The OA circuit was flushed out with fresh OA for 10 minutes. New OA solution was introduced and the first 10 minutes of OA exiting the DOC module was discarded.

At a time designated as "zero time" the weight of the OA reservoir was recorded and OA exiting the module was collected in an empty tared plastic bucket (OA-out bucket). There was no recirculation of the OA solution. The weight of OA in the reservoir was

recorded at 5 minute intervals while the weight of the OA collected in the OA-out bucket was recorded every 3.75 minutes. The water volume reduction in the juice circuit feed vessel was also recorded.

The decrease in the OA reservoir weight, over time was analysed by linear regression analysis (MINITAB), this provided the flow rate of OA into the DOC module ($OA_{IN}$). The increase in the OA-out bucket weight over time was also analysed by linear regression analysis (MINITAB), this provided the flow rate of OA out of the module ($OA_{OUT}$). The flux rate of water across the membrane was calculated from the difference between the $OA_{IN}$ and $OA_{OUT}$ flow rates.

The water flux rate across the membrane was determined for a range of fructose solutions as OA, at concentrations 0.1, 0.2, 0.35, 0.5, 0.6 and 0.7 g (g solution)$^{-1}$. Flux rates were determined after 15, 30, 45, 60, 75, 90 and 105 minutes, at 20°C. For each OA concentration the experiment was carried out in duplicate or triplicate.

### 3.2.19. Visualisation of flow characteristics

To assess the juice circuit flow, amaranth dye solution was placed in the dye feed vessel, which was placed above the juice circuit feed vessel. The dye feed vessel was connected, with PVC tubing and nylon fittings, to the juice circuit at a tee junction just prior to the inlet to the DOC module, as shown in Figure 3.2(a). Flow was controlled with a ball valve placed in the dye inlet PVC tubing. The DOC apparatus was set up as outlined for standard operation [see 3.2.10].

A video camera was placed on a tripod and positioned approximately two metres away from the DOC module. The camera lens was pointed directly at the front flat face of the OA plate, to record the movement of the amaranth dye solution up the juice circuit in the module. Recording on the video camera was started first. The amaranth dye solution was pulsed into the juice circuit using the ball valve. The flow of the amaranth dye solution up the juice circuit was recorded on the video camera. After each pulse of the dye the juice circuit was flushed out with clean water.

The flow conditions up the juice circuit were recorded with the OA circuit empty and with the OA circuit full of 0.6 g (g solution)$^{-1}$ sucrose solution as OA. For each set of conditions the dye was pulsed in six times.

To assess the OA circuit flow, amaranth dye solution was placed in the dye feed vessel placed above the juice circuit feed vessel. The dye feed vessel was connected to the OA

**Figure 3.2. DOC unit flow diagram and dye injection points**

a. Dye injection into the juice circuit
b. Dye injection into the OA circuit

juice circuit

OA circuit

1. Juice circuit feed vessel
2. Juice circuit pump
3. Sampling port for juice circuit, rubber septum
4. Pressure gauge, juice circuit inlet to module
5. DOC module
6. Pressure gauge, juice circuit outlet from module
7. Bleed valve for juice circuit
8. Juice circuit
9. OA circuit
10. OA reservoir
11. OA circuit pump
12. Pressure gauge, OA circuit inlet to module
13. OA balance
14. Dye feed vessel

Not drawn to scale

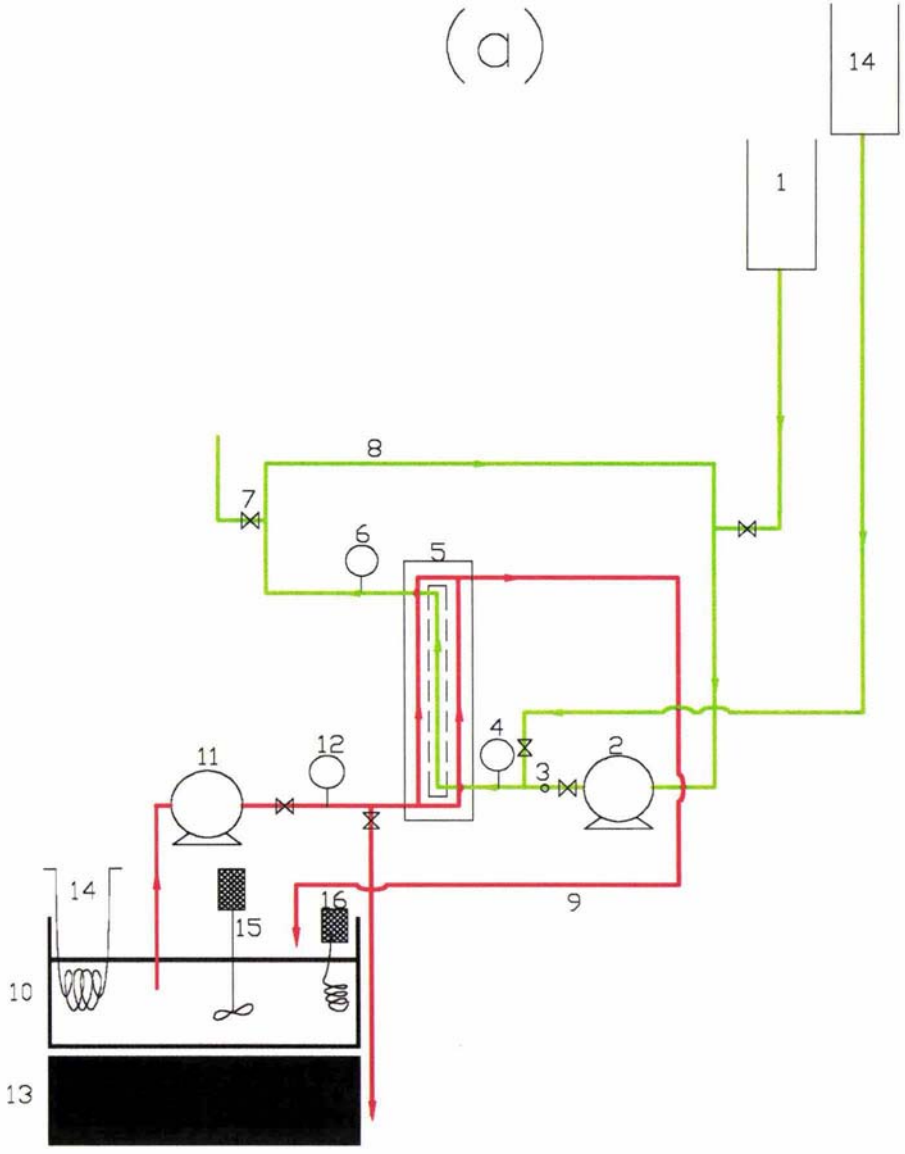
(a)
14
1
8
7
6
5
4
3
2
11
12
14
15
16
9
10
13

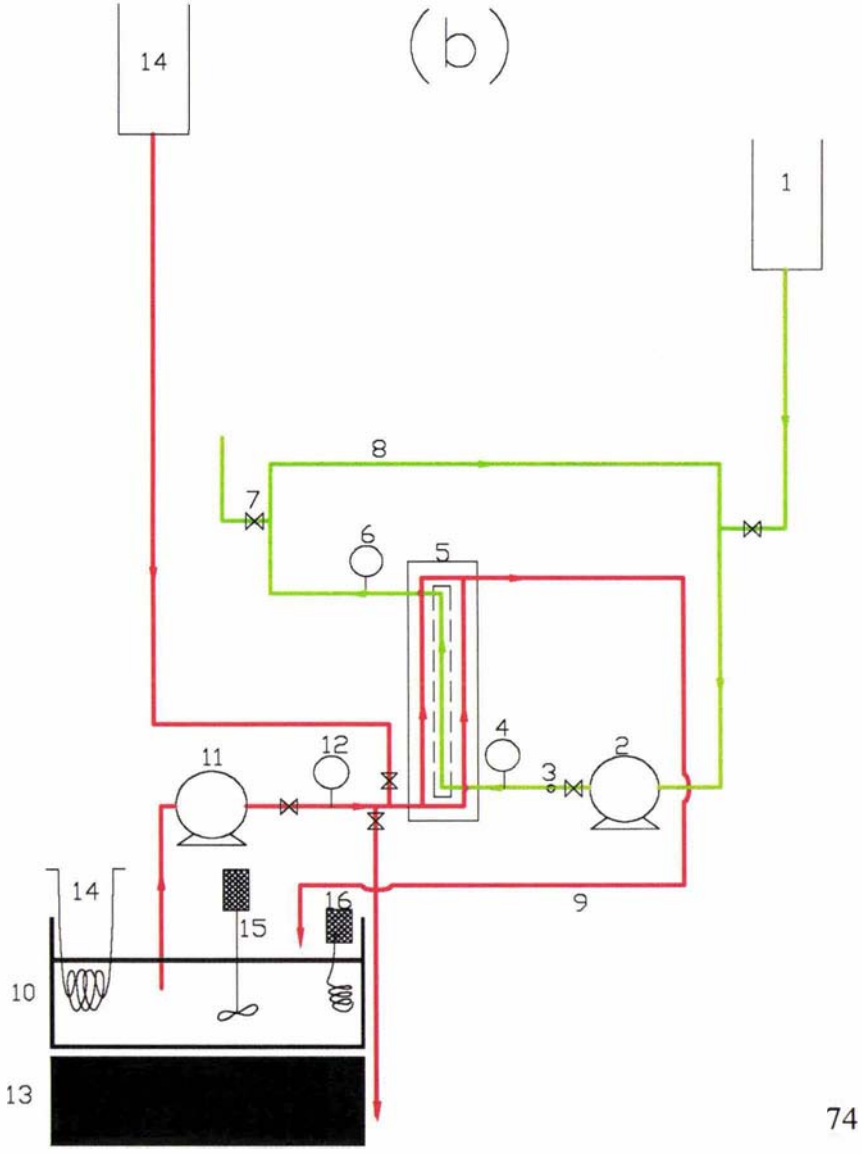
(b)
14
1
8
7
6
5
4
3
2
11
12
14
15
16
9
10
13

circuit at a tee junction just prior to the inlet to the DOC module, as shown in Figure 3.2(b). Flow was controlled with a ball valve placed in the dye inlet PVC tubing. The DOC apparatus was set up as outlined for standard operation [see 3.2.10]. The amaranth dye solution was made up in the OA sugar solution which was being circulated in the OA circuit. The video was operated as before and the amaranth dye solution was pulsed into the OA circuit and the movement of the dye was recorded. After each pulse of the dye, the OA circuit was flushed out with fresh OA.

Osmotic agents circulated in the OA circuit included 0, 0.1, 0.35, 0.5, 0.6 and 0.7 g (g solution)$^{-1}$ fructose solutions, and 0.4, 0.6 g (g solution)$^{-1}$ sucrose solutions. The dye was pulsed in and observed four times for each OA.

### 3.2.20. Determining iso-osmotic concentrations of sugar solutions

In this experiment, the DOC apparatus was used to establish the iso-osmotic concentrations of glucose and sucrose against fructose. A solution of either glucose or sucrose was circulated in the juice circuit while an approximately iso-osmotic solution of fructose was circulated in the OA circuit. Following 24 hours recycling, both solutions had equilibrated and the actual concentration in each circuit was measured.

The DOC apparatus was set up as outlined for standard operation [see 3.2.10] except no OA was introduced into the OA circuit. The juice circuit was drained completely, then flushed with approximately 1 litre of the test solution (glucose or sucrose). The OA circuit was also flushed with the intended fructose solution (2 litres), then drained. Fresh test solution (glucose or sucrose) was then introduced to the juice circuit and continuously recirculated at $5 \times 10^{-6}$ m$^3$ s$^{-1}$. Fresh solution from the juice circuit feed vessel was stopped from entering the juice circuit by closing the ball valve in the feed inlet tubing. A fructose solution with approximately the same iso-osmotic concentration as the test solution was introduced to the OA circuit as outlined under standard operation [see 3.2.10]. The fructose solution (20 kg) was recirculated in the OA circuit at $7 \times 10^{-6}$ m$^3$ s$^{-1}$. The system was allowed to equilibrate for approximately 24 hours, at 20°C. The sugar concentration in both circuits was checked every 3 or 4 hours by removing a small sample from each circuit. The concentrations of both circuits had equilibrated after 15 to 20 hours. Samples from the juice and OA circuits after equilibration were collected, frozen and stored at −20°C for analysis by HPLC.

Three different concentrations of sucrose solutions and one concentration of glucose solution were tested against fructose solutions in duplicated experiments.

## 3.3. Analysis of data

The mean, standard deviation (*sd*) and standard errors about the mean (*SEM*) were calculated for the replicated or triplicated flux rates. The overall standard error of the means was calculated from the pooled estimate of standard deviation (*s*), from the standard deviations of individual means.

$$\textit{Pooled estimate of standard deviation} \quad s = \sqrt{\frac{\sum (df \times sd^2)}{\sum (df)}} \tag{3.3}$$

$$SEM = \frac{s}{\sqrt{n}} \tag{3.4}$$

$n$ - number of samples for each mean
$df$ - degrees of freedom = $(n - 1)$
(Maindonald, 1992)

As outlined in Section 3.2.14 the water flux rate was determined from the rate of change in OA weight over time, using linear regression analysis. The slope ($x$-coefficient) of the regression line was the mass flow rate of water entering the OA circuit across the membrane. A plot of the mass flow rate against the standard error of the slope for all the data showed a straight line could be fitted through the point (0,0) for the data. Therefore, the standard error of the $x$-coefficient was taken to be proportional to the expected value of the $x$-coefficient,

$$SE[x] \approx \kappa E[x] \tag{3.5}$$

$x$ - $x$-coefficient, slope of line of OA weight versus time
$SE[x]$ - standard error of $x$-coefficient
$E[x]$ - expected value of $x$-coefficient
$\kappa$ - proportionality constant

The proportionality constant, $\kappa$, can be calculated from

$$\kappa = \frac{\Sigma SE[x]}{\Sigma x} \tag{3.6}$$

(Maindonald, 1996)

The value of $\kappa$ gives the ratio of the the standard error (*SE*) to the expected value of $x$ (mass flow rate). For both the small and pilot plant DOC modules, $\kappa$ was calculated as 0.008. Therefore, for the mass flow rates (kg $s^{-1}$) determined the standard error (*SE*), $SE[x] = 0.008 \times$ mass flow rate.

The water flux rates (kg $m^{-2}$ $s^{-1}$) were obtained by taking into account the available membrane area for mass transfer. The standard error of the water flux rate obtained was calculated using the following equations,

$$\%Error[flux\ rate] = \left( \sqrt{\left(\frac{SE[x]}{E[x]}\right)^2 + \left(\frac{SE[A_m]}{E[A_m]}\right)^2} \right) \times 100 \quad (3.7)$$

$$SE[flux\ rate] = \%Error[flux\ rate] \times E[flux\ rate] \quad (3.8)$$

$A_m$ - membrane area, $m^2$
$E[A_m]$ - expected value of membrane area, $m^2$
$SE[A_m]$ - standard error of the membrane area, $m^2$
$\%\ Error[flux\ rate]$ - percentage error (fractional error) of mass flux rate
$E[flux\ rate]$ - expected value of mass flux rate, kg $m^{-2}$ $s^{-1}$
$SE[flux\ rate]$ - standard error of mass flux rate, kg $m^{-2}$ $s^{-1}$

### 3.3.1. Comparison of non-linear and linear curves

For non-linear relationships, best fit empirical response curves were fitted to the data sets using the non-linear least squares regression procedure in S-Plus (S-Plus Version 3.3, Statistical Sciences Inc., Washington, USA) (Statistical Sciences, 1995).

Response curves were fitted to each data set for flux rates at different temperatures. The form of the response curves was

$$y = \frac{ax}{(1 + bx)^c} \quad (3.9)$$

$y$ - y axis data
$x$ - x axis data
$a$, $b$, $c$ - constants

The residual standard error ($RSE$) for each curve was provided and the standard error for each parameter in the equation. The residual sum of squares from fitting a single curve ($RSS_O$) to all the data was compared to the residual sum of squares calculated over the individual fitted curves ($RSS_I$) (Draper and Smith, 1981).

Let
$RSS_1$ = (residual standard error from curve 1)$^2$ × $df_1$
$RSS_2$ = (residual standard error from curve 2)$^2$ × $df_2$
$RSS_n$ = (residual standard error from curve $n$)$^2$ × $df_n$

$df_1$ = number of degrees of freedom from curve 1
$df_2$ = number of degrees of freedom from curve 2
$df_n$ = number of degrees of freedom from curve $n$

About the separate curves:
$RSS_I = (RSS_1 + RSS_2 + \ldots + RSS_n)$
$df_I = df_1 + df_2 + \ldots + df_n$

From fitting a single curve to all the data,

$RSS_O$ = (residual standard error)$^2$ × $df_O$
$df_O$ = degrees of freedom for the single curve

$$F_{statistic} = \frac{(RSS_O - RSS_I)/(df_O - df_I)}{(RSS_I/df_I)} \qquad (3.10)$$

The $F_{statistic}$ with degrees of freedom ($df_O - df_I$) and $df_I$, was used to test the null hypothesis that one curve can be fitted to all the data points (i.e. the individual data curves are not different).

This procedure was used to compare flux rate data curves when determining the statistical significance of the effect of temperature, membrane orientation, OA, or module size.

For comparison of linear lines, the same analysis as described above was used to test the null hypothesis. The *RSS* for each fitted line, required for the above analysis was calculated in the linear regression analysis by MINITAB.

### 3.3.2. Best fit polynomial equations for physical properties

Data for physical properties were obtained either from published literature or from experimental work. Polynomial relationships were derived when linear relationships failed to adequately define the physical property. Best fit polynomial equations were derived for the relationships between concentration and refractive index, density, osmosity, and specific conductance. MINITAB was used to fit regression lines to the estimated form of the polynomial equations in order to obtain the best fit equation. The best fit equations were plotted over the published or experimental data points to determine visually the goodness of fit. The sum of the residual standard errors between the fitted line and actual data points was also determined for each fit.

The standard error for each value calculated with the polynomial equations was calculated from the derivative of the equation (Maindonald, 1996). For example, the standard error for density ($SE[\rho]$), when density is estimated from a quadratic relationship, was determined from the standard error of the concentration value ($SE[Y]$) and the derivative of the density function. $SE(Y)$ was obtained from the variability in the experimental data. Therefore, where the quadratic equation for density is

$$\rho = 998.2 + 383Y + 158Y^2 \tag{3.11}$$

then the derivative of the density function is:

$$\frac{d\rho}{dY} = 383 + 316Y \tag{3.12}$$

and

$$SE[\rho] = abs\left(\frac{d\rho}{dY}\right) \times SE[Y] \tag{3.13}$$

$Y$ - solute mass fraction, g (g solution)$^{-1}$
$\rho$ - density solution, kg m$^{-3}$
$SE[Y]$ - standard error of concentration $Y$, g (g solution)$^{-1}$
$SE[\rho]$ - standard error of density at concentration $Y$, kg m$^{-3}$

In another example, osmotic pressure of each OA was estimated using a series of polynomial relationships derived from published data on solution osmosity. The standard error for each estimation of osmotic pressure was calculated from the derivatives of each polynomial equation (Maindonald, 1996). An overall standard error for sugar concentration ($SE[Y]$) was calculated using the pooled standard deviation of data from HPLC analyses. The polynomial relationships required to determine the osmotic pressure of a fructose solution at 20°C are,

$$S = 2.85Y + 5.23Y^2 \tag{3.14}$$

$$\pi = (4.36S + 0.213S^2 + 0.0595S^3) \tag{3.15}$$

therefore, the standard error of the osmotic pressure is:

$$SE[\pi] = \left(abs\left(\frac{dS}{dY}\right) \times abs\left(\frac{d\pi}{dS}\right)\right) \times SE[Y] \tag{3.16}$$

$S$ - osmosity of solution, mol l$^{-1}$
$\pi$ - osmotic pressure, MPa
$SE[Y]$ - standard error of concentration $Y$, g (g solution)$^{-1}$
$SE[\pi]$ - standard error of osmotic pressure at concentration $Y$, MPa

### 3.3.3. Mass Balances

Mass balances were completed over the juice and OA circuits separately first, then over the whole system. Individual water and solute balances were completed to ensure there was no unusual loss or gain of these components. Water lost from the juice circuit was assumed to be taken up in the OA circuit. No solute loss was anticipated but this was also checked. The *SE*'s of the concentration or mass values measured or calculated were determined. The combined errors were handled as described by Cleland (1983). Where values were added or subtracted, the combined *SE* was determined from $\sqrt{(SE_1^2 + SE_2^2)}$. When values were multiplied or divided, the combined *SE* was determined from the percentage error of each value.

The *SE* of the concentration values was determined from refractive index or HPLC data. The refractive index of all samples was measured at least three times. The mean value and its standard deviation (*sd*) was recorded. To obtain a more accurate *SE* of the mean based on a larger degree of freedom, an overall *SE* was determined from a pooled estimate of standard deviation based on the individual standard deviations for all means calculated. This overall *SE* was used in further calculations with each mean value of refractive index. The refractive index value was converted to an equivalent concentration using a polynomial equation and the error in the concentration value was obtained. All samples analysed by HPLC were analysed in duplicate, each with duplicate injections. The solute concentrations were determined from a calibration curve. The mean solute concentration and standard deviation for each sample was determined. As for refractive index, an overall *SE* was determined from a pooled estimate of standard deviation, from individual standard deviations. The mean concentrations determined by HPLC and the overall *SE* were used for subsequent calculations and mass balances.

The *SE* of weights and volumes recorded was determined from the accuracy of the readings taken. The weight of OA in the OA balance NZ was accurate to ± 0.001 kg and in the USA the OA balance was accurate to ± 0.02 kg. The volume in the juice circuit feed vessel and other volume measurements were accurate to ± 5 ml. Volume measurements were converted to mass terms (± *SE*) by first determining the density of the solution from polynomial curves. The "zero time" weight of OA and volume of water in the juice circuit feed vessel was determined by extrapolation of the regression line back to zero time. The flux rate of water across the membrane was obtained by dividing the mass flow rate (kg $s^{-1}$) [see 3.2.14] by the available membrane area ($m^2$). The *SE* for the calculated membrane area was also determined.

# CHAPTER 4
# PHYSICAL PROPERTIES OF AQUEOUS SOLUTIONS

To understand how the DOC apparatus works, it was necessary to obtain information about solution properties and how they were affected by temperature and concentration. In some instances additional information beyond that available in the literature was required or some of the published data needed to be manipulated before it could be used. This chapter contains information on osmotic pressure, viscosity and diffusion coefficients of solutions.

## 4.1. Concentration, refractive index, density and specific conductance

Published data were used to verify the techniques used to determine refractive index, density and specific conductance. Because these published data were incomplete, experimental data were obtained for the aqueous solutions needed for this work (Norris, 1967; Wolf et al., 1984). Calibration curves for refractive index and density of fructose, glucose, sucrose and sodium chloride (NaCl) solutions, and the specific conductance of NaCl are shown in Figures 4.1 to 4.3. All data showed excellent agreement with literature values, where available. The data of Wolf et al. (1984) were used for the polynomial equations for refractive index, density and specific conductance.

During this study actual measurements were made to verify published data. The methods and techniques used were found to be accurate over the full concentration range.

**Solution concentrations**

Solution concentrations expressed as molarity were converted to mass fraction (g (g solution)$^{-1}$) for all experimental and modelling work. Molarity was converted to a mass fraction using the following formula (Weast et al., 1984):

$$Y = \frac{M \times M_E}{\rho} \tag{4.1}$$

$Y$ - solute mass fraction, g (g solution)$^{-1}$

$M$ - solution molarity, mol l$^{-1}$

$M_E$ - molecular weight of solute, g mol$^{-1}$

$\rho$ - solution density, kg m$^{-3}$

**Figure 4.1. Refractive index of aqueous sugar solutions at 20°C**

(a) Fructose
(b) Glucose
(c) Sucrose

—— Published data (Wolf et al., 1984).

o Mean of experimentally determined data. The horizontal lines represent two standard errors about each mean. For some data points two standard errors are smaller than the actual size of the markers, they are not distinguishable on the graphs and appear as one line.

For fructose and glucose, $n = 4$
For sucrose, $n = 7$

Sugar concentrations determined by HPLC.
Refractive index was determined with a refractometer.

(a)

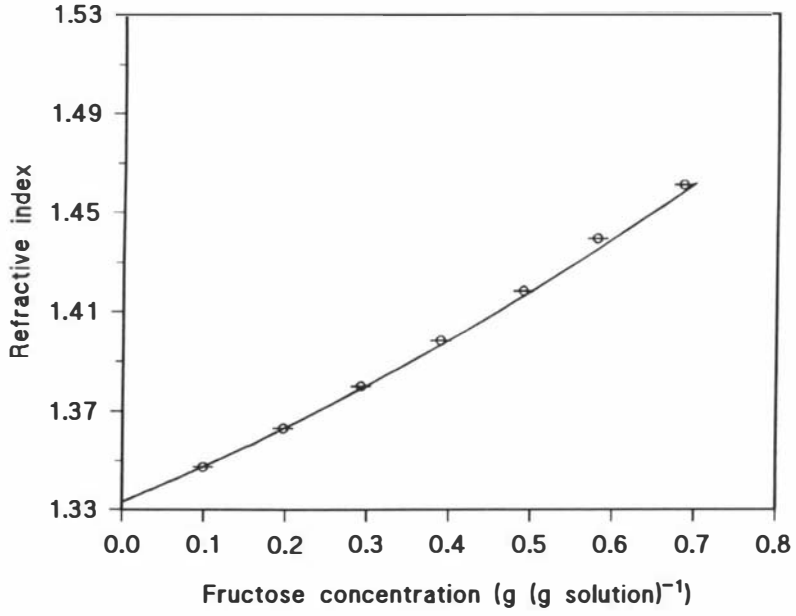
1.53
1.49
1.45
1.41
1.37
1.33
Refractive index
0.0 0.1 0.2 0.3 0.4 0.5 0.6 0.7 0.8
Fructose concentration (g (g solution)$^{-1}$)

(b)

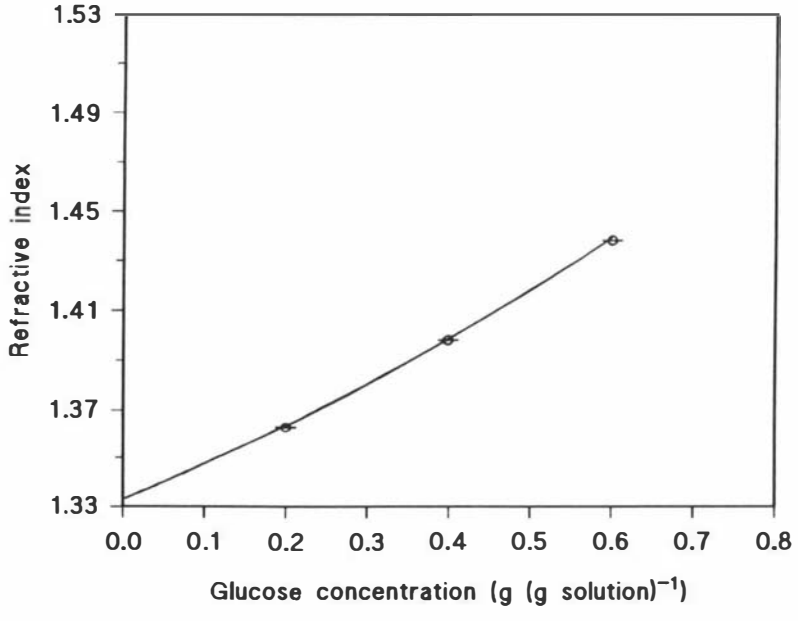
1.53
1.49
1.45
1.41
1.37
1.33
Refractive index
0.0 0.1 0.2 0.3 0.4 0.5 0.6 0.7 0.8
Glucose concentration (g (g solution)$^{-1}$)

(c)

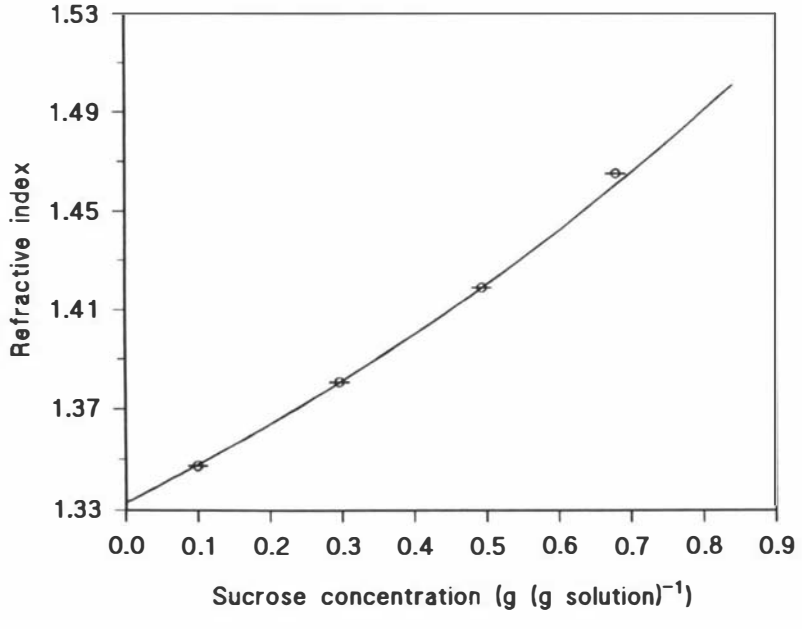
1.53
1.49
1.45
1.41
1.37
1.33
Refractive index
0.0 0.1 0.2 0.3 0.4 0.5 0.6 0.7 0.8 0.9
Sucrose concentration (g (g solution)$^{-1}$)

**Figure 4.2. Density of aqueous sugar solutions at 20°C**

All solution densities presented are corrected values.

(a) Fructose
(b) Glucose
(c) Sucrose

—— Published data (Wolf et al., 1984).

o Mean of experimentally determined data. The horizontal lines represent two standard errors about each mean. For some data points two standard errors are smaller than the actual size of the markers, they are not distinguishable on the graphs and appear as one line.

For all sugars, $n = 2$

Sugar concentrations determined by HPLC and density with a Paar density meter.

(a)

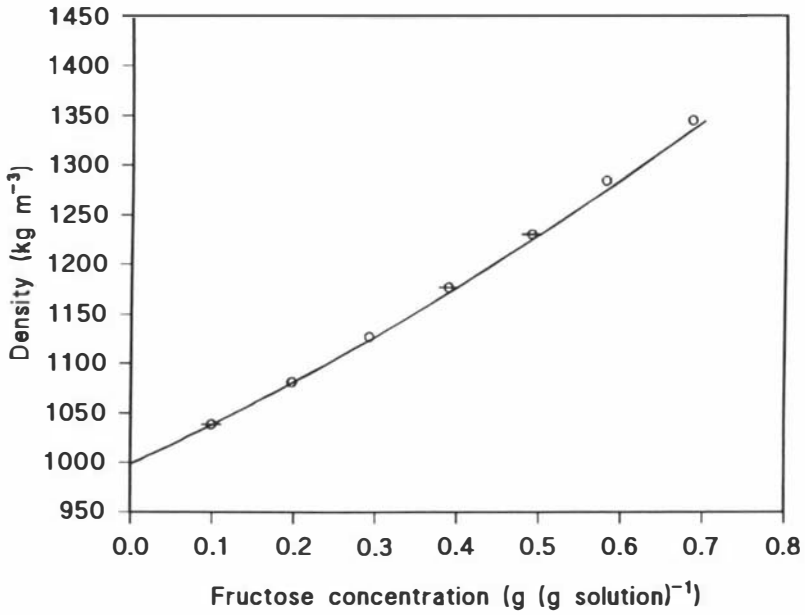
Density (kg m$^{-3}$)
1450
1400
1350
1300
1250
1200
1150
1100
1050
1000
950
0.0
0.1
0.2
0.3
0.4
0.5
0.6
0.7
0.8
Fructose concentration (g (g solution)$^{-1}$)

(b)

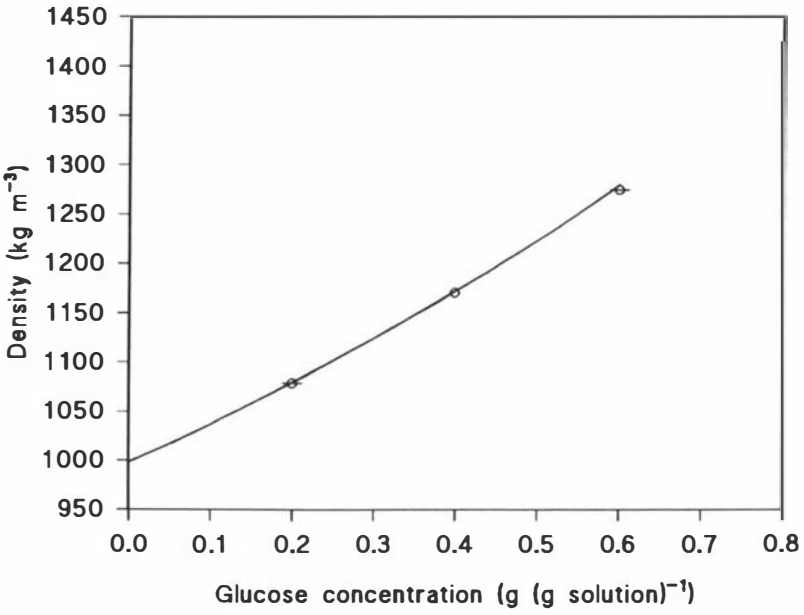
Density (kg m$^{-3}$)
1450
1400
1350
1300
1250
1200
1150
1100
1050
1000
950
0.0
0.1
0.2
0.3
0.4
0.5
0.6
0.7
0.8
Glucose concentration (g (g solution)$^{-1}$)

(c)

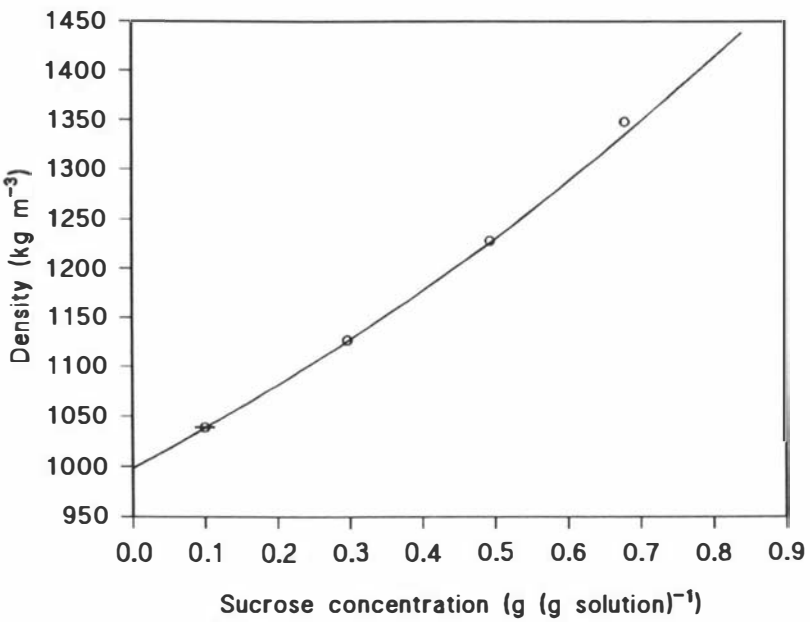
Density (kg m$^{-3}$)
1450
1400
1350
1300
1250
1200
1150
1100
1050
1000
950
0.0
0.1
0.2
0.3
0.4
0.5
0.6
0.7
0.8
0.9
Sucrose concentration (g (g solution)$^{-1}$)

**Figure 4.3. Physical properties of sodium chloride solutions at 20°C**

(a) Refractive index
(b) Density (kg $m^{-3}$)
(c) Specific conductance (mmhos $cm^{-1}$)

— Published data (Wolf et al., 1984).

o Mean of experimentally determined data. The horizontal lines represent two standard errors about each mean. For some data points two standard errors are smaller than the actual size of the markers, they are not distinguishable on the graphs and appear as one line.

For refractive index, $n = 4$.
For density, $n = 6$.
For specific conductance, $n = 4$

Solution concentrations determined by HPLC, refractive index with a refractometer, density with a Paar density meter and conductance with a conductivity meter. Solution densities are corrected values.

(a)

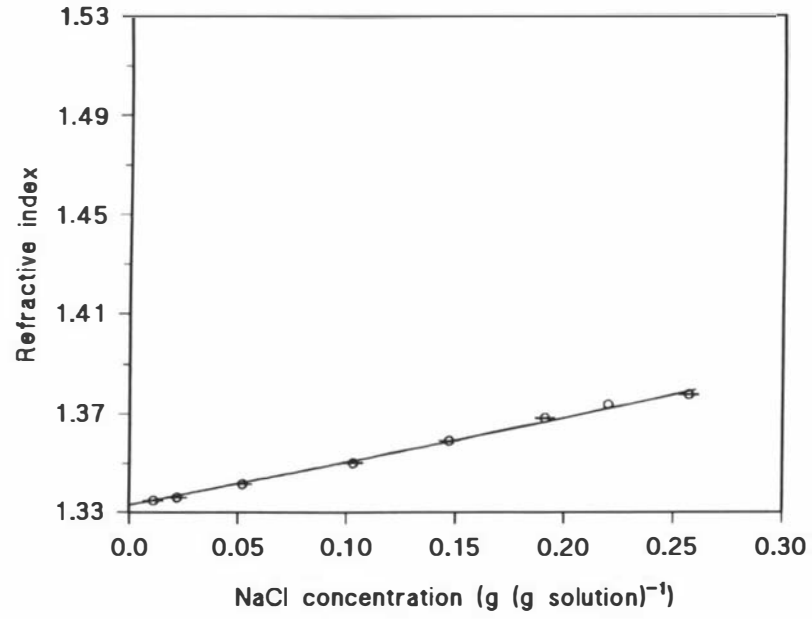
1.53
1.49
1.45
1.41
1.37
1.33
Refractive index
0.0
0.05
0.10
0.15
0.20
0.25
0.30
NaCl concentration (g (g solution)$^{-1}$)

(b)

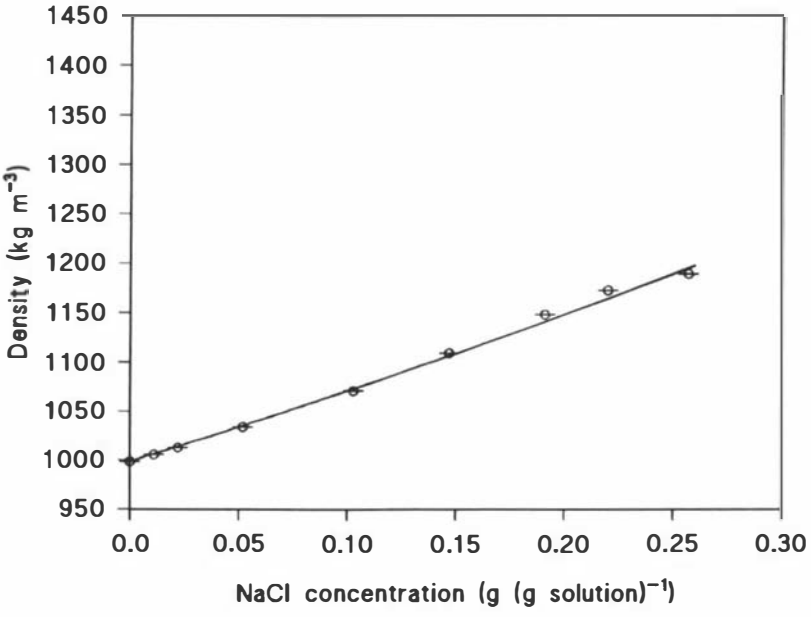
1450
1400
1350
1300
1250
1200
1150
1100
1050
1000
950
Density (kg m$^{-3}$)
0.0
0.05
0.10
0.15
0.20
0.25
0.30
NaCl concentration (g (g solution)$^{-1}$)

(c)

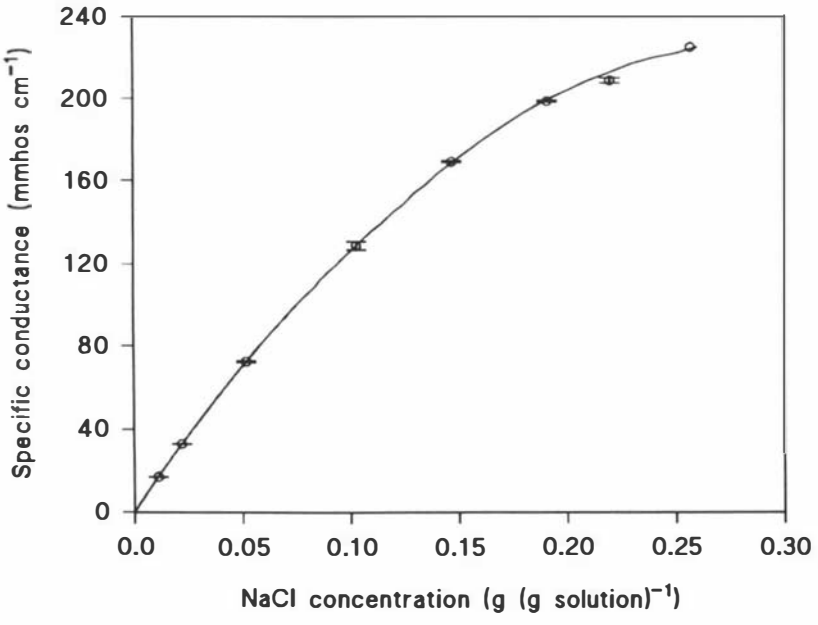
240
200
160
120
80
40
0
Specific conductance (mmhos cm$^{-1}$)
0.0
0.05
0.10
0.15
0.20
0.25
0.30
NaCl concentration (g (g solution)$^{-1}$)

Similarly, solution concentrations expressed as molality were converted to mass fraction (g (g solution)$^{-1}$) by the following equation (Weast et al., 1984):

$$Y = \frac{m \times M_E}{1000 + (m \times M_E)} \tag{4.2}$$

$m$ - solution molality, mol (kg solvent)$^{-1}$

## 4.2. Osmosity and osmotic pressure

To be able to relate solution properties to osmotic pressure of OAs, a relationship between concentration and osmotic pressure was required over a wide range of solution concentrations and temperatures. For aqueous solutions, published data were available on the osmosity of various aqueous solutions. This is a direct measure of the molarity of an iso-osmotic NaCl solution (Wolf et al., 1984). An advantage in using osmosity was that there were also published data for the osmotic pressure of NaCl solutions over the entire concentration and temperature range required (Sourirajan, 1970). For the experimental work required in this study, data for 10 and 20°C were derived by interpolation of the published data and is shown for 20°C in Figure 4.4. Data were also required at 40°C, this was available in the literature (Sourirajan, 1970).

To determine the osmotic pressure of an aqueous solution (NaCl, fructose, glucose or sucrose), the solution concentration (mass fraction, g (g solution)$^{-1}$) was first converted to an equivalent osmosity using the one of the following polynomial equations derived from published data (Wolf et al., 1984),

$$\begin{aligned}
&\textit{NaCl}\ (20°C) && S = 17.1Y + 11.7Y^2 + 4.94Y^3 \\
&\textit{Sucrose}\ (20°C) && S = 1.44Y + 3.05Y^2 + 3.4Y^3 \\
&\textit{Glucose}\ (20°C) && S = 2.82Y + 5.73Y^2 \\
&\textit{Fructose}\ (20°C) && S = 2.85Y + 5.23Y^2
\end{aligned} \tag{4.3}$$

for NaCl: $0 \leq Y \leq 0.38$, sucrose: $0 \leq Y \leq 0.84$, glucose: $0 \leq Y \leq 0.60$, fructose: $0 \leq Y \leq 0.70$

$Y$ - solute mass fraction, g (g solution)$^{-1}$

$S$ - osmosity, molar concentration of NaCl, mol l$^{-1}$

The calibration curves for equivalent osmosity and solution concentration (mass fraction) are shown in Figure 4.5(a), based on published data and extended to cover the concentration range.

**Figure 4.4. Influence of temperature on osmotic pressure of NaCl solutions**

Osmotic pressure data for NaCl at 5, 15, 25 and 35°C obtained from published data (Sourirajan, 1970).

Data at 20°C interpolated from published data.

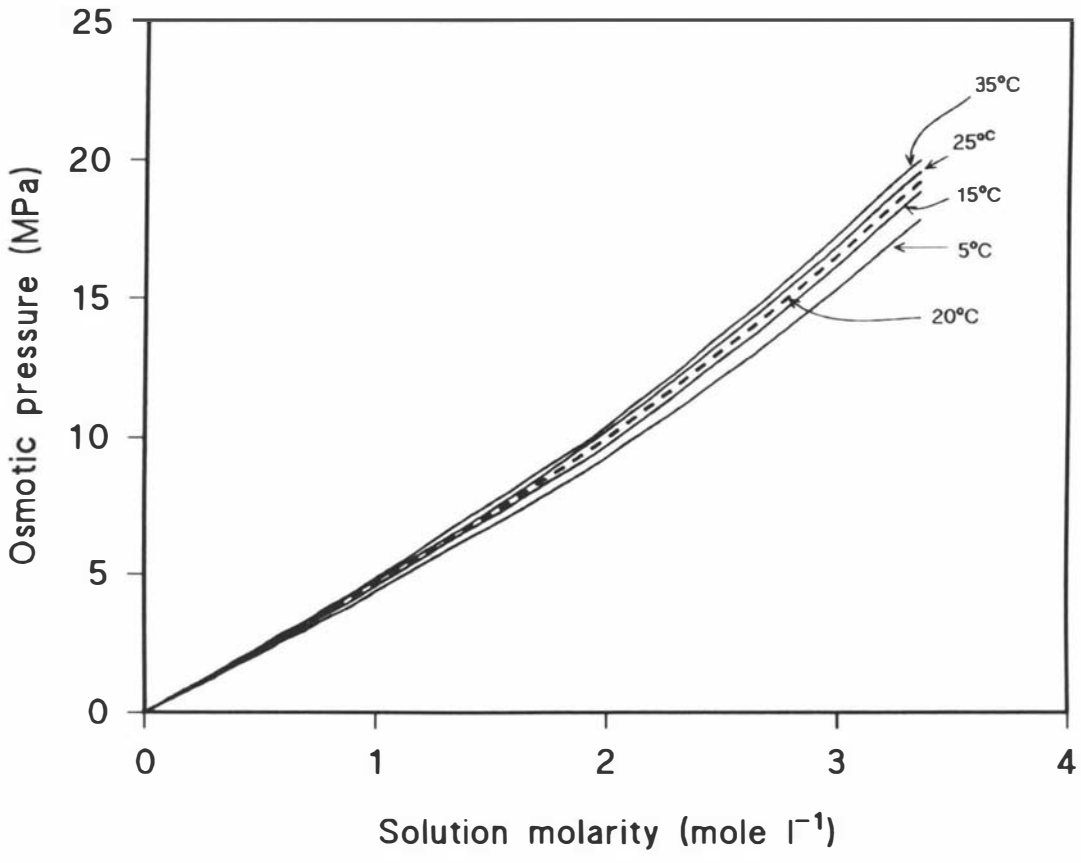
25
20
15
10
5
0
0
1
2
3
4
Osmotic pressure (MPa)
Solution molarity (mole l⁻¹)
35°C
25°C
15°C
5°C
20°C

**Figure 4.5. Calibration curves for determining osmotic pressure using osmosity**

(a) Equivalent osmosity of aqueous solutions for different solution concentrations for NaCl, glucose, fructose and sucrose, at 20°C (Wolf et al., 1984).

(b) Osmotic pressure for the equivalent osmosity (Sourirajan, 1970).

(a)

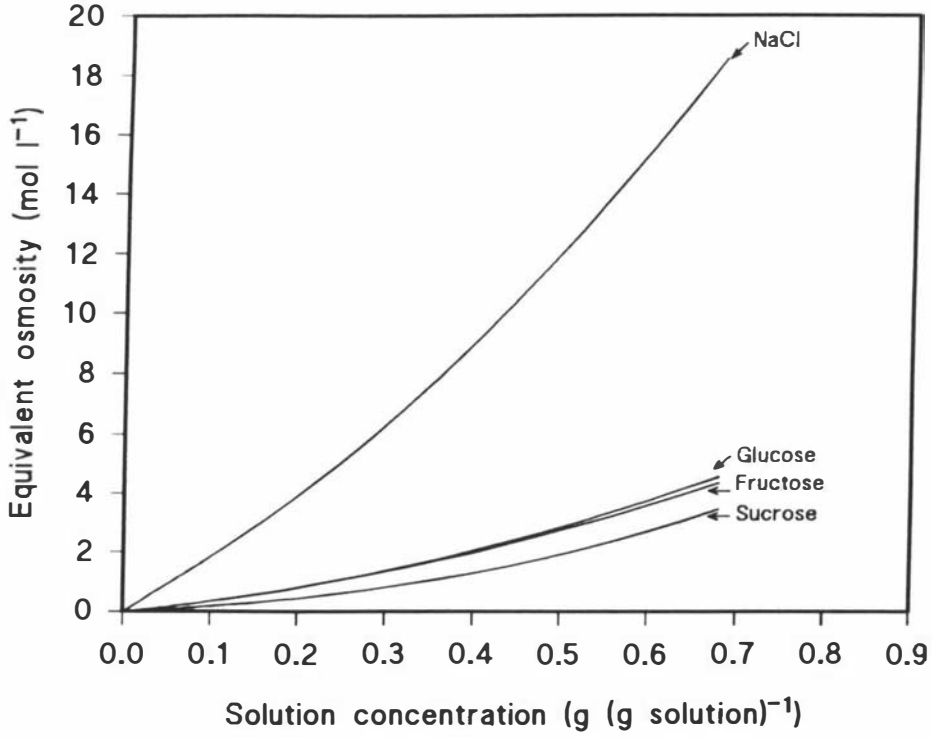
Equivalent osmosity (mol l⁻¹)
20
18
16
14
12
10
8
6
4
2
0
NaCl
Glucose
Fructose
Sucrose
0.0
0.1
0.2
0.3
0.4
0.5
0.6
0.7
0.8
0.9
Solution concentration (g (g solution)⁻¹)

(b)

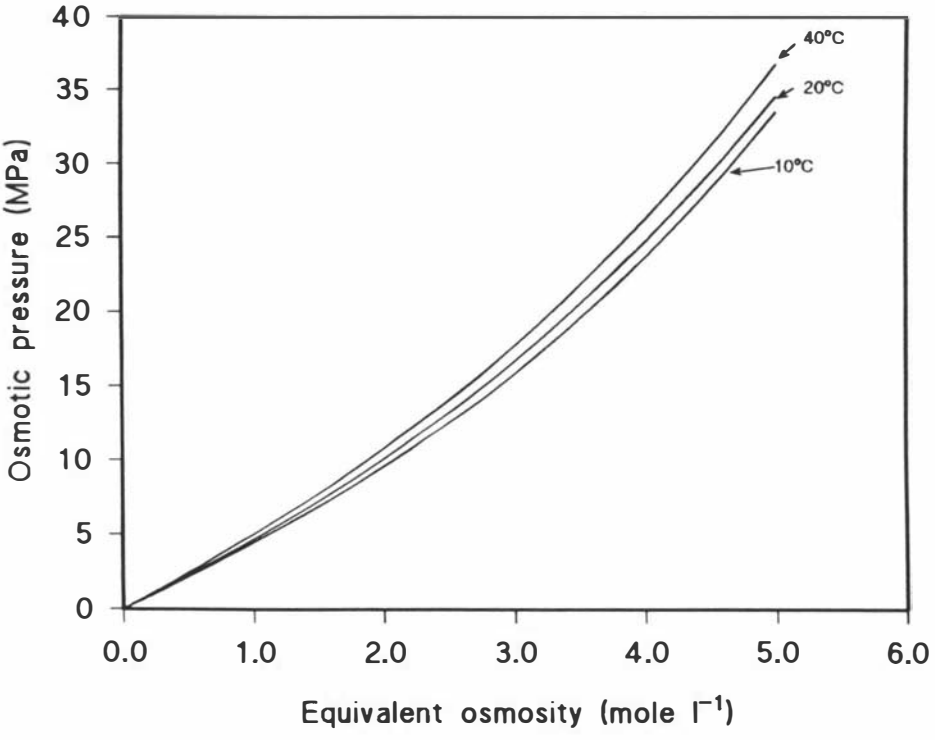
Osmotic pressure (MPa)
40
35
30
25
20
15
10
5
0
40°C
20°C
10°C
0.0
1.0
2.0
3.0
4.0
5.0
6.0
Equivalent osmosity (mole l⁻¹)

The equivalent osmosity determined from concentration was then converted to an equivalent osmotic pressure (MPa) using the following calibration equations derived from published data (Sourirajan, 1970):

$$\begin{aligned} 10^{o}C \quad & \pi = 4.28S + 0.0814S^2 + 0.0808S^3 \\ 20^{o}C \quad & \pi = 4.36S + 0.213S^2 + 0.0595S^3 \\ 40^{o}C \quad & \pi = 4.77S + 0.152S^2 + 0.0727S^3 \end{aligned} \tag{4.4}$$

for $0 \leq S \leq 5.3$

$\pi$ - osmotic pressure, MPa

Note these equations can be used for all solutes for which the equivalent osmosity is known. The calibration curves for 10, 20 and 40°C for osmotic pressure and equivalent osmosity are shown in Figure 4.5(b).

These data agree with published data for NaCl at 20°C, as shown in Figure 4.6. However there were no data for glucose, sucrose or fructose at 20°C. But there was good agreement with published data for glucose at approximately 25°C (Merson and Ginnette, 1972) and for sucrose at 25°C (Sourirajan, 1970) with the values determined using the calibration curves, as shown in Figure 4.6. There were no published data for fructose solutions.

### 4.2.1. Iso-osmotic sugar solutions

The relationship between osmotic pressure and concentration for NaCl and each sugar solution was determined from literature values of osmosity. It was unclear whether these relationships held true for the experimental apparatus being used. Thus the DOC apparatus was used with fructose in the OA circuit and sucrose or glucose of equivalent osmosity in the juice circuit. On equilibration, samples of OA and juice circuit solutions were measured for sugar content. The results are shown in Table 4.1.

These data were compared to those calculated from calibration equations and published data. The results are presented in Figure 4.7. It is clear that the data from calibration equations and experimental data were in excellent agreement.

**Figure 4.6. Solute concentration and osmotic pressure**

NaCl
— at 20°C, estimated from calibration curves [Figure 4.5]
□ at 20°C, interpolated from published data (Sourirajan, 1970).

Sucrose
— at 20°C, estimated from calibration curves [Figure 4.5]
▵ at 25°C, published data (Sourirajan, 1970).

Glucose
— at 20°C, estimated from calibration curves [Figure 4.5]
o at approximately 25°C, published data (Merson and Ginnette, 1972).

Fructose
— at 20°C, estimated from calibration curves [Figure 4.5]

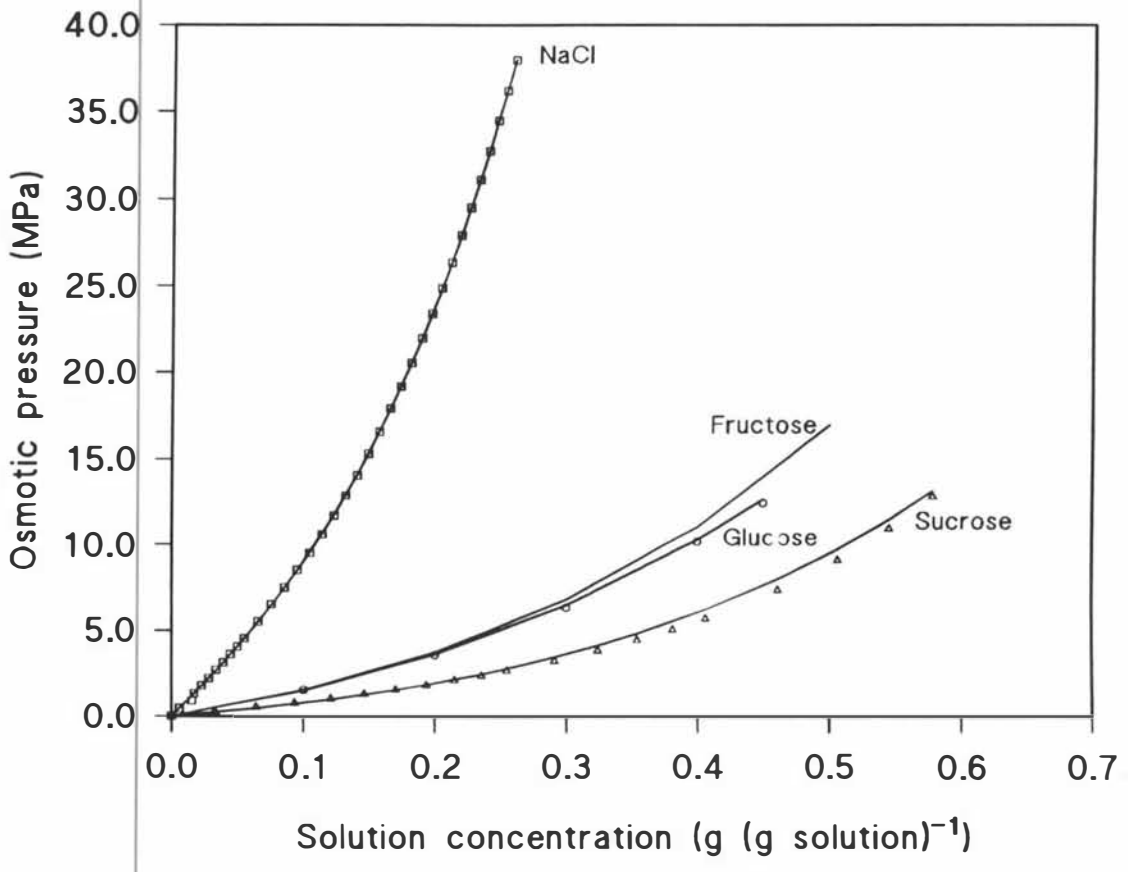
40.0
35.0
30.0
25.0
20.0
15.0
10.0
5.0
0.0
Osmotic pressure (MPa)
NaCl
Fructose
Glucose
Sucrose
0.0
0.1
0.2
0.3
0.4
0.5
0.6
0.7
Solution concentration (g (g solution)$^{-1}$)

**Figure 4.7. Iso-osmotic sugar solutions at 20°C**

——— iso-osmotic concentration of fructose vs. sucrose or fructose vs. glucose solutions calculated from calibration curves [Figure 4.5].

○ mean of experimentally determined data for fructose vs. sucrose. Horizontal lines represent two standard errors of the mean, $n = 2$.

□ mean of experimentally determined data for fructose vs. glucose. Horizontal lines represent two standard errors of the mean, $n = 2$.

For some data points two standard errors are smaller than the actual size of the markers, they are not distinguishable on the graphs and appear as one line.

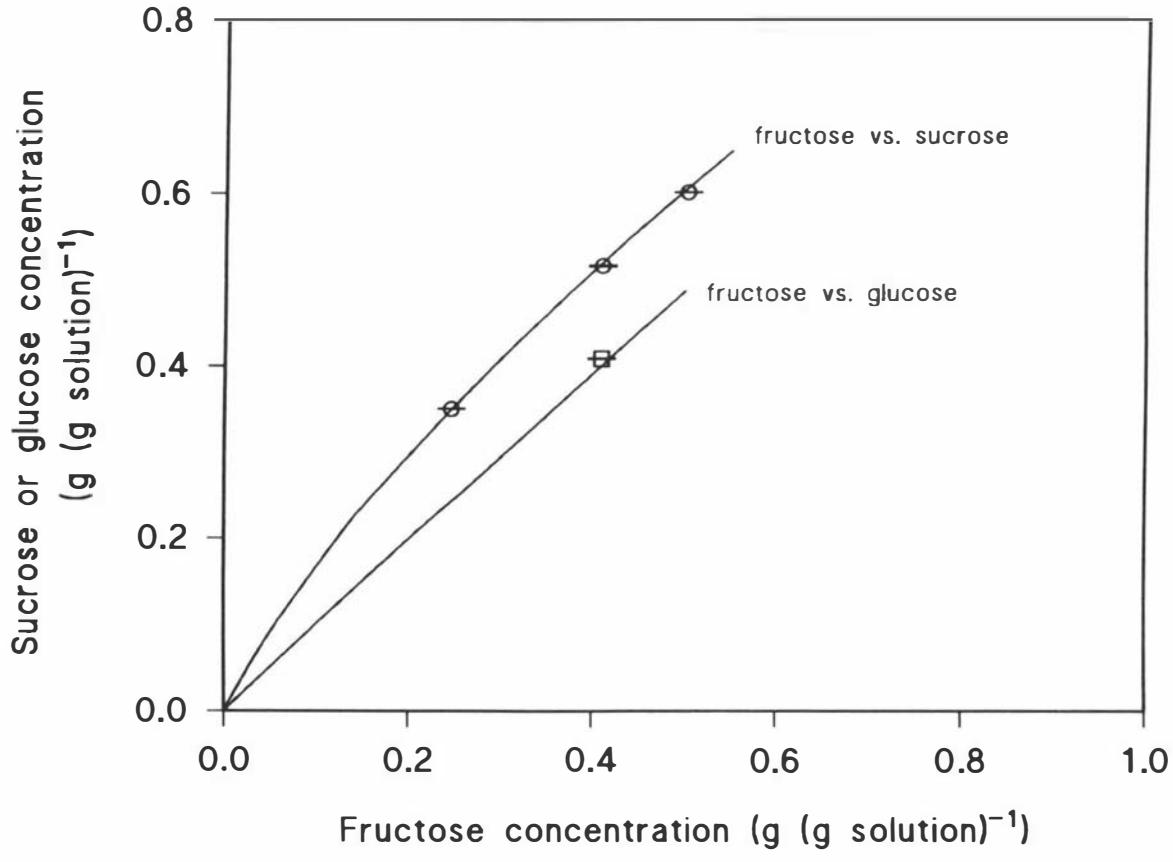
0.8
0.6
0.4
0.2
0.0
0.0
0.2
0.4
0.6
0.8
1.0
fructose vs. sucrose
fructose vs. glucose
Sucrose or glucose concentration
(g (g solution)$^{-1}$)
Fructose concentration (g (g solution)$^{-1}$)

**Table 4.1. Equivalent solution concentrations for iso-osmotic solutions at 20°C**

| Fructose concentration in OA circuit | | | Sugar material and concentration in juice circuit | | |
|---|---|---|---|---|---|
| mass fraction (g (g solution)$^{-1}$) | molarity (mol l$^{-1}$) | molality (mol (kg solution)$^{-1}$) | mass fraction (g (g solution)$^{-1}$) | molarity (mol l$^{-1}$) | molality (mol (kg solution)$^{-1}$) |
| Fructose | | | Sucrose | | |
| 0.25 | 1.53 | 1.85 | 0.35 | 1.18 | 1.57 |
| 0.41 | 2.68 | 3.86 | 0.52 | 1.88 | 3.16 |
| 0.50 | 3.40 | 5.55 | 0.61 | 2.30 | 4.57 |
| | | | Glucose | | |
| 0.41 | 2.68 | 3.86 | 0.41 | 2.68 | 3.86 |

## 4.3. Absolute and relative viscosity of fructose and NaCl solutions

There are few published data available on the viscosity of fructose solutions at different temperatures. The viscosity of fructose solutions at 0.70 g (g solution)$^{-1}$ has been published for various temperatures between -10 and 40°C (Pancoast and Junk, 1980). Published data on the viscosities of glucose and sucrose solutions at 20, 25 and 35°C were available in the literature (Gladden and Dole, 1953; Norris, 1967; Pancoast and Junk, 1980; Wolf et al., 1984).

The absolute viscosities of fructose solutions at 10, 20 and 40°C and NaCl solutions at 20°C were determined experimentally and are presented in Table 4.2. The experimental data for fructose solutions at 20°C agree well with published data (Pancoast and Junk, 1980; Wolf et al., 1984).

The relationship between fructose solution viscosity and concentration (mass fraction) was non-linear. Gladden and Dole (1953) found for glucose and sucrose solutions the $\log_e$(*relative viscosity*) was related linearly to mole fraction at different temperatures.

The fructose solution absolute viscosity data were converted to relative viscosities. A linear relationship between $\log_e$(*relative viscosity*) and mole fraction for fructose

solutions was found, as shown in Figure 4.8. The slope of the linear relationships (constant *b* required to solve Equation (2.52)) are presented in Table 4.3.

**Table 4.2. Absolute viscosities (μ) of aqueous fructose solutions**

| Solution: Concentration (g (g solution)$^{-1}$) | Temperature | | |
|---|---|---|---|
| | 10°C | 20°C | 40°C |
| | $\mu^a$ (kg m$^{-1}$ s$^{-1}$) | $\mu^a$ (kg m$^{-1}$ s$^{-1}$) | $\mu^a$ (kg m$^{-1}$ s$^{-1}$) |
| Fructose: 0.1 | 0.00227 ± 0.00002 | 0.00178 ± 0.00002 | 0.00120 ± 0.00002 |
| Fructose: 0.35 | 0.0064 ± 0.0001 | 0.00464 ± 0.00008 | 0.00275 ± 0.00001 |
| Fructose: 0.49 | 0.0198 ± 0.0000 | 0.0129 ± 0.0002 | 0.00637 ± 0.00002 |
| Fructose: 0.60 | 0.0604 ± 0.0009 | 0.0338 ± 0.0003 | 0.014 ± 0.000 |
| Fructose: 0.65 | 0.127 ± 0.003 | 0.0676 ± 0.0008 | 0.0234 ± 0.0001 |
| Fructose: 0.67 | 0.336 ± 0.004 | 0.158 ± 0.004 | 0.0453 ± 0.0003 |
| NaCl: 0.02 | | 0.00138 ± 0.00001 | |
| NaCl: 0.10 | | 0.00163 ± 0.00000 | |
| NaCl: 0.15 | | 0.00179 ± 0.00001 | |
| NaCl: 0.23 | | 0.00228 ± 0.00002 | |

a. Mean value (± *SEM*) for $n = 2$. Determined using a Bohlin rheometer.

**Table 4.3. Relationship between $\log_e(\mu/\mu_0)$ and mole fraction of fructose solutions at various temperatures**

| | Temperature | $\mu_0^b$ (kg m$^{-1}$ s$^{-1}$) | Constant '*b*' required to solve $\log_e(\mu/\mu_0) = b\,x^c$ (2.51) | Standard deviation of coefficient |
|---|---|---|---|---|
| Fructose | 10°C[a] | 0.001307 | 29.5 | 0.4 |
| | 20°C[a] | 0.001002 | 26.8 | 0.1 |
| | 40°C[a] | 0.000653 | 23.2 | 0.7 |

a. Determined from experimental data [Table 4.2.].
b. Weast et al. (1984).
c. For $0 \leq x \leq 0.2$.

**Figure 4.8. Relative viscosity of aqueous fructose solutions**

Relative viscosity values calculated from the absolute viscosity values determined experimentally [Table 4.2.].

□ 10.0 ± 0.1°C. Mean of experimentally determined data.
$\mu_0$ = 0.001307 kg $m^{-1}$ $s^{-1}$

○ 20.0 ± 0.1°C. Mean of experimentally determined data.
$\mu_0$ = 0.001002 kg $m^{-1}$ $s^{-1}$

△ 40.0 ± 0.1°C. Mean of experimentally determined data.
$\mu_0$ = 0.000653 kg $m^{-1}$ $s^{-1}$

—— Best fit linear regression lines

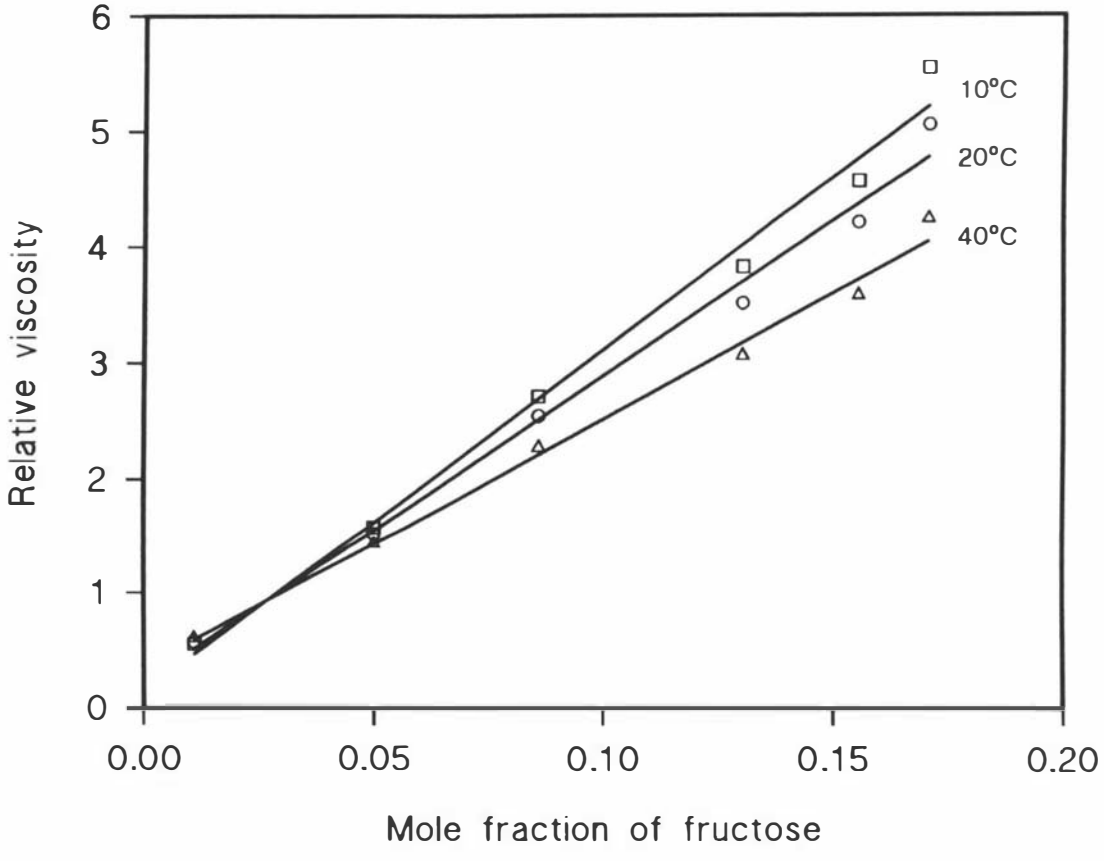
6
5
4
3
2
1
0
Relative viscosity
0.00
0.05
0.10
0.15
0.20
Mole fraction of fructose
10°C
20°C
40°C

A linear relationship for absolute viscosity and concentration for NaCl solutions was not achieved. Thus the calibration curve between absolute viscosity and concentration was used for NaCl solutions, shown in Figure 4.9.

### 4.3.1. Relationship between temperature and viscosity of fructose solutions

From the measured data, the $\log_e$(*absolute viscosity*) for fructose solutions were plotted against $1/T$, as shown in Figure 4.10. The activation energies ($E_a$) for these are presented in Table 4.4.

**Table 4.4. Activation energies for fructose solution viscosity**

| Fructose concentration (g (g solution)$^{-1}$) | Slope $E_d/R$[a] (K) | *sd* of slope | $r^2$ | $E_a$ (J mol$^{-1}$) |
|---|---|---|---|---|
| 0.1 | 1910 | 50 | 0.999 | 15,910 |
| 0.35 | 2430 | 50 | 0.999 | 20,230 |
| 0.49 | 3320 | 90 | 0.999 | 27,600 |
| 0.60 | 4300 | 200 | 0.996 | 35,600 |
| 0.65 | 4970 | 90 | 0.999 | 41,300 |
| 0.67 | 5900 | 100 | 1.00 | 49,000 |

a From regression of line in Figure 4.10.

From the Arrhenius relationships for viscosity and temperature it was determined for a 0.1 g (g solution)$^{-1}$ fructose solution, a 10 degree increase in temperature would result in a 20% reduction in viscosity. For a 0.7 g (g solution)$^{-1}$ a 10 degree increase in temperature would result in a 50% reduction in solution viscosity. A linear relationship was found between the activation energy of viscous flow and mole fraction of fructose solutions as for glucose and sucrose solutions, where

$$E_a\ (viscous) = 11.4 + 196x_F \qquad (4.5)$$

for $0 \leq x_F \leq 0.2$

$E_a$(viscous) - activation energy of viscous flow, J mol$^{-1}$

$x_F$ - mole fraction for fructose solution

**Figure 4.9. Absolute viscosity of NaCl solutions at 20°C**

Absolute viscosities (kg $m^{-1}$ $s^{-1}$) of solutions, determined using a Bohlin rheometer (Bohlin Reologi AB, Sweden).

o Mean of experimentally determined data. Horizontal lines represent two standard errors about each mean, $n$ = 2. For some data points two standard errors are smaller than the actual size of the markers, they are not distinguishable on the graphs and appear as one line. Data points with no standard errors indicate replicate data were identical.

Temperature 20 ± 0.1°C

— Published data at 20°C (Wolf et al., 1984).

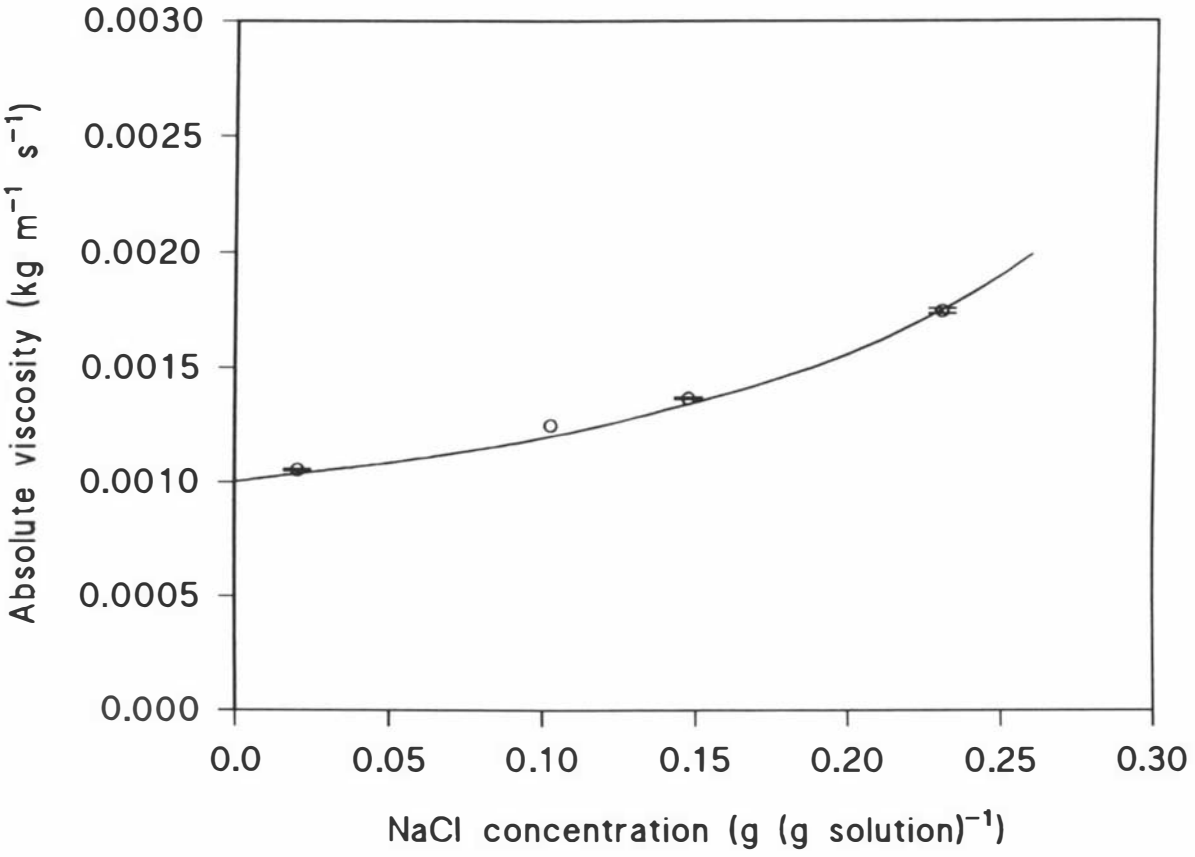
0.0030
0.0025
0.0020
0.0015
0.0010
0.0005
0.000
Absolute viscosity (kg m$^{-1}$ s$^{-1}$)
0.0
0.05
0.10
0.15
0.20
0.25
0.30
NaCl concentration (g (g solution)$^{-1}$)

**Figure 4.10. Relationship between temperature and viscosity of fructose solutions**

Absolute viscosity was determined experimentally using a Bohlin rheometer.

□ Mean of experimentally determined data. Horizontal lines represent two standard errors about each mean, $n = 2$. For some data points two standard errors are smaller than the actual size of the markers, they are not distinguishable on the graphs and appear as one line.

——— Best fit linear regression lines.

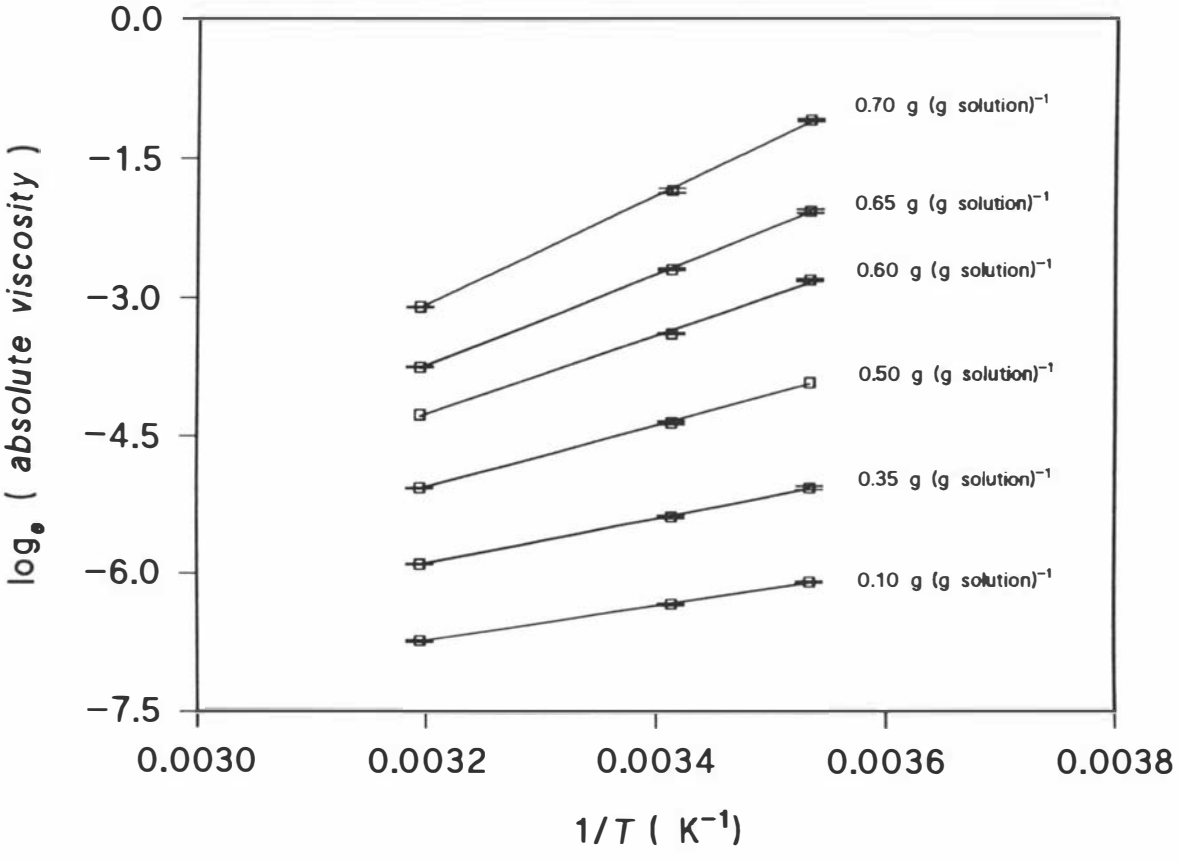
0.0
−1.5
−3.0
−4.5
−6.0
−7.5
0.0030
0.0032
0.0034
0.0036
0.0038
log$_e$ ( absolute viscosity )
1/T ( K$^{-1}$)
0.70 g (g solution)$^{-1}$
0.65 g (g solution)$^{-1}$
0.60 g (g solution)$^{-1}$
0.50 g (g solution)$^{-1}$
0.35 g (g solution)$^{-1}$
0.10 g (g solution)$^{-1}$

## 4.4. Binary diffusion coefficients for fructose and NaCl solutions

Binary diffusion coefficients for fructose solutions were calculated using Equation (2.37). It was assumed that the $\alpha$ term required to satisfy Equation (2.37) could be used for both sugars when determining their binary diffusion coefficients because glucose and fructose molecules have the same molecular weight and have similar shapes.

Using a value of 0.47 for $\alpha$, fructose solution viscosities [Figure 4.8 and Table 4.3], and glucose solution viscosities and diffusion coefficients [from published data (Gladden and Dole, 1953)] at equivalent mole fraction concentrations, Equation (2.37) was solved to determine the binary diffusion coefficients for fructose solutions at 10, 20 and 40°C. These are presented in Figure 4.11.

As found for glucose and sucrose solutions [see 2.5], for fructose solutions a linear relationship was found between the activation energy of diffusion and mole fraction. The relationship is as follows:

$$E_a\ (diffusion) = 17.2 + 121\,x_F \qquad (4.6)$$

for $0 \leq x_F \leq 0.19$.

The activation energy of diffusion can be used to solve Equation (2.40) for determining diffusion coefficients of fructose solutions at different temperatures. The linear equations relating $\log_e (D^o_{AB}/D_{AB})$ to mole fraction for fructose solutions were determined from the calculated diffusion coefficients. Similar relationships were found for glucose and sucrose solutions [see 2.5] (Gladden and Dole, 1953). For fructose solutions the equations and the value for the diffusion coefficient at infinite dilution, $D^o_{AB}$, at different temperatures are present in Table 4.5.

**Figure 4.11. Binary diffusion coefficients for aqueous fructose solutions**

Binary diffusion coefficients ($D_{AB}$) in aqueous fructose solutions, calculated based on method outlined in Section 2.5 using Equations (2.37) and (2.40), and data for glucose solutions.

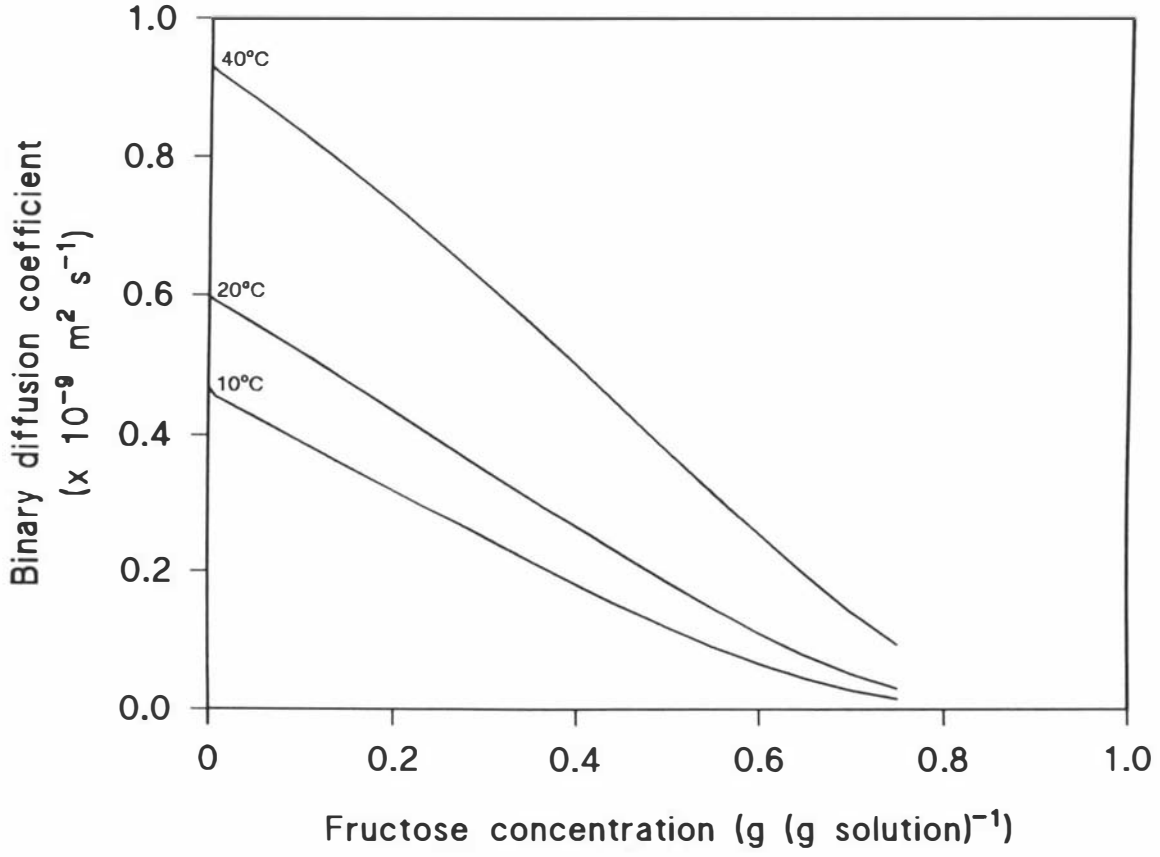
1.0
0.8
0.6
0.4
0.2
0.0
40°C
20°C
10°C
0
0.2
0.4
0.6
0.8
1.0
Binary diffusion coefficient
(x 10⁻⁹ m² s⁻¹)
Fructose concentration (g (g solution)⁻¹)

**Table 4.5. $D^{o}_{AB}$ and the relationship between $\log_e(D^{o}_{AB}/D_{AB})$ and mole fraction for fructose solutions**

| | Temperature | $D^{o}_{AB}$ ($\times 10^{-9}$ m$^2$ s$^{-1}$) | Constant '$a$' required to solve $\log_e(D^{o}_{AB}/D_{AB}) = a\, x^b$ (2.43) | Standard deviation of coefficient |
|---|---|---|---|---|
| Fructose | 10°C[a] | 0.47 | 15.02 | 0.03 |
| | 20°C[a] | 0.60 | 12.96 | 0.01 |
| | 40°C[a] | 0.93 | 9.97 | 0.01 |

a. Determined from data for glucose solutions [see 2.5, Equation (2.37)].
b. For $0 \leq x \leq 0.2$.

As there were no published data for diffusion coefficients of NaCl solutions at 20°C [see 2.5], the mean diffusion coefficient $\bar{D}_{AB}$ was interpolated from a plot of $D_{AB}$ versus temperature. The linear regression equation fitted to the plot between 18 and 35°C, is

$$\bar{D}_{AB} = (-9.82 + 0.038\,T) \times 10^{-9} \qquad (4.7)$$

$T$ - temperature, $291 \leq T \leq 308$ K ($18 \leq T$ °C $\leq 35$)

The standard deviation of the coefficient was 0.002 and $r^2$ 0.99. The mean binary diffusion coefficient at 20°C was calculated as $1.34 \times 10^{-9}$ m$^2$ s$^{-1}$ over the concentration 0 to 0.25 g (g solution)$^{-1}$.

## 4.5. Viscosity and diffusion coefficients of fructose and NaCl solutions

### 4.5.1. Fructose and NaCl solutions used during experimental trials

The viscosity and diffusion coefficients of various fructose and NaCl solutions used during the experimental trials are presented in Table 4.6.

There are large differences between the two OAs, fructose and NaCl, in their solution viscosities and diffusion coefficients. NaCl solutions have viscosities that are 1.3 and up to 90 times lower than fructose solutions over the osmotic pressure range 1.5 to 30 MPa. The diffusion coefficient of NaCl solutions are 2.5 to 25 times greater than in fructose solutions over the same osmotic pressure range.

**Table 4.6. Viscosity and diffusion coefficients of various fructose and NaCl solutions at 20°C**

| | Concentration (g (g solution$^{-1}$ )) | Osmotic pressure (MPa) | Absolute viscosity[a] (kg m$^{-1}$ s$^{-1}$) | Diffusion coefficient[b] ( x 10$^{-10}$ m$^2$ s$^{-1}$) |
|---|---|---|---|---|
| Fructose | 0.10 | 1.5 | 0.00135 | 5.2 |
| | 0.35 | 8.0 | 0.00394 | 3.1 |
| | 0.49 | 14.2 | 0.0105 | 1.9 |
| | 0.69 | 28.9 | 0.131 | 0.6 |
| NaCl | 0.02 | 1.5 | 0.00104 | 13.4 |
| | 0.10 | 9.1 | 0.00119 | 13.4 |
| | 0.15 | 15.5 | 0.00135 | 13.4 |
| | 0.23 | 30.5 | 0.00175 | 13.4 |

a. Viscosity determined from experimental data: for fructose see Figure 4.8 and Table 4.3; for NaCl see Figure 4.9.

b. Diffusion coefficients for fructose determined from published data for glucose and Equation (2.37); diffusion coefficients for NaCl using Equation (4.7).

### 4.5.2. Sucrose, fructose and NaCl solutions at approximate iso-osmotic concentrations

For sucrose, fructose and NaCl solutions with osmotic pressures within the range 7.6 to 9.1 MPa [8.2 ± 0.6 MPa (± *sd*)], the viscosity and diffusion coefficients are presented in Table 4.7.

**Table 4.7. Viscosity and diffusion coefficients of sucrose, fructose and NaCl solutions**

| | Concentration (g (g solution$^{-1}$)) | Osmotic pressure (MPa) | Absolute viscosity[a] (kg m$^{-1}$ s$^{-1}$) | Diffusion coefficient[b] (x 10$^{-10}$ m$^2$ s$^{-1}$) |
|---|---|---|---|---|
| Sucrose, 20°C | 0.45 | 7.6 | 0.0102 | 1.9 |
| Fructose, 10°C | 0.35 | 7.6 | 0.0059 | 2.2 |
| Fructose, 20°C | 0.35 | 8.0 | 0.0039 | 3.1 |
| Fructose, 40°C | 0.35 | 8.5 | 0.0021 | 5.6 |
| NaCl, 20°C | 0.10 | 9.1 | 0.0012 | 13.4 |

a. Viscosity determined from experimental data: for fructose see Figure 4.8 and Table 4.3; for NaCl see Figure 4.9. Viscosity for sucrose from published data (Gladden and Dole, 1953; Norris, 1967; Wolf et al., 1984).

b. Diffusion coefficients for fructose determined from published data for glucose (Gladden and Dole, 1953) and Equation (2.37); for NaCl using Equation (4.7); for sucrose from published data (English and Dole, 1950; Gladden and Dole, 1953; Henrion, 1964).

# CHAPTER 5
# DOC MODULE AND OPERATION

In this chapter the direct osmotic concentration (DOC) module and membranes are described in detail. The DOC membrane characteristics and structure is described and the method used to calculate the available membrane area is presented. Measurements of channel dimensions are presented. The operating conditions for equilibration and the boundary fluid conditions during experimental trials were determined.

## 5.1. DOC module

The DOC module consists of two specially designed polycarbonate plates which form the OA plates and two sheets of DOC membranes. A schematic cross-section of the small laboratory DOC module is shown in Figure 5.1. Within the DOC module two flat membrane sheets were placed parallel to each other. The membranes were held in place between the two OA plates. A rubber seal around the outer edge of the OA plate ensured there was no leakage from the system and kept the membranes taut. The two OA plates clamped together secure the membranes in place and seal off any leaks. The only support between the two membranes occurs at the inlet and outlet. Polycarbonate washers, 10 mm thick, with rubber seals were used to keep the membranes apart at the juice circuit inlet and outlet ports. When the solution flowed in the juice circuit the hydraulic pressure forced the membranes apart and they rested against the support bars in the OA circuit. A detailed drawing of the side view of the module with membranes in place is shown in Figure 5.2(a).

A drawing of the inside face of an OA plate is shown in Figure 5.2(b). Within each OA plate horizontal support bars were fixed at right angles to the flow in the juice circuit. This forced the OA flow to move horizontally across the plate in a zig-zag path. The flow path along each channel was at right angles to the flow in the juice circuit. However, the overall net flow in the OA plates was parallel to that of the juice circuit, with the OA inlet and outlets adjacent to those of the juice. The flow path followed by the osmotic agent in the OA circuit along the horizontal flow channels is shown in Figure 5.3(a). The OA plate can be divided into three sections, as shown in Figure 5.3(b), an inlet and outlet port section and the main mass transfer section.

The pilot plant DOC module was the same design as the small laboratory module. It was made larger by increasing the number of horizontal OA flow channels from 8 and 9 in the small laboratory module to 50 and 51 in the pilot plant module. The end areas

**Figure 5.1. Schematic diagram of the small laboratory DOC module**

Side view of small laboratory DOC module.
Not drawn to scale

juice - dilute solution to be concentrated
OA - osmotic agent, concentrated solution
⊙ - flow direction, out of the page
⊗ - flow direction, into the page

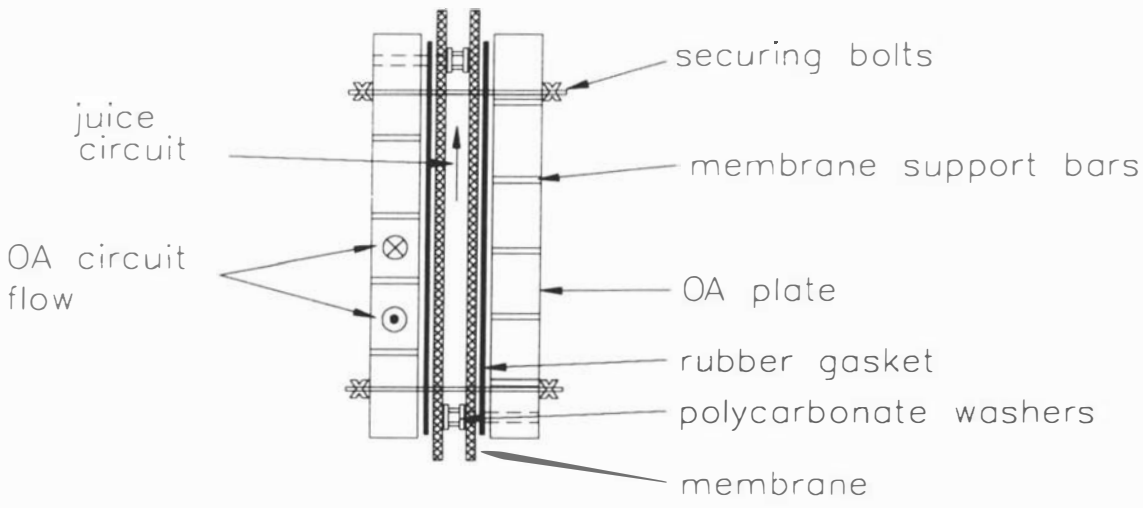
securing bolts
juice circuit
membrane support bars
OA circuit flow
OA plate
rubber gasket
polycarbonate washers
membrane

**Figure 5.2. Drawing of small laboratory DOC module**

(a) Side view of small laboratory DOC module with membranes in place.

(b) OA plate for small laboratory DOC module, a view of the inside face of the plate, which faces the membrane.

Shaded areas - membrane support bars

Drawn to scale, 1 : 5.3, units mm.

(a) MODULE SIDE VIEW

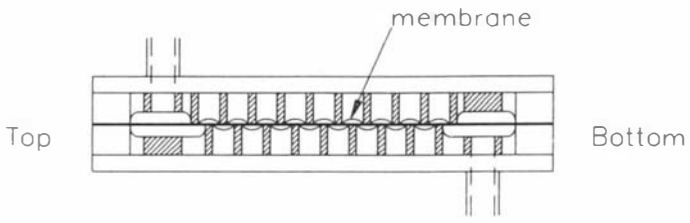


(b) OA PLATE INSIDE VIEW

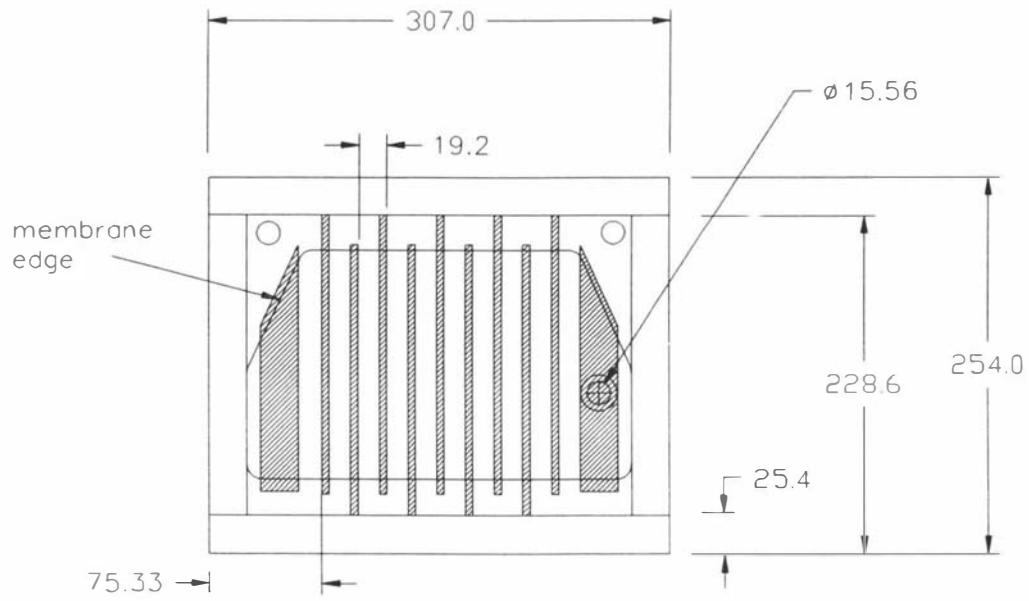

**Figure 5.3. DOC module OA plate**

(a) Module setup:

Juice circuit - water, at 20 ± 1°C
- flow rate $4 \times 10^{-5}$ $m^3$ $s^{-1}$

OA circuit - 0.1 g (g solution)$^{-1}$ fructose solution, at 20°C
- flow rate $7 \times 10^{-6}$ $m^3$ $s^{-1}$

An amaranth dye solution was pulsed into the OA flow immediately prior to entry into the module.

(b) Sections 1 and 3 are the membrane areas around the inlet and outlet ports. The blocks marked 'A' are solid polycarbonate blocks which limit the expansion of the membrane in these two sections. The shaded areas represent the polycarbonate components of the module. There is no contact of OA with the membrane in these areas.

Section 2, represents the main area for mass transfer in the DOC module.

(a)

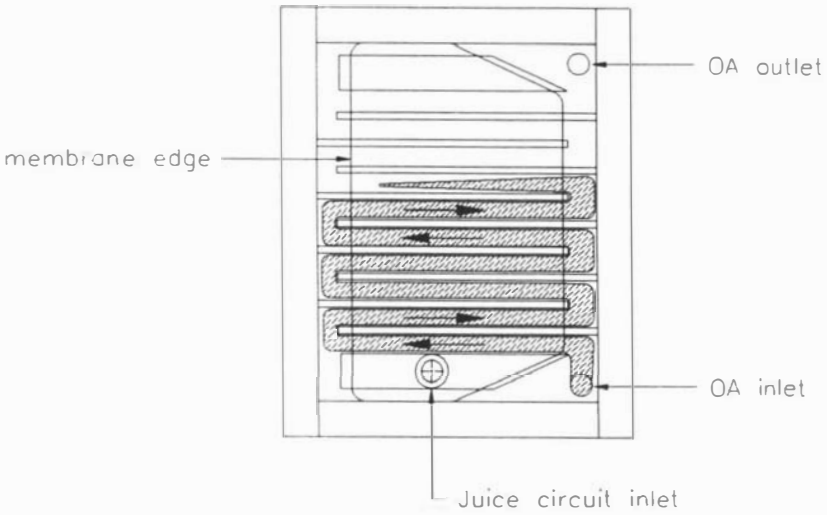
OA outlet
membrane edge
OA inlet
Juice circuit inlet

(b)

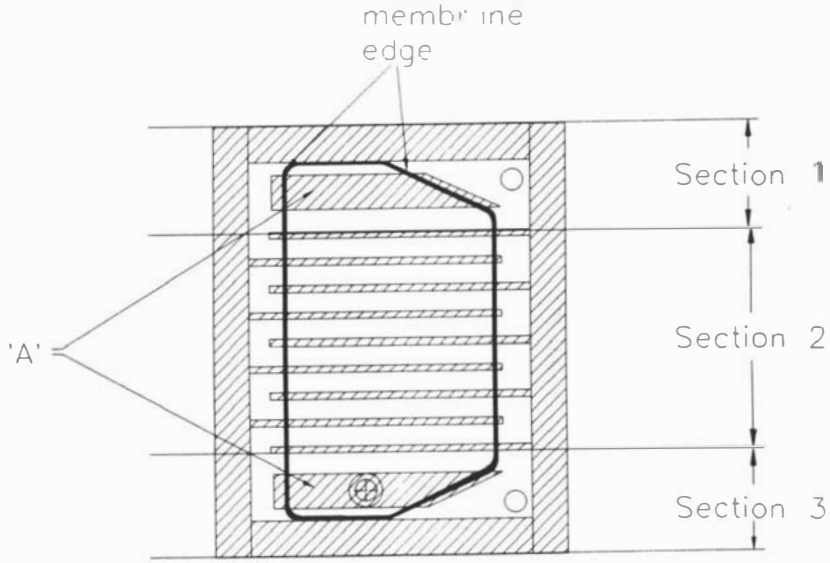
membrane edge
Section 1
Section 2
Section 3
'A'

around the inlet and outlet gaskets were larger to accommodate larger inlet and outlet ports. A schematic drawing of an OA plate from the pilot plant DOC module is shown in Figure 5.4. The pilot plant DOC module was based at Oregon State University, USA.

## 5.2. Flow in the juice circuit

The dilute liquid stream flows through the module between the two membranes in the juice circuit. Due to the alternating spacing of the horizontal membrane support bars, in the OA plates, the flow path of the dilute solution up the juice circuit followed a corrugated path, as shown in Figure 5.5. The flow path resulted in small changes in the direction of flow in the juice circuit (Herron et al., 1994).

The dimensions and flow conditions in the juice circuit are presented in Table 5.1, for the small laboratory and pilot plant DOC modules.

**Table 5.1. Dimensions and flow conditions in the juice circuit of the DOC modules**

| | Small laboratory module | | | Pilot plant module | | |
|---|---|---|---|---|---|---|
| | Mean | *SE* | *n* | Mean | *SE* | *n* |
| Thickness of gap between membranes[a] (m) | 0.0038 | 0.0008 | | 0.0038 | 0.0008 | |
| Width of membrane across the module (m) | 0.1545 | 0.0005 | 2 | 0.1781 | 0.0005 | 6 |
| Cross-sectional area of flow[b] ($\times 10^{-4}$ $m^2$) | 5.9 | 1.2 | | 6.8 | 1.4 | |
| Volumetric flow rate[c] ($\times 10^{-5}$ $m^3$ $s^{-1}$) | 4.0 | 0.1 | 9 | 4.2 | 0.1 | 11 |
| Mean fluid velocity (m $s^{-1}$) | 0.07 | 0.01 | | 0.06 | 0.01 | |

a. Herron (1995).

b. Thickness of membrane gap × total width of membrane.

c. For water only, set by pump speed on experimental unit.

After amaranth dye was pulsed into the juice circuit of both the small and pilot plant DOC modules, the flow up the channel was observed to be well mixed and relatively

**Figure 5.4. OA plate of the pilot plant DOC module**

Not drawn to scale

(Source: Herron et al., 1994)

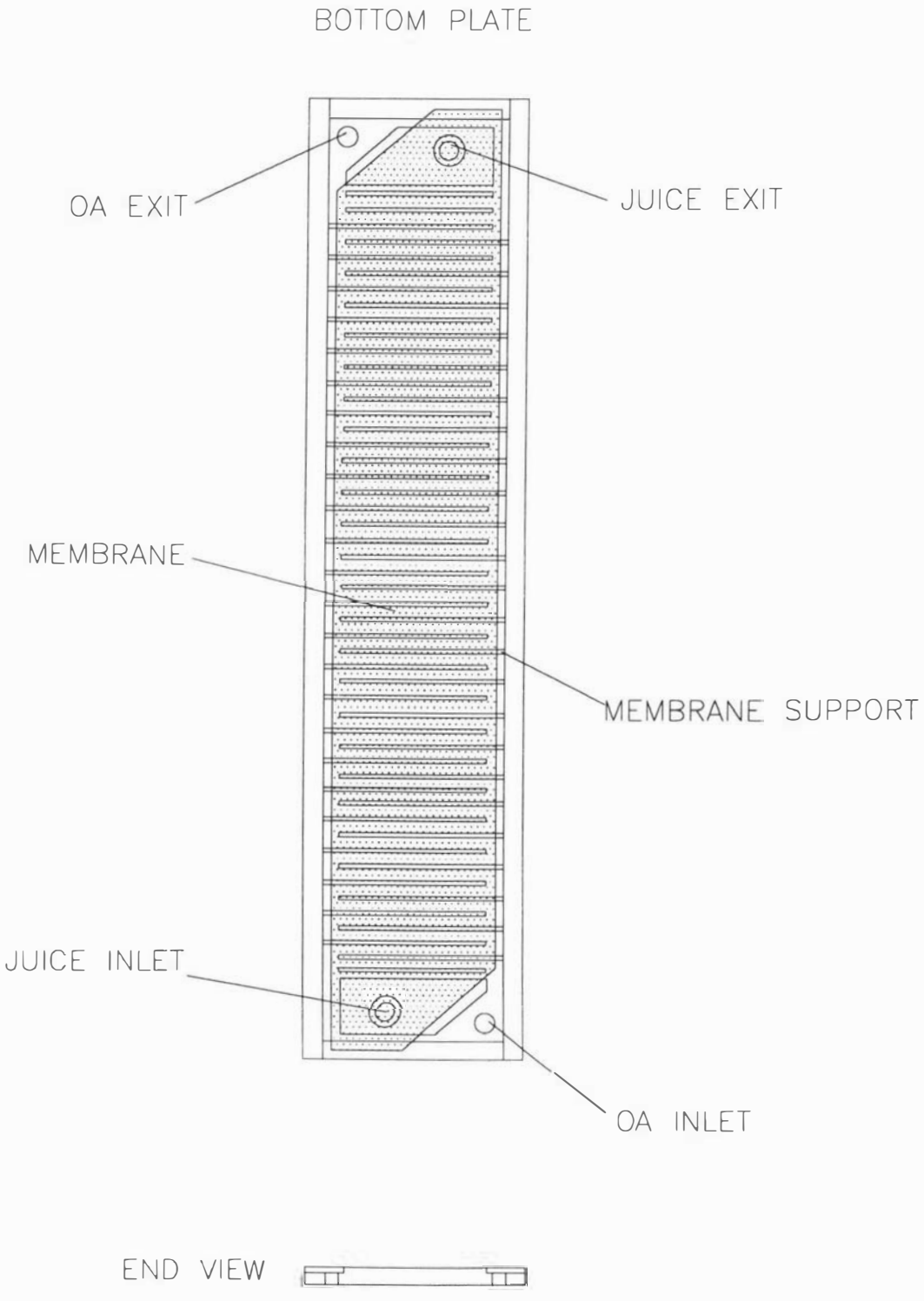
BOTTOM PLATE
OA EXIT
JUICE EXIT
MEMBRANE
MEMBRANE SUPPORT
JUICE INLET
OA INLET
END VIEW

**Figure 5.5. Schematic drawing of side view of DOC module**

Juice circuit flows in the direction of the arrows.
OA circuit flows at right angles to the page, with an overall flow in the same direction as the juice circuit arrows.

⊙ - flow direction, out of the page

⊗ - flow direction, into the page

Two membranes, 1a and 1b, enclose the juice circuit.
Two OA channels, 2a and 2b, represent the OA circuit..

The hydraulic pressure inside the juice circuit was about 15 kPa greater than the hydraulic pressure in the OA circuit. This forced the two membranes apart and against the support bars lining the OA channel. Where there was no support bar, the membrane was forced onto the OA channel. This created a corrugated flow path for the juice circuit up through the module.

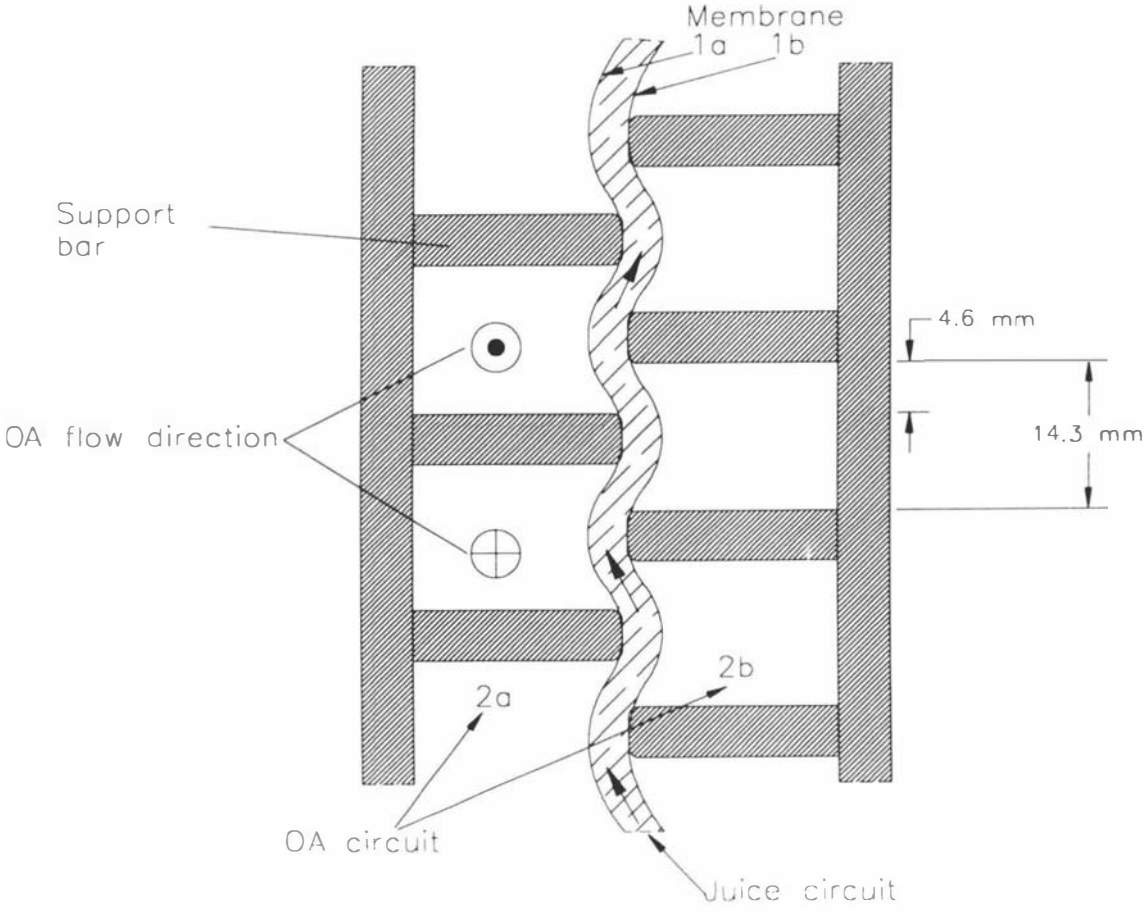
Membrane
1a
1b
Support
bar
4.6 mm
14.3 mm
OA flow direction
2b
2a
OA circuit
Juice circuit

uniform across the width of the module from bottom to top. No channelling was observed. A range of flow and hydraulic conditions were assessed. These conditions are shown in Figure 5.6. There were no visual differences in flow pattern for any of the conditions tested. The typical movement of dye up the DOC module is shown in Figure 5.6. The flow pattern was identical for all OA operating conditions from being left empty to containing 0.7 g (g solution$^{-1}$) fructose solution.

For the pilot plant DOC module, the hydraulic pressure at the module inlet of the juice circuit was higher than that in the small module, this was because of the greater static head of the pilot plant module. The operating hydraulic pressure at the juice circuit inlet was 13.5 - 17 kPa in the small module and 25 - 30 kPa in the pilot plant module.

For all experiments to determine water flux rates, water only was used in the juice circuit.

## 5.3. Flow in the OA circuit

Although the OA enters and exits the module at the same position in the module as the juice circuit, the OA flow was forced perpendicular to the juice circuit flow on a path determined by the horizontal flow channels. The flow characteristics in the OA circuit were examined after amaranth dye was pulsed in the flow channels, as shown in Figure 5.7. The flow characteristics of the OA in the horizontal flow channels was observed to be laminar in both the small laboratory and pilot plant DOC modules.

At the beginning of each horizontal OA channel there was a small amount of mixing but this was quickly dampened out. At lower OA concentrations (0.1 to 0.35 g (g solution)$^{-1}$ fructose) boundary layers gradually formed along the length of each flow channel. At the higher OA concentrations (0.5 to 0.7 g (g solution)$^{-1}$ fructose; 0.4 to 0.6 g (g solution)$^{-1}$ sucrose) the dye travelled down the centre of the flow channels. The boundary layers appeared to form virtually immediately at the entry to each flow channel.

The velocity boundary layer next to the membrane provided some resistance to the mass transfer of water. The existence of boundary layers in the OA flow channels indicated that perfect mixing was not occurring at the membrane surface. Because water exiting the active layer of the membrane diluted the OA at the surface, a concentration gradient was set up within the boundary layers. Thus the concentration of OA at the membrane surface was not the same as the concentration in the OA free-stream. The movement of particles in the boundary layer, due to diffusion or convection, was considered to be

**Figure 5.6. The progress of amaranth dye in the juice circuit**

The juice circuit was equilibrated with water. Then an amaranth dye solution was pulsed into the juice circuit flow at time "zero", and its progress up the module was recorded.

Module setup:

| | |
|---|---|
| Juice circuit | - water at 20 ± 1 °C |
| Volumetric flow rate | - $4 \times 10^{-5}$ $m^3$ $s^{-1}$ |
| Inlet hydraulic pressure, juice circuit | - 13.8 kPa |
| Inlet hydraulic pressure, OA circuit | - 0 kPa |
| Volume within module in the juice circuit | - $\approx 1.26 \times 10^{-4}$ $m^3$ |

The same pattern of flow was observed with the following conditions:

- sucrose solutions in the juice circuit (0.2 to 0.4 g (g solution)$^{-1}$)
- air or fructose (0.1 to 0.7 g (g solution)$^{-1}$) in OA circuit
- volumetric flow rates in juice circuit from $3.3 \times 10^{-5}$ to $6.3 \times 10^{-5}$ $m^3$ $s^{-1}$
- hydraulic pressures in juice circuit from 0 to 31 kPa
- hydraulic pressures in OA circuit from 0 to 7 kPa
- pilot plant DOC module, under similar ranges of operating conditions

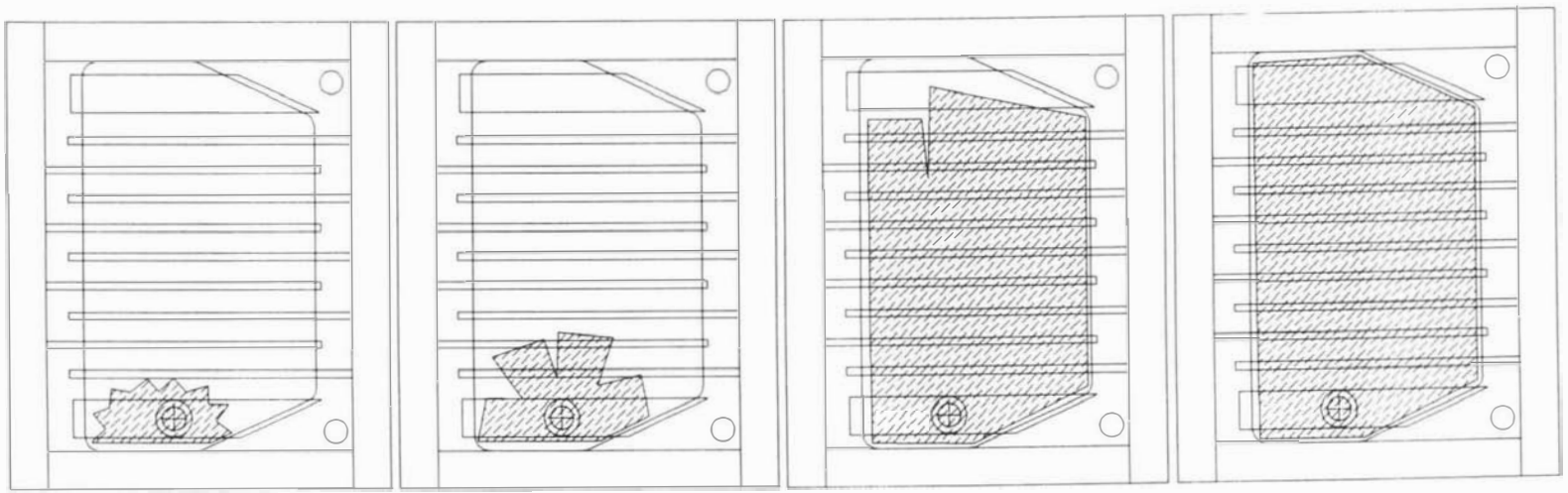

Time after injection of dye

0.10 sec

0.25 sec

0.60 sec

0.65 sec

Amaranth Dye Solution

**Figure 5.7. The progress of amaranth dye in the OA circuit**

The juice circuit was equilibrated with water. Then an amaranth dye solution was pulsed into the OA circuit flow at time "zero", and its progress up the module was recorded.

The flow patterns presented were observed when

(a) fructose solution at 0.10 g (g solution)$^{-1}$, at 20 ± 1 °C

(b) fructose solution at 0.70 g (g solution)$^{-1}$, at 20 ± 1 °C

The progression of the dye up the module is shown after approximately 30 seconds.

| | |
|---|---|
| Juice circuit | - water at 20 ± 1 °C |
| OA circuit | - fructose solutions, at 20 ± 1 °C |
| Juice circuit volumetric flow rate | - $4 \times 10^{-5}$ m$^3$ s$^{-1}$ |
| OA circuit volumetric flow rate | - $7 \times 10^{-6}$ m$^3$ s$^{-1}$ |
| Juice circuit inlet hydraulic pressure | - 13.8 kPa |
| OA circuit inlet hydraulic pressure | - 0 to 6 kPa |

The same pattern of flow was observed in the pilot plant DOC module, under similar ranges of operating conditions.

(a)

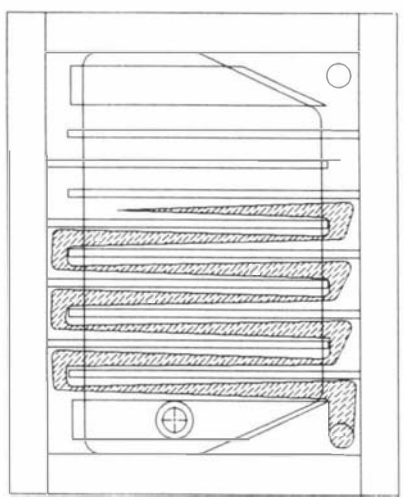

(b)

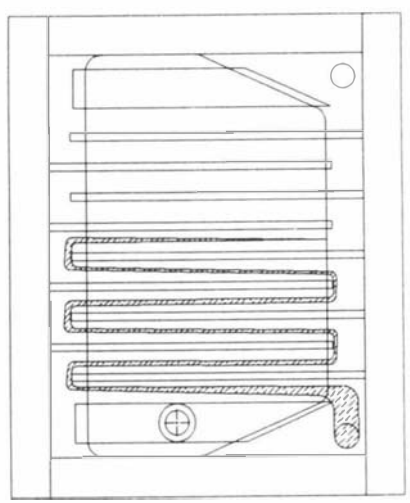

essentially perpendicular to the membrane. Water molecules exiting the membrane surface were not immediately swept away into the free stream of the OA circuit but remained at the surface and slowly diffused outward. The rate at which the water diffused away from the membrane and OA solute diffused toward the membrane, was dependent on the diffusion rates of the solute and water molecules in the boundary layer. The thickness of the boundary layer also influenced the concentration at the membrane surface.

The cross section dimensions of the OA flow channels were virtually the same in both modules. A diagram of an individual OA flow channel is shown in Figure 5.8. The dimensions of the flow channel in the OA circuit, the flow conditions and the corresponding *Re* number for the small laboratory and pilot plant DOC modules are presented in Table 5.2. The *Re* number calculated was based on the free-stream fluid velocity in the centre of the flow channel and the entire channel cross-sectional area of flow [Equation (2.20)]. The *Re* number in the boundary layer is different, based on the boundary layer thickness [Equation (2.54)]. The cross-sectional area of flow in which the flow was at the free-stream velocity was smaller than the channel cross-sectional area of flow. The *Re* number in the free-stream velocity channel would be marginally higher than one calculated from the entire channel. For example, if the boundary layers were 20% of the flow area, the *Re* number for 0.1 g (g solution)$^{-1}$ fructose solution in the small module would be 230 compared to 211 for the entire channel. The flow in the OA flow channels was definitely laminar.

### 5.3.1. Entry length for fully-developed laminar flow

The actual length of the channels was 0.1545 m. The entry length required to allow fully-developed flow in the OA flow channels was calculated for fructose and NaCl solutions according to Equation (2.56). The values for the entry length $L'$ are presented in Table 5.3.

Fully-developed laminar flow implies the boundary layers from the two sides of the flow channel have met and the flow is laminar along the channel. With fructose solutions at 0.5 g (g solution)$^{-1}$ the entry length before fully-developed laminar flow, was calculated to be 0.04 m, a quarter of the length of each flow channel. For fructose solutions at 0.7 g (g solution)$^{-1}$ the entry length was 0.003 m, fully-developed laminar flow was formed almost immediately after entry into the flow channel. Fully-developed laminar flow exists for greater than 50% of the flow channel for fructose solutions greater than 0.5 g (g solution)$^{-1}$.

**Figure 5.8. A single OA flow channel**

Schematic diagram showing the direction of the $x$, $y$ and $z$ coordinates in the OA flow channel.

$Q_m$ - mass flow rate along OA flow channel, kg $s^{-1}$

$m_w$ - mass flow rate of water across membrane per unit area, kg $m^{-2}$ $s^{-1}$

$L_m$ - length of each OA flow channel, 0.1545 ± 0.0005 m

$h$ - equivalent flow channel height; distance between membrane and OA wall when membrane was fully deflected, 0.017 ± 0.001 m

$w$ - width between two membrane support bars, 0.0143 ± 0.0001 m

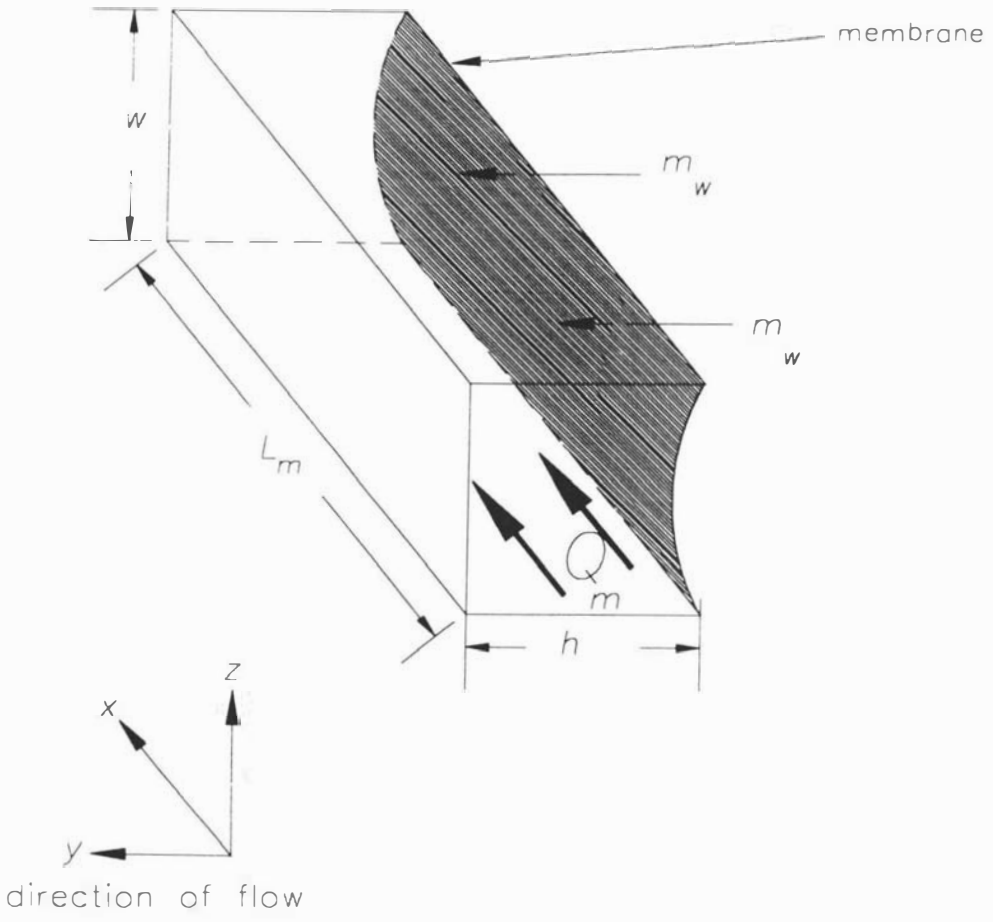
membrane
w
$m_w$
$m_w$
$L_m$
$Q_m$
h
z
x
y
direction of flow

**Table 5.2. Dimensions and flow conditions in the OA circuit**

a. Dimension of channel with no membrane.

b. Cross sectional area of flow = flow channel height × flow channel width

The channel is rectangular therefore the equivalent diameter is calculated using Equation (2.53),

$$D_H = 4 \times \frac{cross\ sectional\ area\ of\ flow}{wetted\ perimeter} \tag{2.53}$$

c. For fructose solutions.

d. Density and viscosity of fructose solutions determined as described in Chapter 4.

e. Reynolds number was calculated using Equation (2.20)

$$Re = \frac{\rho\ U\ D_H}{\mu} \tag{2.20}$$

$\rho$ - fluid density, kg $m^{-3}$

$U$ - free stream velocity, m $s^{-1}$ (= OA bulk stream velocity, based on entire channel width)

$\mu$ - fluid viscosity, kg $m^{-1}$ $s^{-1}$

$D_H$ - equivalent hydraulic diameter of flow channel, m

| DOC module size → | Small laboratory module | | | | | Pilot plant module | | | | |
|---|---|---|---|---|---|---|---|---|---|---|
| DOC module characteristics | Mean | *SE* | *n* | Mean | *SE* | Mean | *SE* | *n* | Mean | *SE* |
| Flow channel width, $w$ (m)[a] | 0.0143 | 0.0001 | 17 | | | 0.0143 | 0.0001 | 103 | | |
| Flow channel height, $h$ (m)[a] | 0.0201 | 0.0001 | 19 | | | 0.0209 | 0.0008 | 103 | | |
| Cross-sectional area of flow (x $10^{-4}$ $m^2$)[b] | 2.87 | 0.01 | | | | 3.0 | 0.1 | | | |
| Perimeter of flow area (m) | 0.0688 | 0.0001 | | | | 0.0704 | 0.0008 | | | |
| $D_H$ (m) | 0.017 | 0.001 | | | | 0.017 | 0.001 | | | |
| Volumetric flow rate (x $10^{-6}$ $m^3$ $s^{-1}$)[c] | 7.0 | 0.3 | | | | 7.0 | 0.3 | | | |
| Mean fluid velocity (m $s^{-1}$) | 0.024 | 0.001 | | | | 0.023 | 0.001 | | | |
| OA: fructose solution[d] (g (g solution $^{-1}$) | 0.10 | 0.01 | | 0.70 | 0.01 | 0.10 | 0.01 | | 0.70 | 0.01 |
| OA density (kg $m^{-3}$) | 1038.5 | 0.1 | | 1334.3 | 0.1 | 1038.5 | 0.1 | | 1334.3 | 0.1 |
| OA viscosity (kg $m^{-1}$ $s^{-1}$) | 0.00135 | 0.00002 | | 0.159 | 0.004 | 0.00135 | 0.00002 | | 0.159 | 0.004 |
| Reynolds number[e] | 211 | | | 3 | | 203 | | | 3 | |

**Table 5.3. Entry length for fully-developed flow at 20°C**

| Concentration (g (g solution)$^{-1}$) | Mole fraction[a] | Density[b] (kg m$^{-3}$) | Viscosity[c] (kg m$^{-1}$ s$^{-1}$) | $Re$[d] | $L'/D_H$[e] | $L'$ (m) |
|---|---|---|---|---|---|---|
| Fructose | | | | | | |
| 0.10 | 0.011 | 1038.1 | 0.00135 | 314.9 | 18.1 | 0.31 |
| 0.30 | 0.041 | 1127.3 | 0.00301 | 152.7 | 8.8 | 0.15 |
| 0.50 | 0.091 | 1229.2 | 0.0114 | 43.9 | 2.5 | 0.04 |
| 0.60 | 0.13 | 1284.9 | 0.0330 | 15.9 | 0.9 | 0.015 |
| 0.70 | 0.19 | 1343.7 | 0.159 | 3.4 | 0.2 | 0.0034 |
| NaCl | | | | | | |
| 0.05 | 0.016 | 1033.7 | 0.00109 | 387.7 | 22.2 | 0.38 |
| 0.15 | 0.052 | 1108.4 | 0.00135 | 336.3 | 19.3 | 0.33 |
| 0.25 | 0.093 | 1188.1 | 0.00190 | 255.6 | 14.6 | 0.25 |

a. Mole fraction ($x$) [Equation (2.41)].

b. Calibration curves Section 4.1 (Wolf et al., 1984).

c. Fructose, experimental data; NaCl, Wolf et al., 1984 .

d. Reynolds number.

e. $L'/D_H \approx 0.0575Re$, Equation (2.56) (Foust et al., 1980).

# 5.4. DOC membranes

## 5.4.1. Membrane structure

The membranes used in the DOC module for experiments were Osmotek Type B membranes. The membrane was examined under a light microscope and the thickness of the membrane was determined. The membrane was asymmetric and consisted of an active membrane layer, its thickness ranged from 10 to 15 μm, and a porous support membrane layer, its thickness ranging from 120 to 150 μm thick. A nylon mesh support was included in the support membrane layer during manufacture (Herron, 1995). A diagram of the membrane is presented in Figure 5.9.

## 5.4.2. Membrane orientation

The membranes used for DOC, being asymmetric can be placed in the module either with the active layer facing the juice circuit and the support layer facing the OA circuit (normal orientation) or vice versa (reversed orientation). When the DOC unit was used for juice concentration, the membranes were placed with the active side facing the juice circuit and the support layer facing the OA circuit.

**Figure 5.9. DOC membrane structure**

am - Active layer of membrane, 10 - 15 μm thick.

sm - Support layer of membrane, porous, 120 -150 μm thick.

Nylon mesh embedded in support layer matrix.

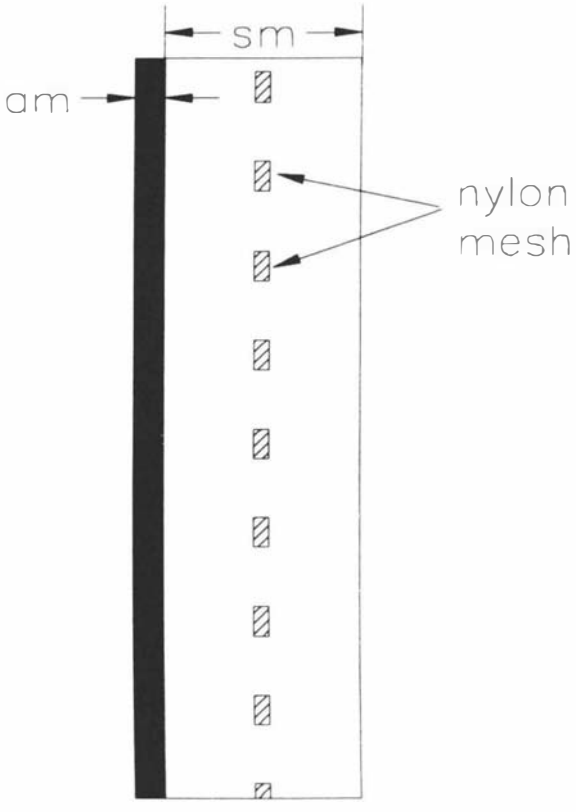
sm
am
nylon
mesh

The active layer was the semi-permeable non-porous membrane layer. The thick support layer was the porous layer consisting of a series of open and tortuous pores. This layer was estimated to be about 50% porous (Herron, 1995). Fifty percent of the layer is open pores and the rest is non-porous membrane material. Due to the support layer's high porosity the solution from the adjacent channel can become trapped in the pores forming an essentially stationary boundary layer.

Resistance to the mass transfer of water was provided by each layer and their influence was quite different. The orientation of the membranes in the DOC module has an influence on the water flux rates (Rautenbach and Albrecht, 1989).

### 5.4.3. Membrane area at equilibrium

The total membrane area available for mass transfer in the DOC modules was calculated by taking into account the membrane deflection, the presence of support bars blocking the membrane and the two end sections around the inlet and outlet ports. The membrane area available in each section of the OA plate divided as shown in Figure 5.3(b) was calculated separately to take into account the membrane deflection in each section.

To estimate the total membrane area, it was assumed at maximum deflection the membrane formed a circular arc, as shown in Figure 5.10. The arc length ($L_a$) of the membrane between the two support members was calculated using the following equation [The derivation of the equation is presented in Appendix A1].

$$\frac{L_a}{w} = \frac{\left(\frac{\Delta}{w}\right)^2 + \frac{1}{4}}{\left(\frac{\Delta}{w}\right)} \sin^{-1}\left(\frac{\left(\frac{\Delta}{w}\right)}{\left(\frac{\Delta}{w}\right)^2 + \frac{1}{4}}\right) \qquad (5.1)$$

$L_a$ - length of membrane arc between two support bars or members, m

$\Delta$ - membrane deflection between two membrane support bars or members, m

$w$ - width between two adjacent membrane support bars or members, m

In sections 1 and 3, a solid piece of polycarbonate attached to the OA plate restricted further deflection of the membrane past it. The extra piece of polycarbonate is shown in Figure 5.3(b). The maximum deflection possible in these sections was limited to 0.00794 m. In these two sections the radius of curvature and arc length, based on this maximum deflection for a rectangular piece of membrane, was calculated using Equation (5.1). The total active membrane area in sections 1 or 3 was estimated for a rectangular

**Figure 5.10. The membrane gap and deflection between two support bars**

(a) Membrane deflection during operation.

(b) Calculated membrane deflection between two spacer bars.

$L_a$ - length of membrane arc between membrane support bars = 0.016 ± 0.009 m

$w$ - width between adjacent membrane support bars = 0.0143 ± 0.0001 m

$\Delta$ - membrane deflection between two support bars = 0.0033 ± 0.0008 m

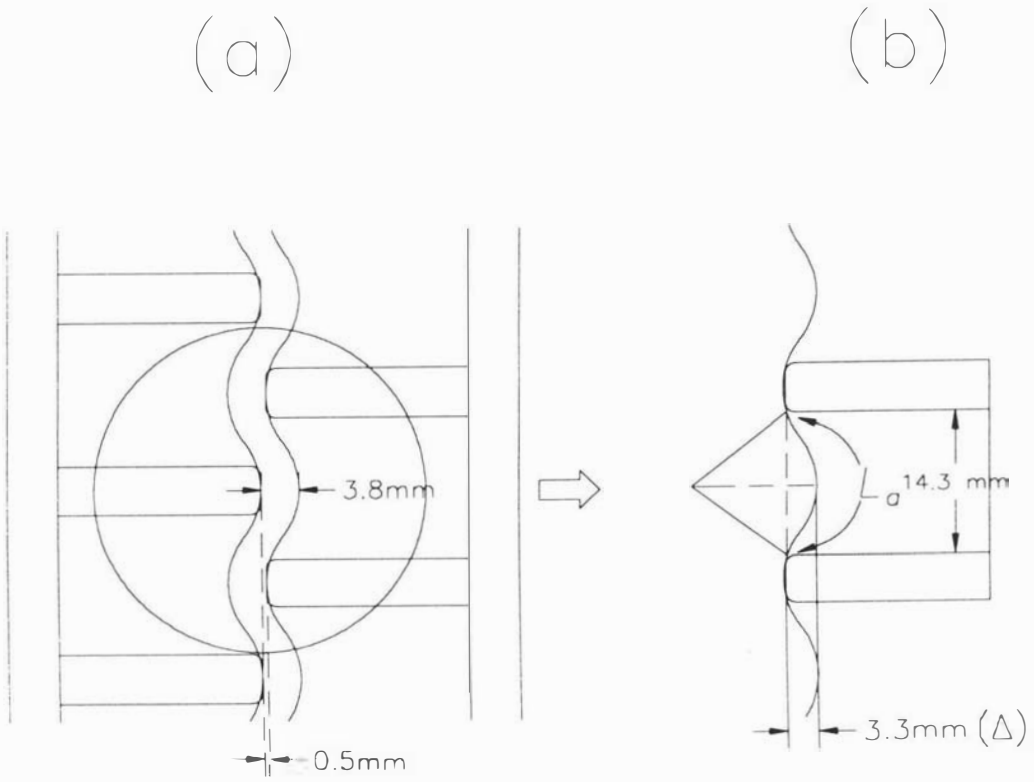
(a)
(b)
3.8mm
0.5mm
α
14.3 mm
3.3mm (Δ)

piece of membrane, taking into account the radius of curvature calculated from the maximum deflection. Then the following were subtracted from the membrane area; missing corners of membrane and the inlet and outlet port areas.

For the small laboratory module, $L_a$ ranged from 0.044 ± 0.002 to 0.055 ± 0.002 m in sections 1 and 3. For the pilot plant module and two OA plates, $L_a$ ranged from 0.089 ± 0.004 to 0.100 ± 0.004 m. The calculated membrane areas in sections 1 and 3 of the small laboratory and pilot plant DOC modules are presented in Table 5.4.

In section 2, the membrane deflection (Δ) was estimated from the thickness of the gap between the two membranes during constant operation and the distance between two opposite support bars (Herron, 1995) [Figure 5.10]. Based on the data of Herron (1995) the membrane deflection was calculated to be 0.0033 ± 0.0008 m, assuming a circular arc was formed by the membrane. The membrane arc length $L_a$, between the two support bars in section 2 was calculated using Equation (5.1) and the following measurements: $w$ = 0.0143 ± 0.0001 m and Δ = 0.0033 ± 0.0008 m. Therefore, $L_a$ = 0.016 ± 0.009 m, between two support bars. The radius of curvature of arc, $r$ = 0.0094 m, θ = 1.73 rad.

The length of each horizontal OA flow channel = membrane length across module, $L_m$. For the small laboratory module; $L_m$ = 0.1545 ± 0.0005 m and for the pilot plant laboratory module; $L_m$ = 0.1781 ± 0.0005 m. Available membrane area between support members = $L_a \times L_m$.

In section 2, the available membrane area = $n \times L_a \times L_m$, where $n$ = number of horizontal flow channels in section 2. In the small laboratory DOC module, there were 17 horizontal flow channels, 8 in one OA plate and 9 in the second. In the pilot plant DOC module, there were 103 horizontal flow channels, 51 in one OA plate and 52 in the second. The membrane areas in section 2 and the total membrane area available for mass transfer, for the two DOC modules, are presented in Table 5.4.

**Table 5.4. Total membrane area available for mass transfer**

| | Membrane area ($m^2$) | |
|---|---|---|
| DOC module → | Small laboratory module | Pilot plant module |
| section 1[a] | 0.0108 ± 0.0004 | 0.0176 ± 0.0009 |
| section 2[b] | 0.043 ± 0.024 | 0.30 ± 0.16 |
| section 3[a] | 0.0106 ± 0.0004 | 0.0166 ± 0.0009 |
| Total | 0.064 ± 0.024 | 0.33 ± 0.17 |
| No. flow channels in section 2[c] (*n*) | 17 | 103 |

a - Section of membrane around the inlet and outlet ports [Figure 5.3(b)].

b - Middle section of the membrane where the support bars are present.

c - For two OA plates.

## 5.4.4. Membrane stretching and membrane gap

The DOC membranes did not remain static during operation. Once liquid was introduced into the juice circuit the membranes stretched until they reached a maximum deflection, at a constant pressure. As the membranes stretched the volume in the juice circuit increased and the gap between the membranes changed. The flow rate of water into the juice circuit was greater than the flow rate of water into the OA circuit for about the first 40 minutes as shown in Figure 5.11. The same results were obtained with fructose solutions at 0.1, 0.3 and 0.7 g (g solution)$^{-1}$ as OAs. It was therefore important to equilibrate the membranes before any measurements were taken.

The membrane gap was determined during constant operation. The gap between the membranes was on average 0.0038 m (error ± 20%) and the front faces of opposite membrane support bars were 0.0005 m apart when the module was closed (Herron, 1995). The measurements supplied by Herron (1995) were used because the membrane gap was not able to be measured on the modules used during this work. Using the value for the membrane gap from Herron (1995) the volume of the juice circuit, in the module, was estimated based on the volume of a thin slab. The volume was calculated to be 1.26 × $10^{-4}$ $m^3$. The hold up volume of the juice circuit, in the module, was measured and found to range from 0.75 × $10^{-4}$ to 1.5 × $10^{-4}$ $m^3$.

The error for the average gap thickness between the membranes was ± 20% (Herron, 1995). To determine the effect of this error on subsequent flux rate calculations, the total membrane area was calculated for the two extreme values of the membrane gap

**Figure 5.11. Water flow rates into and out of juice circuit**

Module setup

Juice circuit - water only at 20.0 ± 0.1 °C
- flow rate $4 \times 10^{-5}$ $m^3$ $s^{-1}$

OA circuit - 0.5 g (g solution)$^{-1}$ fructose solution at 20.0 ± 0.1 °C
- flow rate $7 \times 10^{-6}$ $m^3$ $s^{-1}$

□ - mass flow rate of water entering juice circuit from juice circuit feed vessel

Δ - mass flow rate of water moving out of the juice circuit across the membrane into the OA circuit.

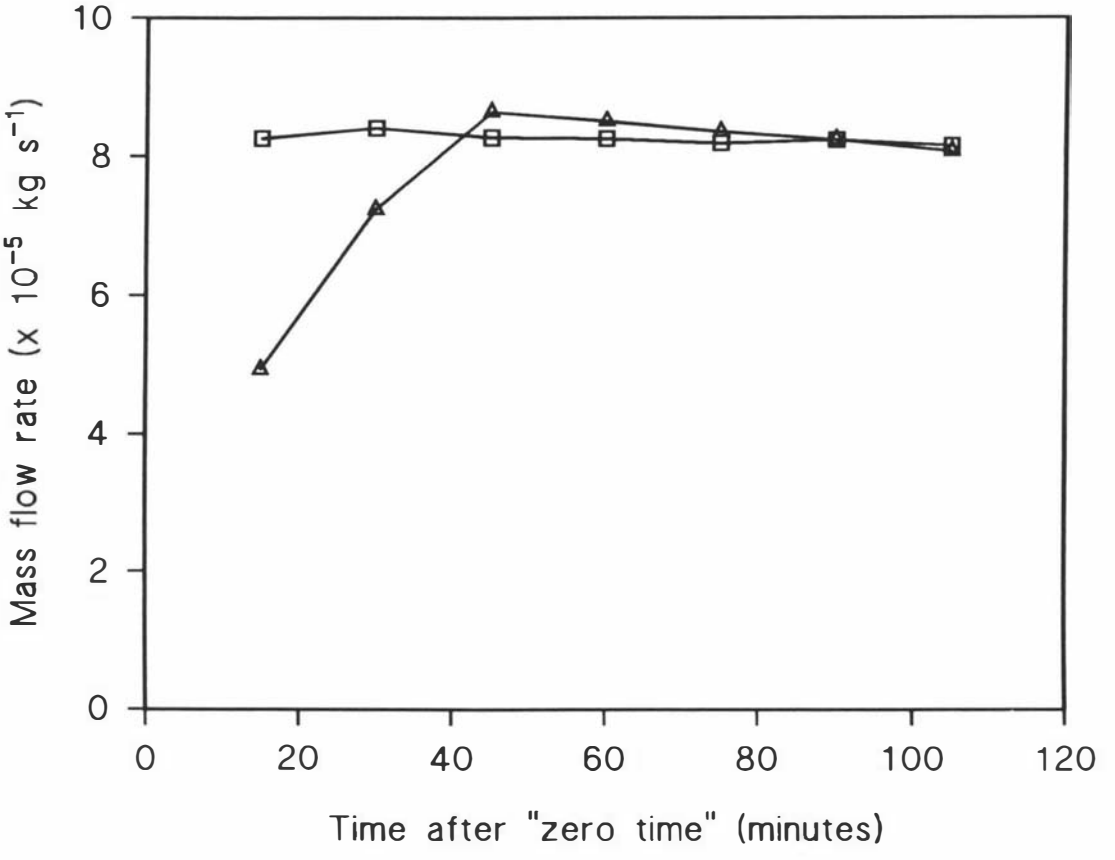
10
8
6
4
2
0
Mass flow rate (x $10^{-5}$ kg $s^{-1}$)
0
20
40
60
80
100
120
Time after "zero time" (minutes)

thickness. That is, for the small DOC unit the membrane area was equal to 0.060 and 0.068 $m^2$, at the two extremes. The mass flux rates calculated with these membrane areas were found to vary by ± 6% compared to using the mean value of 0.064 $m^2$ for membrane area.

### 5.4.5. Salt permeability test for new membranes

The permeability of each new set of membranes to NaCl was used to ascertain that each new batch had similar mass transfer properties to all previous batches. Following three hours of continuous operation, under a standard set of operating conditions, the amount of salt which passed through the membrane into the juice circuit from the OA circuit, containing 0.15 g (g solution)$^{-1}$ NaCl solution, was determined. The DOC unit was not operated at steady state conditions, as the volume of OA was small its concentration decreased over the three hours operation with the uptake of water from the juice circuit. The concentration of the fructose solution in the juice circuit increased from 0.1 g (g solution)$^{-1}$ to approximately 0.2 g (g solution)$^{-1}$. The amount of salt transferred across the membrane was found to be on average 2.3 ± 0.1 g per kg water transferred from the juice circuit under the conditions outlined in Section 3.2.16 ($n$ = 5, with membranes from two different batches).

## 5.5. Equilibration of DOC module

Because the membranes stretched when water was introduced into the juice circuit and continued to do so until maximum deflection was obtained, there was a need to equilibrate the apparatus before recording any data.

In preliminary trials it was found that the concentration of OA exiting the DOC module reached a steady-state after 5 to 10 minutes from start-up. This was found for fructose solutions ranging from 0.1 to 0.7 g (g solution)$^{-1}$. After 10 minutes, any residual water in the OA circuit had been flushed out. The water movement from the juice circuit across the membrane was small. The concentration of OA exiting the DOC module remained relatively constant over the 105 minutes operating period. With 0.7 g (g solution)$^{-1}$ fructose as the OA, its concentration exiting the DOC module was reduced by only 1% after one pass (from six replicate trials).

However, despite the preliminary flushing of the OA circuit following start-up, the membrane continued to stretch for a considerable time and the experimental determination of initial flux rate was very inaccurate and highly variable. To determine the membrane equilibration time required, water flux rates were measured from start-up for a period of two hours operation with no recycling of OA. A range of fructose

concentrations were used. As the best estimate of the true steady-state flux rates, a mean water flux rate was calculated from data collected at 75, 90 and 105 minutes. The difference (residual standard error) between that mean flux rate and the individual measured flux rates at each time period for a given fructose concentration was calculated. The results are shown in Figure 5.12. It can be seen that the measurement of flux rates up to 45 minutes of operation incurred considerable error. The flux rates after 45 minutes operation were within three standard errors of the calculated mean water flux rates. To provide a safety factor, the membranes were equilibrated for 60 minutes prior to data recording.

In the pilot plant DOC module, using similar procedures, it was found that 20 minutes was required to flush the system. A detailed analysis of the membrane equilibration time required for the large DOC module was not completed. It was decided to equilibrate the membranes in the large DOC module for 90 minutes prior to data recording.

## 5.6. Osmotic agent concentration changes after DOC

For ease of operation, pragmatic needs for a reasonable volume of OA, and in accord with recommended system operation, the OA circuit was recirculated through the module during its operation. It was important to keep the OA concentration roughly constant throughout any one experiment. Given the experimental errors involved, it was assessed that the concentration of OA in the reservoir could change by up to 5% from the initial concentration without significantly influencing water flux rates. To facilitate this, the procedure described for experimental operation of DOC apparatus [see 3.2.12] was followed.

To assess the impact of these assumptions, the module was equilibrated as described and operated for 45 minutes. At the end of that time the OA concentration was remeasured. The data are shown in Table 5.5. It is clear that all concentrations remained below the 5% limit chosen for these trials, except for NaCl at 0.23 g (g solution)$^{-1}$. For fructose and NaCl solutions a drop in concentration of 5% will result in a maximum reduction in the osmotic pressure of 3 MPa at 0.7 g (g solution)$^{-1}$ for fructose and 0.23 g (g solution)$^{-1}$ for NaCl.

**Figure 5.12. Water flux rate errors during membrane equilibration period**

Module setup:

Juice circuit - water at 20.0 ± 0.1 °C
- flow rate $4 \times 10^{-5}$ $m^3$ $s^{-1}$

OA circuit - fructose solutions, one pass through the module and no recirculation, at 20.0 ± 0.1 °C
- flow rate $7 \times 10^{-6}$ $m^3$ $s^{-1}$

- Data represent combined results from a range of OA fructose concentrations: 0.1, 0.2, 0.35, 0.5, 0.6 and 0.7 g (g solution)$^{-1}$.

- "Zero time" represents the time when the OA exiting the module was first collected in the tared bucket.

- Individual water flux rate = Increase in mass of OA / membrane area / time (kg $m^{-2}$ $s^{-1}$) [determined in triplicate].

- Mean flux rate for any one concentration = average of data from 75, 90 and 105 minutes.

- Residual standard error = Mean flux rate - Individual water flux rate at time t.

- Overall standard error of mean flux rates = $3.4 \times 10^{-5}$ kg $m^{-2}$ $s^{-1}$ (n = 3).

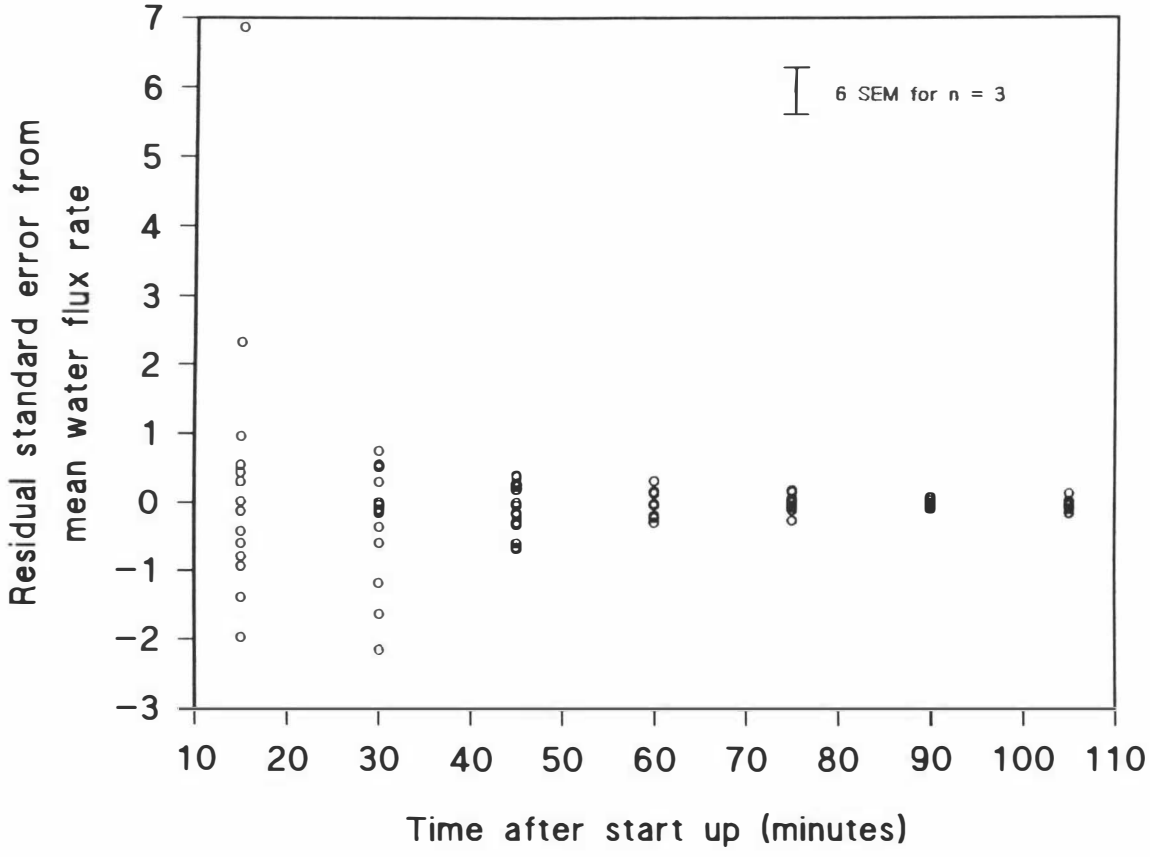
Residual standard error from mean water flux rate
7
6
5
4
3
2
1
0
−1
−2
−3
6 SEM for n = 3
10
20
30
40
50
60
70
80
90
100
110
Time after start up (minutes)

**Table 5.5. Impact of 45 minutes recirculation on OA concentration**

| | |
|---|---|
| Module setup: | |
| Juice circuit | - water |
| | - flow rate $4 \times 10^{-5}$ $m^3$ $s^{-1}$ |
| OA circuit | - OA circulated for 45 minutes after membrane equilibration |
| | - flow rate $7 \times 10^{-6}$ $m^3$ $s^{-1}$ |
| OA concentration | - mean ± *SEM* |
| OA mass | - small laboratory DOC module, approximately 25 kg |
| | - pilot plant DOC module, approximately 56 kg |

| OA solute | Temperature (°C) | Small laboratory module | | | | Pilot plant module | | | |
|---|---|---|---|---|---|---|---|---|---|
| | | Mean concentration (g (g solution)$^{-1}$) | | | | Mean concentration (g (g solution)$^{-1}$) | | | |
| | | Initial | Final | *n* | % change | Initial | Final | *n* | % change |
| Fructose | 10.0 ± 0.1 | 0.1030±0.0001 | 0.1030±0.0001 | 2 | 0.0 | | | | |
| | | 0.352±0.003 | 0.350±0.002 | 2 | 0.6 | | | | |
| | | 0.5050±0.0001 | 0.5004±0.0008 | 2 | 0.9 | | | | |
| | | 0.697±0.002 | 0.692±0.003 | 3 | 0.7 | | | | |
| | 20.0 ± 0.1 | 0.104±0.002 | 0.101±0.001 | 5 | 2.9 | 0.1035±0.0006 | 0.1019±0.0008 | 3 | 1.5 |
| | | 0.352±0.002 | 0.343±0.002 | 6 | 2.6 | 0.3523±0.0001 | 0.3431±0.0001 | 2 | 2.6 |
| | | 0.494±0.003 | 0.487±0.003 | 15 | 1.4 | 0.503±0.004 | 0.488±0.003 | 2 | 3.0 |
| | | 0.693±0.003 | 0.676±0.006 | 7 | 2.5 | 0.68±0.01 | 0.662±0.004 | 3 | 2.6 |
| | 40.0 ± 0.1 | 0.1030±0.0001 | 0.1012±0.0005 | 2 | 1.8 | | | | |
| | | 0.3490±0.0008 | 0.3453±0.0007 | 2 | 1.1 | | | | |
| | | 0.505±0.002 | 0.492±0.003 | 2 | 2.6 | | | | |
| | | 0.696±0.002 | 0.681±0.001 | 2 | 2.2 | | | | |
| NaCl | 20.0 ± 0.1 | 0.0200±0.0003 | 0.0199±0.0003 | 4 | 0.5 | | | | |
| | | 0.1027±0.0004 | 0.0989±0.0009 | 5 | 3.7 | | | | |
| | | 0.1473±0.0005 | 0.1426±0.0006 | 9 | 3.2 | | | | |
| | | 0.2305±0.0004 | 0.218±0.003 | 4 | 5.4 | | | | |

## 5.7. Mass balances

Mass balances were completed for each experimental run with both DOC modules. There were no significant losses of solute or solvent from the DOC system during the experimental runs. Any differences in water or solute masses in the juice or OA circuit were within the experimental errors calculated for both fructose and NaCl OAs and for different operating conditions. In the experimental runs where solute from the OA was detected in the juice circuit, the amount of solute in the juice circuit was less than the experimental error for solute lost from the OA circuit.

# CHAPTER 6
# MASS FLUX RATES IN THE SMALL DOC MODULE

In this chapter the results of water and solute flux rates obtained in the small laboratory DOC module are presented. The influence of OA velocity, osmotic pressure, temperature, nature of osmotic agent, OA viscosity, OA diffusion coefficient and membrane orientation on water flux rate were determined. The evidence of any solute transfer was presented for the different OAs used. The influence of OA and operating conditions on solute flux rate was determined. From these results the resistances to the mass transfer of water from the juice circuit to the OA circuit were ascertained and the factors affecting these resistances were discussed.

## 6.1. Flow velocity and water flux rate

The effect of flow velocities in the juice and OA circuits on water flux rate is presented in Table 6.1.

**Table 6.1. Water flux rates and flow channel velocity at 20°C**

| Juice circuit[a] | | OA circuit[b] | | Water flux rate[d] ($kg\ m^{-2}\ s^{-1}$) |
|---|---|---|---|---|
| Flow rate ($m^3\ s^{-1}$) | Velocity ($m\ s^{-1}$) | Flow rate ($m^3\ s^{-1}$) | Velocity ($m\ s^{-1}$) | |
| $4 \times 10^{-5}$ [c] | 0.07 | $7 \times 10^{-6}$ [c] | 0.024 | 0.00143 ± 0.00004 |
| $7 \times 10^{-5}$ | 0.12 | $7 \times 10^{-6}$ | 0.024 | 0.00148 ± 0.00003 |
| $7 \times 10^{-5}$ | 0.12 | $1.6 \times 10^{-5}$ | 0.055 | 0.00159 ± 0.00004 |

a Juice circuit, water.
b OA, 0.7 g (g solution)$^{-1}$ fructose solution.
c Conditions for standard operation.
d Batch 1, DOC membranes.

The flux rate obtained following a 71.4% increase in juice circuit velocity was not significantly different ($p < 0.05$) to the flux rate obtained under conditions used for standard operation. The flux rate obtained after increasing the velocity in the OA circuit by 125% was not significantly greater ($p < 0.05$) than the flux rate obtained under

standard operating conditions. It would appear that the increase in OA velocity had an insignificant effect on the thickness of the velocity boundary layers.

## 6.2. Impact of osmotic pressure difference on water flux rate

Water flux rates obtained in the DOC unit are presented in Figure 6.1 with respect to the osmotic pressure difference between the juice circuit's free-stream osmotic pressure ($\pi_J$) and the OA circuit's free-stream osmotic pressure ($\pi_{OA}$). As water only was present in the juice circuit $\pi_J = 0$.

Under ideal conditions, the water flux rate should be directly proportional to the osmotic pressure difference (Lonsdale, 1972; Lee et al., 1981; Strathmann, 1981; Cheryan and Nichols, 1992). However, the water flux rate for the DOC system was not linearly proportional to osmotic pressure difference between the two solutions. This shows the DOC system was not ideal, in accord with observations of others (Lonsdale, 1972; Lee et al., 1981; Cheryan and Nichols, 1992). It has been proposed that the asymptotic curve relating water flux rate to osmotic pressure difference between the two bulk solutions was due to the concentration boundary layers next to the membrane and within the porous support layer of the asymmetric membranes (Kessler and Moody, 1976; Lee et al., 1981; Honda and Barclay, 1990).

Osmotic pressure differences were calculated from the two bulk free-stream concentrations on either side of the membrane. This osmotic pressure difference was not the true difference across the membrane because of the concentration boundary layers that exist between the bulk free-stream and the membrane. To calculate the actual osmotic pressure across the membrane the solute concentration adjacent to the membrane must be determined. Resistance to the transfer of water from the membrane to the free-stream was encountered in the boundary layer. On the juice side of the membrane water only was used and there was no concentration boundary layer or resistance to water transfer in this channel.

## 6.3. Influence of temperature on water flux rate

Temperature was considered to have an important influence on water flux rate. The impact of temperature on water flux rates in the DOC module is shown in Figure 6.2. The general shapes of the curves at different operating temperatures are the same. The flux rate curves at the three operating temperatures are statistically different ($p < 0.01$). With increasing operating temperature there was a corresponding increase in the water flux rates obtained in the DOC system.

**Figure 6.1. Impact of osmotic pressure difference on water flux rates in the small laboratory DOC module**

Module set up:

Juice circuit - water only at 20.0 ± 0.1 °C
- flow rate 4 × $10^{-5}$ $m^3$ $s^{-1}$

OA circuit - fructose solutions at 20.0 ± 0.1 °C
- flow rate 7 × $10^{-6}$ $m^3$ $s^{-1}$

o - Mean of experimentally determined data. The horizontal lines represent two standard errors about each mean. The data points are joined by a best fit line. The overall standard error of the means (*SEM*) = 5 x $10^{-5}$ for $n$ = 3.

Number of replicate trials:

| OA concentration (g (g solution)$^{-1}$) | Osmotic pressure difference, $\Delta\pi$[a] (MPa) | Number of trials |
|---|---|---|
| 0.10 | 1.5 | 3 |
| 0.35 | 8.0 | 3 |
| 0.49 | 14.2 | 11 |
| 0.69 | 28.9 | 5 |

a. Osmotic pressure difference, $\Delta\pi = (\pi_{OA} - \pi_J)$ and $\pi_J = 0$.

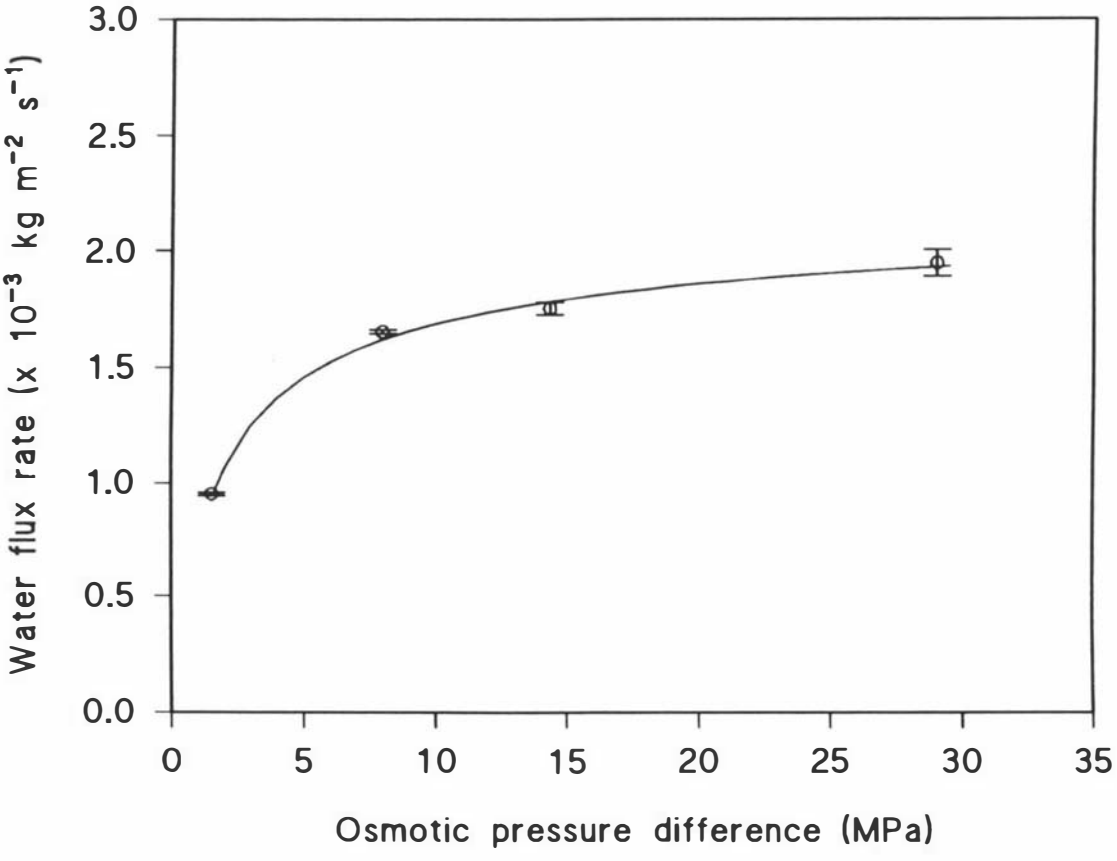
Water flux rate (x $10^{-3}$ kg $m^{-2}$ $s^{-1}$)
3.0
2.5
2.0
1.5
1.0
0.5
0.0
0
5
10
15
20
25
30
35
Osmotic pressure difference (MPa)

**Figure 6.2. Influence of temperature on water flux rates in the small laboratory DOC module**

Module set up:

Juice circuit - water only, flow rate $4 \times 10^{-5}$ $m^3$ $s^{-1}$

OA circuit - fructose solutions, flow rate $7 \times 10^{-6}$ $m^3$ $s^{-1}$

Operating temperatures (± *SEM* for $n = 3$) were: 10.0 ± 0.1 °C; 20.0 ± 0.1 °C; 40.0 ± 0.1 °C

Data points presented are means of experimentally determined data. The horizontal lines represent two standard errors about each mean. The overall standard error of the means (*SEM*) = $6 \times 10^{-5}$ for $n = 2$.

Number of replicate trials:

| Approximate OA concentration (g (g solution)$^{-1}$) | Osmotic pressure difference, $\Delta\pi$[a] (MPa) | Operating temperature | | |
|---|---|---|---|---|
| | | 10°C | 20°C | 40°C |
| 0.10 | 1.5 | 2 | 3 | 2 |
| 0.35 | 8.0 | 2 | 3 | 2 |
| 0.50 | 15.0 | 2 | 11 | 2 |
| 0.70 | 30.0 | 3 | 5 | 2 |

a. Osmotic pressure difference, $\Delta\pi = (\pi_{OA} - \pi_J)$ and $\pi_J = 0$.

Best fit response curves were fitted using non linear least squares regression [see 3.3.1]. Where $y$ = water flux rate, $x$ = osmotic pressure difference and $a$, $b$ and $c$ are constants, the form of the curves was

$$y = \frac{ax}{(1 + bx)^c}$$

The value of the coefficients for each temperature are:

| | *a* | *b* | *c* |
|---|---|---|---|
| Fructose, 10°C | 0.0021 | 2.64 | 0.83 |
| Fructose, 20°C | 0.0012 | 0.69 | 0.95 |
| Fructose, 40°C | 0.0013 | 0.54 | 0.92 |

The $F_{statistic}$ calculated from the residual mean square of a single curve fit to all the data and the residual mean square from the individual fitted curves was 104.2, degrees of freedom 6 and 3.

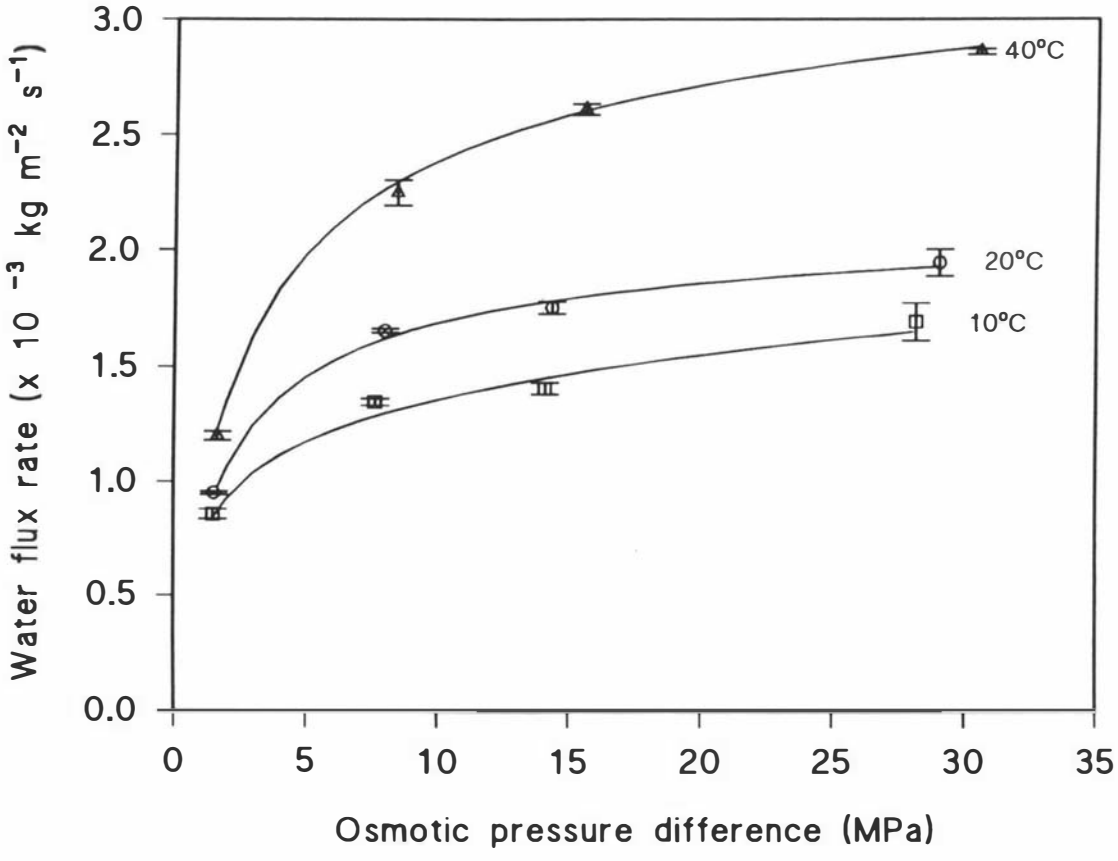
Water flux rate (x 10 -3 kg m-2 s-1)
3.0
2.5
2.0
1.5
1.0
0.5
0.0
0
5
10
15
20
25
30
35
Osmotic pressure difference (MPa)
40°C
20°C
10°C

The relationship between water flux rate and temperature was found to fit an Arrhenius relationship, shown in Figure 6.3. The activation energies ($E_a$) determined from the slopes of each graph are presented in Table 6.2.

**Table 6.2. Activation energies for water flux during DOC**

| Fructose concentration (g (g solution)$^{-1}$) | Slope $E_a/R^a$ (K) | *sd* of slope | $r^2$ | $E_a$ (J mol$^{-1}$) |
|---|---|---|---|---|
| 0.1 | 980 | 50 | 0.997 | 8,180 |
| 0.35 | 1490 | 70 | 0.998 | 12,440 |
| 0.5 | 1823 | 2 | 1.00 | 15,156 |
| 0.7 | 1500 | 200 | 0.990 | 13,000 |

a. Determined from regression analysis of Arrhenius plots.

Using these data it was determined that for every one degree Kelvin rise in temperature, there was a corresponding 1 to 2% increase in the flux rate using fructose OA solutions from 0.1 to 0.7 g (g solution)$^{-1}$. For RO, using cellulose acetate membranes, water flux rates were also found to increase with operating temperature. Lonsdale (1972) found the flux rate during RO increased by 3% for every increase in degrees Kelvin, with activation energies of 20 - 25 kJ mol$^{-1}$. There are no similar data published for DOC.

Temperature affects solution properties such as viscosity and diffusion coefficients, and this may be a key reason for the differences in flux rates. As the viscosity of a solution decreases with increasing temperature, the diffusion coefficient of the solution increases. The rate at which the water molecules could diffuse away from the membrane would affect the concentration and driving force for water transfer at the membrane edge. The effect of temperature on diffusion coefficients for fructose solutions was shown in Figure 4.11. For a fructose solution at 0.5 g (g solution)$^{-1}$ as the OA, the diffusion coefficient increases by 50% between 10 and 20°C and by 110% between 20 and 40°C. Water flux rates with this OA, increased by 30% between 10 and 20°C and 45% between 20 and 40°C.

Temperature may also have an effect on the membrane and membrane transport properties. The mechanism of transfer of water and solute across the active layer of a semi-permeable membrane is considered to be solution and diffusion (Merton 1966; Lonsdale, 1972; Rautenbach and Albrecht, 1989). The solution and diffusion processes

**Figure 6.3. Relationship between temperature and water flux rate for fructose solutions**

Module set up:
Juice circuit - water only, flow rate $4 \times 10^{-5}$ $m^3$ $s^{-1}$
OA circuit - fructose solutions, flow rate $7 \times 10^{-6}$ $m^3$ $s^{-1}$

Data points presented are means of experimentally determined data. The horizontal lines represent two standard errors about each mean.

Linear regressions were carried out on the mean mass flux rate values.

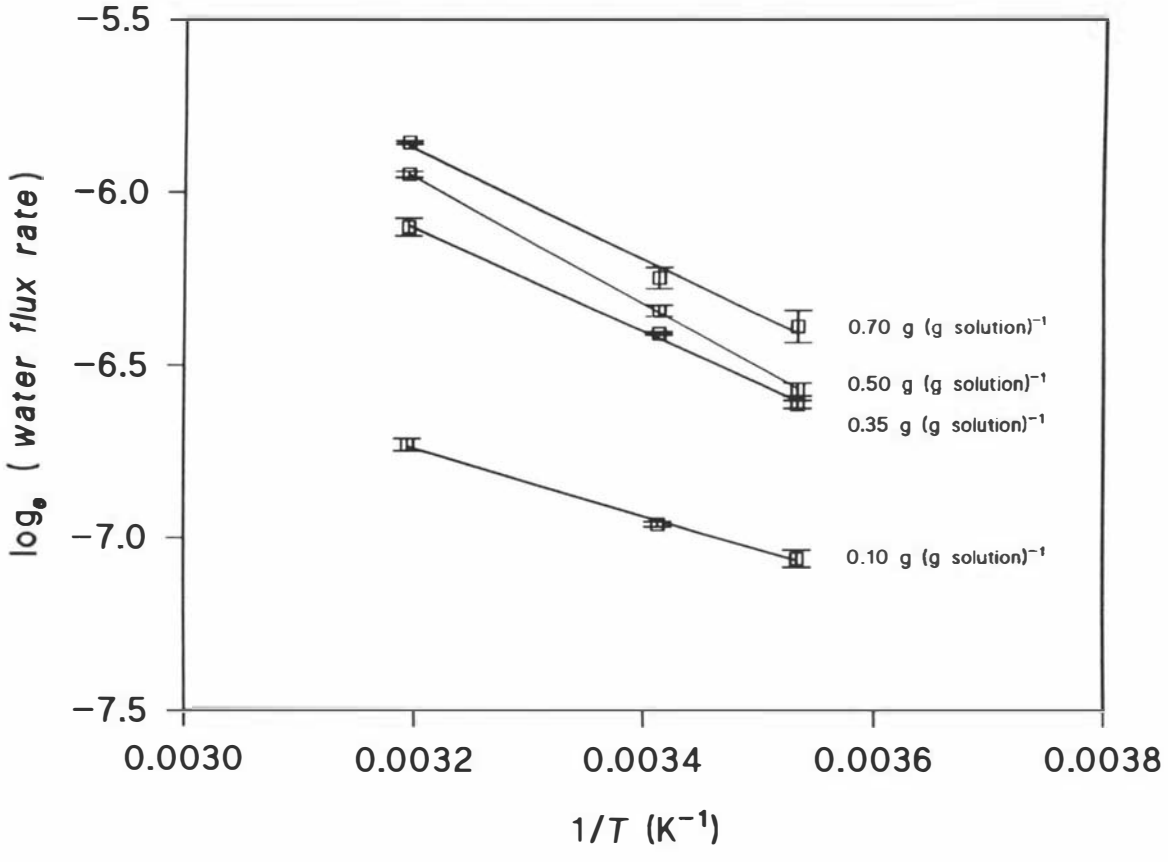
−5.5
−6.0
−6.5
−7.0
−7.5
0.0030
0.0032
0.0034
0.0036
0.0038
log$_e$ ( water flux rate )
1/T (K$^{-1}$)
0.70 g (g solution)$^{-1}$
0.50 g (g solution)$^{-1}$
0.35 g (g solution)$^{-1}$
0.10 g (g solution)$^{-1}$

are both influenced by temperature, mediated through the membranes capability to solubilise molecules and the ease of diffusion through the membrane matrix. For solvent flux described by the solution-diffusion model, the term outside the brackets in Equation (2.24) is equivalent to the membrane constant. This term is dependent on the diffusion coefficient in the membrane, solute concentration in the membrane, and on temperature (Merton, 1966; Rautenbach and Albrecht, 1989).

The temperature dependent properties of the membrane were not measured in this study. The DOC system was not operated at a temperature above the maximum temperature (40°C) for the DOC membrane recommended by the membrane manufacturer. Above the maximum temperature the membrane properties may change (Herron, 1995).

## 6.4. Water flux rates and OA solution properties

### 6.4.1. Water flux rates using NaCl

The viscosity and diffusion coefficients of the OA solution were considered to have important influences on the water flux rate. The OA solution viscosity and diffusion coefficients could be altered by varying the solute in solutions at iso-osmotic concentrations, or by varying the temperature.

The water flux rates were determined using NaCl as the OA solution. NaCl gave solutions with different viscosities and diffusion coefficients to fructose [Table 4.6]. The molecular weight of NaCl is much less than that of fructose and in solutions NaCl is ionic. The results are presented in Figure 6.4. For comparative purposes the water flux rates using fructose are shown on the same graph.

The two curves were significantly different ($p < 0.001$). Water flux rates obtained with NaCl as OA are on average two times greater than for fructose at the same osmotic pressure. The best fit curve used for statistical analysis of the fructose data was also found to fit the data for NaCl. This indicates that the increase in flux rate with osmotic pressure for the two OAs follows a similar trend and the factors influencing flux rate were likely to be the same for the two OAs.

### 6.4.2. Water flux rate and OA solution viscosity

To test the importance of viscosity, water flux rates were determined with OA solutions at approximately iso-osmotic concentrations but with different solution viscosities. The difference in solution viscosities were achieved by using different OA solutes or by varying the temperature. The results are presented in Figure 6.5. Viscosity data for the OA solutions are presented in Table 4.7. For solutions of high viscosity, small changes

**Figure 6.4. Water flux rates using NaCl or fructose solution in small laboratory DOC module**

Module set up:

Juice circuit - water only, at 20.0 ± 0.1 °C, flow rate $4 \times 10^{-5}$ $m^3$ $s^{-1}$

OA circuit - NaCl or fructose solutions, at 20.0 ± 0.1 °C

- flow rate $7 \times 10^{-6}$ $m^3$ $s^{-1}$

Data points presented are means of experimentally determined data. The horizontal lines represent two standard errors about each mean. The overall standard error of means (*SEM*) = 5 x $10^{-5}$ for $n$ = 3.

Number of replicate trials:

| NaCl | | | Fructose | | |
|---|---|---|---|---|---|
| OA concentration (g (g solution)$^{-1}$) | Osmotic pressure difference, $\Delta\pi^a$ (MPa) | No. trials | OA concentration (g (g solution)$^{-1}$) | Osmotic pressure difference, $\Delta\pi^a$ (MPa) | No. trials |
| 0.02 | 1.5 | 2 | 0.10 | 1.5 | 3 |
| 0.10 | 9.1 | 3 | 0.35 | 8.0 | 3 |
| 0.15 | 15.5 | 3 | 0.49 | 14.2 | 11 |
| 0.23 | 30.5 | 2 | 0.69 | 28.9 | 5 |

a. Osmotic pressure difference, $\Delta\pi = (\pi_{OA} - \pi_J)$ and $\pi_J = 0$.

Best fit response curves were fitted using non linear least squares regression [see 3.3.1]. Where $y$ = water flux rate, $x$ = osmotic pressure difference and $a$, $b$ and $c$ are constants, the form of the curves was

$$y = \frac{ax}{(1 + bx)^c}$$

The value of the coefficients for each osmotic agent are:

| | $a$ | $b$ | $c$ |
|---|---|---|---|
| Fructose, 20°C | 0.0012 | 0.69 | 0.95 |
| NaCl, 20°C | 0.0016 | 0.63 | 0.77 |

The $F_{statistic}$ calculated from the error mean square of a single curve fit to all the data and the error mean square from the individual fits was 230.4, degrees of freedom 9, 4.

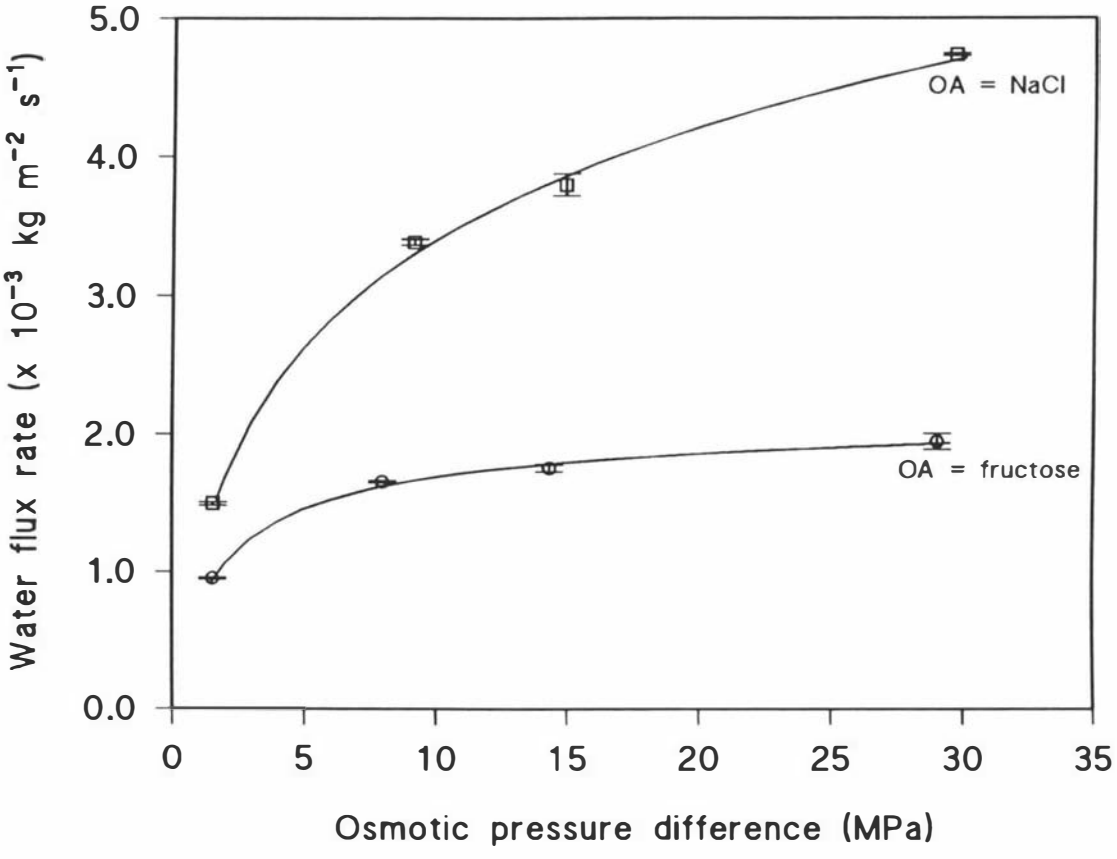
Water flux rate (x $10^{-3}$ kg $m^{-2}$ $s^{-1}$)
5.0
4.0
3.0
2.0
1.0
0.0
0
5
10
15
20
25
30
35
Osmotic pressure difference (MPa)
OA = NaCl
OA = fructose

**Figure 6.5. Water flux rates for approximate iso-osmotic OA solutions with different solution viscosities**

Module set up:
Juice circuit - water only, at 20.0 ± 0.1 °C, flow rate $4 \times 10^{-5}$ $m^3$ $s^{-1}$
OA circuit - sucrose, fructose and NaCl solutions, flow rate $7 \times 10^{-6}$ $m^3$ $s^{-1}$

○ - NaCl, 0.10 g (g solution)$^{-1}$ at 20.0 ± 0.1 °C, osmotic pressure 7.6 MPa
◊ - fructose, 0.35 g (g solution)$^{-1}$ at 40.0 ± 0.1 °C, osmotic pressure 7.6 MPa
△ - fructose, 0.35 g (g solution)$^{-1}$ at 20.0 ± 0.1 °C, osmotic pressure 8.0 MPa
□ - fructose, 0.35 g (g solution)$^{-1}$ at 10.0 ± 0.1 °C, osmotic pressure 8.5 MPa
▽ - sucrose, 0.45 g (g solution)$^{-1}$ at 20.0 ± 0.1 °C, osmotic pressure 9.1 MPa

Data points presented are means of experimentally determined data. The horizontal lines represent two standard errors about each mean. The overall standard error of means (*SEM*) = 2 x $10^{-5}$ for $n = 3$.

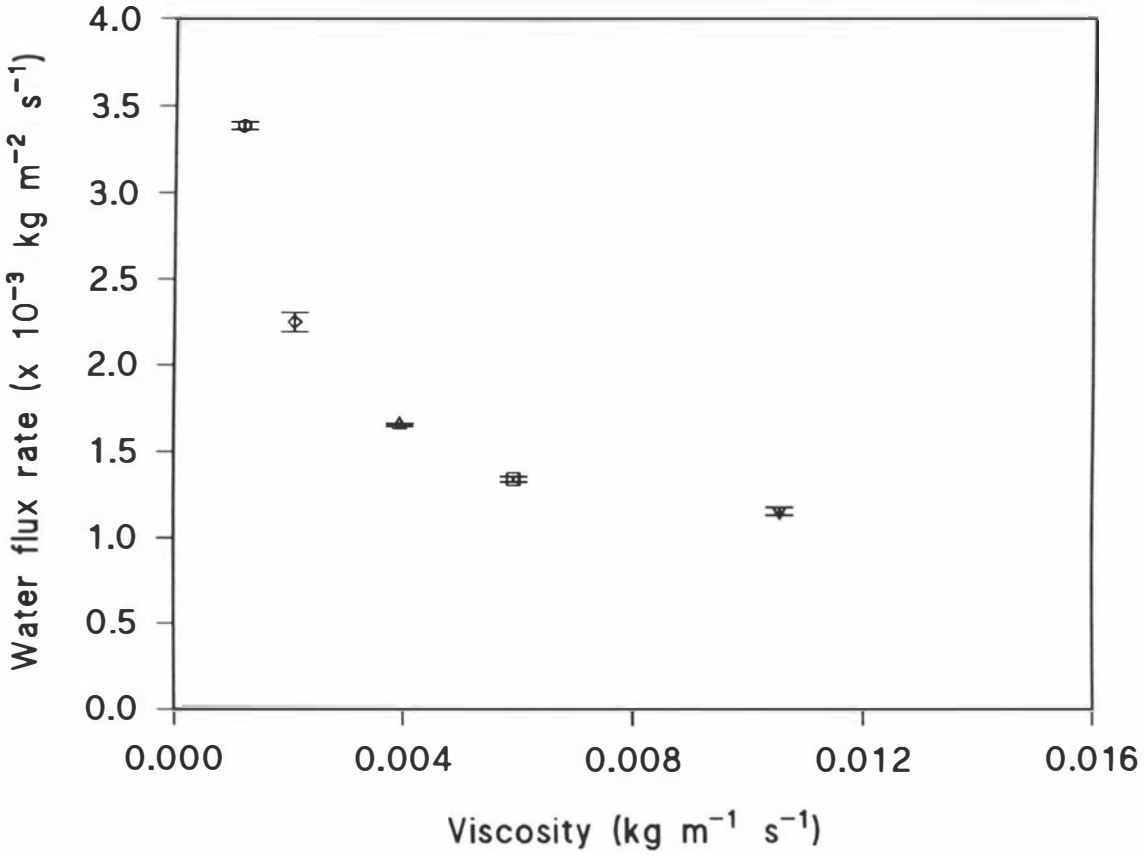
Water flux rate (x $10^{-3}$ kg $m^{-2}$ $s^{-1}$)
4.0
3.5
3.0
2.5
2.0
1.5
1.0
0.5
0.0
0.000
0.004
0.008
0.012
0.016
Viscosity (kg $m^{-1}$ $s^{-1}$)

in viscosity had relatively little influence on the water flux rate. The water flux rate was inversely proportional to viscosity but was not a linear relationship even when plotted on a $\log_e$:$\log_e$ scale.

For a large number of membrane systems (including MF, UF and RO) and feed streams, the flux rates are inversely proportional to the fluid viscosity (Porter, 1990).

### 6.4.3. Water flux rate and solution diffusion coefficients

Diffusion coefficients are also known to influence flux rates. Diffusion coefficients are influenced by viscosity, but to a lesser extent in solutions with viscosities greater than $5 \times 10^{-3}$ kg m$^{-1}$ s$^{-1}$ (Hiss and Cussler, 1973). The relationship between water flux rates and diffusion coefficients is presented in Figure 6.6. Diffusion coefficient data for the OA solutions were presented in Table 4.7.

There was also a non-linear relationship between flux rate and diffusion coefficients. The solutions with diffusion coefficients greater than $3 \times 10^{-10}$ m$^2$ s$^{-1}$ correspond to solutions with viscosities less than $5 \times 10^{-3}$ kg m$^{-1}$ s$^{-1}$. A linear correlation between flux rate and diffusion coefficients was found for solutions with diffusion coefficients greater than $3 \times 10^{-10}$ m$^2$ s$^{-1}$.

The viscosity and diffusion coefficient of an OA solution definitely influenced the water flux rate across the membrane. In solutions with high viscosities and low diffusion coefficients (e.g. fructose), the water which was transported across the membrane diffused away slowly into the bulk OA. In solutions with low viscosities and high diffusion coefficients (e.g. NaCl) water exiting the membrane into the OA encountered less resistance and diffused quickly away from the membrane surface to be replaced by OA solute molecules. In a sugar solution the water molecules have to break a number of hydrogen bonds for diffusion (Gladden and Dole, 1953). Therefore, solute molecules in OA solutions with relatively high viscosities and low diffusion coefficients can not diffuse at a sufficient rate to maintain the maximum solute concentration at the membrane surface and hence can not maintain the maximum osmotic pressure driving force possible.

Changing the OA solution properties by changing the bulk free-stream OA concentration, solute or temperature affected the boundary layer thickness [Equation (2.55)] and resistances to water transfer in the boundary layer. The concentration gradient across the boundary layer, and therefore, the diffusion rate across the boundary layer varied with different solution properties. Lower solution viscosities resulted in

**Figure 6.6. Water flux rates for approximate iso-osmotic OA solutions with varying solution diffusion coefficients**

Module set up:
Juice circuit - water only, at 20.0 ± 0.1 °C, flow rate $4 \times 10^{-5}$ $m^3$ $s^{-1}$
OA circuit - sucrose, fructose and NaCl solutions, flow rate $7 \times 10^{-6}$ $m^3$ $s^{-1}$

o - NaCl, 0.10 g (g solution)$^{-1}$ at 20.0 ± 0.1 °C, osmotic pressure 7.6 MPa
◊ - fructose, 0.35 g (g solution)$^{-1}$ at 40.0 ± 0.1 °C, osmotic pressure 7.6 MPa
▵ - fructose, 0.35 g (g solution)$^{-1}$ at 20.0 ± 0.1 °C, osmotic pressure 8.0 MPa
□ - fructose, 0.35 g (g solution)$^{-1}$ at 10.0 ± 0.1 °C, osmotic pressure 8.5 MPa
▽ - sucrose, 0.45 g (g solution)$^{-1}$ at 20.0 ± 0.1 °C, osmotic pressure 9.1 MPa

Data points presented are means of experimentally determined data. The horizontal lines represent two standard errors about each mean. The overall standard error of means (*SEM*) = 2 x $10^{-5}$ for $n = 3$.

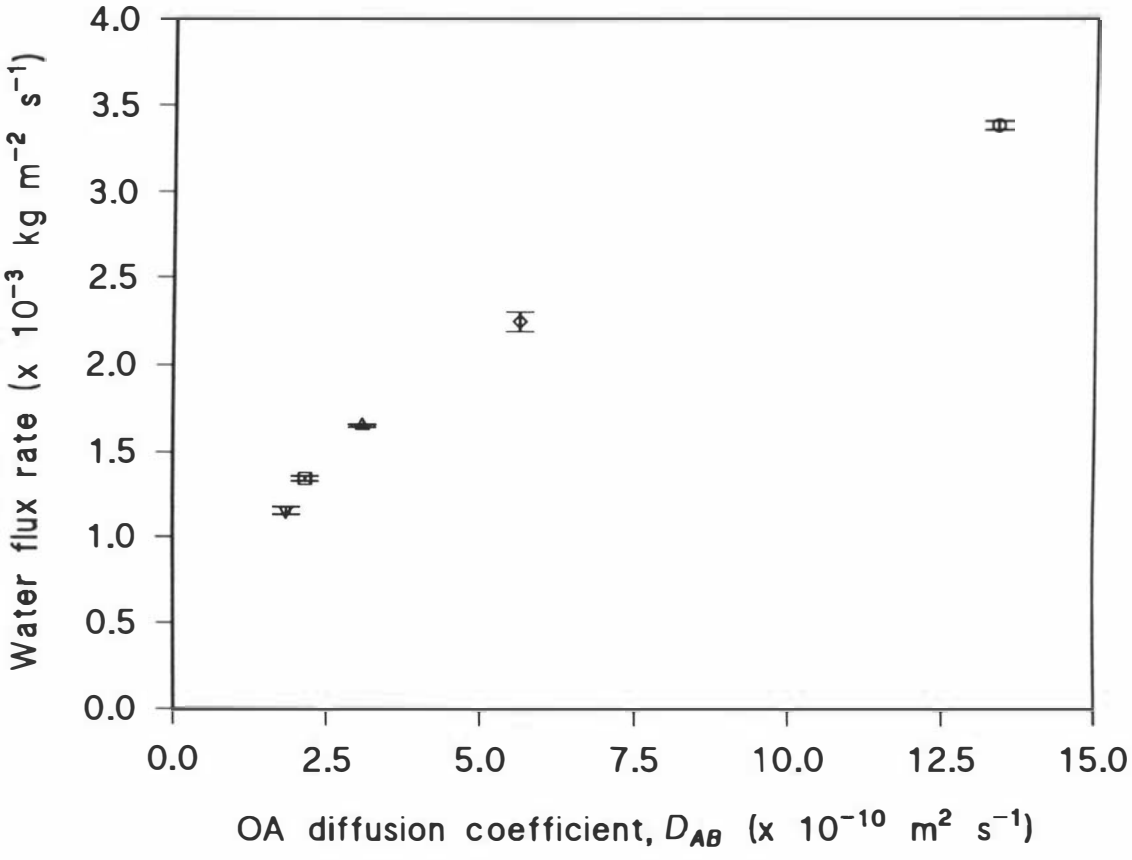
Water flux rate (x $10^{-3}$ kg $m^{-2}$ $s^{-1}$)
4.0
3.5
3.0
2.5
2.0
1.5
1.0
0.5
0.0
0.0
2.5
5.0
7.5
10.0
12.5
15.0
OA diffusion coefficient, $D_{AB}$ (x $10^{-10}$ $m^2$ $s^{-1}$)

thinner boundary layers at constant velocity. Thinner boundary layers provided less resistance to water transfer and the water will reach the OA free-stream more quickly.

## 6.5. Water flux rate and membrane orientation

The impact of fluid dynamics and boundary layer in the OA channel, OA solute, OA concentration and OA solution properties on water flux rates have been determined. The influence of the membrane and membrane properties on the water flux rate will now be considered.

The membranes used for DOC were asymmetric membranes which consisted of an active membrane layer and a porous support membrane layer. When the membranes were set up for normal DOC operation, the active layer was placed adjacent to the juice circuit while the support layer of the membrane faced the OA circuit. It was possible to set up the module with the membranes reversed. In that instance, the active layer of the membranes were placed adjacent to the OA circuit, while the support layers faced the juice circuit. Resistances to the transfer of water were present in both the active and support membrane layers.

The water flux rates obtained for both membrane orientations are presented in Figure 6.7. All curves are significantly different ($p < 0.001$). When the membranes were orientated with the active layer facing the OA circuit, the water flux rates were on average 2.7 and 1.7 times greater for fructose and NaCl, respectively, than when the membranes were set up for normal operation. For each OA the flow conditions in the OA channel were kept constant and the boundary layer in the OA channel was identical for both orientations. The results indicate that the porous support layer had a large impact on water flux rates.

When the membranes were orientated with the active layer facing the OA circuit the support layer in the juice circuit provided no resistance to the movement of water towards the membranes. When the membranes were orientated for normal operation the support layer facing the OA channel contributed a large resistance to the water transfer and reduced the water flux rate by approximately 63% using fructose as OA and by approximately 40% using NaCl as OA.

It was believed that the resistance to transfer of water through the support layer was due to three factors. Firstly, the porosity of the membrane determined some of the resistance. The support layer was estimated to be about 50% porous, i.e. 50% of the membrane material contains open pores while the rest was non-porous membrane material (Herron,

**Figure 6.7. Water flux rates for different membrane orientations**

Module set up:

Juice circuit - water only, at 20.0 ± 0.1 °C, flow rate $4 \times 10^{-5}$ $m^3$ $s^{-1}$

OA circuit - fructose and NaCl solutions, at 20.0 ± 0.1 °C, flow rate $7 \times 10^{-6}$ $m^3$ $s^{-1}$

o - active layer of membrane facing the juice circuit, OA = fructose (Fructose 1)

□ - active layer of membrane facing the juice circuit, OA = NaCl (NaCl 1)

Δ - active layer of membrane facing the OA circuit, OA = fructose (Fructose 2)

◊ - active layer of membrane facing the OA circuit, OA = NaCl (NaCl 2)

Data points presented are means of experimentally determined data. The horizontal lines represent two standard errors about each mean. The overall standard error of means ($SEM$) = 5 x $10^{-5}$ for $n$ = 3.

Number of replicate trials:

| Membrane orientation, active layer facing: | Fructose | | | NaCl | | |
|---|---|---|---|---|---|---|
| | OA concentration (g (g solution)$^{-1}$ | $\Delta\pi^a$ (MPa) | No. trials | OA concentration (g (g solution)$^{-1}$ | $\Delta\pi^a$ (MPa) | No. trials |
| juice circuit | 0.10 | 1.5 | 3 | 0.02 | 1.5 | 2 |
| | 0.35 | 8.0 | 3 | 0.10 | 9.1 | 3 |
| | 0.49 | 14.2 | 11 | 0.15 | 15.5 | 3 |
| | 0.69 | 28.9 | 5 | 0.23 | 30.5 | 2 |
| OA circuit | 0.10 | 1.5 | 2 | 0.02 | 1.5 | 2 |
| | 0.34 | 7.6 | 3 | 0.10 | 9.1 | 2 |
| | 0.48 | 13.6 | 4 | 0.15 | 15.5 | 2 |
| | 0.67 | 27.0 | 2 | 0.22 | 28.1 | 2 |

a. Osmotic pressure difference, $\Delta\pi = (\pi_{OA} - \pi_J)$ and $\pi_J = 0$.

Best fit response curves were fitted using non linear least squares regression [see 3.3.1. and Figure 6.2]. The value of the coefficients for each osmotic agent are:

| | $a$ | $b$ | $c$ |
|---|---|---|---|
| Fructose: active facing juice | 0.0012 | 0.69 | 0.95 |
| Fructose: active facing OA | 0.0027 | 0.99 | 0.74 |
| NaCl: active facing juice | 0.0016 | 0.63 | 0.77 |
| NaCl: active facing OA | 0.0019 | 0.29 | 0.85 |

The $F_{statistic}$ calculated from the error mean square of a single curve fit to all the data and the error mean square from the individual fits was 230.4, degrees of freedom 9, 4.

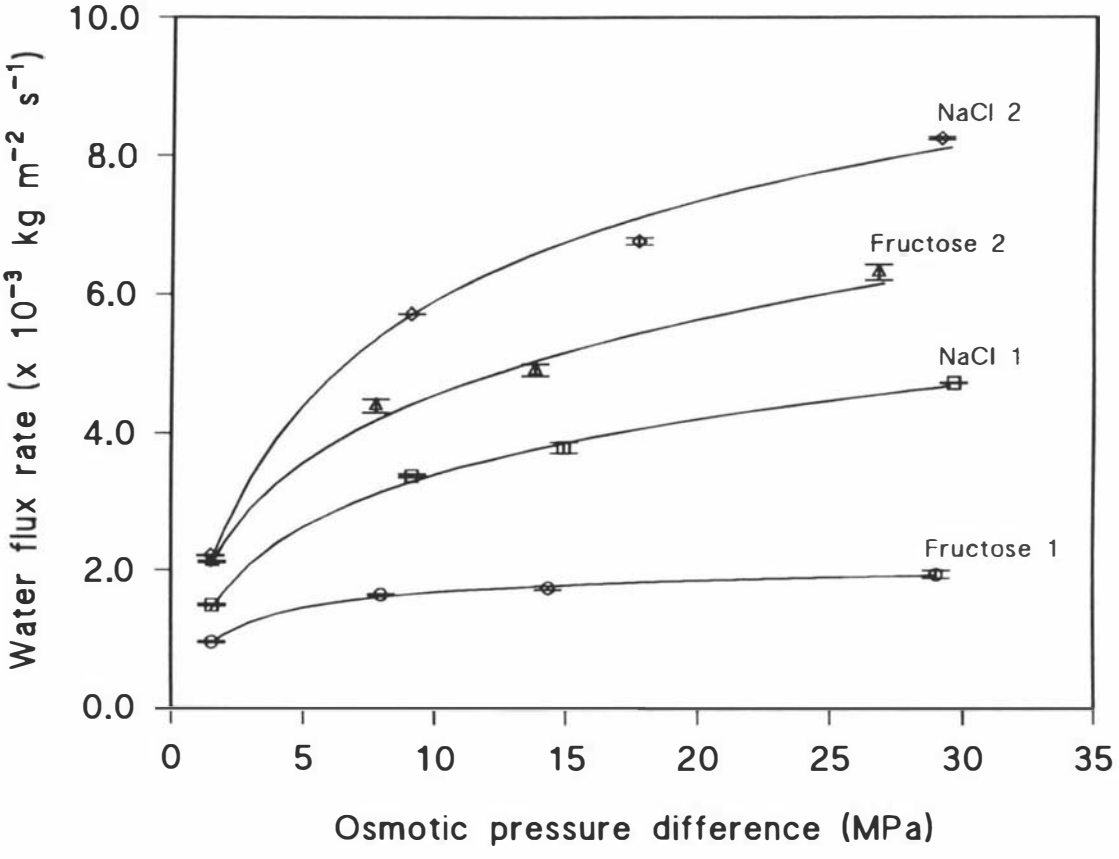
Water flux rate (x $10^{-3}$ kg $m^{-2}$ $s^{-1}$)
10.0
8.0
6.0
4.0
2.0
0.0
0
5
10
15
20
25
30
35
Osmotic pressure difference (MPa)
NaCl 2
Fructose 2
NaCl 1
Fructose 1

1995). Water entering the support layer from the active layer would travel through the open pores as they provided the least resistance to flow compared to the membrane material. Therefore, the less porous the support layer was, the greater the resistance to water transfer. Secondly, the presence of the nylon mesh provided some resistance to water transfer by providing a physical discontinuity in the support material. A small pressure drop occurred across the support layer due to the resistances to flow in this layer. The third factor contributing to the resistance in the support layer was within the pores themselves. During normal operation the pores faced the OA solution and were thus filled with the OA solution. This essentially formed a stationary concentration boundary layer through which the water had to diffuse. The presence of the OA solution in the pores reduced the diffusion rate of the water out to the OA flow channel. When NaCl was used as the OA, the OA solution viscosities were lower and diffusion coefficients were higher, therefore, the diffusion rate across the support layer was greater than for fructose as OA.

With the membrane orientated with the active layer facing the OA channel, the water exiting the active layer had to diffuse across the boundary layer to reach the OA free-stream. The water flux rate across the boundary layer would be higher with NaCl OA solutions. The solution viscosities in NaCl solutions were considerably lower than in an iso-osmotic fructose solution, therefore, for the same flow channel velocity, the velocity boundary layers would be thinner with NaCl solutions as OA.

## 6.6. Solute transfer during DOC

As water was always used in the juice circuit, and water mass flow was always from the juice to the OA side, any solute moving against the water flow could readily be detected as a contaminant in the juice circuit. Prior to each run, after the equilibration period, there was no solute detected in the juice circuit. The water in the juice circuit was analysed after 45 minutes operation and the results are presented in Table 6.3. Under normal operation, the DOC membrane's rejection was on average 99.0% for NaCl and 99.9% for fructose. The mass of NaCl transferred across the membrane was four times greater than for fructose at the same osmotic pressure driving force and temperature. No sucrose was detected in the juice circuit when it was used as the OA.

The relationship between solute flux and solute molecular weight is shown in Figure 6.8. The DOC membranes reportedly had a molecular weight cut-off of 100 g $mol^{-1}$ (Beaudry and Lampi, 1990(a)). As the molecular weight's of sucrose (342.3 g $mol^{-1}$) and fructose (180.16 g $mol^{-1}$) are both greater than 100 g $mol^{-1}$ it was expected both would be rejected by the DOC membranes. One possible reason for the fructose transfer may be

**Table 6.3. Solute movement across the DOC membrane**

Module set up:
Juice circuit - water only, flow rate $4 \times 10^{-5}$ $m^3$ $s^{-1}$
OA circuit - fructose and NaCl solutions, flow rate $7 \times 10^{-6}$ $m^3$ $s^{-1}$
Mean operating temperatures (± *SEM* for $n = 3$) were: 10.0 ± 0.1°C; 20.0 ± 0.1°C;
40.0 ± 0.1°C
Small DOC module membrane area = 0.064 ± 0.024 $m^2$
Pilot plant DOC module membrane area = 0.33 ± 0.17 $m^2$

Mean values for solute movement across the membrane into the juice circuit after 45 minutes.

The standard error of means (*SEM*) were calculated from a pooled standard deviation from all individual results. The *SEM* was calculated for various values of *n*, where *n* was the number of replicate trials from which results were obtained.

% *R* = % *Rejection*

$$\%\ Rejection = \left(1 - \frac{Y_J}{Y_{OA}}\right) \times 100$$

$Y_J$ - concentration of solute in juice circuit after 45 minutes, (g (g solution)$^{-1}$
$Y_{OA}$ - concentration of solute in OA circuit, (g (g solution)$^{-1}$
(Sudak, 1990; Field, 1993)

| | | Active layer facing juice circuit : Small module | | | | Active layer facing OA circuit : Small module | | | | Active layer facing juice circuit : Pilot plant module | | | |
|---|---|---|---|---|---|---|---|---|---|---|---|---|---|
| Osmotic agent | Concentration (g (g solution)$^{-1}$) | Solute in JC (x $10^{-3}$ kg) | *SEM* (x $10^{-3}$) | *n* | %*R* | Solute in JC (x $10^{-3}$ kg) | *SEM* (x $10^{-3}$) | *n* | %*R* | Solute in JC (x $10^{-3}$ kg) | *SEM* (x $10^{-3}$) | *n* | %*R* |
| Fructose | 0.10 @ 10°C | 0 | 0.02 | 2 | 100.0 | | | | | | | | |
| | 0.10 @ 20°C | 0 | 0.02 | 3 | 100.0 | 0.06 | 0.02 | 2 | 99.81 | 0.25 | 0.02 | 3 | 99.74 |
| | 0.10 @ 40°C | 0.10 | 0.02 | 2 | 99.68 | | | | | | | | |
| | 0.35 @ 10°C | 0.02 | 0.02 | 2 | 99.98 | | | | | | | | |
| | 0.35 @ 20°C | 0.05 | 0.02 | 3 | 99.95 | 0.18 | 0.02 | 3 | 99.83 | 0.41 | 0.02 | 2 | 99.88 |
| | 0.35 @ 40°C | 0.18 | 0.02 | 2 | 99.84 | | | | | | | | |
| | 0.50 @ 10°C | 0.05 | 0.02 | 2 | 99.97 | | | | | | | | |
| | 0.50 @ 20°C | 0.08 | 0.01 | 9 | 99.95 | 0.14 | 0.01 | 4 | 99.91 | 0.50 | 0.02 | 2 | 99.89 |
| | 0.50 @ 40°C | 0.19 | 0.02 | 2 | 99.88 | | | | | | | | |
| | 0.70 @ 10°C | 0.08 | 0.02 | 3 | 99.97 | | | | | | | | |
| | 0.70 @ 20°C | 0.10 | 0.01 | 5 | 99.95 | 0.24 | 0.02 | 2 | 99.89 | 0.68 | 0.02 | 3 | 99.89 |
| | 0.70 @ 40°C | 0.21 | 0.02 | 2 | 99.90 | | | | | | | | |
| NaCl | 0.02 @ 20°C | 0.119 | 0.002 | 2 | 98.15 | 0.185 | 0.002 | 2 | 97.04 | | | | |
| | 0.10 @ 20°C | 0.286 | 0.002 | 3 | 99.11 | 0.500 | 0.002 | 2 | 98.43 | | | | |
| | 0.15 @ 20°C | 0.222 | 0.002 | 3 | 99.52 | 0.552 | 0.002 | 2 | 98.80 | | | | |
| | 0.23 @ 20°C | 0.403 | 0.002 | 2 | 99.44 | 0.841 | 0.002 | 2 | 98.81 | | | | |

**Figure 6.8. Solute flux rates of different molecular weight solutes in the small laboratory DOC module**

Module set up:

Membrane - active layer facing the juice circuit

Juice circuit - water only, 20.0 ± 0.1 °C, flow rate $4 \times 10^{-5}$ $m^3$ $s^{-1}$

OA circuit - sucrose, fructose and NaCl solutions, at 20.0 ± 0.1 °C, flow rate $7 \times 10^{-6}$ $m^3$ $s^{-1}$

Data points presented are means of experimentally determined data. The horizontal lines represent two standard errors about each mean.

□ - OA = NaCl,0.02 g (g solution)$^{-1}$, number of replicates ($n$) = 2

○ - OA = NaCl, 0.10 g (g solution)$^{-1}$, $n$ = 3

△ - OA = NaCl, 0.146 g (g solution)$^{-1}$, $n$ = 3

◊ - OA = NaCl, 0.22 g (g solution)$^{-1}$, $n$ = 2

■ - OA = Fructose, 0.10 g (g solution)$^{-1}$, $n$ = 3

● - OA = Fructose, 0.35 g (g solution)$^{-1}$, $n$ = 3

▲ - OA = Fructose, 0.49 g (g solution)$^{-1}$, $n$ = 9

◆ - OA = Fructose, 0.69 g (g solution)$^{-1}$, $n$ = 5

▼ - OA = Sucrose, 0.45 g (g solution)$^{-1}$, $n$ = 3

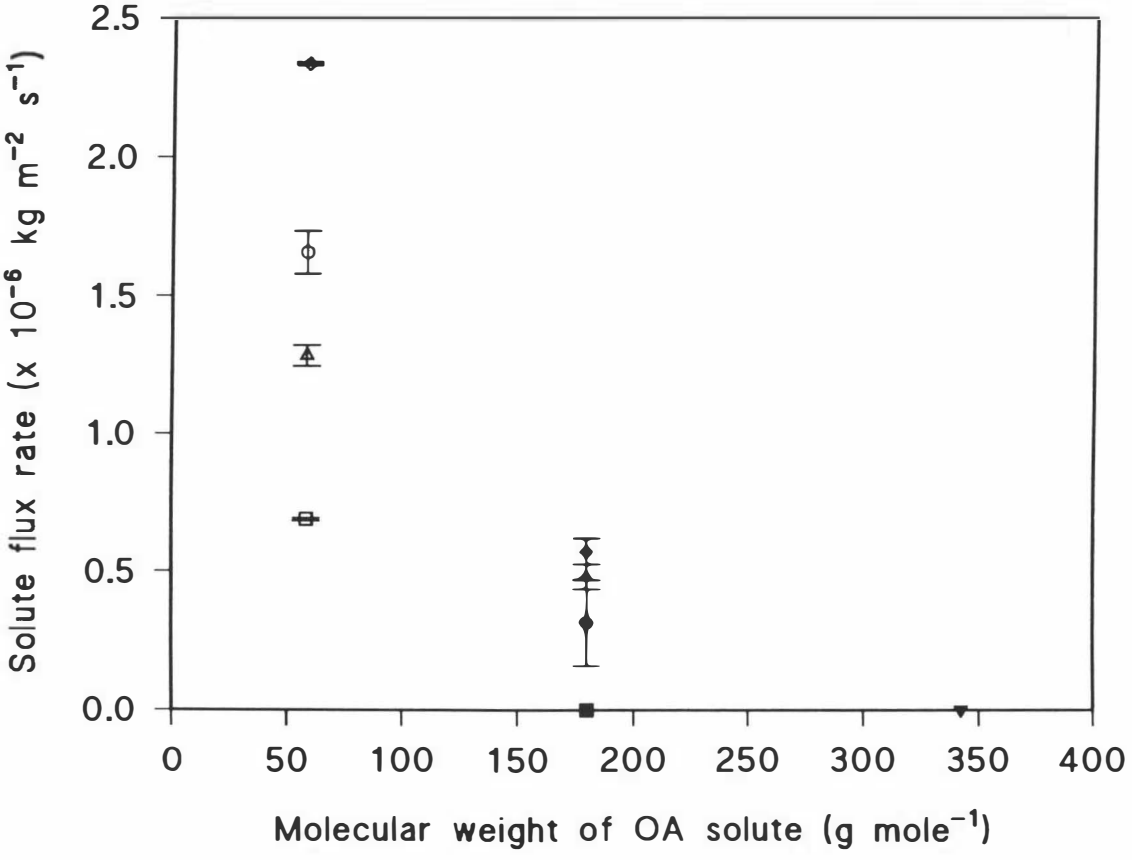
Solute flux rate (x $10^{-6}$ kg $m^{-2}$ $s^{-1}$)
2.5
2.0
1.5
1.0
0.5
0.0
0
50
100
150
200
250
300
350
400
Molecular weight of OA solute (g $mole^{-1}$)

that fructose has an affinity for the membrane polymer and may be partially soluble in the membrane. Cellulose acetate membranes provide good conditions for hydrogen bonding (Reid and Breton, 1959). Another possibility for its transfer may be that the true molecular weight rejection of the DOC membranes used was greater than 100 g $mol^{-1}$.

The amount of solute transferred across the membrane after 45 minutes was plotted against OA concentration and results are presented in Figure 6.9. Given these solute flux rates for 1 $m^2$ of membrane, 2 g of fructose or 8 g of NaCl would transfer across the membrane per hour at 20°C for the highest solute concentrations tested. The solute flux was directly proportional to the chemical potential gradient across the membrane which was the concentration gradient (Merton, 1966; Lonsdale, 1972).

When the membranes were reversed so the active layer was facing the OA circuit, solute molecules could diffuse without restraint to the active layer replacing water molecules coming across the membrane. With greater solute concentrations maintained at the interface between the active layer and the OA stream, the amount of solute transfer occurring was expected to increase. This was the case, as was shown in shown in Figure 6.9. The solute flux rate was approximately twice that observed for the normal membrane orientation. This increased solute flux rate corresponds to the water flux rates which were approximately two times greater with the active layer facing the OA circuit.

There was a definite linear relationship between temperature and solute flux at different OA concentrations as shown by the linear regression lines in Figure 6.10. With an increase in temperature there was the corresponding decrease in viscosity and increase in diffusion coefficients in the the OA solution. Higher diffusion coefficients resulted in the rapid diffusion of solute molecules to the membrane, therefore, maintaining the concentration gradient across the membrane and increasing the likelihood of solute transfer. Solute flux rate was found to be significantly different ($p < 0.02$) at the different OA concentrations shown in Figure 6.10 after comparison of the linear regression lines.

It has already been noted that water flux rate increased with an increase in OA concentration, increase in temperature, decrease in viscosity and with the reversal of the membrane orientation. It was found that solute flux rate increased for the same conditions as those responsible for increasing the water flux rate as shown in Figure 6.11. The solution-diffusion model for mass transfer across semi-permeable

**Figure 6.9. Solute flux rates as influenced by OA solute concentration**

Module set up:
Juice circuit - water only, at 20.0 ± 0.1 °C, flow rate $4 \times 10^{-5}$ $m^3$ $s^{-1}$
OA circuit - fructose and NaCl solutions, at 20.0 ± 0.1 °C, flow rate $7 \times 10^{-6}$ $m^3$ $s^{-1}$

(a) o - fructose, active membrane layer facing the juice circuit
Δ - fructose, active membrane layer facing the OA circuit

(b) o - NaCl, active membrane layer facing the juice circuit
Δ - NaCl, active membrane layer facing the OA circuit

Data points presented are means of experimentally determined data. The horizontal lines represent two standard errors about each mean.
Number of replicate trials:

| | Fructose (g g(solution)$^{-1}$) | | | | NaCl (g g(solution)$^{-1}$) | | | |
|---|---|---|---|---|---|---|---|---|
| Membrane | 0.10 | 0.35 | 0.49 | 0.69 | 0.02 | 0.10 | 0.15 | 0.23 |
| active facing juice | 3 | 3 | 9 | 5 | 2 | 3 | 2 | 3 |
| active facing OA | 2 | 3 | 3 | 2 | 2 | 2 | 2 | 2 |

Fructose determined by HPLC.
NaCl determined by increase in specific conductance.

(a)

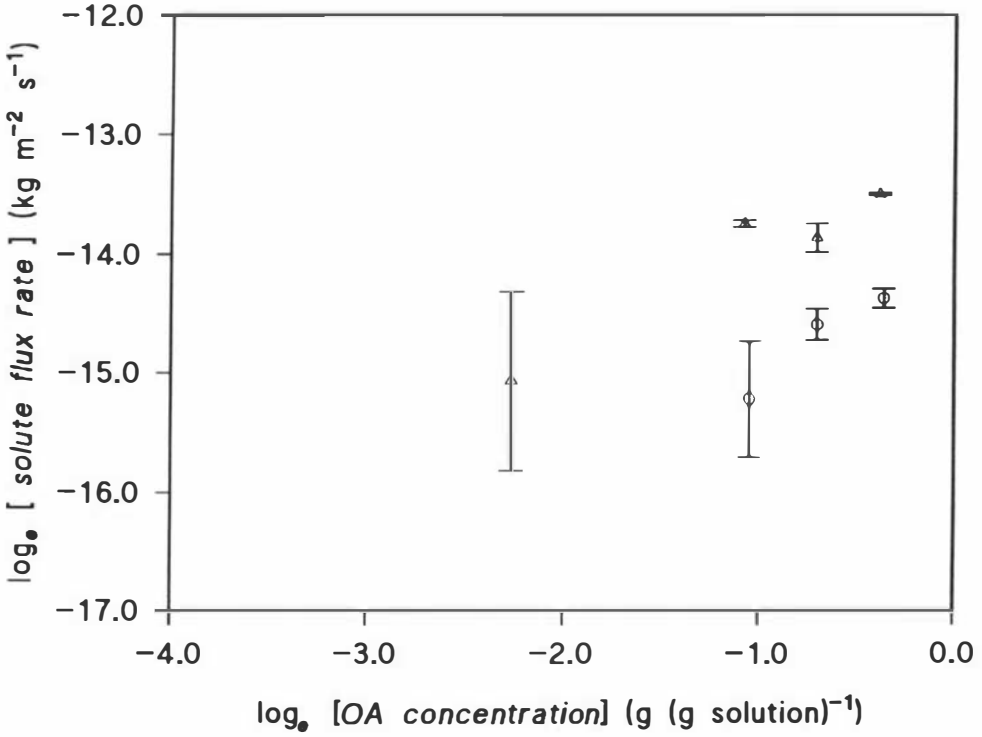
−12.0
−13.0
−14.0
−15.0
−16.0
−17.0
−4.0
−3.0
−2.0
−1.0
0.0
log$_e$ [ solute flux rate ] (kg m$^{-2}$ s$^{-1}$)
log$_e$ [OA concentration] (g (g solution)$^{-1}$)

(b)

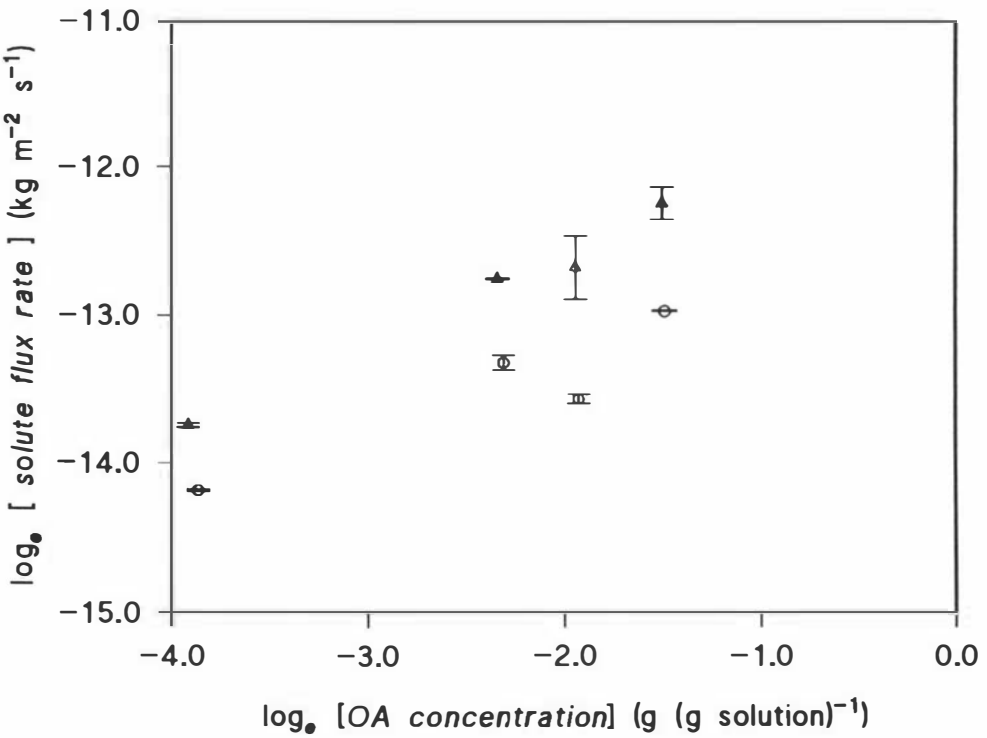
−11.0
−12.0
−13.0
−14.0
−15.0
−4.0
−3.0
−2.0
−1.0
0.0
log$_e$ [ solute flux rate ] (kg m$^{-2}$ s$^{-1}$)
log$_e$ [OA concentration] (g (g solution)$^{-1}$)

**Figure 6.10. Fructose solute flux rates as influenced by temperature**

Module set up:
Membrane - active layer facing the juice circuit
Juice circuit - water only, flow rate $4 \times 10^{-5}$ $m^3$ $s^{-1}$
OA circuit - fructose solutions, flow rate $7 \times 10^{-6}$ $m^3$ $s^{-1}$
Mean operating temperatures (± *SEM* for n = 3) were:
10.0 ± 0.1 °C ($\log_e$ = 5.64), 20.0 ± 0.1 °C ($\log_e$ = 5.68), 40.0 ± 0.1 °C ($\log_e$ = 5.75)

○ - 0.35 g (g solution)$^{-1}$
△ - 0.49 g (g solution)$^{-1}$
□ - 0.69 g (g solution)$^{-1}$

Data points presented are means of experimentally determined data. The horizontal lines represent two standard errors about each mean.
Number of replicate trials:

| Fructose concentration (g (g solution)$^{-1}$) | Operating temperature | | |
|---|---|---|---|
| | 10°C | 20°C | 40°C |
| 0.35 | 2 | 3 | 2 |
| 0.49 | 2 | 9 | 2 |
| 0.69 | 3 | 5 | 2 |

Linear regression was carried out using all individual data values. The equation of the lines were of the form

$$\log_e (\textit{solute flux rate}) = a \log_e (\textit{temperature}) - c$$

The value of the coefficients for each OA concentration are:

| | *a* | *c* |
|---|---|---|
| Fructose, 0.35 g (g solution)$^{-1}$ | 19.9 | 123.3 |
| Fructose, 0.49 g (g solution)$^{-1}$ | 14.1 | 89.8 |
| Fructose, 0.69 g (g solution)$^{-1}$ | 11.1 | 72.1 |

The $F_{statistic}$ calculated from the residual sum of squares of a single line fit to all the data and the residual sum of squares from the individual fitted lines was 4.0, degrees of freedom 4 and 24.

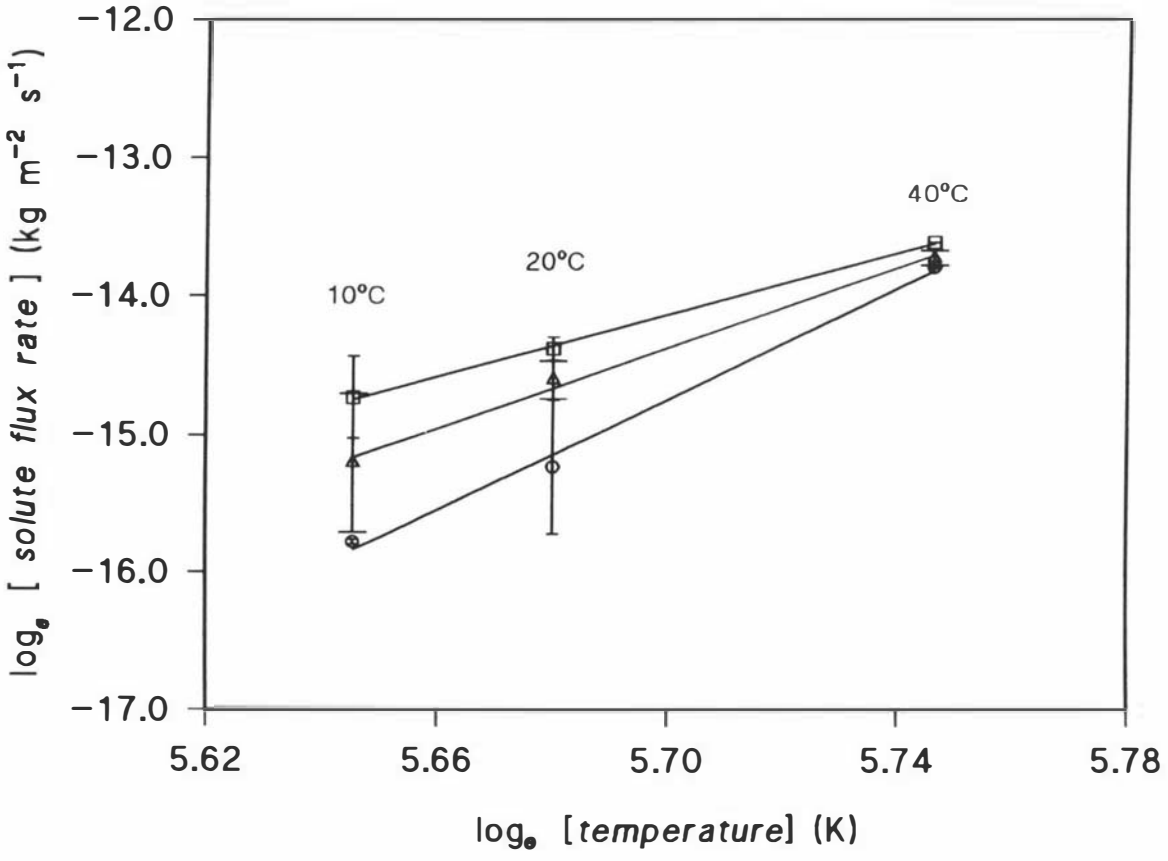
−12.0
−13.0
−14.0
−15.0
−16.0
−17.0
5.62
5.66
5.70
5.74
5.78
10°C
20°C
40°C
log$_e$ [ solute flux rate ] (kg m$^{-2}$ s$^{-1}$)
log$_e$ [temperature] (K)

**Figure 6.11. Solute and water flux rates in the small laboratory DOC module**

Module set up:

Membrane - active layer facing the juice circuit

Juice circuit - water only, at 20.0 ± 0.1 °C, flow rate $4 \times 10^{-5}$ $m^3$ $s^{-1}$

OA circuit - fructose and NaCl solutions, flow rate $7 \times 10^{-6}$ $m^3$ $s^{-1}$

Individual results from each trial presented.

(a) □ - fructose 0.69 g (g solution)$^{-1}$, at 10.0 ± 0.1 °C

△ - fructose 0.69 g (g solution)$^{-1}$, at 20.0 ± 0.1 °C

▽ - fructose 0.69 g (g solution)$^{-1}$, at 40.0 ± 0.1 °C

◇ - fructose 0.49 g (g solution)$^{-1}$, at 10.0 ± 0.1 °C

○ - fructose 0.49 g (g solution)$^{-1}$, at 20.0 ± 0.1 °C

■ - fructose 0.49 g (g solution)$^{-1}$, at 40.0 ± 0.1 °C

▲ - fructose 0.35 g (g solution)$^{-1}$, at 10.0 ± 0.1 °C

▼ - fructose 0.35 g (g solution)$^{-1}$, at 20.0 ± 0.1 °C

◆ - fructose 0.35 g (g solution)$^{-1}$, at 40.0 ± 0.1 °C

◦ - fructose 0.10 g (g solution)$^{-1}$, at 10.0, 20.0 and 40.0 ± 0.1 °C

(b) □ - NaCl 0.02 g (g solution)$^{-1}$, at 20.0 ± 0.1 °C

△ - NaCl 0.10 g (g solution)$^{-1}$, at 20.0 ± 0.1 °C

▽ - NaCl 0.15 g (g solution)$^{-1}$, at 20.0 ± 0.1 °C

◇ - NaCl 0.22 g (g solution)$^{-1}$, at 20.0 ± 0.1 °C

(a)

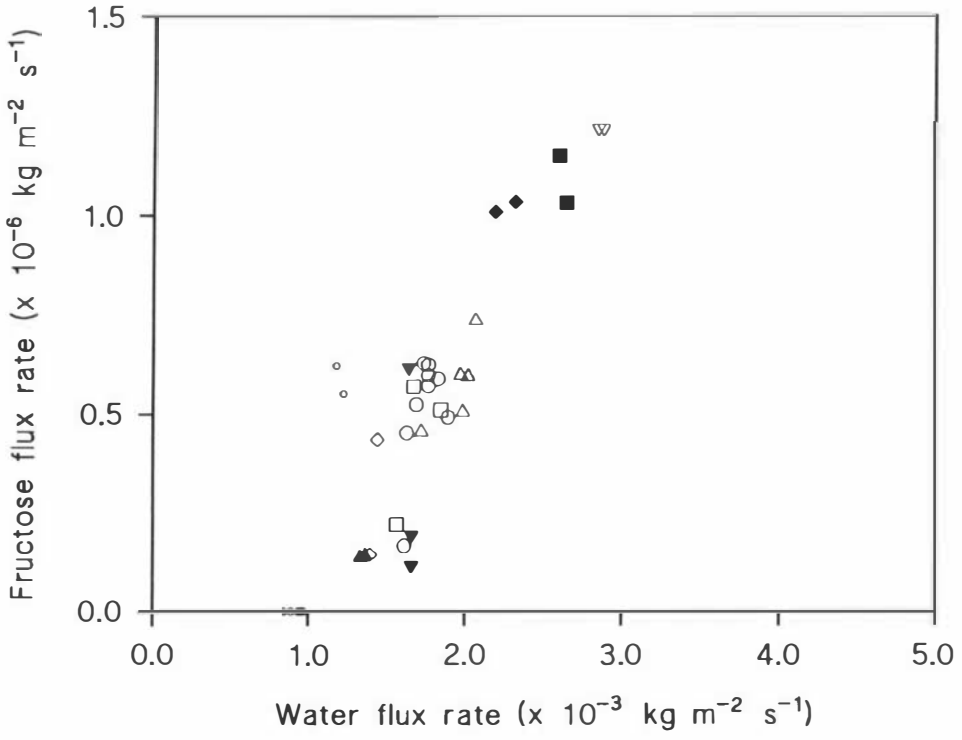
Fructose flux rate (x 10⁻⁶ kg m⁻² s⁻¹)
1.5
1.0
0.5
0.0
0.0
1.0
2.0
3.0
4.0
5.0
Water flux rate (x 10⁻³ kg m⁻² s⁻¹)

(b)

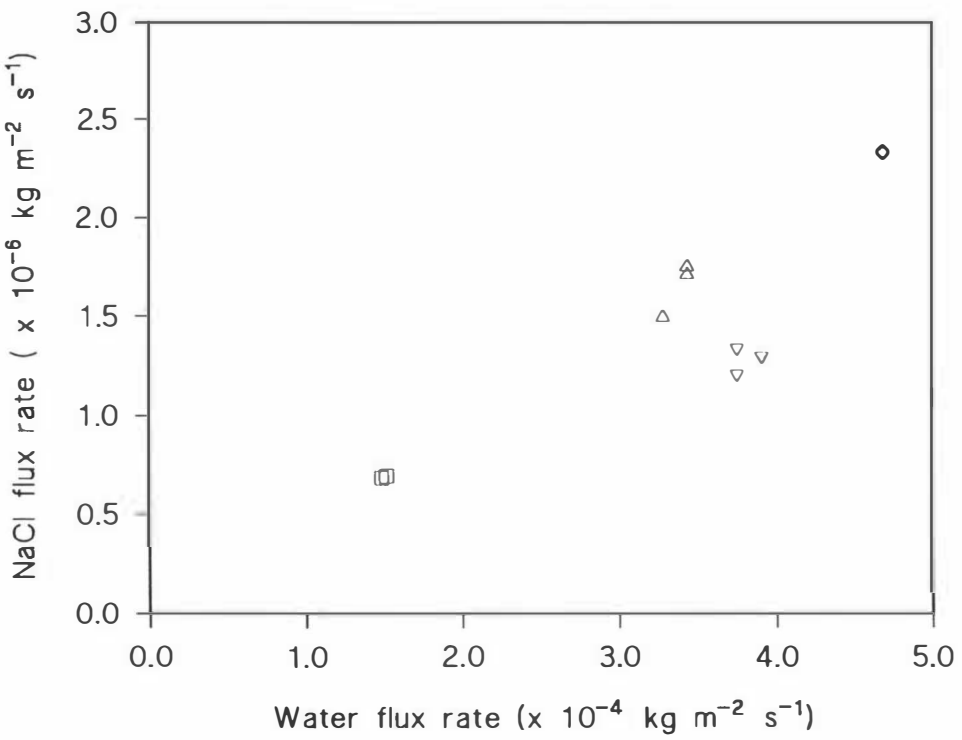
NaCl flux rate ( x 10⁻⁶ kg m⁻² s⁻¹)
3.0
2.5
2.0
1.5
1.0
0.5
0.0
0.0
1.0
2.0
3.0
4.0
5.0
Water flux rate (x 10⁻⁴ kg m⁻² s⁻¹)

membranes in RO processes assumes no coupling between solute and solvent flows (Rautenbach and Albrecht, 1989; Cheryan and Nichols, 1992). The driving force for solute and water transfer is a concentration and a pressure gradient, respectively. Whereas, in DOC the solute and water fluxes appeared to be coupled as the driving force for transfer of both solutes and water was the concentration gradient or osmotic pressure gradient across the membrane (Rautenbach and Albrecht, 1989).

Raspberry juice was concentrated with DOC, using high fructose corn syrup as the OA. Stable carbon isotope analysis of the raspberry juice concentrate showed no transfer of OA sugars through the membrane (Wrolstad et al., 1993). The membranes used by Wrolstad et al. (1993) were a different type of DOC membrane to the Type B membranes used during this research.

## 6.7. Membrane constant '*C*' for solvent transfer across active membrane layer

Based on the solution-diffusion model for mass transfer across the active layer of the membrane, the membrane constant $C$, is the water flux characteristic membrane constant which must be determined from experimental data (Rautenbach and Albrecht, 1989). The constant gives a measure of the resistance of the membrane active layer to transfer of the solvent, in this case water. It is specific to the membrane and the solutions used to determined its value. The membrane constant will differ for different membrane materials, methods of construction and membrane thicknesses. The value of the membrane constant is dependent on temperature and operating hydraulic pressure (Rautenbach and Albrecht, 1989). As the hydraulic pressure over the membranes was relatively small and constant, hydraulic pressure was not considered to affect the value of the membrane constant for DOC.

To determine the membrane constant for the DOC active membrane layer for fructose as the OA, the slope of the line for ideal water flux rates vs. increasing osmotic pressure was estimated. Ideal water flux rates are obtained from a DOC system with active membrane layer only and no boundary layers in either flow channel.

For the membrane orientated with the active layer facing the OA (reverse orientation), the gradient of a line from zero to the water flux rate measured at 0.1 g (g solution)$^{-1}$ fructose OA (1.5 MPa) was used as an estimate of the gradient of an ideal water flux rate line. For 0.1 g (g solution)$^{-1}$ fructose solution, the diffusion coefficient was calculated to be $5.1 \times 10^{-10}$ m$^2$ s$^{-1}$ at 20°C [Figure 4.11]. The diffusion coefficient for infinite dilution ($D^o_{AB}$) for fructose solutions was $6.0 \times 10^{-10}$ m$^2$ s$^{-1}$ at 20°C [Table 4.5].

A solution at infinite dilution is virtually water, therefore, the boundary layers would not be significant and there would be no resistance to water transfer into the OA free-stream. Because these two diffusion coefficients were very similar it was concluded that the diffusion rate in a 0.1 g (g solution)$^{-1}$ fructose solution would also be very similar to the diffusion rate in a fructose solution at infinite dilution. Therefore, for membranes in the reverse orientation and using 0.1 g (g solution)$^{-1}$ fructose as OA, the water flux rate was considered to be the same for an ideal system.

For NaCl as the OA, the gradient of the ideal water flux rate line was determined from a line between zero and the water flux rate measured at 0.02 g (g solution)$^{-1}$ NaCl solution when membranes were in the reverse orientation. For the membrane constant at 10 and 40°C the gradients of the lines for the ideal water flux rate were estimated by assuming the gradients varied with temperature at the same rate as observed for normal membrane orientation. No data was obtained at different temperatures for reversed membrane orientation.

The membrane constants for the active membrane layer determined for fructose and NaCl as OAs, water in the juice circuit and Osmotek Type B DOC membranes are presented in Table 6.4. The hydraulic pressure difference across the membrane was less than 20 kPa.

**Table 6.4. Membrane constants for the active layer of DOC membranes**

| OA solution | Temperature (°C) | Membrane constant[a], $C$, (kg m$^{-2}$ s$^{-1}$ Pa$^{-1}$) |
|---|---|---|
| Fructose | 10 | $1.3 \times 10^{-9}$ |
| Fructose | 20 | $1.4 \times 10^{-9}$ |
| Fructose | 40 | $1.6 \times 10^{-9}$ |
| NaCl | 20 | $1.5 \times 10^{-9}$ |

a. Based on flux rates obtained with membranes in reverse orientation and Osmotek Type B DOC membranes.

A number of values for $C$ have been reported for RO systems with a number of different membranes and solutions (Sourirajan, 1970; Rautenbach and Albrecht, 1989). The values in Table 6.4 were of the same order of magnitude as those reported for cellulose acetate

based RO membranes. No membrane constants have been published for DOC membranes.

## 6.8. Resistances to water transfer in the DOC module

It is clear from the results presented in this chapter that there are multiple resistances to water flow from the juice to the OA free-stream. A schematic view of these resistances is shown in Figure 6.12. If water only was kept in the juice circuit, as was done for these trials, it was reasonable to assume that there was no concentration boundary layer on the juice circuit side of the membrane. Operating temperatures were kept constant, therefore, there were no temperature boundary layers on either side of the membrane.

When the membranes were orientated with the active layer facing the juice circuit, water from the juice circuit diffused through the active membrane layer (resistance $R_1$), where the resistance was determined by the membrane structure and was estimated by the membrane constant, $C$. The water then diffused through the OA solution trapped and stationary in the support layer pores (resistance $R_2$). The support layer was essentially a stationary concentration boundary layer. The water then diffused across the velocity and concentration boundary layers in the OA flow channel (resistance $R_3$), before reaching the OA free-stream. The resistance in the support layer ($R_2$) was determined by the nature of the support layer (porosity and tortuosity) and by the solution properties of the OA forming the stationary concentration boundary layer. The resistance in the velocity and concentration boundary layers ($R_3$) was dependent on flow dynamics and OA solution properties.

When the membranes were reversed so the active layer was facing the OA circuit there was no stationary trapped layer of OA within the porous support layer. Resistance due to any solute transfer across the membrane was considered to be negligible. Thus water diffused through the support layer unhindered (resistance $R_2 = 0$). The resistances to water transfer in this orientation were in the active layer ($R_1$) and the OA channel velocity and concentration boundary layers ($R_3$). This was consistent with experimental data and the observations of Rautenbach and Albrecht (1989).

**Figure 6.12. Membrane orientation and resistances**

(a) Active layer facing towards the juice circuit
(b) Active layer facing towards the OA circuit

am - active membrane layer
sm - support membrane layer
bl - boundary layer in OA channel
$R_1$ - resistance in active layer
$R_2$ - resistance in support layer
$R_3$ - resistance in boundary layer

Not drawn to scale

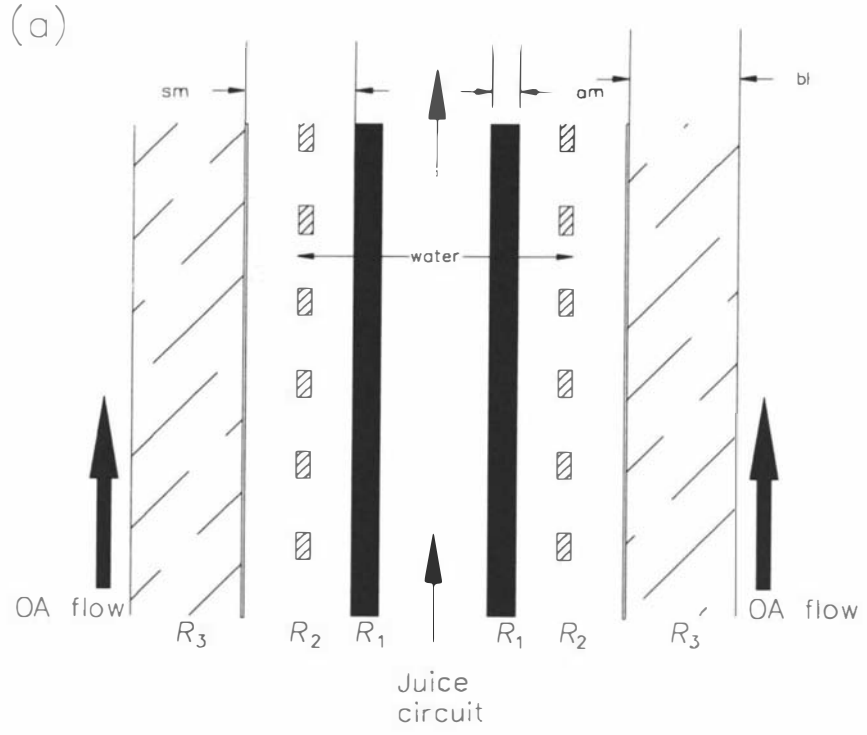
(a)
sm
am
bl
water
OA flow
OA flow
$R_3$
$R_2$
$R_1$
$R_1$
$R_2$
$R_3'$
Juice
circuit

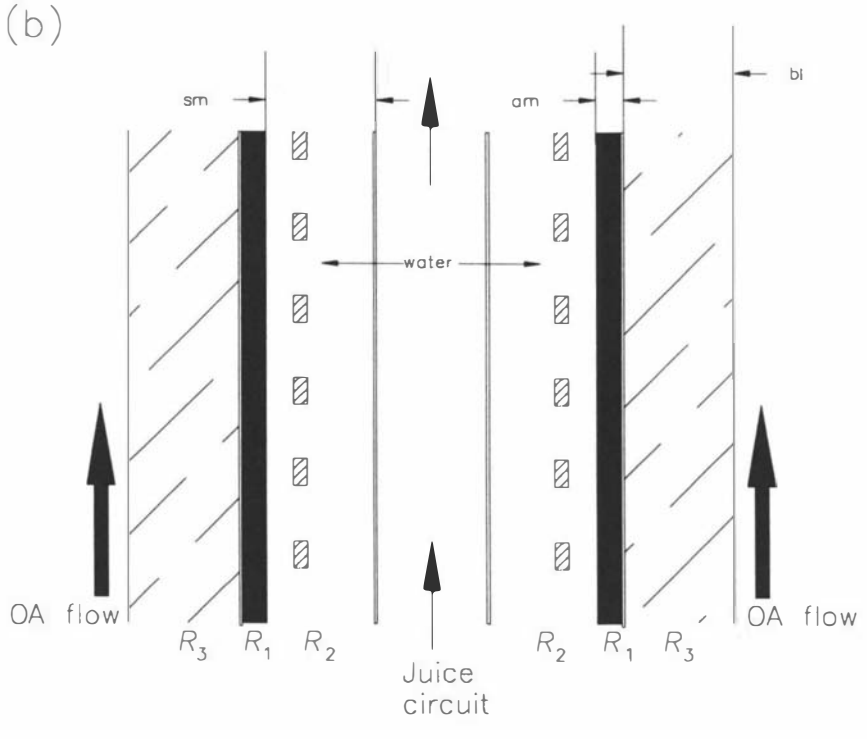
(b)
sm
am
bl
water
OA flow
OA flow
$R_3$
$R_1$
$R_2$
$R_2$
$R_1$
$R_3'$
Juice
circuit

The water flux rate in an ideal system was determined by the osmotic pressure difference across the membrane,

$$m_w = C\Delta\pi \tag{6.1}$$

The water flux rate in the DOC system with normal membrane orientation was related to the osmotic pressure driving force and the resistances, $R_1$, $R_2$ and $R_3$, by the following equation:

$$m_w = \frac{\Delta\pi}{(R_1 + R_2 + R_3)} \tag{6.2}$$

The resistance in the active layer ($R_1$) was estimated by the membrane constant [see 6.7], hence, $R_1 \approx 1/C$. $R_1$ was constant for all OA solution concentrations, for each solute type and each temperature. $\Delta\pi$ is the osmotic pressure difference between the two bulk free-streams. The water flux rate obtained with membranes reversed was related to resistances $R_1$ and $R_3$ by the following equation:

$$m_w = \frac{\Delta\pi}{(R_1 + R_3)} \tag{6.3}$$

$R_3$ was determined using this equation for different values of $\Delta\pi$. Therefore, Equation (6.2) was solved for $R_2$ using the water flux rate obtained with membranes orientated for normal operation. Then the total resistance to transfer of water for this membrane orientation was calculated by summing the resistances ($R_1 + R_2 + R_3$). The percentage contribution of each resistance to the total resistance was calculated for different OA concentrations and are presented in Table 6.5 for normal membrane orientation.

For 0.1 g (g solution)$^{-1}$ fructose and 0.02 g (g solution)$^{-1}$ NaCl as OA the velocity and concentration boundary layers ($R_3$) contributed to only 1 and 4% of the total resistance to water flux, respectively. Therefore, the assumption made in Section 6.7 to estimate the membrane constants, that the boundary layer resistance at these concentrations was small, was confirmed.

The percentage resistance contributed by each layer to the total resistance was dependent on the OA concentration and the type of OA. The absolute resistance in the active layer was constant for all concentrations but its contribution to the total resistance decreased with increasing OA concentration. With increased OA concentrations the water molecules must overcome the added resistance to flow contributed by the changing solution properties, increased solution viscosity and lower diffusion coefficients. The rate of diffusion across the support layer and boundary layers ($R_2$ and $R_3$) controls the water flux rate into the OA free-stream.

**Table 6.5. Contributions of individual resistances**

| OA solution | OA concentration (g (g solution)$^{-1}$) | $\%R_1$[a] | $\%R_2$[b] | $\%R_3$[c] |
|---|---|---|---|---|
| Fructose | 0.10 | 44 | 55 | 1 |
| | 0.35 | 15 | 62 | 23 |
| | 0.50 | 9 | 64 | 27 |
| | 0.70 | 5 | 69 | 26 |
| NaCl | 0.02 | 64 | 32 | 4 |
| | 0.10 | 25 | 41 | 34 |
| | 0.15 | 17 | 44 | 39 |
| | 0.23 | 11 | 43 | 46 |

a. Resistance in the active membrane layer (determined for normal membrane orientation from experimental data).

b. Resistance in the porous support layer (determined for normal membrane orientation from experimental data).

c. Resistance in the velocity boundary layer (determined for normal membrane orientation from experimental data).

When fructose was used as the OA, the support layer contributed the greatest resistance to transfer of water at all concentrations. At concentrations of 0.35 g (g solution)$^{-1}$ fructose and above, the support layer contributed 65% of all the resistances and the velocity and concentration boundary layers in the OA channel contributed approximately 25% of the total resistance to water transfer. When NaCl was used as the OA, at concentrations of 0.1 g (g solution)$^{-1}$ NaCl and above, the amount of resistance encountered in the support layer (approximately 43%), and velocity and concentration boundary layers (approximately 40%) were similar.

## 6.9. Actual water flux rate across membrane

Although the DOC membranes were heterogenous the osmotic transfer of water occurred only across the active layer of the membrane. This layer was essentially homogeneous and non-porous. The water flux rate across the active layer was proportional to the osmotic pressure difference across this layer. The true osmotic pressure difference was not the difference between the bulk concentrations in the juice (water) and OA circuits. The concentration at the surface of the active layer facing the juice circuit was assumed

to be equal to water. On the other side of the active layer the concentration was much less than that of the bulk OA free-stream concentration.

With the membranes orientated for normal operation, the mechanism driving the transfer of water across the support layer was different to that across the active layer, being a combination of a concentration gradient and a small pressure drop across it. Diffusion, governed by Fick's law, took place in the OA solution trapped in the support layer pores and voids (Bird et al., 1960). A small pressure drop across the support layer developed because the water molecules travelled from a very dense membrane layer, of relatively high resistance, into the open OA flow channel, of relatively low resistance. The mass transfer across the porous support layer due to the pressure gradient can be described by Darcy's law for flow through porous media (Bird et al., 1960; Vennard and Street, 1982).

Within the velocity and concentration boundary layers the transport is in the direction normal to the membrane due primarily to diffusion, convection and transference (Jonsson and Boesen, 1984).

In order to model the DOC system and to determine the rate of water transfer from the juice circuit into the OA free stream, the concentration gradients across the three layers need to be determined. The only concentrations which were measured directly were that in the juice circuit and that in the OA bulk free-stream. The thickness of the different membrane layers was measured, the membrane constant was determined from experimental data, the porosity of the support layer was estimated (Herron, 1995) and the channel dimensions were measured. The unknowns to be determined were the boundary layer thickness, the concentration at the interface between different layers and the concentration gradients across the different layers.

# CHAPTER 7
# WATER FLUX RATES IN THE PILOT PLANT DOC MODULE

A pilot plant DOC module supplied by Osmotek Inc., Oregon, was tested in the USA and water flux rates were compared to those obtained in the small laboratory DOC module.

## 7.1. Scaling up water flux rates to the pilot plant DOC module

The pilot plant DOC module had approximately five times the membrane area of the small laboratory DOC module. Flow velocities in the juice and OA circuits were adjusted to be the same as the small laboratory DOC unit.

The water flux rates determined at 20°C for both DOC modules are presented in Figure 7.1. There was no significant difference in flux rates between the two modules. Therefore, results obtained on the small module were good estimates of flux rates in a pilot plant DOC module of the same design.

The channel geometry in the two modules was the same. The main differences between the two modules was: (1) the pilot plant module had an increased membrane area and; (2) the static head in the pilot plant module was greater and the inlet hydraulic pressures were slightly higher. It appears these differences did not have a significant effect on the water flux rates.

**Figure 7.1. Water flux rates in the small laboratory and pilot plant DOC modules**

Module set up:
Juice circuit - water, at 20.0 ± 0.1 °C, flow rate $4 \times 10^{-5}$ $m^3$ $s^{-1}$
OA circuit - fructose solutions, 20.0 ± 0.1 °C, flow rate $7 \times 10^{-6}$ $m^3$ $s^{-1}$

o - Data points represent mean water flux rates determined on small laboratory DOC module. The horizontal lines represent two standard errors about each mean. The standard error of the means (*SEM*) = 4.6 x $10^{-5}$ for $n$ = 3.

Δ - Data points represent mean water flux rates determined on pilot plant DOC module. The horizontal lines represent two standard errors about each mean. The standard error of the means (*SEM*) = 4.6 x $10^{-5}$ for $n$ = 3.

Number of replicate trials:

| Approximate OA concentration (g (g solution)$^{-1}$) | $\Delta\pi^a$ (MPa) | Module size | |
|---|---|---|---|
| | | Small | Pilot plant |
| 0.10 | 1.5 | 3 | 3 |
| 0.35 | 8.0 | 3 | 2 |
| 0.50 | 15.0 | 11 | 2 |
| 0.70 | 30.0 | 5 | 3 |

a. Osmotic pressure difference, $\Delta\pi = (\pi_{OA} - \pi_J)$ and $\pi_J = 0$.

A best fit response curve was fitted using non linear least squares regression [see 3.3.1 and Figure 6.2]. The value of the coefficients for the single curve are:

| | *a* | *b* | *c* |
|---|---|---|---|
| Fructose, single curve for both modules | 0.0012 | 0.74 | 0.93 |

The $F_{statistic}$ calculated from the error mean square of a single curve fit to all the data and the error mean square from the individual fits was 6.9, degrees of freedom 3, 2 ; this is not significant at p = 0.05.

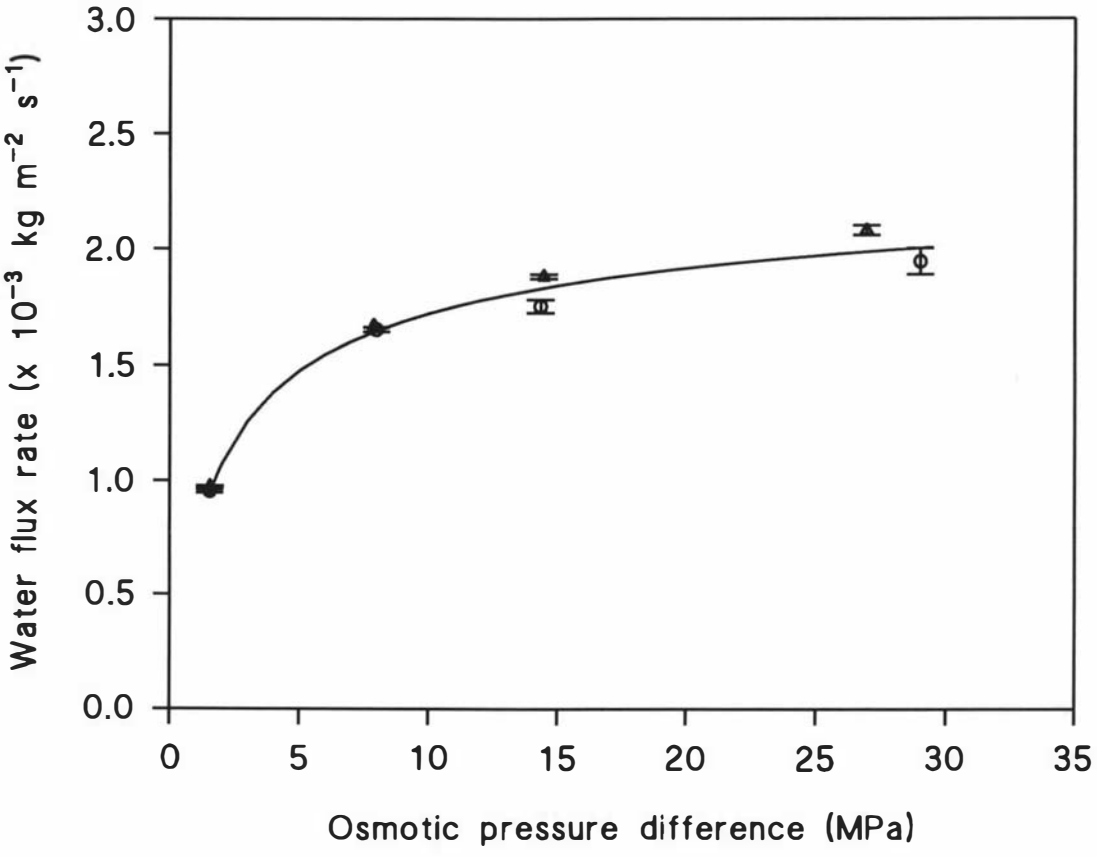
Water flux rate (x $10^{-3}$ kg $m^{-2}$ $s^{-1}$)
3.0
2.5
2.0
1.5
1.0
0.5
0.0
0
5
10
15
20
25
30
35
Osmotic pressure difference (MPa)

# CHAPTER 8
# MATHEMATICAL MODEL FOR DOC

The DOC process was mathematically modelled to describe and understand the overall transport processes involved, and the relationships between water flux, boundary concentrations and resistances. The mass transfer characteristics of the DOC system in relation to the solution properties and the fluid mechanics in the system were also defined. This DOC system has not been thoroughly modelled and tested with extensive experimental data.

The mathematical model for the DOC process was developed over a number of stages. At the end of each stage the validity of earlier assumptions was evaluated. A summary of the stages in the development of the model is presented. A detailed description of the final model found to describe the DOC process is presented, including its derivation and testing.

## 8.1. Development of the unsteady state DOC model

The DOC process was first modelled as an unsteady state process over the entire DOC system, including module, juice feed and OA vessels, juice and OA circuits and pumps. This model took into account changes in concentration on both juice and OA circuits over time. Concentration changes due to convection, at different positions up the DOC module and around the unit, were determined. The contribution to concentration changes due to diffusion were neglected as being small. It was assumed in this initial model that the concentration of the solution in the juice circuit would increase in concentration after one pass through the module.

The water flux rate across the membrane was initially assumed to increase linearly with the osmotic pressure difference between the two bulk solutions in the juice and OA circuits. The asymmetric structure of the membrane and the boundary layers in the OA flow channel were neither considered nor included in this model. This model assumed an homogenous membrane with perfect mixing of solutions on each side. The equations for the unsteady state model are presented in Appendix A2. The water mass flux rate was not linearly related to the osmotic pressure driving force between the two bulk solutions. The assumption that perfect mixing was occurring on both sides of the membranes was therefore found to be invalid.

## 8.2. Development of the steady state DOC model

### 8.2.1. Water flux rate across the active layer

A schematic diagram of the DOC membrane in the three possible membrane orientations, with concentration gradients and boundaries marked is presented in Figure 8.1.

The theoretical model used to describe the water flux rate across the membrane during DOC was based on the solution-diffusion model for mass transfer across an homogeneous membrane (Lee et al., 1981; Rautenbach and Albrecht, 1989).

Water flux rate across the active layer is defined by

$$m_w = C\,[\pi(Y_1) - \pi(0)] = C\pi(Y_1) \qquad (8.1)$$

$m_w$ - water mass flux rate, kg $m^{-2}$ $s^{-1}$

$\pi(Y_1)$ - osmotic pressure of solution $Y_1$, at the surface of the active layer, on the opposite side to the juice circuit, Pa

$\pi(0)$ - osmotic pressure of water in the juice circuit = 0, Pa

$C$ - membrane constant, kg $m^{-2}$ $s^{-1}$ $Pa^{-1}$

To estimate the actual water flux rate across the active layer the concentration $Y_1$ was determined mathematically.

### 8.2.2. Water flux rate across the support layer

When the membranes were configured for normal operation with the active layer facing the juice circuit, water exiting the active layer had to travel across the support layer to reach the OA flow channel and OA free-stream. The equations describing mass flux rates and concentration gradients across the support layer were derived. These equations are applicable to the support layer in Cases 1 and 2 shown in Figure 8.1. The water flux rate across the support layer was determined from the concentration and pressure gradients across it. It can be shown mathematically that the hydraulic pressure gradient can be eliminated, thereby, leaving only the concentration gradient across the support layer to be determined for the water flux rate.

The water flux rate exiting the active layer can be described by Equation (8.1). The water flux rate through the support layer is

**Figure 8.1. DOC membrane and OA channel boundary layer**

(a) - Active layer facing the juice circuit, support layer facing the OA circuit and boundary layer present in OA flow channel (Case 1).

(b) - Active layer facing the juice circuit, support layer facing the OA circuit but with no boundary layer in the OA flow channel (Case 2)

(c) - Active layer facing the OA circuit, support layer facing the juice circuit and boundary layer present in OA flow channel, (Case 3).

am - active membrane layer
sm - support membrane layer
bl - boundary layer in OA channel
$Y_1$ - concentration at surface of active layer (OA side) which determines the osmotic pressure driving force across the layer, g (g solution)$^{-1}$
$Y_0$ - concentration at interface between support layer and velocity boundary layer, g (g solution)$^{-1}$
$Y_C$ - concentration of OA in OA channel free-stream, g (g solution)$^{-1}$
$d_a$ - thickness of active membrane layer
$d_s$ - thickness of support membrane layer
$\delta$ - thickness of velocity boundary layer
$x$ - direction parallel along membrane
$y$ - direction perpendicular to membrane
$u$ - velocity in $x$ direction, m s$^{-1}$
$v$ - velocity in $y$ direction, m s$^{-1}$

(a)

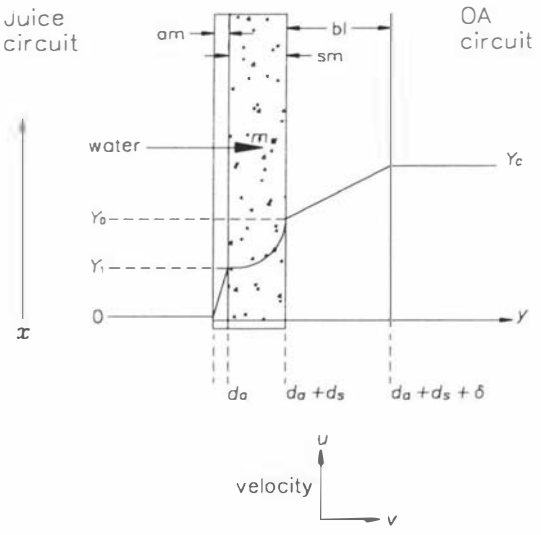
Juice circuit
am
bl
sm
OA circuit
water
$m_w$
$Y_c$
$Y_0$
$Y_1$
0
y
x
$d_a$
$d_a + d_s$
$d_a + d_s + \delta$
u
velocity
v

(b)

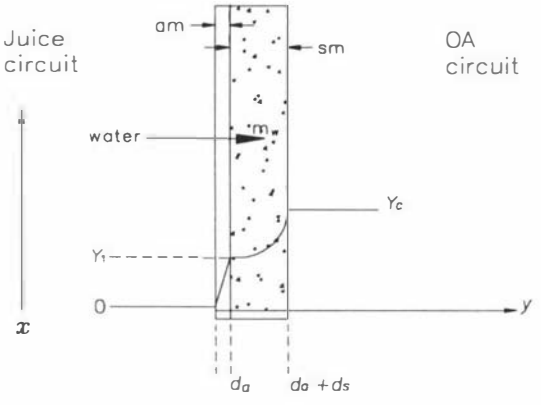
Juice circuit
am
sm
OA circuit
water
$m_w$
$Y_c$
$Y_1$
0
y
x
$d_a$
$d_a + d_s$

(c)

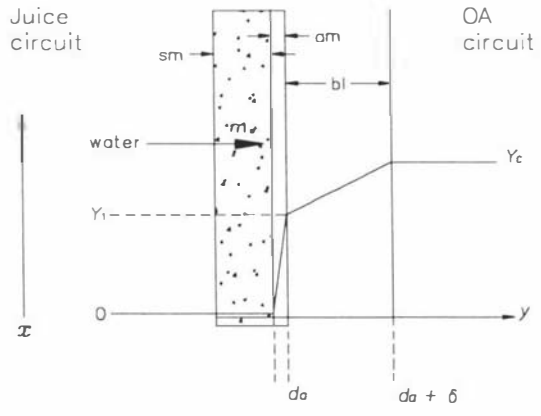
Juice circuit
sm
am
bl
OA circuit
water
$m_w$
$Y_c$
$Y_1$
0
y
x
$d_a$
$d_a + \delta$

$$m_w = -\rho(Y)\frac{\varepsilon D_{wf}(Y)}{\tau}\frac{d}{dy}(1 - Y) - (1 - Y)\rho(Y)\frac{k_p}{\mu(Y)}\frac{dp}{dy} \qquad (8.2)$$

*diffusion flux* *Darcy's law*

$\varepsilon$ - porosity of membrane support layer

$\tau$ - tortuosity of membrane support layer

$k_p$ - permeability of porous media, $m^2$

$p$ - hydraulic pressure, Pa

$D_{wf}(Y)$ - binary diffusion coefficient of water in an aqueous fructose solution at concentration $Y$, $m^2\ s^{-1}$

The measured solute flux rate through the membrane was relatively small compared to the water flux rate. Thus for the purposes of modelling the DOC system, to determine the water flux rate, the solute flux rate was assumed to be negligible. Therefore, the solute flux rate, in this case the fructose flux rate, through the support layer is:

$$m_f = -\rho(Y)\frac{\varepsilon D_{fw}(Y)}{\tau}\frac{dY}{dy} - Y\rho(Y)\frac{k_p}{\mu(Y)}\frac{dp}{dy} = 0 \qquad (8.3)$$

$$\rightarrow \quad \rho(Y)\frac{k_p}{\mu(Y)}\frac{dp}{dy} = -\rho(Y)\frac{1}{Y}\frac{\varepsilon D_{fw}(Y)}{\tau}\frac{dY}{dy} \qquad (8.4)$$

$m_f$ - fructose mass flux rate, kg $m^{-2}\ s^{-1}$

$D_{fw}(Y)$ - binary diffusion coefficient of fructose in an aqueous fructose solution at concentration $Y$, $m^2\ s^{-1}$

Substituting Equation (8.4) into Equation (8.2) gives

$$m_w = \rho(Y)\frac{\varepsilon D_{wf}(Y)}{\tau}\frac{dY}{dy} + \frac{1 - Y}{Y}\rho(Y)\frac{\varepsilon D_{fw}(Y)}{\tau}\frac{dY}{dy} \qquad (8.5)$$

$$\rightarrow \quad m_w = \rho(Y)\frac{\varepsilon}{\tau}\left[D_{wf}(Y) + \frac{1 - Y}{Y}D_{fw}(Y)\right]\frac{dY}{dy} \qquad (8.6)$$

as $D_{wf}(Y) = D_{fw}(Y)$, therefore,

$$m_w = \frac{\varepsilon}{\tau}\rho(Y)D_{fw}(Y)\left[1 + \frac{1 - Y}{Y}\right]\frac{dY}{dy} \qquad (8.7)$$

$$If \quad D_e(Y) = \frac{\varepsilon}{\tau}D_{fw}(Y) \quad then \qquad (8.8)$$

$$m_w = \rho(Y)\, D_e(Y)\, \frac{1}{Y}\frac{dY}{dy} \tag{8.9}$$

This equation describes the water flux rate in the support layer for the membranes orientated for normal operation. By integrating Equation (8.9) the concentration gradient across the support layer can be determined.

At steady state, within the support layer $D_{fw}(Y) \approx D_{fw}(Y_1) = \text{constant}$
$\rho(Y) \approx \rho(Y_1) = \text{constant}$

Integrating across the support layer

$$\rho(Y_1)\, D_e(Y_1)\, \frac{1}{Y}\frac{dY}{dy} = m_w \tag{8.10}$$

$$\left[\rho(Y_1) D_e(Y_1) \log_e Y\right]_{Y_1}^{Y_0} = \left[m_w y\right]_{d_s}^{d_s + d_s} \tag{8.11}$$

$$\rho(Y_1) D_e(Y_1) \log_e \frac{Y_0}{Y_1} = m_w d_s \tag{8.12}$$

$$\log_e \frac{Y_0}{Y_1} = \frac{m_w d_s}{\rho(Y_1) D_e(Y_1)} \tag{8.13}$$

$$Y_1 = Y_0 \exp\left( - \frac{m_w d_s}{\rho(Y_1) D_e(Y_1)} \right) \tag{8.14}$$

and substituting in Equation (8.1) for $m_w$ gives

$$Y_1 = Y_0 \exp\left( - \frac{C\, \pi(Y_1)\, d_s}{\rho(Y_1)\, D_e(Y_1)} \right) \tag{8.15}$$

This equation describes the concentration gradient across the support layer and was used to determine the concentration $Y_1$ at the interface between the active layer and the support layer of the membrane when membranes were orientated for Cases 1 or 2. For Case 1 the concentration $Y_0$ at the interface between the support layer and the velocity boundary layer must be determined first. This equation was not used to solve for the concentration at the active layer surface when the membranes were reversed (Case 3).

For this situation the concentration gradient across the velocity boundary layer was determined.

## 8.2.3. Water flux rate across velocity boundary layer

As water was used experimentally in the juice circuit, there were no velocity boundary layers providing resistance to the water movement on the juice side of membrane. Thus a velocity boundary layer was considered only on the OA side of the membrane, either adjacent to the support layer, under normal operation (Case 1), or adjacent to the active layer, when the membranes were reversed (Case 3). The water flux rate and concentration gradient across the velocity boundary layer was determined for two cases; firstly for a boundary layer which gradually grew along the length of the flow channel and secondly, for a fully-developed laminar boundary layer in the OA flow channel. A diagram of the OA flow channel is presented in Figure 8.2.

The literature states that the concentration boundary layer is usually less than the velocity boundary layer (Incropera and De Witt, 1985). But, in this study it has been assumed that the two layers were equal and diffusion was occurring right across the boundary layer. Concentration boundary layers did not exist on the three solid polycarbonate walls of the flow channel as the concentration across them was constant at $Y_C$, the OA free-stream concentration.

### 8.2.3.1. Growing velocity boundary layer in OA flow channel

In this case it was assumed that the two boundary layers along the membrane remain relatively thin. Velocity boundary layers on the polycarbonate walls of the flow channel were also thin and they did not interfere with one another. The velocity profile across the boundary layer was assumed to be uniform, except for at the surface where $y = 0$, for $0 < y < \delta(x)$:

$$u = U\left[1 - \left(1 - \frac{y}{\delta}\right)^{\alpha}\right] \tag{8.16}$$

$u$ - velocity in the x direction, m $s^{-1}$

$U$ - bulk free-stream velocity in x direction, m $s^{-1}$

$\delta$ - velocity boundary layer thickness, m

$\alpha$ - power term for velocity profile equation, $\alpha > 1$

**Figure 8.2. OA flow channel**

Schematic diagram showing the direction of the $x$, $y$ and $z$ coordinates in the OA flow channel used for modelling the DOC process.

$Q_m$ - mass flow rate along OA flow channel, kg $s^{-1}$

$m_w$ - mass flow rate of water across membrane per unit area, kg $m^{-2}$ $s^{-1}$

$L_m$ - length of each OA flow channel, 0.1545 ± 0.0005 m

$h$ - equivalent flow channel height; distance between membrane and OA wall when membrane was fully deflected, 0.017 ± 0.001 m

$w$ - width between two membrane support bars, 0.0143 ± 0.0001 m

$u$, $v$, $\omega$ - corresponding velocity components in x, y, z directions

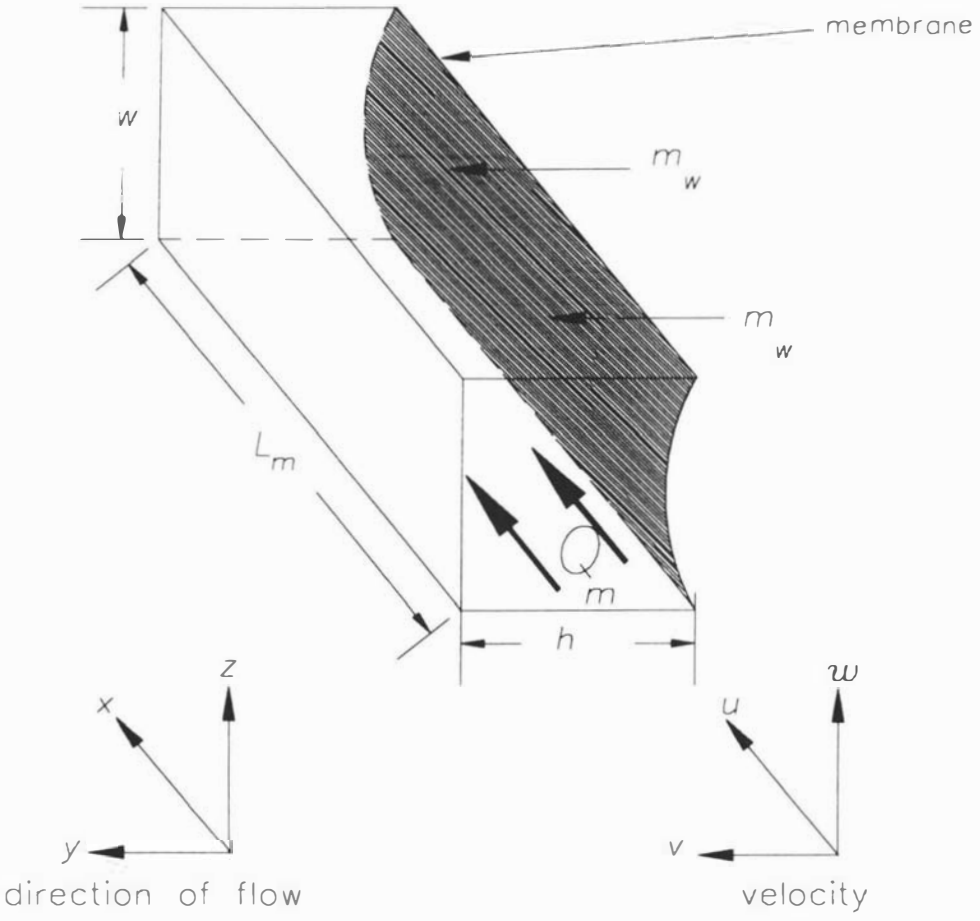
membrane
w
$m_w$
$m_w$
$L_m$
$Q_m$
h
z
x
y
direction of flow
w
u
v
velocity

For steady incompressible two-dimensional flow, the governing equations for mass and momentum in the boundary layer were obtained by solving the equations for conservation of mass and momentum.

A differential equation for the boundary layer thickness was obtained by integration of the governing equations determined while taking into account the introduction of water flux at the edge of the boundary layer, entering on the $y$-coordinate [A complete derivation of this equation is presented in Appendix A3]. The differential equation derived for the boundary layer thickness is as follows:

$$\frac{d}{dx}(\delta^2) = \frac{2(\alpha + 1)(2\alpha + 1)}{\alpha U}\left[\frac{F(Y_C)}{\rho(Y_0)} + \frac{\alpha\mu(Y_0)}{\rho(Y_0)} - \alpha\int_{Y_0(x)}^{Y_C}\frac{\mu(Y)}{[\rho(Y)]^2}\left(1 - \frac{F(Y)}{F(Y_C)}\right)^{\alpha-1}\frac{d\rho}{dY}dY\right] \tag{8.17}$$

*where*
$$F(Y) = \int_{Y_0(x)}^{Y}\frac{\rho(Y)D_{fw}(Y)}{Y}dY \tag{8.18}$$

Integration of Equation (8.17) along the length of the membrane provided the thickness of the boundary layer at each position. The boundary layer thickness at each position $x_n$ was determined from the thickness at the previous position $x_{n-1}$ along the membrane. Two dimensional flow in the $x$ and $y$ directions only was evaluated.

The water flux perpendicular to the membrane is due to a bulk flow from the osmotic flux plus diffusion based on Fick's law. The equation for the water flux rate across the velocity boundary layer is:

$$m_w(x) = \frac{F(Y_C)}{\delta(x)} \tag{8.19}$$

The concentration of the OA at the membrane surface was estimated using the following equation

$$Y_0 = Y_C - \frac{C\,\delta(x)\,\pi(Y_1)}{\left\{\dfrac{\frac{1}{2}[\rho(Y_0) + \rho(Y_C)]\ \frac{1}{2}[D_{fw}(Y_0) + D_{fw}(Y_C)]}{\frac{1}{2}(Y_0 + Y_C)}\right\}} \tag{8.20}$$

Equations (8.17) to (8.20) apply to Case 1 for normal membrane orientation, when the support layer is present facing the OA flow channel. These equations can be used to

solve for Case 3, when the variable $Y_0$ is replaced by $Y_1$ the concentration at the interface between the active layer and velocity boundary layer.

For normal operation, the OA concentration at the interface between the active and support layers was estimated knowing the concentration gradients across the support and velocity boundary layers, and the velocity boundary layer thickness. The water flux rate across the active membrane layer was then determined using Equation (8.1). The solution of this model produced water flux rates much smaller than experimental results. The velocity boundary layer thickness was over-estimated and became larger than the actual channel dimensions.

**8.2.3.2. Fully-developed laminar flow in OA flow channel**

To overcome the problem with the over-estimation of the boundary layer thickness, the flow in the OA flow channels was then modelled as fully-developed laminar flow. The flow in the OA flow channels under the conditions operated, for fructose and NaCl solutions, was determined to be laminar. Although fully-developed laminar flow exists in the flow channels with fructose solutions greater than 0.5 g (g solution)$^{-1}$ only, the DOC process was modelled assuming fully-developed laminar flow was occurring for the full range of OA solutions and concentrations tested.

In fully-developed laminar flow the velocity boundary layers would form on all four walls and meet in the middle of the flow channel. In this model the movement of the water and OA, in the OA flow channel, in the $x$, $y$ and $z$ directions were taken into account [Figure 8.2]. Looking at the flow within the OA flow channel, in the $x$ direction, the total OA solute flow was constant, but the water mass flow increased as the flow moved along the OA flow channel taking up water from the membrane. The velocity profile along the OA flow channel with fully-developed flow was assumed to be uniform along its length.

For normal membrane orientation and Case 1, the OA concentration ($Y_0$) at the support layer and velocity boundary layer interface can be estimated from the concentration in the bulk solution ($Y_C$) and the OA flow channel dimensions using an equation describing the concentration gradient across the velocity boundary layer. Using $Y_0$, the OA concentration ($Y_1$) at the active and support layer interface was estimated from the concentration gradient across the support layer. For reversed membrane orientation and Case 3, the OA concentration ($Y_1$) at the active layer and velocity boundary layer interface can be estimated from the concentration in the bulk solution ($Y_C$) and the OA

flow channel dimensions using the equation describing the concentration gradient across the velocity boundary layer.

For fully-developed laminar flow the equation describing the concentration gradient across the velocity boundary layer will be derived for normal membrane orientation (Case 1).

For steady incompressible flow of a fluid with uniform density, $\rho$, parallel to the horizontal plane $y = 0$,

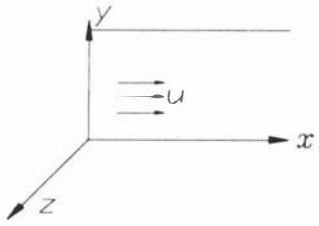


The equations for conservation of mass (for incompressible flow),

$$\nabla \cdot \vec{u} = 0 \tag{8.21}$$

and the Navier-Stokes equation (for incompressible laminar flow),

$$\rho \frac{\partial \vec{v}}{\partial t} + \rho(\vec{v} \cdot \nabla)\vec{v} = -\nabla p + \rho \vec{g} + \mu \nabla^2 \vec{v} \tag{8.22}$$

and the following boundary conditions: at $y = 0$, $u = 0$; at $y = h$, $u = 0$; at $z = 0$, $u = 0$; at $z = w$, $u = 0$, were used to derive the following partial differential equation which is the form of the velocity function, where $G_P$ is the pressure gradient in the $x$ direction, $dP/dx$:

$$\frac{\partial^2 u}{\partial y^2} + \frac{\partial^2 u}{\partial z^2} = -\frac{G_P}{\mu} \tag{8.23}$$

where $\mu = \mu(Y)$. Using Fourier series, let

$$u = \sum_{m=1}^{\infty} \sum_{n=1}^{\infty} u_{mn} \sin \frac{m\pi y}{h} \sin \frac{n\pi z}{w} \tag{8.24}$$

$h$ - distance between membrane and OA plate outside wall, m

$w$ - distance between spacers, width, m

$m, n$ - number of periods in Fourier series

To satisfy the boundary conditions, determine the coefficients for $u_{mn}$ to satisfy the partial differential equation, Equation (8.23). First, substitute the sum for $u$ [Equation (8.24)] into the partial differential equation:

$$\sum_{m=1}^{\infty}\sum_{n=1}^{\infty}\left(-\frac{m^2\pi^2}{h^2}-\frac{n^2\pi^2}{w^2}\right)u_{mn}\sin\frac{m\pi y}{h}\sin\frac{n\pi z}{w}=-\frac{G_P}{\mu} \qquad (8.25)$$

Then, $$\int_0^w\int_0^h \ldots\ldots \sin\frac{p\pi y}{h}\sin\frac{q\pi z}{w}\,dy\,dz$$

(assume that $\int$ and $\Sigma$ can be interchanged)

$$-\sum_{m=1}^{\infty}\sum_{n=1}^{\infty}\left(\frac{m^2}{h^2}+\frac{n^2}{w^2}\right)\pi^2 u_{mn}\int_0^h \sin\frac{m\pi y}{h}\sin\frac{p\pi y}{h}\,dy\int_0^w \sin\frac{n\pi z}{w}\sin\frac{q\pi z}{w}\,dz$$

$$=\frac{G_P}{\mu}\int_0^h \sin\frac{p\pi y}{h}\,dy\int_0^w \sin\frac{q\pi z}{w}\,dz \qquad (8.26)$$

$p$, $q$ - number of periods in Fourier series

Using the orthogonality of the sine functions:

$$\int_0^h \sin\frac{m\pi y}{h}\sin\frac{p\pi y}{h}\,dy = 0 \quad for \quad m \neq p$$
$$= \frac{h}{2} \quad for \quad m = p \qquad etc. \qquad (8.27)$$

After integration and substitution of $m$, $n$ with $p$, $q$:

$$-\left(\frac{p^2}{h^2}+\frac{q^2}{w^2}\right)\pi^2 u_{pq}\frac{h}{2}\frac{w}{2} = -\frac{G_P}{\mu}\frac{(1-\cos p\pi)}{p\pi/h}\frac{(1-\cos q\pi)}{q\pi/w}$$
$$= 0 \quad for \quad p, q \quad both \quad even$$
$$= -\frac{4G_P hw}{\mu pq\pi^2} \quad for \quad p, q \quad both \quad odd \qquad (8.28)$$

Therefore, $u_{mn} = 0$ for $m$ or $n$ even. For $m$, $n$ both odd,

$$\left(\frac{m^2}{h^2} + \frac{n^2}{w^2}\right)\pi^2 u_{mn}\frac{hw}{4} = \frac{4G_P hw}{\mu mn\pi^2} \tag{8.29}$$

or

$$u_{mn} = \frac{16G_P}{\mu\pi^4}\frac{1}{mn(m^2/h^2 + n^2/w^2)} \tag{8.30}$$

So, substituting the equation for $u_{mn}$ into Equation (8.24) gives,

$$u = \sum_{m=1}^{\infty}\sum_{n=1}^{\infty}\frac{16G_P}{\mu\pi^4}\frac{1}{mn(m^2/h^2 + n^2/w^2)}\sin\frac{m\pi y}{h}\sin\frac{n\pi z}{w} \tag{8.31}$$

where m and n are both odd. If the total mass flow at a cross-section of the flow channel is $Q_m$,

$$\int_0^w\int_0^h \rho u\,dydz = Q_m \tag{8.32}$$

$\rho = \rho(Y)$

$Q_m$ - total mass flow along OA flow channel, kg $s^{-1}$

Then, assuming density, $\rho$, and viscosity, $\mu$, are constant,

$$Q_m = \frac{16G_P\rho}{\mu\pi^4}\sum_{m=1}^{\infty}\sum_{n=1}^{\infty}\frac{1}{mn(m^2/h^2 + n^2/w^2)}\frac{2h}{m\pi}\frac{2w}{n\pi}$$

$$= \frac{64G_P\rho hw}{\mu\pi^6}\sum_{m=1}^{\infty}\sum_{n=1}^{\infty}\frac{1}{m^2n^2(m^2/h^2 + n^2/w^2)} \tag{8.33}$$

for $m$, $n$ both odd.

Therefore,

$$\frac{16G_P}{\mu\pi^4} = \frac{\frac{Q_m\pi^2}{4\rho wh}}{\sum_{m=1}^{\infty}\sum_{n=1}^{\infty}\frac{1}{m^2n^2(m^2/h^2 + n^2/w^2)}} \tag{8.34}$$

and Equation (8.31) can be written

$$u = \frac{Q_m \pi^2}{4\rho wh} \frac{\sum_{m=1}^{\infty}\sum_{n=1}^{\infty} \frac{1}{mn(m^2/h^2 + n^2/w^2)} \sin\frac{m\pi y}{h} \sin\frac{n\pi z}{w}}{\sum_{m=1}^{\infty}\sum_{n=1}^{\infty} \frac{1}{m^2n^2(m^2/h^2 + n^2/w^2)}} \quad (8.35)$$

At $x = 0$ (entrance), $\rho = \rho_C$, $Q_m = Q_{mC}$ (total mass flow at channel entry, kg $s^{-1}$), therefore,

$$u_{mn} = \frac{Q_{mC} \pi^2}{4\rho_C wh} \frac{\frac{1}{mn(m^2/h^2 + n^2/w^2)}}{\sum_{m=1}^{\infty}\sum_{n=1}^{\infty} \frac{1}{m^2n^2(m^2/h^2 + n^2/w^2)}} \quad (8.36)$$

$$\int_0^h u(y)dy = \frac{Q_{mC}}{\rho_C w} \quad (8.37)$$

or for $x > 0$,

$$Q_m = Q_{mC} + \int_0^w \int_0^{L_x} m_w(x,z)dxdz \quad (8.38)$$

For three dimensional flow in the OA flow channel [Figure 8.2], the fluid velocity $\vec{v} = (u, v, w)$. The water mass flux rate (per unit area) within the flow channel (kg $m^{-2}$ $s^{-1}$) is given by

$$\vec{q}_{mw} = (1 - Y)\rho(Y)\vec{v} + \rho(Y)D_{wf}(Y)[-\nabla(1 - Y)] \quad (8.39)$$

Fructose mass flux rate (per unit area) along the flow channel (kg $m^{-2}$ $s^{-1}$) is given by

$$\vec{q}_{mf} = Y\rho(Y)\vec{v} + \rho(Y)D_{fw}(Y)[-\nabla Y] \quad (8.40)$$

At $y = 0$, $u = w = 0$ i.e. $\vec{v} = (0, v, 0)$

$\vec{q}_{mw} = (0, m_w(x,z), 0)$

$\vec{q}_{mf} = (0, 0, 0)$

and Equation (8.39) and (8.40) give for water:

$$m_w(x,z) = \left[(1 - Y)\rho(Y)v + \rho(Y)D_{wf}(Y)\frac{\partial Y}{\partial y}\right]_{y=0} \quad (8.41)$$

and for fructose,

$$0 = \left[ Y\rho(Y)v - \rho(Y)D_{fw}(Y)\frac{\partial Y}{\partial y} \right]_{y=0} \tag{8.42}$$

Rearranging Equation (8.42)

$$[\rho(Y)v]_{y=0} = \left[ \frac{\rho(Y)\, D_{fw}(Y)\, \frac{\partial Y}{\partial y}}{Y} \right]_{y=0} \tag{8.43}$$

and substituting this into Equation (8.41) gives

$$m_w(x,z) = \rho(Y) \left[ \left( \frac{1-Y}{Y} D_{fw}(Y) + D_{wf}(Y) \right) \frac{\partial Y}{\partial y} \right]_{y=0} \tag{8.44}$$

Now $D_{wf}(Y) = D_{fw}(Y)$, therefore

$$m_w(x,z) = \left[ \frac{1}{Y} \rho(Y) D_{fw}(Y) \frac{\partial Y}{\partial y} \right]_{y=0} \tag{8.45}$$

and

$$\left[ \frac{\partial Y}{\partial y} \right]_{y=0} = \left[ \frac{Y}{\rho(Y)D_{fw}(Y)} \right]_{y=0} m_w(x,z) \tag{8.46}$$

For $x > 0$, write $Y(x, 0, z) = Y_0(x, z)$ then,

$$Y(x,y,z) = Y(x,0,z) + \left[ \frac{\partial Y}{\partial y} \right]_{y=0} \frac{y}{1!} + \left[ \frac{\partial^2 Y}{\partial y^2} \right]_{y=0} \frac{y^2}{2!} + \ldots \tag{8.47}$$

(Taylor series expanded about $y = 0$).

Substituting Equation (8.46) into Equation (8.47) gives

$$Y(x,y,z) = Y_0(x,z) + \left[ \frac{Y}{\rho(Y)D_{fw}(Y)} \right]_{y=0} m_w(x,z)\, y + a_2 y^2 + a_3 y^3 + \ldots \tag{8.48}$$

or

$$Y(x,y,z) = Y_0(x,z) + \frac{Y_0(x,z)\, m_w(x,z)}{\rho(Y_0(x,z))\, D_{fw}(Y_0(x,z))}\, y + a_2 y^2 + a_3 y^3 + \ldots \tag{8.49}$$

or

$$Y(x,y,z) = Y_0(x,z) \left\{ 1 + \frac{m_w(x,z)}{\rho(Y_0(x,z))\, D_{fw}(Y_0(x,z))} \left[ y + b_2 y^2 + b_3 y^3 + \ldots \right] \right\} \tag{8.50}$$

where

$$b_n = b_n(x,z) = \frac{\rho(Y_0(x,z))\, D_{fw}(Y_0(x,z))}{Y_0(x,z)\, m_w(x,z)}\, a_n(x,z) \tag{8.51}$$

and where

$$a_n(x,z) = \frac{1}{n!} \left[ \frac{\partial^n Y}{\partial y^n} \right]_{y=0}, \quad n = 2,3,\ldots \tag{8.52}$$

The total mass flow of fructose along the flow channel is constant with respect to $x$:

$$Q_{mf} = \int_0^w \int_0^h \rho(Y)\, Y u \; dydz = constant \tag{8.53}$$

where $\rho = \rho(Y)$, $Y = Y(x, y, z)$, $u = u(x, y, z)$. Note that the water mass flow increases with increasing $x$ along the flow channel.

Assume that at the entry to the channel, $Y = Y_C$ , $\rho = \rho(Y_C) = \rho_C$ , $u = u(0, y, z) = u_C(y, z)$ then,

$$Q_{mf} = \int_0^w \int_0^h \rho_C\, Y_C\, u_C(y,z)\; dydz \tag{8.54}$$

$$Q_{mf} = Y_C \int_0^w \int_0^h \rho_C\, u_C(y,z)\; dydz \tag{8.55}$$

$$Q_{mf} = Y_C\, Q_{mC} \tag{8.56}$$

where $Q_{mC}$ is the total mass flow at the channel entry (kg $s^{-1}$) [Equation (8.37)].

The flow of water (per unit area) through the membrane active layer into the boundary layer is

$$m_w(x,z) = C\pi(Y_1(x,z)) \tag{8.57}$$

Conservation of water along the flow channel from left to right →

$$\int_0^w \int_0^h (1 - Y)\rho(Y)\, u\, dydz = (1 - Y_C)Q_{mC} + \int_0^w \int_0^x m_w(x,z)\, dxdz \tag{8.58}$$

Conservation of fructose along the flow channel from left to right →

$$\int_0^w \int_0^h Y\rho(Y)\, u\, dydz = Y_C Q_{mC} = constant \tag{8.59}$$

The total mass flow through cross-section of flow channel at position $x$ is, from Equations (8.32) and (8.38),

$$\int_0^w \int_0^h \rho(Y)\, u\, dydz = Q_{mC} + \int_0^w \int_0^{L_m} m_w(x,z)\, dxdz \tag{8.60}$$

or, using Equation (8.57),

$$\int_0^w \int_0^h \rho(Y)\, u\, dydz = Q_{mC} + \int_0^w \int_0^{L_m} C\pi(Y_1(x,z))\, dxdz \tag{8.61}$$

Now, substituting Equation (8.50) into the left hand side (LHS) of Equation (8.59) gives

$$\int_0^w \int_0^h \rho(Y)\, Y_0(x,z) \left\{1 + \frac{m_w(x,z)}{\rho(Y_0(x,z))\, D_{fw}(Y_0(x,z))} \left[y + b_2 y^2 + \ldots\right]\right\} u\, dydz = Y_C Q_{mC} \tag{8.62}$$

Rearrangement gives

$$\int_0^w \int_0^h \rho(Y)\, Y_0(x,z)\, u\, dydz + \int_0^w \int_0^h \frac{\rho(Y) Y_0(x,z) m_w(x,z)}{\rho(Y_0(x,z))\, D_{fw}(Y_0(x,z))} \left[y + b_2 y^2 + \ldots\right] u\, dydz = Y_C Q_{mC} \tag{8.63}$$

Now, suppose that variation in $Y$ across the width ($z$-direction) of the channel is small i.e. $Y = Y(x, y)$, $Y_0 = Y_0(x)$, $m_w = m_w(x)$, etc, but

$$u = u(x,y,z) = \sum_{m=1}^{\infty} \sum_{n=1}^{\infty} u_{mn}(x) \sin\frac{m\pi y}{h} \sin\frac{n\pi z}{w} \tag{8.64}$$

for m, n both odd. Therefore, Equation (8.63) can be written, after integration with respect to $z$ ($\int_0^w \ldots dz$),

$$\int_0^w \int_0^h \rho(Y(x,y))\, Y_0(x) \sum_{m=1}^{\infty} \sum_{n=1}^{\infty} u_{mn}(x) \sin\frac{m\pi y}{h} \sin\frac{n\pi z}{w}\, dy dz$$
$$+ \int_0^w \int_0^h \frac{\rho(Y(x,y))\, Y_0(x) m_w(x)}{\rho(Y_0(x))\, D_{fw}(Y_0(x))} [y + b_2 y^2 + \ldots] \sum_{m=1}^{\infty} \sum_{n=1}^{\infty} u_{mn}(x) \sin\frac{m\pi y}{h} \sin\frac{n\pi z}{w}\, dy dz$$
$$= Y_C Q_{mC} \tag{8.65}$$

Knowing that

$$\int_0^w \sin\frac{n\pi z}{w}\, dz = \frac{2w}{n\pi} \tag{8.66}$$

then,

$$\frac{2w}{\pi} Y_0(x) \sum_{n=1}^{\infty} \left\{ \frac{1}{n} \sum_{m=1}^{\infty} \left[ \int_0^h \rho(Y(x,y)) u_{mn}(x) \sin\frac{m\pi y}{h}\, dy \right] \right\}$$
$$+ \frac{2w}{\pi} \frac{Y_0(x) m_w(x)}{\rho(Y_0(x))\, D_{fw}(Y_0(x))} \sum_{n=1}^{\infty} \left\{ \frac{1}{n} \sum_{m=1}^{\infty} \left[ \int_0^h \rho(Y(x,y))\, (y + b_2 y^2 + \ldots)\, u_{mn}(x) \sin\frac{m\pi y}{h}\, dy \right] \right\}$$
$$= Y_C Q_{mC} \tag{8.67}$$

for m and n both odd. Now, substituting Equation (8.64) into Equation (8.61) gives, after integration with respect to $z$,

$$\frac{2w}{\pi} \sum_{n=1}^{\infty} \left\{ \frac{1}{n} \sum_{m=1}^{\infty} \left[ \int_0^h \rho(Y(x,y)) u_{mn}(x) \sin\frac{m\pi y}{h}\, dy \right] \right\} = Q_{mC} + w \int_0^{L_m} C\pi(Y_0(x))\, dx \tag{8.68}$$

Substitution of the LHS Equation (8.68) into Equation (8.67) gives

$$Y_0(x) \left\{ Q_{mC} + w \int_0^{L_m} C\pi(Y_1(x))\, dx + \frac{2w}{\pi} \frac{m_w(x)}{\rho(Y_0(x))\, D_{fw}(Y_0(x))} \sum_{n=1}^{\infty} \left\{ \frac{1}{n} \sum_{m=1}^{\infty} \left[ \int_0^h \rho(Y(x,y))\, [y + b_2 y^2 + \ldots]\, u_{mn}(x) \sin\frac{m\pi y}{h}\, dy \right] \right\} \right\}$$
$$= Y_C Q_{mC} \tag{8.69}$$

for m and n both odd. If variation with $x$ is small, $Y_0(x) = Y_0$ and

$$Y_0 \left\{ Q_{mC} + wL_m C\pi(Y_1) + \frac{2w}{\pi} \frac{m_w(x)}{\rho(Y_0) D_{fw}(Y_0)} \sum_{n=1}^{\infty} \left\{ \frac{1}{n} \sum_{m=1}^{\infty} \left[ \int_0^h \rho(Y(y)) \left[ y + b_2 y^2 + \ldots \right] u_{mn}(x) \sin \frac{m\pi y}{h} \, dy \right] \right\} \right\} = Y_C Q_{mC}$$

(8.70)

For x > 0, the expression $(wL_m C\pi(Y_1))$ is much smaller than the third term:

$$\frac{2w}{\pi} \frac{m_w(x)}{\rho(Y_0) D_{fw}(Y_0)} \sum_{n=1}^{\infty} \left\{ \frac{1}{n} \sum_{m=1}^{\infty} \left[ \int_0^h \rho(Y(y)) \left[ y + b_2 y^2 + \ldots \right] u_{mn}(x) \sin \frac{m\pi y}{h} \, dy \right] \right\}$$

approximately by a factor of $10^7$. Further approximate by writing $\rho(Y) = \rho(Y_C) = \rho_C$ then,

$$Y_0 \left\{ Q_{mC} + \frac{2w}{\pi} \frac{C\pi(Y_1)}{\rho(Y_0) D_{fw}(Y_0)} \sum_{n=1}^{\infty} \left\{ \frac{1}{n} \sum_{m=1}^{\infty} \left[ \int_0^h \rho_C \left[ y + b_2 y^2 + \ldots \right] u_{mn}(x) \sin \frac{m\pi y}{h} \, dy \right] \right\} \right\} = Y_C Q_{mC}$$

(8.71)

Substituting in Equation (8.36) for $u_{mn}$ gives

$$Y_0 \left\{ Q_{mC} + \frac{2w}{\pi} \frac{C\pi(Y_1)}{\rho(Y_0) D_{fw}(Y_0)} \rho_C \frac{Q_{mC} \pi^2}{4 \rho_C w h} \sum_{m=1}^{\infty} \sum_{n=1}^{\infty} \left[ \frac{\frac{1}{mn(m^2/h^2 + n^2/w^2)}}{\sum_{m=1}^{\infty} \sum_{n=1}^{\infty} \frac{1}{m^2 n^2 (m^2/h^2 + n^2/w^2)}} \right] \int_0^h \left[ y + b_2 y^2 + \ldots \right] \sin \frac{m\pi y}{h} \, dy \right\} = Y_C Q_{mC}$$

(8.72)

Dividing by $Q_{mC}$ and simplifying gives

$$Y_0 \left\{ 1 + \frac{C\pi(Y_1)}{2\rho(Y_0) D_{fw}(Y_0)} \frac{\pi}{h} \sum_{m=1}^{\infty} \sum_{n=1}^{\infty} \left[ \frac{\frac{1}{mn(m^2/h^2 + n^2/w^2)}}{\sum_{m=1}^{\infty} \sum_{n=1}^{\infty} \frac{1}{m^2 n^2 (m^2/h^2 + n^2/w^2)}} \right] \int_0^h \left[ y + b_2 y^2 + \ldots \right] \sin \frac{m\pi y}{h} \, dy \right\} = Y_C$$

(8.73)

This equation can be used to solve for $Y_0$. In particular, using the simplifications already made,

$$b_n = \frac{\rho(Y_0)D_{fw}(Y_0)}{Y_0 C\pi(Y_1)} \frac{1}{n!}\left[\frac{\partial^n Y}{\partial y^n}\right]_{y=0} \tag{8.74}$$

However, note that at the top of the channel, $y = h$, we have $\vec{v} = \vec{\sigma}$ (i.e. a no-slip boundary). The vertical component of $\vec{q}_{mf}$ is zero, so $\partial Y/\partial y = 0$ at the solid boundary. If we let

$$\frac{\partial Y}{\partial y} = 1 + 2b_2 y = 0 \qquad at\ y = h, \tag{8.75}$$

then $b_2 = -1/2h$ and

$$y + b_2 y^2 + \ldots = \left(y - \frac{y^2}{2h}\right) + small\ terms \tag{8.76}$$

Substituting Equation (8.76) into Equation (8.73) then gives,

$$Y_0\left\{1 + \frac{C\pi(Y_1)}{2\rho(Y_0)D_{fw}(Y_0)} \frac{\pi}{h} \sum_{m=1}^{\infty}\sum_{n=1}^{\infty}\left[\frac{\frac{1}{mn(m^2/h^2 + n^2/w^2)}}{\sum_{m=1}^{\infty}\sum_{n=1}^{\infty}\frac{1}{m^2n^2(m^2/h^2 + n^2/w^2)}}\right]\int_0^h \left[y - \frac{y^2}{2h}\right]\sin\frac{m\pi y}{h}\,dy\right\} + small\ terms = Y_C \tag{8.77}$$

Simplified

$$Y_0\left\{1 + \frac{C\pi(Y_1)h}{\rho(Y_0)D_{fw}(Y_0)} I\right\} = Y_C \tag{8.78}$$

and

$$Y_0 = \frac{Y_C}{1 + \dfrac{C\pi(Y_1)h}{\rho(Y_0)D_{fw}(Y_0)} I} \tag{8.79}$$

Equations (8.78) and (8.79) describe the concentration gradient across the velocity boundary layer for normal operation, where:

$$I = \frac{\pi}{2h^2} \sum_{m=1}^{\infty} \sum_{n=1}^{\infty} \left[ \frac{\dfrac{1}{mn(m^2/h^2 + n^2/w^2)}}{\sum_{m=1}^{\infty} \sum_{n=1}^{\infty} \dfrac{1}{m^2n^2(m^2/h^2 + n^2/w^2)}} \right] \int_0^h \left[ y - \frac{y^2}{2h} \right] \sin \frac{m\pi y}{h} \, dy + \textit{small terms}$$

(8.80)

where the "*small terms*" is

$$\textit{small terms} = \frac{\pi}{2h^2} \sum_{m=1}^{\infty} \sum_{n=1}^{\infty} \left[ \frac{\dfrac{1}{mn(m^2/h^2 + n^2/w^2)}}{\sum_{m=1}^{\infty} \sum_{n=1}^{\infty} \dfrac{1}{m^2n^2(m^2/h^2 + n^2/w^2)}} \right] \int_0^h \left[ b_3 y^3 + .... \right] \sin \frac{m\pi y}{h} \, dy$$

(8.81)

Solving the first integral in Equation (8.80) results in

$$I = \sum_{m=1}^{\infty} \sum_{n=1}^{\infty} \left[ \frac{\dfrac{1}{mn(m^2/h^2 + n^2/w^2)}}{\sum_{m=1}^{\infty} \sum_{n=1}^{\infty} \dfrac{1}{m^2n^2(m^2/h^2 + n^2/w^2)}} \right] \frac{\pi}{2h^2} \left( \frac{h^2}{2m\pi} + \frac{2h^2}{m^3\pi^3} \right) + \textit{small terms}$$

(8.82)

$$I = \sum_{m=1}^{\infty} \sum_{n=1}^{\infty} \left( \frac{1}{4m} + \frac{1}{m^3\pi^2} \right) \left[ \frac{\dfrac{1}{mn(m^2/h^2 + n^2/w^2)}}{\sum_{m=1}^{\infty} \sum_{n=1}^{\infty} \dfrac{1}{m^2n^2(m^2/h^2 + n^2/w^2)}} \right] + \textit{small terms}$$

(8.83)

The first term on the RHS of Equation (8.83) was solved for values of $m$ and $n$ (both odd) using an iterative procedure. For $m$ = 11 and $n$ = 11, the first term of the RHS of Equation (8.83) was found to equal 0.34. Therefore, $I = 0.34 \times I_R$. The correction factor ($I_R$) required for $I$ took into account the remaining integrals, covering the "*small terms*" not evaluated. The integral '$I$' represents the relationship between the velocity profile and the concentration profile. The need for the correction factor ($I_R$) was an indication that the velocity and concentration profiles did not fit a parabolic shape as initially assumed, but possibly one of higher order.

Equation (8.78) describes the concentration gradient across the fully-developed laminar boundary layer. It can be used to determine the concentration $Y_0$ at the interface between the membrane and the boundary layer in the OA flow channel for normal operation

(Case 1). Combining the equations for fully-developed laminar flow [Equation (8.78) and (8.83)] with those for active layer [Equation (8.1)], the porous support layer [Equation (8.15)], the theoretical water flux rate at steady state can be determined. This combined mathematical model takes into account the resistances in the active, support and velocity boundary layers.

For reversed membranes and Case 3, Equation (8.78) can be used to determine the concentration gradient across the velocity boundary layer by replacing the variable $Y_0$ with $Y_1$, the concentration at the active layer interface.

The assumptions made during development of this model for three dimensional flow:

1. Solute flux = 0 and $\pi_J = 0$.
2. At steady state, within the support layer $D_{fw}(Y) \approx D_{fw}(Y_1)$ = constant and $\rho(Y) \approx \rho(Y_1)$ = constant.
3. The size of the velocity and concentration boundary layers adjacent to the membrane in the OA flow channel were equal and diffusion was occurring right across the boundary layers.
4. Conservation of mass and momentum in OA flow channels, and flow was incompressible.
5. Fully-developed laminar flow in OA flow channel.
6. Uniform velocity flow profile along the boundary layer having a parabolic shape.
7. Density, $\rho$, and viscosity, $\mu$, within the boundary layer are constant.
8. Mass flow of solute along the flow channel is constant with respect to $x$ and the water mass flow increases with $x$ along the flow channel.
9. At entry to the flow channel : $Y = Y_C$ , $\rho = \rho(Y_C) = \rho_C$ , $u = u(0, y, z) = u_C(y, z)$, $Q_{mC}$ is the total mass flow at the channel entry.
10. Variation in $Y$ across the width ($z$-direction) of the channel is small, therefore, $Y = Y(x, y)$, $Y_0 = Y_0(x)$, $m_w = m_w(x)$.
11. At the top of the channel, $y = h$, $\vec{v} = \vec{\sigma}$ (i.e. a no-slip boundary).
12. The vertical component of $\vec{q}_{mf}$ is zero, so $\partial Y/\partial y = 0$ at the solid boundary.

## 8.3. Solution of DOC model for mass flux rate of water

A summary of the equations derived to describe the concentration gradients across the membrane and boundary layers, and the equation used to determine the membrane water flux rate during DOC are presented in Table 8.1.

**Table 8.1. Summary of DOC model**

| | |
|---|---|
| Boundary layer[a] | $Y_0 \left\{ 1 + \frac{C\pi(Y_1)h}{2\rho(Y_0)D_{fw}(Y_0)} I \right\} = Y_C$ <br> Equation (8.78) |
| Support layer[b] | $Y_1 = Y_0 \exp\left( - \frac{C\ \pi(Y_1)\ d_s}{\rho(Y_1)\ D_e(Y_1)} \right)$ $\qquad D_e(Y) = \frac{e}{\tau} D_{fw}(Y)$ <br> Equation (8.15) |
| Active layer | $m_w = C\ \pi(Y_1)$ <br> Equation (8.1) |

a. Model assumes fully-developed laminar flow in OA flow channel.

b. The membrane is orientated for normal operation, with active layer facing the juice circuit and the support layer facing the OA circuit.

The model was solved for three possible membrane orientations:

**Case 1.** Active layer facing the juice circuit, support layer facing the OA circuit and a fully-developed boundary layer in OA flow channel (normal membrane orientation) [Figure 8.1 (a)];

**Case 2.** Active layer facing the juice circuit and support layer facing the OA circuit, no velocity boundary layers in OA channel [Figure 8.1. (b)].

**Case 3.** Active layer facing the OA circuit, no support layer in OA channel and fully-developed boundary layer in OA flow channel (reversed membrane orientation) [Figure 8.1 (c)];

**Case 1.** Values for the OA concentrations $Y_1$ and $Y_0$ were determined from the OA bulk concentration, $Y_C$. In summary, the procedure used to determine $Y_1$ was to initially guess its value (e.g. $0.5Y_C$), and to use that value to calculate $Y_0$ and then $Y_C$ using Equations (8.15) and (8.78). If the value of $Y_C$ calculated from the guessed values of $Y_1$ and $Y_0$ was equal to the experimental value of $Y_C$ in the OA channel, the guess of $Y_1$ was assumed to be correct.

A flow diagram of the iterative procedure used to solve for $Y_1$ and $Y_0$ at each position along the membrane is shown in Figure 8.3. If the difference between the calculated and experimental $Y_C$ was equal to zero the value guessed for $Y_1$ was correct, thereby, giving the correct value for $Y_0$. If not, a second guess of $Y_1$ was taken based on the difference calculated above using the following procedure. If the difference was less than zero the guess of $Y_1$ was originally too large. Therefore, the next guess of $Y_1$ was taken as a value half way between the previous guess and $Y_{1\,min}$. If the difference was greater than zero the guess of $Y_1$ was originally too small. Therefore, the next guess of $Y_1$ was taken as a value half way between the previous guess and $Y_{1\,max}$. With the new guess for $Y_1$, Equations (8.15) and (8.78) were again solved and the value of the difference determined. This process was continued until the difference was equal to zero or within a small pre-set tolerance.

Having calculated a value for $Y_1$ the water flux rate across the membrane was determined for each position along the membrane using Equation (8.1). The total water flux rate was calculated by summing the individual water flux rates over the whole available membrane area.

The diffusion coefficient of the solution in the concentration boundary layer in the support layer was estimated by the effective diffusion coefficient for a solution at concentration $Y_1$ [$D_e(Y_1)$], Equation (8.8)]. In the velocity boundary layer the binary diffusion coefficient was determined from the solution concentration $Y_0$ [$D_{fw}(Y_0)$].

**Case 2.** The model was also solved for the presence of the active and support layers but for no velocity boundary layer. The concentration in the OA flow channel adjacent to the support layer was $Y_C$. The concentration at the interface between the active and support layer $Y_1$ provides the driving force for water transfer across the active layer. $Y_1$ was determined iteratively from $Y_C$ using Equation (8.15), in which the variable $Y_0$ was replaced by the variable $Y_C$. The water flux rate was determined from $Y_1$.

**Figure 8.3. Flow diagram of iterative procedure to solve for concentration $Y_1$**

Procedure to solve for $Y_1$ for normal membrane orientation, Case 1.

| | |
|---|---|
| $Y_1$ | - concentration at interface between active and support layer, g (g solution)$^{-1}$ |
| $Y_0$ | - concentration at interface between support layer and velocity boundary layer, g (g solution)$^{-1}$ |
| $Y_C$ | - concentration of OA in OA channel free-stream, g (g solution)$^{-1}$ |
| $m_w$ | - water flux rate, kg m$^{-2}$ s$^{-1}$ |
| $d_s$ | - thickness of support layer, m |
| $\rho(Y)$ | - density of solution at concentration $Y$, kg m$^{-3}$ |
| $D_{fw}(Y)$ | - binary diffusion coefficient of fructose in aqueous fructose solution at concentration $Y$, m$^2$ s$^{-1}$ |
| $LHS$ | - left hand side of Equation (8.78) |
| $C$ | - membrane constant, kg m$^{-2}$ s$^{-1}$ Pa$^{-1}$ |
| $I$ | - integral function describing velocity and concentration profiles across the OA channel. |

For Case 2, Equation (8.15) is only solved and for Case 3, Equation (8.78) is only solved.

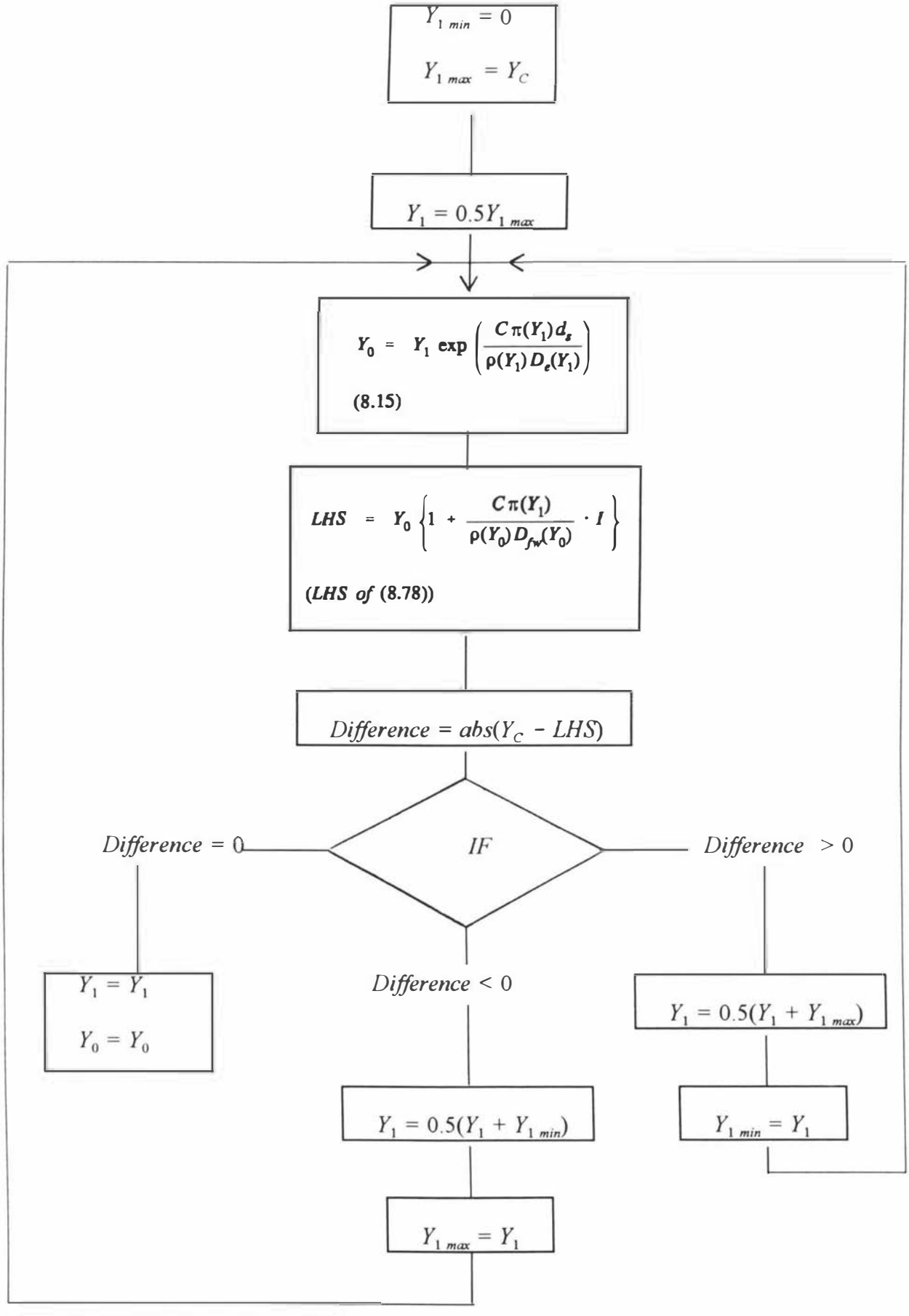
$Y_{1\,min} = 0$
$Y_{1\,max} = Y_C$
$Y_1 = 0.5Y_{1\,max}$
$Y_0 = Y_1 \exp\left(\frac{C\pi(Y_1)d_s}{\rho(Y_1)D_e(Y_1)}\right)$
(8.15)
$LHS = Y_0\left\{1 + \frac{C\pi(Y_1)}{\rho(Y_0)D_{fw}(Y_0)} \cdot I\right\}$
(LHS of (8.78))
Difference = abs($Y_C$ - LHS)
IF
Difference = 0
Difference < 0
Difference > 0
$Y_1 = Y_1$
$Y_0 = Y_0$
$Y_1 = 0.5(Y_1 + Y_{1\,min})$
$Y_{1\,max} = Y_1$
$Y_1 = 0.5(Y_1 + Y_{1\,max})$
$Y_{1\,min} = Y_1$

**Case 3.** The model was solved for the presence of the active membrane and velocity boundary layer only, no support layer was present in the OA flow channel [Figure 8.1 (c)]. The concentration at the interface between the active layer and velocity boundary layer, $Y_1$, was determined iteratively from $Y_C$ using Equation (8.78) where the variable $Y_0$ was replaced with $Y_1$. The water flux rate at each position along the membrane was calculated from the value of $Y_1$ determined.

A program was written in Pascal language (Turbo Pascal 7, Borland International, California, USA) to the solve the equations of the DOC model using the above iterative procedures. The DOC model determined the water flux rate and the concentration profiles across the membrane support and velocity boundary layers for the three different cases described above. The complete program is presented in Appendix A4.

## 8.4. Testing the model with experimental data

### 8.4.1 Water flux rates

The experimental data on water flux rates determined with the small laboratory DOC module, using fructose and NaCl as the osmotic agents, were used to test the theoretical model for DOC. Cases 1 and 3 were tested. No experimental data were collected to test Case 2.

The OA channel dimensions, standard data and functions used to solve the DOC model are presented in Table 8.2. The values for the membrane constant $C$ used to solve the model were determined from the experimental data. For fructose, $C = 1.4 \times 10^{-9}$ kg m$^{-2}$ s$^{-1}$ Pa$^{-1}$ and for NaCl, $C = 1.5 \times 10^{-9}$ kg m$^{-2}$ s$^{-1}$ Pa$^{-1}$, at 20°C. A porosity ($\varepsilon$) of 0.5 was assumed based on information provided by Herron (1995). For cylindrical perpendicular pores the tortuosity ($\tau$) is equal to unity (Mulder, 1992). As the tortuosity of the membrane was unknown initially, it was first assumed to be unity. It was found later that a tortuosity of 1.2 for the support layer provided theoretical flux rates that agreed well with experimental results.

In the mathematical model it was assumed that the concentration and velocity profiles in the OA flow channel were parabolic in shape. The correction factor ($I_R$) was an indication that the velocity and concentration profiles did not fit this shape, but possibly one of higher order. $I_R$ is used to correct this assumption, about the flow profile, for the actual flow in the OA flow channel. Different values for $I_R$ were determined for each OA solution used. The values of $I_R$ required to solve the mathematical model were found to be 0.023 for fructose and 0.05 for NaCl. The velocity and concentration profiles in

**Table 8.2. Data and functions used to solve the mathematical model for the small laboratory DOC module at 20°C**

| | | |
|---|---|---|
| OA channel dimensions | Flow channel length, $L_m$ | 0.1545 ± 0.0005 m |
| | Flow channel width, $w$ | 0.0143 ± 0.0001 m |
| | Equivalent channel width[a], $w_1$[b] | 0.030 ± 0.003 m |
| | Equivalent channel width[a], $w_2$[c] | 0.016 ± 0.009 m |
| | Equivalent channel width[a], $w_3$[d] | 0.039 ± 0.003 m |
| | Equivalent flow channel height[e], $h$ | 0.017 ± 0.001 m |
| | No. of flow channel for section 1, 2 & 3 | 2, 17, 2 |
| | Total membrane area | 0.064 ± 0.024 $m^2$ |
| | Membrane support layer thickness | 150 μm |
| Velocity, OA channel, $U$ | | 0.03 m $s^{-1}$ |
| Membrane constant, $C$ | fructose | $1.4 \times 10^{-9}$ kg $m^{-2}$ $s^{-1}$ $Pa^{-1}$ |
| | NaCl | $1.5 \times 10^{-9}$ kg $m^{-2}$ $s^{-1}$ $Pa^{-1}$ |
| Density of water | at 20°C | 998.2 kg $m^{-3}$ |
| Viscosity of water, $\mu_0$ | at 10°C<br>at 20°C<br>at 40°C | 0.001307 kg $m^{-1}$ $s^{-1}$<br>0.001002 kg $m^{-1}$ $s^{-1}$<br>0.000653 kg $m^{-1}$ $s^{-1}$ |
| Molecular weight | fructose<br>NaCl<br>water | 180.16 g $mol^{-1}$<br>58.44 g $mol^{-1}$<br>18.0 g $mol^{-1}$ |
| $D^o_{AB}$ at infinite dilution | fructose at 10°C<br>fructose at 20°C<br>fructose at 40°C | $4.7 \times 10^{-10}$ $m^2$ $s^{-1}$<br>$6.0 \times 10^{-10}$ $m^2$ $s^{-1}$<br>$9.3 \times 10^{-10}$ $m^2$ $s^{-1}$ |
| | NaCl at 20°C | $1.34 \times 10^{-9}$ $m^2$ $s^{-1}$ |
| Functions at 20°C | density : fructose (kg $m^{-3}$) | $998.2 + 383Y + 158Y^2$[f] |
| | density : NaCl (kg $m^{-3}$) | $998.2 + 697Y + 251Y^2$ |
| | viscosity : fructose (kg $m^{-1}$ $s^{-1}$) | $\log_e(\mu/\mu_0) = 26.8x_F$[g] |
| | viscosity : NaCl (kg $m^{-1}$ $s^{-1}$) | $\mu_0(1 + 1.7Y - 1.6Y^2 + 36.5Y^3)$ |
| | diffusion coefficient : fructose ($m^2$ $s^{-1}$) | $\log_e(D^o_{AB}/D_{AB}) = 12.96x_F$ |
| | osmosity : fructose (mol $l^{-1}$) | $2.85Y + 5.23Y^2$ |
| | osmosity : NaCl (mol $l^{-1}$ ) | $17.1Y + 11.7Y^2 + 4.94Y^3$ |
| | osmotic pressure: fructose and NaCl MPa | $4.36S + 0.213S^2 + 0.0595S^3$[h] |

a Equivalent channel width for section taking into account full membrane deflection. Equivalent channel width = available membrane area/$L_m$.

b Average for sections 1 and 3, plate 1.

c OA plate section 2 only, $w_2 = L_a$.

d Average for section 1 and 3, plate 2.

e Equivalent flow channel height for fully deflected membrane, m.

f Mass fraction, g (g solution)$^{-1}$.

g Mole fraction.

h Osmosity, mol $l^{-1}$.

the boundary layers were affected by the viscosity of the solution in the flow channel. High viscosity solutions would result in higher shear and steeper velocity gradients at the channel wall or membrane. Fructose and NaCl solutions have very different viscosities, hence with each solution the velocity profiles in the flow channels were different, requiring different values of $I_R$ for each solution.

For Case 1, the water flux rates determined by the mathematical model were found to agree well with the experimental data for fructose and NaCl. For Case 3, the water flux rates from the mathematical model were again found to agree well with the experimental data obtained when the membranes were reversed. The results for these two cases are presented in Figure 8.4. The theoretical results for Case 2 are also presented. For Case 1 only, the theoretical water flux rates determined for different operating temperatures are presented in Figure 8.5. Water flux rates are presented with respect to the osmotic pressure difference ($\Delta\pi$) between the juice circuit's free-stream osmotic pressure ($\pi_J$) and the OA circuit's free-stream osmotic pressure ($\pi_{OA}$). The value of $\pi_J = 0$ and $\pi_{OA} = \pi(Y_C)$.

The mathematical model successfully predicted flux rates for Case 1 over the osmotic pressure range tested (1.5 to 30 MPa). This was true for different OAs (fructose, NaCl) and different temperatures (10, 20 and 40°C).

In Case 3, with membrane reversed, the model was a successful predictor of flux rates for fructose OA at 20°C. However, it was a poor estimate for NaCl as OA, at concentrations above 15 MPa.

The results confirm that support and velocity boundary layer resistances were very important in determining the flux rate of water across the DOC membrane. Using the theoretical data the percentage contribution of each resistance: active layer ($R_1$), support layer ($R_2$) and velocity boundary layer ($R_3$) to the total resistance to water transfer was calculated for the two OAs. For selected OA concentrations the theoretical and experimental percentage resistances are presented in Table 8.3.

Except for the lowest OA concentrations the theoretical resistances agreed with values determined from experimental data.

**Figure 8.4. Theoretical and experimental water flux rates for fructose and NaCl as osmotic agents**

Module set up:
Juice circuit - water only, at 20.0 ± 0.1°C, flow rate $4 \times 10^{-5}$ $m^3$ $s^{-1}$
OA circuit - fructose and NaCl solutions, at 20 ± 0.1°C, flow rate $7 \times 10^{-6}$ $m^3$ $s^{-1}$

Osmotic pressure difference, $\Delta\pi = (\pi_{OA} - \pi_J)$. Data points presented are means of experimentally determined data. The horizontal lines represent two standard errors about each mean.

------ Case 1 - theoretical data for model including: active layer (am), support layer (sm) and fully-developed boundary layer (fdbl)

– – Case 2 - theoretical data for model including: active and support layers only (am and sm)

—— Case 3 - theoretical data for model including: active layer (am) and fully-developed boundary layer (fdbl)

(a) Fructose solutions as OA
Theoretical values determined using mathematical model derived for DOC
$C = 1.4 \times 10^{-9}$ kg $m^{-2}$ $s^{-1}$ $Pa^{-1}$, $d_s = 150$ μm, $I_R = 0.023$

o Experimental data : membrane orientated with active layer facing juice circuit

Δ Experimental data : membrane orientated with active layer facing OA circuit

(b) NaCl solutions as OA
Theoretical values determined using mathematical model derived for DOC
$C = 1.5 \times 10^{-9}$ kg $m^{-2}$ $s^{-1}$ $Pa^{-1}$, $d_s = 150$ μm, $I_R = 0.05$

□ Experimental data : membrane orientated with active layer facing juice circuit

◊ Experimental data : membrane orientated with active layer facing OA circuit

(a)

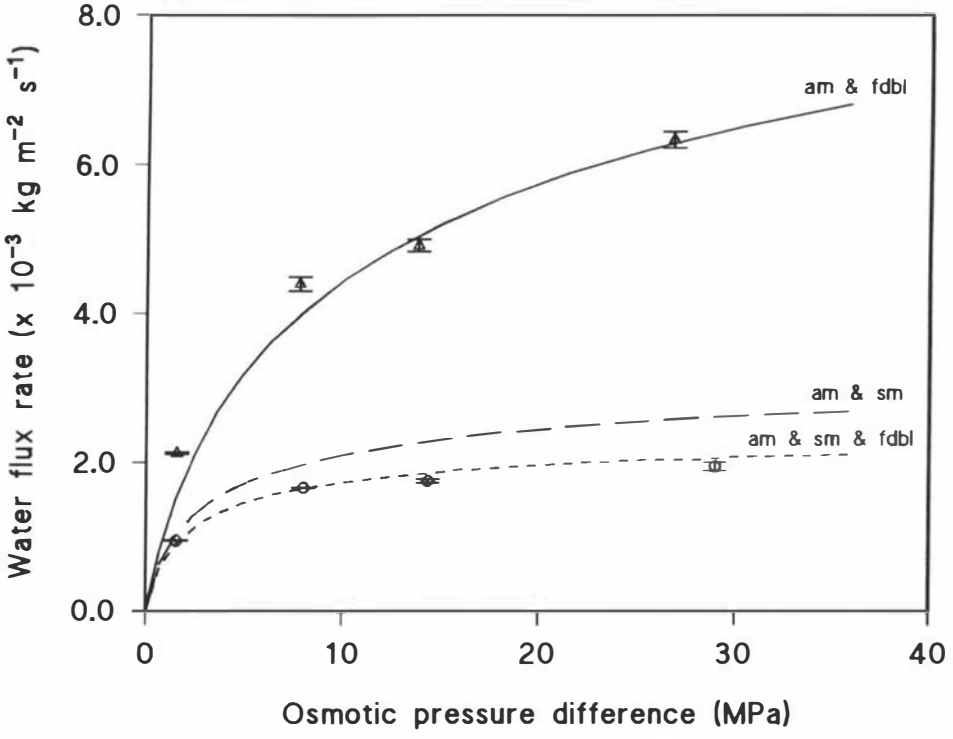
8.0
6.0
4.0
2.0
0.0
Water flux rate (x 10⁻³ kg m⁻² s⁻¹)
am & fdbl
am & sm
am & sm & fdbl
0
10
20
30
40
Osmotic pressure difference (MPa)

(b)

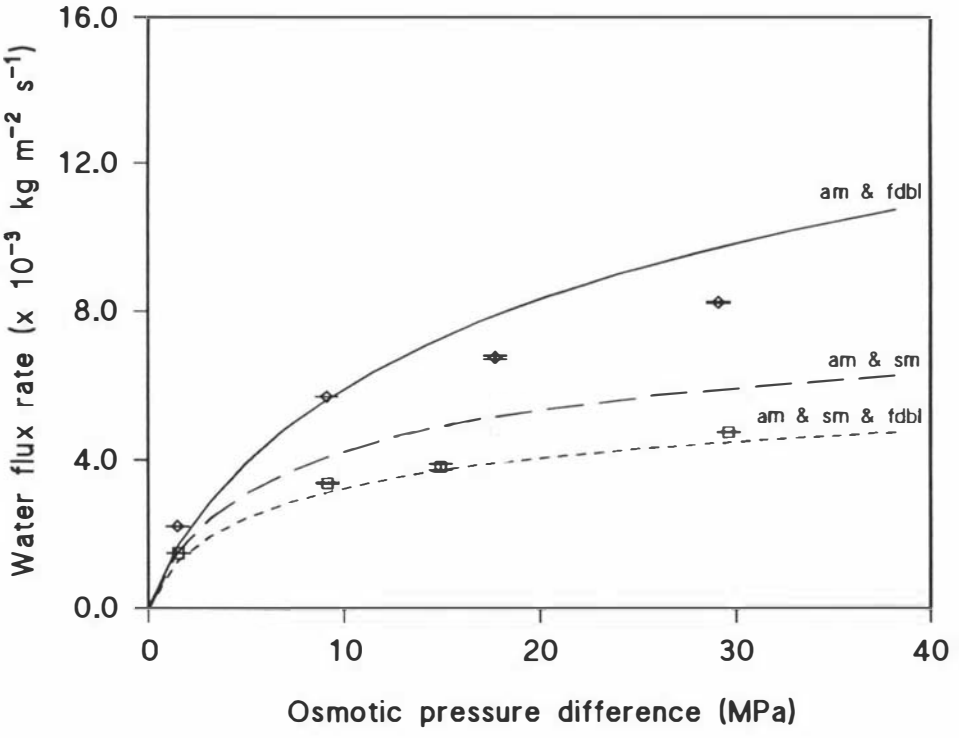
16.0
12.0
8.0
4.0
0.0
Water flux rate (x 10⁻³ kg m⁻² s⁻¹)
am & fdbl
am & sm
am & sm & fdbl
0
10
20
30
40
Osmotic pressure difference (MPa)

**Figure 8.5. Theoretical and experimental flux rates at various temperatures using fructose**

Module set up:
Juice circuit - water only, flow rate $4 \times 10^{-5}$ $m^3$ $s^{-1}$
OA circuit - fructose solutions, flow rate $7 \times 10^{-6}$ $m^3$ $s^{-1}$
Operating temperatures (± *SEM* for $n = 3$) were: 10.0 ± 0.1 °C; 20.0 ± 0.1 °C; 40.0 ± 0.1 °C

Data points presented are means of experimentally determined data. The horizontal lines represent two standard errors about each mean.

For Case 1 (active layer (am), support layer (sm) and fully-developed boundary layer (fdbl)), theoretical values determined using mathematical model derived for DOC

——— - theoretically determined data
10°C $C = 1.3 \times 10^{-9}$ kg $m^{-2}$ $s^{-1}$ $Pa^{-1}$, $d_s = 150$ μm, $I_R = 0.023$
20°C $C = 1.4 \times 10^{-9}$ kg $m^{-2}$ $s^{-1}$ $Pa^{-1}$, $d_s = 150$ μm, $I_R = 0.023$
40°C $C = 1.6 \times 10^{-9}$ kg $m^{-2}$ $s^{-1}$ $Pa^{-1}$, $d_s = 150$ μm, $I_R = 0.023$

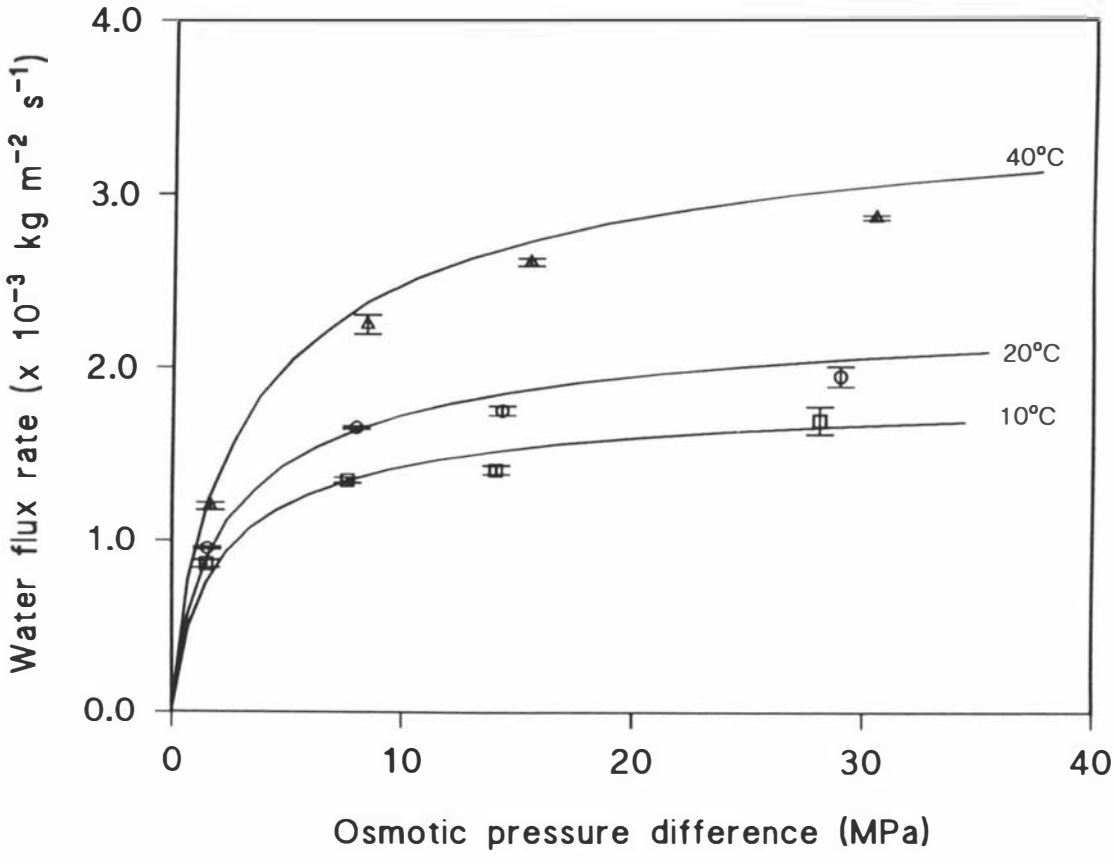
4.0
3.0
2.0
1.0
0.0
0
10
20
30
40
Water flux rate (x $10^{-3}$ kg $m^{-2}$ $s^{-1}$)
Osmotic pressure difference (MPa)
40°C
20°C
10°C

**Table 8.3. Contributions of individual resistances determined from theoretical and experimental data**

| | | Theoretical[a] | | | Experimental[b] | | |
|---|---|---|---|---|---|---|---|
| OA solution | OA concentration (g (g solution)$^{-1}$) | $\%R_1$[c] | $\%R_2$[d] | $\%R_3$[e] | $\%R_1$[c] | $\%R_2$[d] | $\%R_3$[e] |
| Fructose | 0.10 | 40 | 43 | 17 | 44 | 55 | 1 |
| | 0.35 | 13 | 63 | 24 | 15 | 62 | 23 |
| | 0.50 | 8 | 67 | 25 | 9 | 64 | 27 |
| | 0.70 | 5 | 70 | 25 | 5 | 69 | 26 |
| NaCl | 0.02 | 57 | 24 | 19 | 64 | 32 | 4 |
| | 0.10 | 23 | 44 | 33 | 25 | 41 | 34 |
| | 0.15 | 16 | 49 | 35 | 17 | 44 | 39 |
| | 0.23 | 10 | 55 | 35 | 11 | 43 | 46 |

a. For normal membrane orientation, determined from theoretical values using Equations (6.1) to (6.3).

b For normal membrane orientation, determined from experimental data using Equations (6.1) to (6.3) [see 6.8].

c. Resistance in the active membrane layer.

d. Resistance in the porous support layer.

e. Resistance in the velocity boundary layer.

If the same flow conditions and characteristics in the DOC module are maintained then reducing the thickness of the support layer and possibly reducing the amount of mesh material used will lead to a reduction in support layer resistances. The presence of the nylon mesh in the support layer was reported to reduce the flux rate through this layer (Herron, 1995). As the model assumes fully-developed laminar flow, any increase in the velocity of the OA solution in the OA flow channel will not affect the resistances and the water flux rate significantly while the flow remains laminar. As discussed in Section 6.8 the OA solution properties also have a large influence on the resistances and hence the water flux rates.

The actual osmotic pressure driving force across the active layer can be determined from the concentration at the surface of the active membrane layer facing the OA channel ($Y_1$). The mathematical model was used to determine the actual concentration of solute at the active layer for different concentrations ($Y_C$) of fructose and NaCl OAs. The only

variable data input into the model was the concentration ($Y_C$) of OA in the bulk free-stream. The actual osmotic pressure difference across the active layer ($\pi(Y_1)$) calculated from the mathematical model was plotted against experimentally determined flux rates, as shown in Figure 8.6. Linear relationships were found. This supports the assumption that mass transfer across the active layer was by osmosis.

### 8.4.2. Concentration profiles across membrane

Using the theoretical equations which described the concentration gradients across the support and boundary layers [Equations (8.15) and (8.78)], the concentration profiles across these layers were determined and are presented in Figure 8.7. The concentration gradients correspond to the water flux rates curves presented in Figure 8.4 for fructose as OA.

The concentration profiles across the support layer show the resistance to the transfer of water away from the active layer. As water exits the active layer it meets a large resistance in the support layer. The water moves slowly away from the active layer and is replaced by the OA solute; this is shown in the exponential concentration gradient. The concentration gradient across the boundary layer has been assumed to be linear as shown in the concentration profiles.

## 8.5. Steady state water flux rates

Assuming fully-developed laminar flow in the OA flow channel resulted in a model for the Osmotek DOC system which estimated water flux rates in good agreement with experimental data. The model can be used to estimate water flux rates for the DOC module, for water only in the juice circuit and for a number of osmotic agents provided various physical properties are known. The mathematical model assuming fully-developed laminar flow predicts the DOC water flux rates better than the first velocity boundary layer model derived for growing boundary layers in OA flow channel.

In deriving the mathematical model it was assumed the solution-diffusion model was the most appropriate for describing the water flux across the active layer. Diffusion across the support layer and velocity boundary layer was governed by Fick's law of diffusion. In the porous support layer an effective diffusion coefficient was used, as the water was diffusing through a porous medium not a continuous solution as in the velocity boundary layer. The effective diffusion coefficient takes into account the porosity and tortuosity of the porous layer. The rate of water transfer across the active, support and velocity

**Figure 8.6. Relationship between the theoretical actual osmotic pressure driving force and experimental water flux rates**

Module set up:
Juice circuit - water only, at 20.0 ± 0.1°C, flow rate $4 \times 10^{-5}$ $m^3$ $s^{-1}$
OA circuit - fructose and NaCl solutions, at 20 ± 0.1°C, flow rate $7 \times 10^{-6}$ $m^3$ $s^{-1}$

Actual osmotic pressure driving force determined with theoretical mathematical model. Data points presented are means of experimentally determined data. The horizontal lines represent two standard errors about each mean. The overall standard error of means (*SEM*) = 5 x $10^{-5}$ for $n$ = 3. Best fit linear regression lines are presented.

(a) Fructose
o - active layer of membrane facing the juice circuit (Fructose 1, am & sm & fdbl)
Δ - active layer of membrane facing the OA circuit (Fructose 2, am & fdbl)

(b) NaCl
□ - active layer of membrane facing the juice circuit (NaCl 1, am & sm & fdbl)
◊ - active layer of membrane facing the OA circuit (NaCl 2, am & fdbl)

| Membrane orientation, active layer facing: | Fructose | | | NaCl | | |
|---|---|---|---|---|---|---|
| | OA concentration[a] (g (g solution)$^{-1}$ | Approx. $\Delta\pi$[b] (MPa) | Actual $\Delta\pi$[c] (MPa) | OA concentration[a] (g (g solution)$^{-1}$ | Approx. $\Delta\pi$[b] (MPa) | Actual $\Delta\pi$[c] (MPa) |
| juice circuit | 0.10 | 1.5 | 0.6 | 0.02 | 1.5 | 0.9 |
| | 0.35 | 8.0 | 1.2 | 0.10 | 9.1 | 2.1 |
| | 0.49 | 14.2 | 1.3 | 0.15 | 15.5 | 2.5 |
| | 0.69 | 28.9 | 1.5 | 0.23 | 30.5 | 3.0 |
| OA circuit | 0.10 | 1.5 | 1.1 | 0.02 | 1.5 | 1.1 |
| | 0.34 | 7.6 | 2.8 | 0.10 | 9.1 | 3.7 |
| | 0.48 | 13.6 | 3.6 | 0.15 | 15.5 | 4.9 |
| | 0.67 | 27.0 | 4.4 | 0.22 | 28.1 | 6.4 |

a. OA concentration ($Y_C$) in the OA circuit bulk free-stream used during experimental trials.
b. Osmotic pressure difference, $\Delta\pi = (\pi_{OA} - \pi_J)$ and $\pi_J = 0$, calculated from the two bulk free-streams.
c. Actual osmotic pressure difference across the active layer determined by the mathematical model.

(a)

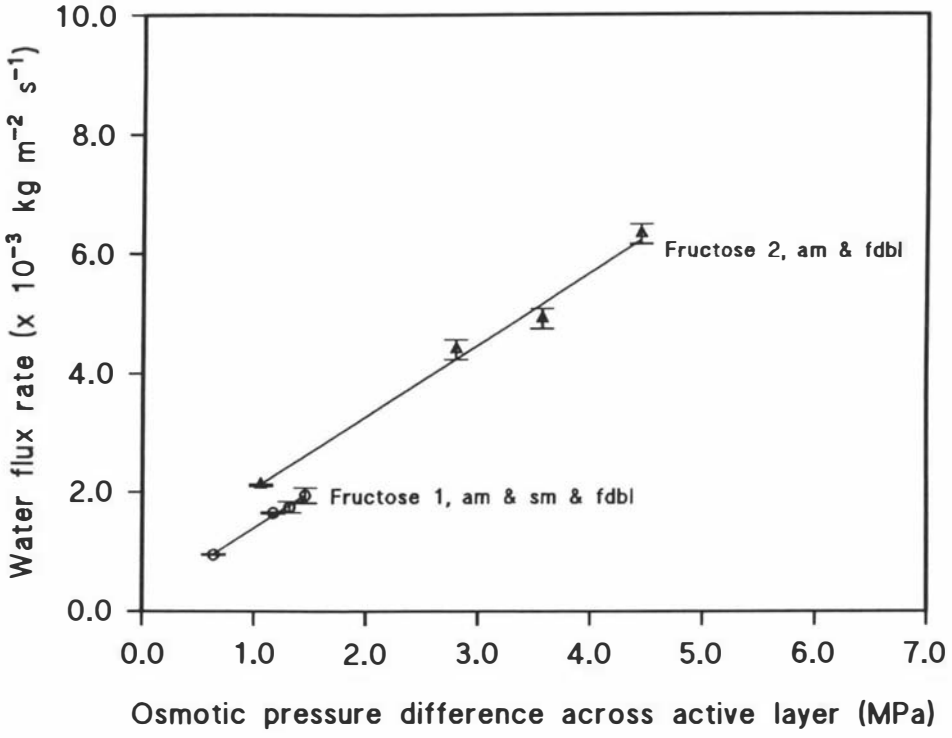
Water flux rate (x $10^{-3}$ kg $m^{-2}$ $s^{-1}$)
10.0
8.0
6.0
4.0
2.0
0.0
0.0
1.0
2.0
3.0
4.0
5.0
6.0
7.0
Fructose 2, am & fdbl
Fructose 1, am & sm & fdbl
Osmotic pressure difference across active layer (MPa)

(b)

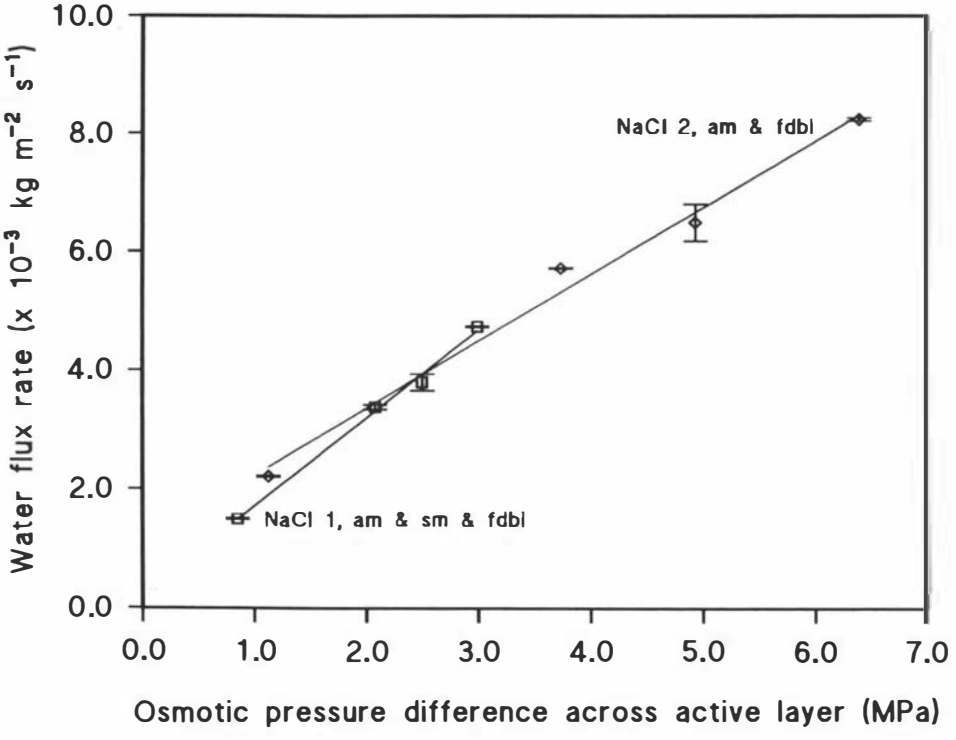
Water flux rate (x $10^{-3}$ kg $m^{-2}$ $s^{-1}$)
10.0
8.0
6.0
4.0
2.0
0.0
0.0
1.0
2.0
3.0
4.0
5.0
6.0
7.0
NaCl 2, am & fdbl
NaCl 1, am & sm & fdbl
Osmotic pressure difference across active layer (MPa)

**Figure 8.7. Concentration profiles across support and boundary layers in DOC membrane**

For fructose as the OA, concentration profiles calculated using theoretical equations describing concentration gradients across the support layer of membrane and the fully-developed laminar boundary layer.

Solute concentration $Y$ (g (g solution)$^{-1}$) at various distances along the support layer or fully-developed boundary layer (m). Active layer not drawn to scale.

(a) Active layer (am) and fully-developed boundary layer (fdbl) (Case 3).

(b) Active layer (am) and support layer (sm) (Case 2).

(c) Active layer (am) and support layer (sm) and fully-developed boundary layer (fdbl) (Case 1). The concentration profile at the start of the boundary layer up to 0.001 m is shown.

(d) Active layer (am) and support layer (sm) and fully-developed boundary layer (fdbl) (Case 1).

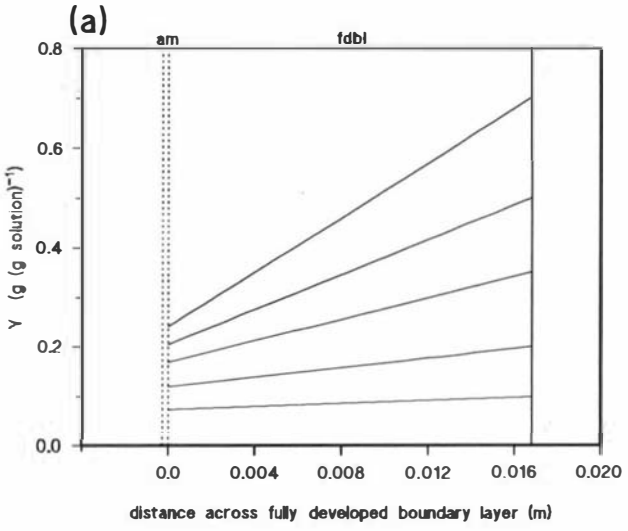
(a)
am
fdbl
0.8
0.6
0.4
0.2
0.0
Y (g (g solution)$^{-1}$)
0.0
0.004
0.008
0.012
0.016
0.020
distance across fully developed boundary layer (m)

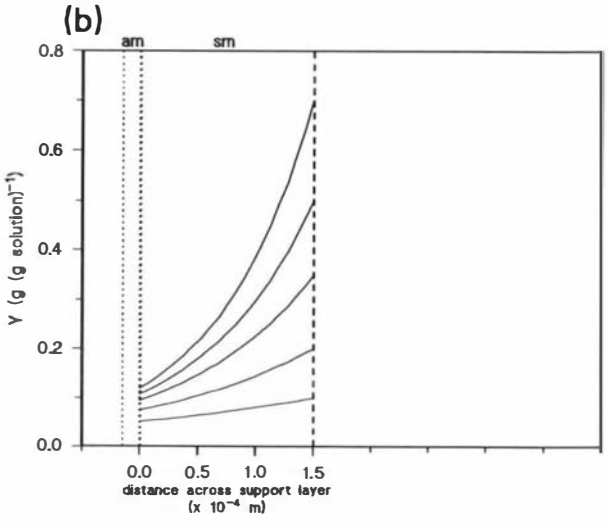
(b)
am
sm
0.8
0.6
0.4
0.2
0.0
Y (g (g solution)$^{-1}$)
0.0
0.5
1.0
1.5
distance across support layer
(x $10^{-4}$ m)

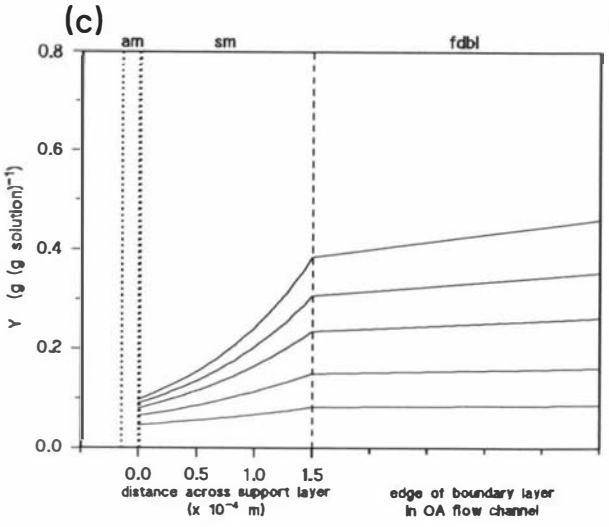
(c)
am
sm
fdbl
0.8
0.6
0.4
0.2
0.0
Y (g (g solution)$^{-1}$)
0.0
0.5
1.0
1.5
distance across support layer
(x $10^{-4}$ m)
edge of boundary layer
in OA flow channel

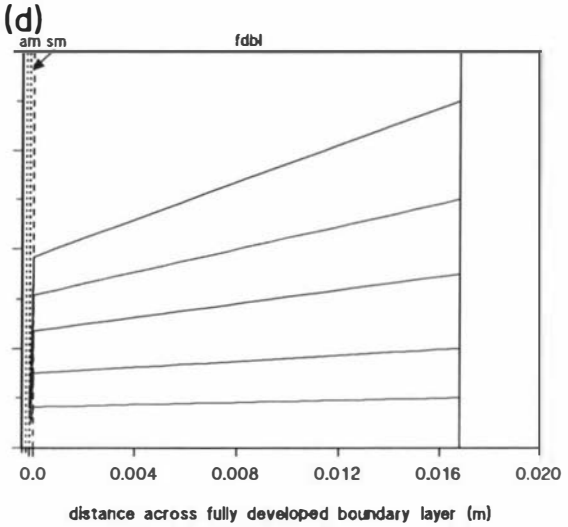
(d)
am sm
fdbl
0.0
0.004
0.008
0.012
0.016
0.020
distance across fully developed boundary layer (m)

boundary layers was well predicted by the mathematical model derived using these mass transfer theories.

The overall resistances in the two membrane layers and the velocity boundary layer were taken into account in the mathematical model. The greatest resistance to the flow of water from the juice circuit to the OA flow channel was the presence of the support layer. For fructose as the OA, at concentrations greater then 0.2 g (g solution)$^{-1}$ the support layer and velocity boundary layer reduced the flux rate by approximately 61% and 18%, respectively. For NaCl as the OA, at concentrations greater than 0.1 g (g solution)$^{-1}$ the flux rate was reduced by approximately 50% and 24%, respectively by each layer. Resistances in the support and velocity boundary layer were found to increase with OA concentration.

The experimental and theoretical results obtained agree with the findings of Rautenbach and Albrecht (1989), that the support layer provided a considerable resistance to the water transfer across the membrane. They also found with normal membrane orientation large increases in the OA concentration in the OA bulk free-stream would only lead to small increases in flux rates.

Rautenbach and Albrecht (1989) modelled DOC for an asymmetric membrane. The resistances in the membrane and velocity boundary layers described as mass transfer coefficients were determined empirically. The mass transfer across the membrane support and boundary layers was described by Fick's law. The governing equation for the support layer also took into account the porosity of the support layer and was based on the pore model. They assumed solute transfer occurred across the membrane. Their model took into account the asymmetric nature of the membrane and concentration boundary layers but they did not test the model with DOC experimental data. They provided the final equations for solving for flux rates, but the mass transfer coefficients needed to be determined from experimental data. The mass transfer coefficients were not estimated to test their DOC model. The models were presented for the two membrane orientations and they calculated that greater fluxes would be obtained with the active layer facing the OA as was found with the Osmotek Inc. DOC system.

The mathematical model for DOC proposed by Moody and Kessler (1976) was based on the assumption that an infinite supply of water from the dilute solution was available and its concentration did not change. A concentration polarisation layer formed on the dilute side of the membrane and solute concentration decreased near the membrane surface on the OA side. Their model assumed two un-stirred films or concentration

boundary layers of unknown thickness at the membrane. The concentrations of solute in the OA or dilute solution were assumed to be equal to the bulk concentrations at a distance, the thickness of the boundary layer, away from the membrane. Solute rejection by the membrane was assumed to be less than 100% but greater than 90%. The DOC system modelled in this study had an infinite supply of water from the juice side when water only was present. The concentration does not change and we assumed no concentration boundary layers developed. In this current study negligible solute transfer was assumed for modelling purposes. Moody and Kessler (1976) derived the model for an homogenous membrane, not an asymmetric membrane with a porous support layer. Therefore, this model was not suitable for the Osmotek DOC system.

The empirical model proposed by Beaudry and Lampi (1990(a)) assumed the water flux rate was directly proportional to the concentration difference across an homogenous membrane. The proportionality constant was determined empirically from a sum of all resistances from the membrane and boundary layers. As this model did not take into account the asymmetric nature of the membrane, and it also used the bulk solution concentration to determine the osmotic pressure driving force across the membrane it was considered to be unsuitable for the DOC system tested.

# CHAPTER 9
# CONCLUSIONS AND RECOMMENDATIONS

## 9.1. Conclusions

1. The transport of water molecules from the juice stream, containing water only, to the OA free-stream was achieved across three unique sets of resistances present in: the semi-permeable non-porous active membrane layer, the porous membrane support layer and the boundary layer in the OA flow channel.

2. The contribution of the active, support or boundary layers to the total resistance to water transfer was dependent on the OA type, OA concentration and temperature.

3. At 20°C, for fructose OA at 0.50 g (g solution)$^{-1}$ the active layer contributed 9% of the total resistances, the support layer 64% and the boundary layers in the OA channel 27%. For NaCl OA at an iso-osmotic concentration (0.15 g (g solution)$^{-1}$) the resistances contributed by each layer were 17%, 44% and 39%, respectively. For both OAs the resistances to water transfer in the support layer and OA channel boundary layers were highly significant and greatly influenced the overall water flux rates obtained in the DOC system.

4. The mechanism for water transfer across the active layer was osmosis. Water transfer across the concentration boundary layer in the support layer was by diffusion and porous flow. Across the velocity and concentration boundary layers in the OA channel water transferred by diffusion.

5. The OA solution properties were found to have a significant influence on water flux rates. These properties include solute type, solute concentration, solution viscosity, and diffusion coefficient of the water or solute in the solution.

6. The DOC membranes were asymmetric, and their orientation greatly influenced water flux rates. Highest flux rates were obtained with the active layer adjacent to the OA flow channel and water in the juice circuit.

7. The operating temperature had a large influence on the water flux rates. Increased operating temperatures led to increased flux rates. Temperature also had an effect on the solution viscosities and diffusion coefficients.

8. The DOC process of Osmotek Inc. was successfully mathematically modelled by: using the solution-diffusion model for the transport in the active layer; taking into account the porous nature of the support layer, and; by assuming fully-developed laminar flow in the OA flow channels. The model was found to successfully predict water flux rates for two different osmotic agents, at different temperatures and for the different membrane orientations.

## 9.2. Recommendations for future work

1. Investigate the presence of solutes in the juice circuit on mass flux rates. Determine the additional resistance to the mass transfer of water contributed by the concentration and velocity boundary layers on the juice side of the membrane. Update the mathematical model for DOC to include solutions in the juice circuit with a starting solute concentration as found in single strength juices.

2. Investigate other membranes suitable for DOC which may have greater permeability to water and have less resistance overall to the transfer of water. Investigate other DOC membrane systems. Determine the water flux rates experimentally and using the theoretical mathematical model derived for DOC.

3. Investigate the level of solute transfer occurring during DOC, especially while concentrating real solutions. Retention of valuable flavour compounds is important for high quality liquid foods such as fruit juice concentrates.

## 9.3. Recommendations for operating DOC processes

1. Reduce the thickness of the porous support layer while maintaining membrane strength.

2. Improve mixing on the OA side of the membrane.

3. Use osmotic agents which exert high osmotic pressures and have low solution viscosities, high diffusion coefficients and that do not permeate through the membrane.

# CHAPTER 10
# SUMMARY

The objectives of this research were to:

1. Define the system parameters (channel geometry, fluid properties, membrane characteristics), operating and boundary conditions of a DOC module.
2. Determine the mass transfer properties of the membrane to solute and solvent.
3. Define the resistances in the system to solute and solvent flow.
4. Mathematically model the DOC process.

DOC is a non-thermal, low pressure, continuous membrane concentration technique for liquids. It uses osmosis to drive the transfer of water across a semi-permeable membrane. In the DOC process, a solution with a high osmotic pressure (the osmotic agent, OA) is circulated on one side of the membrane. A more dilute solution to be concentrated (juice) is circulated on the other side of the membrane. As these two fluids recirculate water transfers across the membrane from the juice to the OA side in an attempt to equalize the concentrations (osmotic pressures). This results in the dilute solution becoming more concentrated and the OA more dilute.

The DOC apparatus consists of two OA plates between which are placed two flat membrane sheets. The juice circuit flows between the membrane sheets and the OA circuit flows up the two plates contacting the other side of the membranes. A slightly higher hydraulic pressure in the juice circuit ensures the two membranes stay apart. In the juice circuit, the flow channel is not straight but follows a designed corrugated path. This ensures the flow in the channel remains turbulent, as was observed in this study. The flow in the OA flow channel was laminar and co-current to the juice channel. Boundary layers were observed in the flow channels. Water has to diffuse across the boundary layer adjacent to the membrane in order to reach the OA free-stream.

The DOC membranes are asymmetric, cellulose acetate based membranes which consist of a thin semi-permeable non-porous active skin layer (15 μm) and a thick porous support layer (150 μm). A nylon mesh is incorporated into the porous support layer for increased strength. It was claimed that the active layer effectively excludes the passage of solutes with a nominal molecular weight cut-off of 100 g $mol^{-1}$. Ions such as $Na^+$ and $Cl^-$ were able to penetrate the membrane, but only to a small degree. The membrane's rejection of fructose was on average 99.9%, while for NaCl it was on average 99.0%.

As fructose has a molecular weight of 186.16 g $mol^{-1}$ the nominal molecular weight cut-off of the membrane must have been greater than 100 g $mol^{-1}$.

For normal operation the membranes were orientated with the active layer facing the juice circuit and the support layer facing the OA circuit. Because water only was circulated in the juice circuit in this study there were no boundary layers present on this side of the membrane (osmotic pressure = 0). The osmotic pressure difference between the juice circuit and the OA circuit free-stream ($\Delta\pi = \pi_{OA}$) was not used directly to calculate the actual membrane water flux rate but was used to give an approximation of the osmotic pressure driving force. With fructose OA solutions, the relationship between steady state water flux rates and $\Delta\pi$ was asymptotic. The flux rates increased at a steady rate up to $\Delta\pi$ = 15 MPa after which the flux rates began to level off. The flux rate at $\Delta\pi$ = 15 MPa was 1.75 ± 0.05 × $10^{-3}$ kg $m^{-2}$ $s^{-1}$ at 20°C. The flux rate at $\Delta\pi$ = 30 MPa was only 10% higher.

Increasing the operating temperature resulted in increased flux rates. Water flux rates at 40°C were 50% higher than at 20°C. The flux rate curves were found to follow the same asymptotic shape with $\Delta\pi$ at different temperatures.

With NaCl as OA, flux rates were twice that of fructose and the increase in flux rate with $\Delta\pi$ followed the same asymptotic curve as for fructose OA. Using sucrose instead of fructose at an iso-osmotic concentration resulted in a 33% decrease in the water flux rates.

The viscosities of iso-osmotic NaCl, fructose and sucrose solutions at 8 MPa and 20°C, were 0.0012, 0.004 and 0.011 kg $m^{-1}$ $s^{-1}$, respectively. The binary diffusion coefficients for these solutions were 13.4, 3.1 and 1.9 × $10^{-10}$ $m^2$ $s^{-1}$. The solution properties of the OA had a significant impact on the water flux rates achieved. OA solution viscosity and diffusion coefficients had a strong influence on the diffusion rate of water through the support and velocity boundary layers.

When the membranes were reversed, with the active layer facing the OA circuit, the water flux rates obtained were 40 to 60% higher than the flux rates obtained with the membranes orientated for normal operation, observed with fructose and NaCl OAs at 20°C. With this orientation the resistances to water transfer were provided by the active layer, and the velocity and concentration boundary layers.

When the membrane was orientated for normal operation the resistances to transfer of water from the juice circuit to the OA free-stream were present in the active ($R_1$) and support ($R_2$) membrane layers, and in the velocity and concentration boundary layers ($R_3$) in OA channel. The resistances in the active layer were dependent on membrane properties. OA solution filled the pores in the support layer and formed a stationary concentration boundary layer through which water had to diffuse to reach the OA channel. Water moved through the stationary layer by diffusion, driven by the concentration gradient across it (Fick's law) and by a small pressure drop across the layer (Darcy's law for flow through porous media). Resistances in the support layer were dependent on the structure of the layer and OA solution properties.

The resistances in the velocity and concentration boundary layers were dependent on the solution properties and on the thickness of the boundary layer which was determined by flow dynamics and solution viscosity. Water transferred across this layer by diffusion.

The percentage contribution of each resistance to the transfer of water was found to be dependent on the OA type and concentration. The absolute resistance in the active layer was constant for all concentrations but its contribution to the total resistance decreased with increasing OA concentration. The resistance in the active layer was estimated by the membrane constant ($C$), determined experimentally at 20°C to be $1.4 \times 10^{-9}$ and $1.5 \times 10^{-9}$ kg m$^{-2}$ s$^{-1}$ Pa$^{-1}$ for fructose and NaCl, respectively. For fructose OA at 0.50 g (g solution)$^{-1}$ the support ($R_2$) and boundary ($R_3$) layers contributed 64% and 27% of the total resistances, respectively, with the remaining 9% from the active layer ($R_1$). For an iso-osmotic NaCl OA (0.15 g (g solution)$^{-1}$) the resistances contributed by the active ($R_1$), support ($R_2$) and boundary ($R_3$) layers were 17%, 44%, and 39%, respectively.

The resistances to water transport in the support and velocity boundary layers were found to be highly significant and greatly influenced the overall water flux rates obtained in the DOC system.

Diffusion was the key mechanism for water transfer across the support and boundary layers. The OA solution diffusion coefficient and viscosity had a major influence on the water flux rates. The conditions became less favourable for diffusion at higher solute concentrations as the diffusion coefficient decreased and viscosities increased. This correlated with the increased resistances in the support and boundary layers.

Water diffused across the active layer by osmosis. The water diffused away from the active layer slowly, the rate being dependent on the diffusion coefficient of the solution in the concentration boundary layer adjacent. The concentration at the surface of the active layer was diluted, therefore, reducing the osmotic pressure driving force across the active layer and the water flux rate. In order to predict the water flux rate across the membrane, into the OA free-stream, the actual OA concentration at the active layer surface had to be determined.

A mathematical model was developed which was based on solution-diffusion transport through the active layer, diffusion and porous flow through the support layer, and diffusion across the velocity boundary layer in the OA flow channel. The DOC system was successfully modelled when fully-developed laminar flow was assumed in the OA flow channel. The water flux rate across the membrane was calculated after determining the concentration gradients across the support layer and velocity boundary layer in the OA flow channel and the OA concentration at the active layer surface. The concentration and velocity boundary layers in the OA flow channel were assumed to be equal.

For normal membrane orientation, the concentration gradient across the velocity boundary layer was determined using the following equation:

$$Y_0 \left\{ 1 + \frac{C\pi(Y_1)h}{\rho(Y_0)D_{fw}(Y_0)} I \right\} = Y_C \qquad (8.78)$$

where $Y_C$ was the solute concentration in the OA free-stream, $Y_0$ the solute concentration at the interface between the velocity boundary layer and support layer, and $Y_1$ the solute concentration at the surface of the active layer, between the active and support layers. The concentration gradient across the support layer was determined by the following equation:

$$Y_1 = Y_0 \exp\left( - \frac{C\ \pi(Y_1)\ d_s}{\rho(Y_1)\ D_e(Y_1)} \right) \qquad (8.15)$$

$D_e(Y_1)$ is the effective diffusion coefficient in the support layer. The actual osmotic pressure driving force across the the active layer which determines the water flux rate was determined from the concentration at the surface of the active membrane layer facing the OA channel ($Y_1$). The relationship between the actual osmotic pressure driving force ($\pi(Y_1)$) and the water flux rate was assumed to be linear and determined by the following equation:

$$m_w = C\,\pi(Y_1) \qquad (8.1)$$

The mathematical model was tested with experimental data for fructose and NaCl OAs, and with the two membrane orientations. For normal membrane orientation the mathematical model successfully predicted the experimental flux rates over the osmotic pressure range tested (1.5 to 30 MPa) for different OAs (fructose, NaCl) and at different temperatures (10, 20 and 40°C) (± 2 *SEM*). For the membranes reversed the model also successfully predicted the experimental flux rates over the same osmotic pressure range for fructose as OA (± 3 *SEM*). For NaCl OA, with membranes reversed, theoretical flux rates did not agree with experimental flux rates at $\Delta\pi > 15$ MPa.

The mathematical model was used to calculate the actual solute concentration at the active layer which determined the actual osmotic pressure driving force across the membrane. The theoretically calculated actual osmotic pressure differences were linearly related to the experimental water flux rates. This supports the assumption that the mass transfer across the active layer is by osmosis.

# APPENDIX

# A1. Derivation of equation to calculate membrane arc length

## List of Nomenclature

$L_a$ - length of membrane arc between two membrane support bars, m

$r$ - arc radius, m

$w$ - width between two adjacent membrane support bars, width of OA flow channel, m

$\Delta$ - membrane deflection between two membrane support bars, m

$\theta$ - angle of arc

## Derivation

Deflection of membrane ($\Delta$) from the central axis:

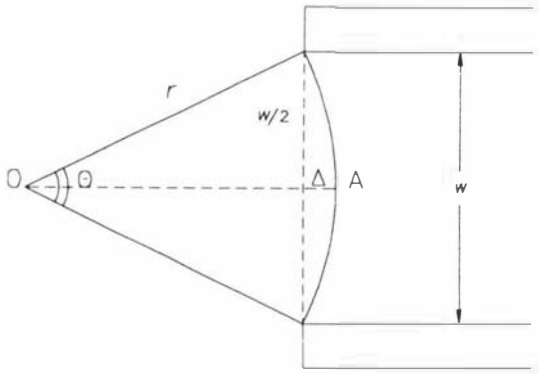


Along the line OA:

$$r = r\cos\left(\frac{\theta}{2}\right) + \Delta \quad \rightarrow \quad \cos\left(\frac{\theta}{2}\right) = 1 - \frac{\Delta}{r} \qquad \text{(A1.1)}$$

Also:

$$\sin\frac{\theta}{2} = \frac{\left(\frac{w}{2}\right)}{r} \qquad \text{(A1.2)}$$

$$\sin^2\frac{\theta}{2} + \cos^2\frac{\theta}{2} \quad \Rightarrow \quad \left(1 - \frac{\Delta}{r}\right)^2 + \left(\frac{w}{2r}\right)^2 = 1 \qquad \text{(A1.3)}$$

Expand and simplify:

$$\times r^2 : \qquad (r - \Delta)^2 + \frac{w^2}{4} = r^2 \qquad \text{(A1.4)}$$

$$\Delta^2 - 2r\Delta + \frac{w^2}{4} = 0$$

Solve for $r$:

$$r = \frac{\Delta^2 + \frac{w^2}{4}}{2\Delta} \qquad \text{(A1.6)}$$

therefore

$$\sin\frac{\theta}{2} = \frac{\left(\frac{w}{2}\right)}{r} = \frac{\Delta w}{\Delta^2 + \frac{w^2}{4}} \qquad \text{(A1.7)}$$

$$= \frac{\Delta/w}{(\Delta/w)^2 + 1/4} \qquad \text{(A1.8)}$$

$$\frac{\theta}{2} = \sin^{-1}\left(\frac{\Delta/w}{(\Delta/w)^2 + 1/4}\right) \qquad \text{(A1.9)}$$

Now, arc length $L_a = r\,\theta$, therefore

$$\frac{L_a}{w} = \frac{r\theta}{w} = \frac{2r}{w} \cdot \frac{\theta}{2} \qquad \text{(A1.10)}$$

$$= \frac{\Delta^2 + w^2/4}{\Delta w} \cdot \frac{\theta}{2} \qquad \text{(A1.11)}$$

$$\frac{L_a}{w} = \frac{\left(\frac{\Delta}{w}\right)^2 + \frac{1}{4}}{\left(\frac{\Delta}{w}\right)} \sin^{-1}\left(\frac{\left(\frac{\Delta}{w}\right)}{\left(\frac{\Delta}{w}\right)^2 + \frac{1}{4}}\right) \qquad \text{(A1.12)}$$

This equation applies for $\Delta \leq w/2$.

# A2. Mathematical modelling of DOC as an unsteady state process

## List of Nomenclature

$A$ - cross sectional area of flow, $m^2$

$A_m$ - membrane area, $m^2$

$A_{mL}$ - available membrane area per unit length of flow, $m^2$

$A_n$ - cross sectional area of flow in juice circuit, $m^2$

$\overline{A}_n$ - average cross sectional area of flow in juice circuit, $m^2$

$B_n$ - cross sectional area of flow in the OA circuit, $m^2$

$\overline{B}_n$ - average cross sectional area of flow in OA circuit, $m^2$

$C$ - membrane constant, kg $m^{-2}$ $s^{-1}$ $Pa^{-1}$

$K_m$ - available membrane area per unit length of flow divided by the cross sectional flow area within the module

L - length of flow channel, m

$m_w$ - water mass flux rate, kg $m^{-2}$ $s^{-1}$

$m_w(x,t)$ - water mass flux rate at position $x$ and at time $t$, kg $m^{-2}$ $s^{-1}$

$p$ - pressure, Pa

$P_n$ - volumetric flow rate in the juice circuit, $m^3$ $s^{-1}$

$\hat{P}_3$ - volumetric flow rate from juice circuit pump, $m^3$ $s^{-1}$

$Q$ - volumetric flow rate, $m^3$ $s^{-1}$

$Q(t)$ - volumetric flow rate at time $t$, $m^3$ $s^{-1}$

$\hat{Q}_3$ - volumetric flow rate from OA circuit pump, $m^3$ $s^{-1}$

$Q_n$ - volumetric flow rate in the OA circuit, $m^3$ $s^{-1}$

$R_n$ - length of each flow section, juice circuit, m

$S_n$ - length of each flow section, OA circuit, m

$t$ - time, s

$u$ - velocity in the juice circuit direction, m $s^{-1}$

$u(x, t)$ - velocity in the juice circuit at position $x$ and at time $t$, m $s^{-1}$

$v$ - velocity in the OA circuit direction, m $s^{-1}$

$v(x, t)$ - velocity in the OA circuit at position $x$ and at time $t$, m $s^{-1}$

$V$ - volume, $m^3$

$V_a$ - volume in OA reservoir tank, $m^3$

$x$ - horizontal distance parallel to the flow channel, m

$X$ - solute mass fraction, in juice circuit, g (g solution)$^{-1}$

$X(x, t)$ - solute mass fraction in juice circuit at position $x$ and at time $t$, g (g solution)$^{-1}$

| | |
|---|---|
| $Y$ | - solute mass fraction in OA circuit, g (g solution)$^{-1}$ |
| $Y(x,t)$ | - solute mass fraction in OA circuit at position $x$ and at time $t$, g (g solution)$^{-1}$ |

*Greek symbols*

| | |
|---|---|
| $\pi$ | - osmotic pressure, MPa |
| $\pi_J(X)$ | - osmotic pressure of solution in juice circuit at concentration $X$, MPa |
| $\pi_C(Y)$ | - osmotic pressure of solution in OA circuit at concentration $Y$, MPa |
| $\rho$ | - fluid or solution density, kg m$^{-3}$ |
| $\rho'$ | - derivative of density as a function of concentration |

*Subscripts*

| | |
|---|---|
| 1 | - module section of OA or juice circuit |
| 2 | - feed inlet section of juice circuit or OA reservoir section of OA circuit |
| 3 | - pump section of juice circuit or pump section of OA circuit |
| *a* | - OA reservoir |
| *C* | - bulk OA free-stream solution, at flow channel entry |
| *F* | - juice feed |
| *J* | - juice circuit solution |
| n | - section of the juice circuit, 1,2 or 3 |
| *w* | - water |

## A2.1. Derivation of mathematical model

The DOC process was modelled as an unsteady state process, over the entire unit, taking into account changes in concentration on both the juice and OA circuits over time. The driving force for mass transfer was assumed to be the concentration difference between the bulk juice and bulk OA streams. The mass flux was also assumed to be proportional to the driving force based on the following equation.

$$m_w = C(\pi_{OA} - \pi_J) \qquad \text{(A2.1)}$$

This model describes the change in solute concentration in a small laboratory scale module and the adjoining tubing with respect to position and time. It models the transport of solvent through the membrane and then describes the changes in concentration and flow rate in both the juice and OA circuits relative to position and time in the two circuits. The change in concentration throughout the module and tubing can be determined at any point in time.

The contribution due to diffusion was neglected as being small. The diffusion rate is much less than the advection rate therefore transport was assumed to be due purely to convection. The ratio between the diffusion distance and the distance travelled in the module was $10^4$, therefore diffusion has little effect. Concentration changes, due to convection, at different positions up the DOC module and around the unit were determined. It was assumed the concentration of the solution in the juice circuit would change after one pass through the module.

The equations proposed to describe the change in concentration throughout the module and tubing were derived from first principles based on flow through a uniform pipe. Calculations are based on mass flows.

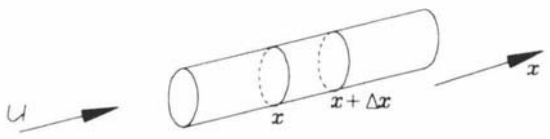


For flow in a tube of uniform cross-sectional area '$A$'. Assume uniform velocity $u(x,t)$ in the $x$ direction along the axis of the tube, fluid density is $\rho(x,t)$. During the time interval $\Delta t$, the net increase in mass within the tube length $\Delta x$ is balanced by the net in flow.

$$(\rho A \Delta x)_{t+\Delta t} - (\rho A \Delta x)_t \approx (\rho u A)_x \Delta t - (\rho u A)_{x+\Delta x} \Delta t \qquad \text{(A2.2)}$$

$\div A \Delta x \Delta t$

$$\frac{\rho_{t+\Delta t} - \rho_t}{\Delta t} \approx - \frac{(\rho u)_{x+\Delta x} - (\rho u)_x}{\Delta x} \qquad \text{(A2.3)}$$

$$\lim \begin{matrix} \Delta t \to 0 \\ \Delta x \to 0 \end{matrix}$$

$$\frac{\partial \rho}{\partial t} + \frac{\partial}{\partial x}(\rho u) = 0 \qquad \text{(A2.4)}$$

*Total mass flow*

Equation (A2.4) can be written

$$\frac{D\rho}{Dt} + \rho \frac{\partial u}{\partial x} = 0 \qquad \text{(A4.5)}$$

$$\text{where} \quad \frac{D}{Dt} \equiv \frac{\partial}{\partial t} + u\frac{\partial}{\partial x} \tag{A2.6}$$

*Solute mass flow*

$$\frac{\partial}{\partial t}(\rho X) + \frac{\partial}{\partial x}(\rho X u) = 0 \tag{A2.7}$$

$$or \quad \rho\frac{DX}{Dt} + X\left(\frac{D\rho}{Dt} + \rho\frac{\partial u}{\partial x}\right) = 0 \tag{A2.8}$$

$X$ - solute mass fraction (g (g solution)$^{-1}$)

Using Equation (A2.5) and substituting into Equation (A2.8), then

$$\rightarrow \quad \frac{DX}{Dt} = 0 \tag{A2.9}$$

i.e., relative to the frame of reference moving with the fluid, $X$ does not change with time.

If fluid density depends only on the solute concentration $X$, then $\rho = \rho(X)$ and Equation (A2.5) becomes

$$\rho'\frac{DX}{Dt} + \rho\frac{\partial u}{\partial x} = 0 \tag{A2.10}$$

where $\rho' = d\rho/dX$ and, using Equation (A2.9) ,

$$\frac{\partial u}{\partial x} = 0 \tag{A2.11}$$

Then $u = u(t)$ and the volumetric flow rate

$$Q = Au(t) = Q(t) \tag{A2.12}$$

A flow diagram showing boundary points and direction of flow is presented in Figure A2.1. A dilute solution circulates in the juice circuit. As water is lost through the membrane (between positions 0 to $R_1$), the volume of water lost is replaced by dilute feed, with concentration $X_F$, at $R_2$. Hence, solute accumulates in the juice circuit and steady state is never reached, i.e. there is always an osmotic pressure driving force acros the membrane. If steady state is reached no loss of water occurs therefore no

**Figure A2.1. Flow diagram of DOC unit used for unsteady state modelling**

$A_n$ - cross sectional area of flow in juice circuit, $m^2$
$B_n$ - cross sectional area of flow in OA circuit, $m^2$
$P_n$ - volumetric flow rate in juice circuit, $m^3\ s^{-1}$
$Q_n$ - volumetric flow rate in OA circuit, $m^3\ s^{-1}$
$R_n$ - length of each flow section in juice circuit, m
$S_n$ - length of each flow section in OA circuit, m
$X_n$ - solute mass fraction in juice circuit
$Y_n$ - OA solute mass fraction in OA circuit
$V_a$ - volume of OA in OA reservoir, $m^3$
$m_w$ - water mass flow rate per unit area of membrane, $m^2$
n - section of DOC unit, 1,2 and 3
$x$ - position on the x axis
$t$ - time, s
1 - in module
2 - between module and juice feed inlet or between module and OA reservoir
3 - between feed inlet and module, including pump or between OA reservoir and module, including pump.

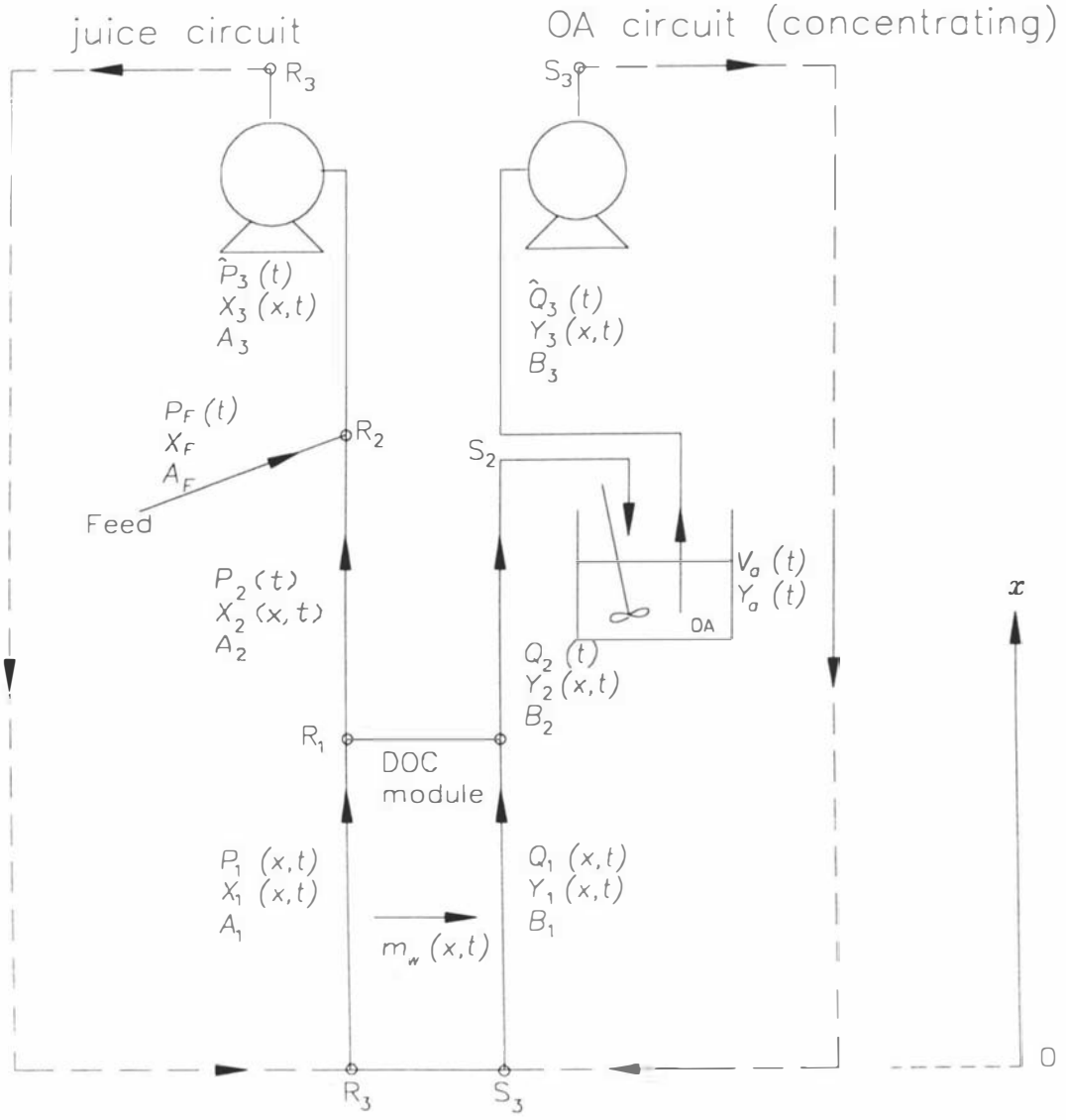
juice circuit
OA circuit (concentrating)
R3
S3
P̂3 (t)
X3 (x,t)
A3
Q̂3 (t)
Y3 (x,t)
B3
PF (t)
XF
AF
Feed
R2
S2
P2 (t)
X2 (x,t)
A2
Va (t)
Ya (t)
OA
Q2 (t)
Y2 (x,t)
B2
R1
DOC
module
P1 (x,t)
X1 (x,t)
A1
Q1 (x,t)
Y1 (x,t)
B1
mw (x,t)
x
0
R3
S3

concentration takes place. In the OA circuit, the OA flows past the membrane taking up the water and then returns to the OA reservoir, which is kept well mixed. The OA is continuously pumped from the reservoir and through the DOC module.

Initially, at time zero, the juice circuit is at concentration $X_F$ (dilute juice concentration) and the OA circuit is at concentration $Y_a$. There is no mass transfer of water ($m_w$) occurring across the membrane until $t_0 + \Delta t$. The model follows the process until the controlled stop point is met, such as, there is no more feed solution or when the concentration difference is so small that it becomes no longer practical to run the unit. The DOC process has been modelled for a batch process.

Assumptions which were made when developing the model for the direct osmotic concentration unit:

1. The driving force for mass flux of water across the membrane can be assumed to be provided by the osmotic pressure difference between the bulk juice and OA circuits.
2. There is no solute transport across the membrane.
3. Solute accumulates in the juice circuit and steady state is never attained.
4. Rigid walled uniform tubes are used.
5. Area of flow in the tubes is constant and cross-sectional area of flow does not change with time.
6. Thermal affects are ignored.
7. The hydraulic pressures on the juice side and inside the module are constant, not dependent on position and time i.e. $p_J(x,t) \rightarrow p_J$ and $p_C(x,t) \rightarrow p_C$.
8. Hydraulic pressure differences between the juice side and the OA side are small i.e. $(p_J - p_C)$ is small.
9. $\bar{A}_1(x,t)$ and $\bar{B}_1(x,t)$ are representative of membrane area in the module. $\bar{A}_1(x,t)$ and $\bar{B}_1(x,t)$ are independent of position and time. The membrane area inside the module remains constant.
10. Concentration polarisation or boundary layer affects are ignored. Also transport resistances in porous support and boundary layers are ignored.
11. Flow of OA is modelled flowing co-current to juice flow inside module.

Subscripts C - represents concentrating circuit containing the OA
J - represents the juice circuit containing the dilute solution

## A2.2. Mass balances over DOC unit

In the juice circuit, $\rho = \rho_J(X(x,t))$ where $X(x,t)$ = mass fraction of solute at position x and at time $t$.

• in the module

$X = X_1(x,t)$, $u = u_1(x,t)$

$Q = \bar{A}_1\, u_1(x,t) = P_1(x,t)$ $\qquad 0 \le x \le R_1$

where

$Q$ - flow rate in circuit, $m^3\ s^{-1}$

$P_n$ - flow rate in juice circuit, $m^3\ s^{-1}$

$Q_n$ - flow rate in OA circuit, $m^3\ s^{-1}$

$\bar{A}_n$ - average cross sectional area of flow in juice circuit, $m^2$

$u$ - velocity in juice circuit, $m\ s^{-1}$

$v$ - velocity in OA circuit, $m\ s^{-1}$

n - section 1, 2, or 3.

• in outlet section:

$X = X_2(x,t)$, $u = u_2(x,t)$

$Q = A_2\, u_2(t) = P_2(t)$ $\qquad R_1 \le x \le R_2$

• in juice feed:

$X = X_F$, $u = u_F(t)$

$Q = A_F\, u_F(t) = P_F(t)$ $\qquad 0 \le x \le R_F$

• in pump section:

$X = X_3(x,t)$, $u = u_3(t)$ $[= \hat{U}(t)]$

$Q = A_3\, u_3(t)$ $[= A_3\, \hat{U}(t)] = \hat{P}_3(t)$ $\qquad R_2 \le x \le R_3$

In the OA circuit, $\rho = \rho_c(Y(x,t))$, where $Y(x,t)$ = mass fraction of OA solute at position $x$ and at time $t$,

• in the module:

$X = Y_1(x,t)$, $u = v_1(x,t)$

$Q = \bar{B}_1\, u_1(x,t) = Q_1(x,t)$ $\qquad 0 \le x \le R_1$

• in outlet section:

$X = Y_2(x,t)$, $u = v_2(t)$

$Q = B_2\, u_2(x,t) = Q_2(t)$ $\qquad R_1 \le x \le S_2$

• in the OA reservoir

$X = Y_a(t)$

$V = V_a(t)$ where $V_a(t)$ = volume of OA

• in pump section:

$X = Y_3(x,t)$, $u = v_3(t)$ $[= \hat{V}(t)]$

$Q = B_3\, u_3(t)\ [= B_3 \hat{V}(t)] = \hat{Q}_3(t)$ $\qquad S_2 \le x \le S_3$

( ˆ values are determined by pump rates.)

## A2.3. Flow in the DOC module

Flow in the module is described as:

$$(\rho A \Delta x)_{t+\Delta t} - (\rho A \Delta x)_t \approx (\rho u A)_x \Delta t - (\rho u A)_{x+\Delta x} \Delta t \mp m_w(x,t) A_m \Delta x \Delta t \qquad \text{(A2.13)}$$

where $m_w(x,t)$ is the mass flow rate of water across the membrane per unit area of membrane and $A_m$ is the available membrane area per unit length of the flow; (-) sign on juice side, (+) sign on the OA side.

$\div A\, \Delta x\, \Delta t$ and $\quad \lim \begin{matrix} \Delta t \to 0 \\ \Delta x \to 0 \end{matrix}$

$$\frac{\partial \rho}{\partial t} + \frac{\partial}{\partial x}(\rho u) = \mp K_m m_w(x,t) \qquad 0 \le x \le R_1 \qquad \text{(A2.14)}$$

where

$$K_m = \frac{A_{mL}}{A} \qquad \text{(A2.15)}$$

$K_m$ is the available membrane area per unit length of flow divided by the cross-sectional flow area within the module, which is assumed to be constant. Since the flow areas on each side of the membrane are different, $K_m$ will have a different value on each side.

On the juice side

$$K_m = \frac{A_{mL}}{A_1} = K_{mJ} \qquad \text{(A2.16)}$$

On the OA side

$$K_m = \frac{A_{mL}}{B_1} = K_{mC} \qquad \text{(A2.17)}$$

Total mass flow:

$$\frac{\partial \rho}{\partial t} + \frac{\partial}{\partial x}(\rho u) = \mp K_m m_w \tag{A2.18}$$

$$or \qquad \frac{D\rho}{Dt} + \rho \frac{\partial u}{\partial x} = \mp K_m m_w \tag{A2.19}$$

*Solute mass flow:* there is no solute flow across the membrane, Equations (A2.7) and (A2.8) presented earlier

$$\frac{\partial}{\partial t}(\rho X) + \frac{\partial}{\partial x}(\rho X u) = 0$$

$$or \qquad \rho \frac{DX}{Dt} + X\left(\frac{D\rho}{Dt} + \rho \frac{\partial u}{\partial x}\right) = 0$$

Using Equation (A2.19) in Equation (A2.8):

$$\rho \frac{DX}{Dt} = \mp K_m X m_w \tag{A2.20}$$

If $\rho = \rho(X)$, then Equation (A2.8) becomes

$$\rho \frac{DX}{Dt} + X\left(\rho' \frac{DX}{Dt} + \rho \frac{\partial u}{\partial x}\right) = 0 \tag{A2.21}$$

$$or \qquad X \frac{\partial u}{\partial x} = -\left(1 + X \frac{\rho'}{\rho}\right) \frac{DX}{Dt} \tag{A2.22}$$

Using Equation (A2.20):

$$\frac{\partial u}{\partial x} = \mp \frac{K_m}{\rho}\left(1 + X \frac{\rho'}{\rho}\right) m_w \tag{A2.23}$$

So in the module, $X$ and $u$ satisfy Equations (A2.20) and (A2.23)

$$\frac{DX}{Dt} = \pm \frac{A_{mL}}{\rho A} X m_w \tag{A2.24}$$

where $Q = u A$, $A_{mL} = K_m A$

$$\frac{\partial Q}{\partial x} = \mp \frac{A_{mL}}{\rho}\left(1 + X\frac{\rho'}{\rho}\right) m_w \qquad \text{(A2.25)}$$

An empirical equation based on the solution-diffusion model for solvent flow across a reverse osmosis membrane (Lonsdale, 1972; Rautenbach and Albrecht, 1989; Cheryan and Nichols, 1992), is used initially to describe the mass transfer through the membrane.

$$m_w = C\,[\pi_C(Y) - \pi_f(X)] \qquad \text{(A2.26)}$$

In the module the juice changes concentration as it moves up the module and with time. The concentration change is due to the loss of water across the membrane dependent on the osmotic pressure difference between the juice and the osmotic agent. The rate of water loss across the membrane is described by Equation (A2.26).

The governing equations derived for the DOC process are as follows, they have been written in terms of $X$, $Y$, $P$ and $Q$.

Juice circuit

The change in concentration and flow rate of the dilute solution in the juice circuit, with respect to position and time is described by the following equations

• in the module

$$\frac{\partial X_1}{\partial t} + \frac{P_1}{\overline{A_1}}\frac{\partial X_1}{\partial x} = \frac{A_{mL_j}}{\rho_f(X_1)\overline{A_1}} X_1 m_w \qquad \text{(A2.27)}$$

$$\frac{\partial P_1}{\partial x} = -\frac{A_{mL_j}}{\rho_f(X_1)}\left[1 + X_1\frac{\rho_f'(X_1)}{\rho_f(X_1)}\right] m_w \qquad \text{(A2.28)}$$

for $0 < x < R_1$

• in outlet section

$$\frac{\partial X_2}{\partial t} + \frac{P_2}{A_2}\frac{\partial X_2}{\partial x} = 0 \qquad \text{(A2.29)}$$

for $R_1 < x < R_2$

• in pump section

$$\frac{\partial X_3}{\partial t} + \frac{P_3}{A_3}\frac{\partial X_3}{\partial x} = 0 \qquad \text{(A2.30)}$$

for $R_2 < x < R_3$

Osmotic agent (OA) circuit

For the OA circuit the equations for the change in concentration and flow rate of concentrating agent in the OA circuit, with respect to position and time is described by the following equations

• in the module

$$\frac{\partial Y_1}{\partial t} + \frac{Q_1}{B_1}\frac{\partial Y_1}{\partial x} = -\frac{A_{mL_c}}{\rho_C(Y_1)B_1} Y_1 m_w \qquad \text{(A2.31)}$$

$$\frac{\partial Q_1}{\partial x} = \frac{A_{mL_c}}{\rho_C(Y_1)}\left[1 + Y_1\frac{\rho_C'(Y_1)}{\rho_C(Y_1)}\right] m_w \qquad \text{(A2.32)}$$

for $0 < x < R_1$

• in outlet section

$$\frac{\partial Y_2}{\partial t} + \frac{Q_2}{B_2}\frac{\partial Y_2}{\partial x} = 0 \qquad \text{(A2.33)}$$

for $R_1 < x < S_2$

• in pump section

$$\frac{\partial Y_3}{\partial t} + \frac{Q_3}{B_3}\frac{\partial Y_3}{\partial x} = 0 \qquad \text{(A2.34)}$$

for $S_2 < x < S_3$

OA reservoir

The OA in the reservoir is assumed to be well mixed. The concentration and the volume of the OA is dependent on time only

*Total mass flow*:

$$\frac{d}{dt}\left[\rho_C(Y_a(t))V_a(t)\right] = \rho_C(Y_2(S_2,t))v_2(t)B_2 - \rho_C(Y_a(t))v_3(t)B_3 \qquad \text{(A2.35)}$$

*Solute mass flow:*

$$\frac{d}{dt}\left[\rho_C(Y_a(t))V_a(t)Y_a(t)\right] = \rho_C(Y_2(S_2,t))v_2(t)B_2Y_2(S_2,t) - \rho_C(Y_a(t))v_3(t)B_3Y_a(t)$$

(A2.36)

Equation (A2.35) becomes

$$\rho_C'(Y_a(t))V_a(t)\frac{dY_a}{dt} + \rho_C(Y_a(t))\frac{dV_a}{dt} = \rho_C(Y_2(S_2,t))Q_2(t) - \rho_C(Y_a(t))Q_3(t)$$

(A2.37)

Equation (A2.36) becomes

$$\left[\rho_C(Y_a(t)) + \rho_C'(Y_a(t))Y_a(t)\right]V_a(t)\frac{dY_a}{dt} + \rho_C(Y_a(t))Y_a(t)\frac{dV_a}{dt}$$
$$= \rho_C(Y_2(S_2,t))Q_2(t)Y_2(S_2,t) - \rho_C(Y_a(t))Q_3(t)Y_a(t)$$

(A2.38)

Now if Equation (A2.37) is multiplied by $Y_a(t)$ and subtracted from Equation (A2.38), this results in,

$$\rho_C(Y_a(t))V_a(t)\frac{dY_a}{dt} = \rho_C(Y_2(S_2,t))Q_2(t)\left[Y_2(S_2,t) - Y_a(t)\right] \qquad \text{(A2.39)}$$

Substituting Equation (A2.39) into Equation (A2.38) gives

$$\rho_C(Y_a(t))\frac{dV_a}{dt} = \rho_C(Y_2(S_2,t))Q_2(t)\left\{1 - \frac{\rho_C'(Y_a(t))}{\rho_C(Y_a(t))}\left[Y_2(S_2,t) - Y_a(t)\right]\right\} - \rho_C(Y_a(t))Q_3(t)$$

(A2.40)

Across membrane module

$$m_w(x,t) = C\,[\pi_C(Y_1(x,t)) - \pi_J(X_1(x,t))] \tag{A2.41}$$

## A2.4. Boundary conditions

The following boundary conditions are written in terms of continuity of total mass and solute mass flow.

For the juice circuit

at $x = 0$

*total mass flow:*

$$\rho_J(X_3(R_3,t))u_3(t)A_3 = \rho_J(X_1(0,t))u_1(0,t)\overline{A_1} \tag{A2.42}$$

*solute mass flow:*

$$\rho_J(X_3(R_3,t))u_3(t)A_3X_3(R_3,t) = \rho_J(X_1(0,t))u_1(0,t)\overline{A_1}X_1(0,t) \tag{A2.43}$$

$$X_3(R_3,t) = X_1(0,t) \tag{A2.44}$$

$$P_3(t) = P_1(0,t) \tag{A2.45}$$

at $x = R_1$

*total mass flow:*

$$\rho_J(X_1(R_1,t))u_1(R_1,t)\overline{A_1} = \rho_J(X_2(R_1,t))u_2(t)A_2 \tag{A2.46}$$

*solute mass flow:*

$$\rho_J(X_1(R_1,t))u_1(R_1,t)\overline{A_1}X_1(R_1,t) = \rho_J(X_2(R_1,t))u_2(t)A_2X_2(R_1,t) \tag{A2.47}$$

$$X_1(R_1,t) = X_2(R_1,t) \tag{A2.48}$$

$$P_1(R_1,t) = P_2(t) \tag{A2.49}$$

at $x = R_2$

*total mass flow:*

$$\rho_J(Y_2(R_2,t))u_2(t)A_2 + \rho_J(X_F)u_F(t)A_F = \rho_J(X_3(0,t))u_3(t)A_3 \quad \text{(A2.50)}$$

*solute mass flow:*

$$\rho_J(Y_2(R_2,t))u_2(t)A_2X_2(R_2,t) + \rho_J(X_F)u_F(t)A_FX_F = \rho_J(X_3(0,t))u_3(t)A_3X_3(0,t) \quad \text{(A2.51)}$$

$$X_3(0,t) = \frac{\rho_J(X_2,t)P_2(t)X(R_2,t) + \rho_J(X_F)P_F(t)X_F}{\rho_J(X_2,t)P_2(t) + \rho_J(X_F)P_F(t)} \quad \text{(A2.52)}$$

and

$$P_3(t) = \frac{\rho_J(X_2,t)P_2(t) + \rho_J(X_F)P_F(t)}{\rho_J(X(0,t))} \quad \text{(A2.53)}$$

rearranging Equation (A2.50)

$$\rho_J(X_F)P_F(t) = \rho_J(X_3(0,t))P_3(t) - \rho_J(X_2(R_2,t))P_2(t) \quad \text{(A2.54)}$$

Substitute for $\rho_J(X_F)P_F(t)$ in Equation (A2.50)

$$X_3(0,t) = \frac{\rho_J(X_2(R_2,t))P_2(t)X_2(R_2,t) + \rho_J(X_3(0,t))P_3(t)X_F - \rho_J(X_2(R_2,t))P_2(t)X_F}{\rho_J(X_3(0,t))P_3(t)} \quad \text{(A2.55)}$$

$$X_3(0,t) = X_F + \frac{\rho_J(X_2(R_2,t))P_2(t)\,[X_2(R_2,t) - X_F]}{\rho_J(X_3(0,t))P_3(t)} \quad \text{(A2.56)}$$

$$P_F(t) = \frac{\rho_J(X_3(0,t))P_3(t) - \rho_J(X_2(R_2,t))P_2(t)}{\rho_J(X_F)} \quad \text{(A2.57)}$$

For OA circuit:

at $x = 0$

*total mass flow:*

$$\rho_C(Y_3(S_3,t))v_3(t)B_3 = \rho_C(Y_1(0,t))v_1(0,t)\overline{B_1} \quad \text{(A2.58)}$$

*solute mass flow:*

$$\rho_C(Y_3(S_3,t))v_3(t)B_3Y_3(S_3,t) = \rho_C(Y_1(0,t))v_1(0,t)\overline{B_1}Y_1(0,t) \quad \text{(A2.59)}$$

$$Y_3(S_3,t) = Y_1(0,t) \quad \text{(A2.60)}$$

$$Q_3(t) = Q_1(0,t) \quad \text{(A2.61)}$$

at $x = R_1$

*total mass flow:*

$$\rho_C(Y_1(R_1,t))v_1(R_1,t)\overline{B_1} = \rho_C(Y_2,t))v_2(t)B_2 \quad \text{(A2.62)}$$

*solute mass flow:*

$$\rho_C(Y_1(R_1,t))v_1(R_1,t)\overline{B_1}Y_1(R_1,t) = \rho_C(Y_2,t))v_2(t)B_2Y_2(0,t) \quad \text{(A2.63)}$$

$$Y_1(R_1,t) = Y_2(0,t) \quad \text{(A2.64)}$$

$$Q_1(R_1,t) = Q_2(t) \quad \text{(A2.65)}$$

at $x = S_2$

$$Y_a(t) = Y_3(S_2,t) \quad \text{(A2.66)}$$

## A2.5. Solution of equations for unsteady state DOC model

These equations have been solved by numerical analysis, the following variables were solved for with respect to position and time

$X_1(x,t)$, $P_1(x,t)$, $X_2(x,t)$, $X_3(x,t)$, $Y_1(x,t)$, $Q_1(x,t)$, $Y_2(x,t)$, $Y_3(x,t)$, $m_w(x,t)$

The following variables were solved with respect to time only

$P_2(t)$, $P_F(t)$, $Q_2(t)$, $V_a(t)$, $Y_a(t)$

Functions for density ($\rho$) and osmotic pressure ($\pi$) were determined for each solute in aqueous solution from published or experimentally determined data [Chapter 4].

$\rho_J(X)$, $\rho_J'(X)$, $\rho_C(Y)$, $\rho_C'(Y)$, $\pi_J(X)$, $\pi_C(Y)$

The value for the membrane constant $C$ used to solve the model was determined from the experimental data. For fructose, $C = 1.4 \times 10^{-9}$ kg m$^{-2}$ s$^{-1}$ Pa$^{-1}$. A computer program written in Turbo Pascal language solves the above equations by numerical analysis. A presentation of the results obtained from the program is shown in Figure A2.2.
$X_F = 0.1$ g (g solution)$^{-1}$, $Y_a = 0.7$ g (g solution)$^{-1}$, $V_a = 0.01$ m$^3$,
$P_3 = 4 \times 10^{-5}$ m$^3$ s$^{-1}$, $Q_3 = 7 \times 10^{-6}$ m$^3$ s$^{-1}$, $C = 1.4 \times 10^{-9}$ kg s$^{-1}$ m$^{-2}$ Pa$^{-1}$

For a batch process, the graphs in Figure A2.2. show that based on the input values, eventually the solute concentrations and the osmotic pressures in the juice and OA circuits equilibrate to a constant value. This was when no further transfer of water takes place as there was no driving force for mass transfer. At this same point in time, the mass flux of water across the membrane and the flow of dilute feed into the juice circuit stops. The volumetric flow rate in the juice circuit, in the module section, was initially lower than the flow rate out of the pump due to the loss of water through the membrane and conversely for the OA circuit it was higher than in the pump section.

From the program, data can be obtained on the concentration at any point ($x$) along the juice or OA circuits. This data is not presented.

The unsteady state model can be used to estimate the changes in solute concentration at any time during the concentration process. The model is for a batch process if allowed to continue for a set time period. The assumption that the mass flux rate of water across the membrane can be estimated by the osmotic pressure difference between the bulk juice and OA circuits leads to an over-estimation of the mass flux rate over time. The membrane was not homogeneous as originally assumed and concentration boundary layers were present providing resistance to mass transfer. Therefore the model for DOC was modified to incorporate the resistances to the flux of water, present in the membrane and the flow channels. The actual osmotic pressure driving force on the two sides adjacent to the active membrane layer were calculated to determine the actual flux rate across the membrane. The assumption that the concentration of the solution in the juice circuit would change after one pass was also tested.

Rautenbach and Albrecht (1989) discussed the use of iterative numerical methods to solve for changes in solute concentration and flux rate along the length of a tubular membrane.

**Figure A2.2. Unsteady state modelling results for DOC module**

Results obtained from a Pascal program written to solve the equations for an unsteady state process during concentration of a dilute solution by DOC.

$X_F$ = 0.10
$Y_a(0)$ = 0.70
$V_a(0)$ = 0.01 $m^3$
$P_3$ = $4.0 \times 10^{-5}$ $m^3$ $s^{-1}$
$Q_3$ = $7.0 \times 10^{-6}$ $m^3$ $s^{-1}$
*dt* = 1 seconds
*t(final)* = 10 hours
C = $1.4 \times 10^{-9}$ kg m $^{-2}$ $s^{-1}$ $Pa^{-1}$

$X_1[0,n]$, $Y_1[0,n]$ - solute mass fractions in juice and OA circuits at inlet to DOC module at position 0
$V_a(t)$ - volume of OA in OA reservoir
$P_1[M1,n]$, $Q_1[M1,n]$ - volumetric flow rates exiting the module at position $R_1$
$P_F[n]$ - volumetric flow rate of dilute feed into the juice circuit at position $R_2$
$m_w[0,n]$ - mass flux rate of water across the membrane at position 0.

(a) Solute concentration (mass fraction) versus time
(b) Volume in OA reservoir versus time.
(c) Volumetric flow rate in juice and OA circuits versus time
(d) Volumetric flow rate of dilute feed into juice circuit
(e) Mass flux rate of water across the membrane versus time

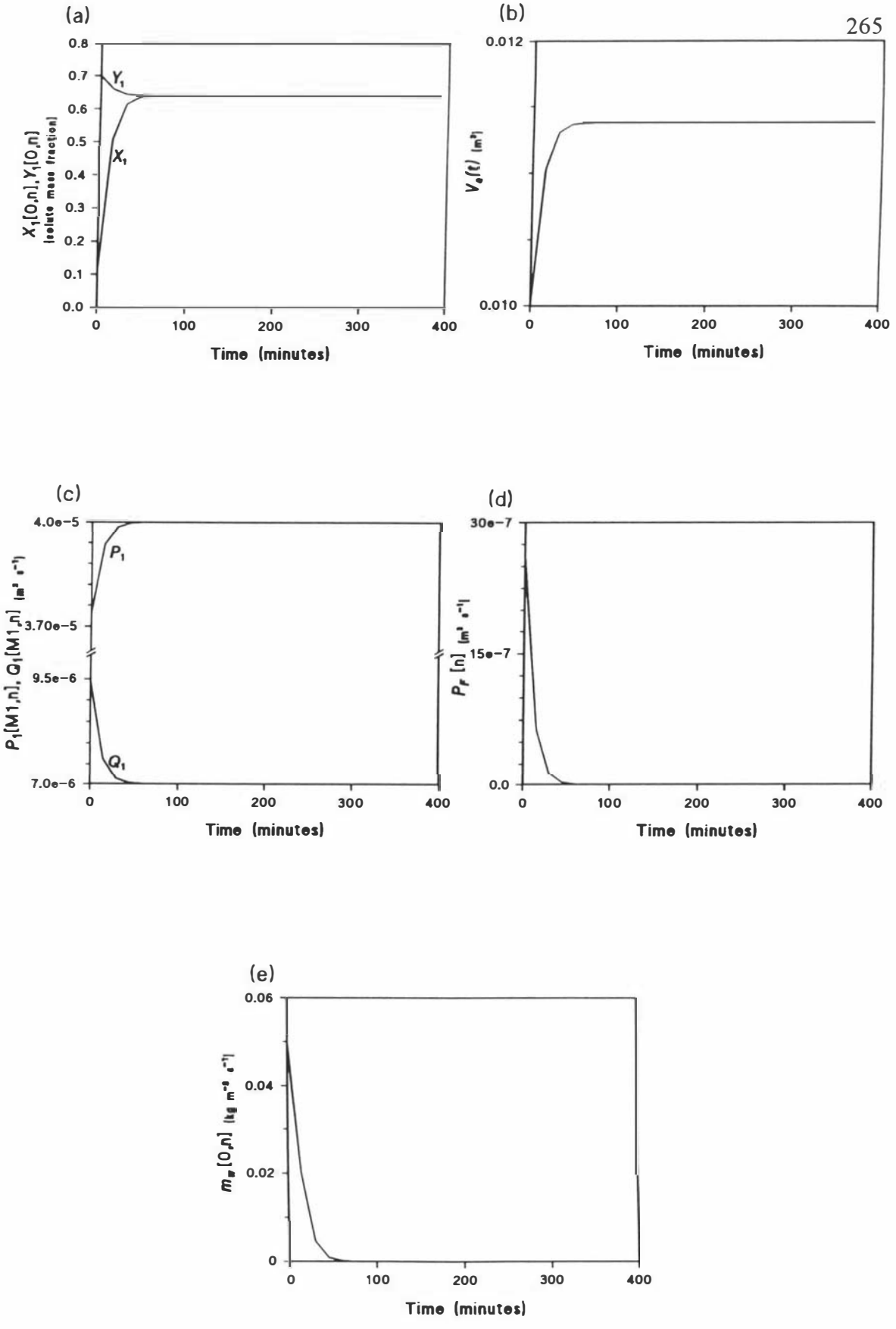
(a)
$X_1[0,n], Y_1[0,n]$ (solute mass fraction)
$Y_1$
$X_1$
Time (minutes)
(b)
$V_e(t)$ [m³]
Time (minutes)
(c)
$P_1[M1,n], Q_1[M1,n]$ [m³ s⁻¹]
$P_1$
$Q_1$
Time (minutes)
(d)
$P_F[n]$ [m³ s⁻¹]
Time (minutes)
(e)
$m_F[0,n]$ [kg m⁻³ s⁻¹]
Time (minutes)

# A3. Mathematical model derived for growing velocity boundary layer

## List of Nomenclature

$C$ - membrane constant, kg $m^{-2}$ $s^{-1}$ $Pa^{-1}$

$D_{wf}$ - binary diffusion coefficient of water in an aqueous fructose solution, $m^2$ $s^{-1}$

$D_{fw}$ - binary diffusion coefficient of fructose in an aqueous fructose solution, $m^2$ $s^{-1}$

$F(Y)$ - integral function of $Y$

$m_w$ - water mass flux rate, kg $m^{-2}$ $s^{-1}$

$m_w(x)$ - water mass flux rate at position $x$, kg $m^{-2}$ $s^{-1}$

$u$ - velocity in the $x$ direction, m $s^{-1}$

$U$ - bulk free-stream velocity in $x$ direction, m $s^{-1}$

$v$ - velocity in the y direction, m $s^{-1}$

$x$ - horizontal distance parallel to the membrane, m

$x$ - coordinate

$y$ - distance perpendicular to the membrane (across membrane or away from the membrane), m

$y$ - coordinate

$Y$ - solute mass fraction, solute mass fraction in OA circuit, g (g solution)$^{-1}$

*Greek symbols*

$\alpha$ - power term for velocity profile equation

$\delta$ - velocity boundary layer thickness, m

$\delta(x)$ - velocity boundary layer thickness as a function of $x$, m

$\mu$ - fluid or solution viscosity, kg $m^{-1}$ $s^{-1}$

$\mu(Y)$ - viscosity of solution at concentration $Y$, kg $m^{-1}$ $s^{-1}$

$\pi$ - osmotic pressure, MPa

$\pi(Y)$ - osmotic pressure of solution at concentration $Y$, MPa

$\rho$ - fluid or solution density, kg $m^{-3}$

$\rho(Y)$ - density of solution at concentration $Y$, kg $m^{-3}$

*Subscripts*

0 - position at the interface between the membrane and the velocity boundary layer

$C$ - bulk OA free-stream solution

$f$ - fructose

$w$ - water

## Derivation

This derivation was for a membrane orientated for normal operation. By solving the equations that express the conservation of mass and momentum in the boundary layer, it is possible to predict the boundary layer flow field for a two-dimensional case. The derivation of this model is described here. A schematic diagram of a growing boundary layer was shown in Figure 2.2(b) [Section 2.7].

Conservation of mass

Mass is conserved at any point in the boundary layer flow field, velocity $\vec{u}$. The equation of conservation of mass for a fluid of density $\rho$ is

$$\frac{\partial \rho}{\partial t} + \nabla \cdot (\rho \vec{u}) = 0 \qquad \text{(A3.1)}$$

This equation can be written as

$$\frac{D\rho}{Dt} + \rho \nabla \cdot \vec{u} = 0 \qquad \text{(A3.2)}$$

where, for 1 dimensional flow,

$$\frac{D}{Dt} = \frac{\partial}{\partial t} + u\frac{\partial}{\partial x} \qquad \text{(A3.3)}$$

For steady incompressible two-dimensional flow, $\vec{u} = (u, v, 0)$ in $(x, y, z)$ directions, where $u = u(x,y)$, $v = v(x,y)$. Incompressibility is expressed by

$$\frac{D\rho}{Dt} = 0 \quad \rightarrow \quad u\frac{\partial \rho}{\partial x} + v\frac{\partial \rho}{\partial y} = 0 \qquad \text{(A3.4)}$$

Where $\rho = \rho(Y)$. From Equation (A3.2),

$$\nabla \cdot \vec{u} = 0 \quad \rightarrow \quad \frac{\partial u}{\partial x} + \frac{\partial v}{\partial y} = 0 \qquad \text{(A3.5)}$$

Steady flow means $\partial\rho/\partial t = 0$, and from Equation (A3.1),

$$\nabla \cdot (\rho \vec{u}) = 0 \quad \rightarrow \quad \frac{\partial}{\partial x}(\rho u) + \frac{\partial}{\partial y}(\rho v) = 0 \qquad \text{(A3.6)}$$

For conservation of momentum, using Navier-Stokes equation for steady laminar flow in the $x$-direction, with constant pressure in the free stream outside the boundary layer:

$$\rho\left(u\frac{\partial u}{\partial x} + v\frac{\partial u}{\partial y}\right) = \frac{\partial}{\partial y}\left(\mu\frac{\partial u}{\partial y}\right) \qquad \text{(A3.7)}$$

where $\mu = \mu(Y)$. Now, using Equation (A3.5),

$$u\frac{\partial u}{\partial x} = \frac{\partial}{\partial x}(u^2) - u\frac{\partial u}{\partial x} = \frac{\partial}{\partial x}(u^2) + u\frac{\partial v}{\partial y} \tag{A3.8}$$

Substituting into Equation (A3.7) gives

$$\rho\left[\frac{\partial}{\partial x}(u^2) + \frac{\partial}{\partial y}(uv)\right] = \frac{\partial}{\partial y}\left(\mu\frac{\partial u}{\partial y}\right) \tag{A3.9}$$

$$\therefore \quad \frac{\partial}{\partial x}(u^2) + \frac{\partial}{\partial y}(uv) = \frac{1}{\rho}\frac{\partial}{\partial y}\left(\mu\frac{\partial u}{\partial y}\right) \tag{A3.10}$$

The boundary layer thickness at any point along the $x$ axis is $\delta(x)$. Integrating the above equation $\int_0^{\delta(x)} dy$

$$\int_0^{\delta}\frac{\partial}{\partial x}(u^2)dy + [uv]_0^{\delta} = \int_0^{\delta}\frac{1}{\rho}\frac{\partial}{\partial y}\left(\mu\frac{\partial u}{\partial y}\right)dy \tag{A3.11}$$

$$\int_0^{\delta}\frac{\partial}{\partial x}(u^2)dy + U\,v(x,\delta) = \int_0^{\delta}\frac{1}{\rho}\frac{\partial}{\partial y}\left(\mu\frac{\partial u}{\partial y}\right)dy \tag{A3.12}$$

where $U = u(x, \delta)$ is the free-stream flow velocity [Figure 2.2(b)] and $u(x, 0) = 0$.

• Similar integration of Equation (A3.5) gives

$$\int_0^{\delta}\frac{\partial u}{\partial x}dy + [v]_0^{\delta} = 0 \tag{A3.13}$$

or

$$\int_0^{\delta}\frac{\partial u}{\partial x}dy + v(x,\delta) - v(x,0) = 0 \tag{A3.14}$$

But

$$v(x,0) = \frac{m_w(x)}{\rho(x,0)} = \frac{m_w(x)}{\rho(Y_0(x))} \tag{A3.15}$$

where $Y_0 = Y_0(x)$,

$$\therefore \quad v(x,\delta) = \frac{m_w(x)}{\rho(Y_0)} - \int_0^{\delta}\frac{\partial u}{\partial x}dy \tag{A3.16}$$

Substituting this equation into Equation (A3.12) gives

$$\int_0^{\delta}\frac{\partial}{\partial x}(u^2)dy + U\left[\frac{m_w(x)}{\rho(Y_0)} - \int_0^{\delta}\frac{\partial u}{\partial x}dy\right] = \int_0^{\delta}\frac{1}{\rho}\frac{\partial}{\partial y}\left(\mu\frac{\partial u}{\partial y}\right)dy \tag{A3.17}$$

or

$$\int_0^{\delta} \frac{\partial}{\partial x}(u^2)dy - U\int_0^{\delta} \frac{\partial u}{\partial x}\,dy = -U\frac{m_w(x)}{\rho(Y_0)} + \int_0^{\delta} \frac{1}{\rho}\frac{\partial}{\partial y}\left(\mu\frac{\partial u}{\partial y}\right)dy \qquad \text{(A3.18)}$$

where U is constant to a good approximation (free-stream flow velocity). The LHS of Equation (A3.18) is

$$\int_0^{\delta} \frac{\partial}{\partial x}[u^2 - Uu]dy = -\frac{d}{dx}\int_0^{\delta} u(U - u)dy$$

since $u(x,0) = 0$ and $u(x, \delta) = U$. So (A3.18) becomes

$$\frac{d}{dx}\int_0^{\delta} u(U - u)dy = U\frac{m_w(x)}{\rho(Y_0)} - \int_0^{\delta} \frac{1}{\rho}\frac{\partial}{\partial y}\left(\mu\frac{\partial u}{\partial y}\right)dy \qquad \text{(A3.19)}$$

To solve for $\delta$, the velocity profile was assumed to have a parabolic shape,

$$u = U\left[1 - \left(1 - \frac{y}{\delta}\right)^2\right] \qquad \text{(A3.20)}$$

For a more generalised flow profile with a power term = $\alpha$

$$u = U\left[1 - \left(1 - \frac{y}{\delta}\right)^{\alpha}\right] \qquad \text{(A3.21)}$$

Now

$$\int_0^{\delta} u(U - u)dy = U^2\left[-\frac{\delta}{\alpha + 1}\left(1 - \frac{y}{\delta}\right)^{\alpha + 1} + \frac{\delta}{2\alpha + 1}\left(1 - \frac{y}{\delta}\right)^{2\alpha + 1}\right]_0^{\delta} \qquad \text{(A3.22)}$$

$$= U^2\delta\,\frac{\alpha}{(\alpha + 1)(2\alpha + 1)} \qquad \text{(A3.23)}$$

The integral on the RHS of Equation (A3.19) takes into account the changing properties of the solutions (viscosity $\mu$ and density $\rho$), which change with concentration ($Y$). To evaluate this integral some relationships between mass flux and concentrations will be defined. Firstly,

$$m_w(x) = \rho(Y_0)v(x,0) \qquad \text{(A3.24)}$$

Variations of properties within the boundary layer are small in the $x$-direction compared with variation in the $y$-direction. The mass flux of water in the $y$-direction is given by the sum of an advected term due to the net mass flux away from the membrane and a diffused flux (given by Fick's law):

$$m_w(x) = (1 - Y)\rho(Y)v - \rho(Y)D_{wf}(Y)\frac{\partial}{\partial y}(1 - Y)$$

Similarly the fructose mass flux perpendicular to the membrane

$$m_f(x) = Y\rho(Y)v - \rho(Y)D_{fw}(Y)\frac{\partial Y}{\partial y}$$

But $m_f(x) = 0$ since there was assumed no solute transfer across the membrane. Therefore,

$$\rho(Y)v = \frac{\rho(Y)D_{fw}(Y)\frac{\partial Y}{\partial y}}{Y}$$

and substitution into the expression for water mass flux gives

$$m_w(x) = \frac{1 - Y}{Y}\rho(Y)D_{fw}(Y)\frac{\partial Y}{\partial y} + \rho(Y)D_{wf}(Y)\frac{\partial Y}{\partial y}$$

as $D_{wf}(Y) = D_{fw}(Y)$

$$m_w(x) = \rho(Y)\frac{D_{fw}(Y)}{Y}\frac{\partial Y}{\partial y} \qquad \text{(A3.25)}$$

$D_{fw}(Y)$ is the diffusion coefficient of fructose in an aqueous solution of concentration $Y$. Now, $m_w$ is a function of $x$ only, and so, writing

$$\frac{\rho(Y)D_{fw}(Y)}{Y}\frac{\partial Y}{\partial y} = m_w(x) \qquad \text{(A3.26)}$$

and, using the calculus theorem

$$\frac{\partial}{\partial y}\left(\int_0^Y \frac{\rho(Y)D_{fw}(Y)}{Y}dY\right) = m_w(x) \qquad \text{(A3.27)}$$

then, integrating with respect to $y$,

$$\int_0^Y \frac{\rho(Y)D_{fw}(Y)}{Y}dY = m_w(x)y + B(x) \qquad \text{(A3.28)}$$

where $B$ is a function of $x$ only. Using boundary conditions at the bottom and top of the boundary layer:

$$Y = Y_0 \quad at \quad y = 0 \rightarrow \int_0^{Y_0(x)} \frac{\rho(Y)D_{fw}(Y)}{Y}dY = B(x) \qquad \text{(A3.29)}$$

$$Y = Y_C \quad at \quad y = \delta(x) \rightarrow \int_0^{Y_C} \frac{\rho(Y)D_{fw}(Y)}{Y}dY = m_w(x)\delta(x) + B(x) \qquad \text{(A3.30)}$$

subtraction gives

$$\int_{Y_0(x)}^{Y_C} \frac{\rho(Y)D_{fw}(Y)}{Y}dY = m_w(x)\delta(x) \qquad \text{(A3.31)}$$

Substitute Equations (A3.29) and (A3.31) for $B(x)$ and $m_w(x)$ into (A3.28) and rearrange:

$$\int_0^{Y} \frac{\rho(Y)D_{fw}(Y)}{Y}dY = \frac{y}{\delta(x)}\int_{Y_0(x)}^{Y_C} \frac{\rho(Y)D_{fw}(Y)}{Y}dY + \int_0^{Y_0(x)} \frac{\rho(Y)D_{fw}(Y)}{Y}dY \qquad \text{(A3.32)}$$

to give:

$$\int_{Y_0(x)}^{Y} \frac{\rho(Y)D_{fw}(Y)}{Y}dY = \frac{y}{\delta(x)}\int_{Y_0(x)}^{Y_C} \frac{\rho(Y)D_{fw}(Y)}{Y}dY \qquad \text{(A3.33)}$$

$$\therefore \quad \frac{y}{\delta(x)} = \frac{F(Y)}{F(Y_C)} \qquad \textit{where} \quad F(Y) = \int_{Y_0(x)}^{Y} \frac{\rho(Y)D_{fw}(Y)}{Y}dY \qquad \text{(A3.34)}$$

So now, from Equation (A3.21) and using Equation (A3.34), $\delta = \delta(x)$,

$$\frac{\partial u}{\partial y} = \frac{U\alpha}{\delta}\left(1 - \frac{y}{\delta}\right)^{\alpha - 1} \qquad \text{(A3.35)}$$

$$= \frac{U\alpha}{\delta}\left(1 - \frac{F(Y)}{F(Y_C)}\right)^{\alpha - 1} \qquad \text{(A3.36)}$$

Now, taking the integral on the RHS of Equation (A3.19), using integration by parts and where $\rho = \rho(Y)$,

$$\int_0^{\delta} \frac{1}{\rho}\frac{\partial}{\partial y}\left(\mu\frac{\partial u}{\partial y}\right)dy = \left[\frac{1}{\rho}\mu\frac{\partial u}{\partial y}\right]_0^{\delta} + \int_0^{\delta} \mu\frac{\partial u}{\partial y}\frac{1}{\rho^2}\frac{\partial \rho}{\partial y}dy \qquad \text{(A3.37)}$$

substitution from (A3.35) gives,

$$\int_0^{\delta} \frac{1}{\rho}\frac{\partial}{\partial y}\left(\mu\frac{\partial u}{\partial y}\right)dy = \left[\frac{1}{\rho}\mu\frac{U\alpha}{\delta}\left(1 - \frac{y}{\delta}\right)^{\alpha - 1}\right]_0^{\delta} + \int_0^{\delta} \mu\frac{\partial u}{\partial y}\frac{1}{\rho^2}\frac{\partial \rho}{\partial y}dy \qquad \text{(A3.38)}$$

$$= -\frac{\mu(Y_0)}{\rho(Y_0)}\frac{U\alpha}{\delta} + \int_0^{\delta} \mu\frac{\partial u}{\partial y}\frac{1}{\rho^2}\frac{\partial \rho}{\partial y}dy \qquad \text{(A3.39)}$$

Now

$$\rho = \rho(Y) \quad \Rightarrow \quad \frac{\partial \rho}{\partial y} = \frac{d\rho}{dY}\frac{\partial Y}{\partial y}$$

$$\therefore \int_0^{\delta} \mu \frac{\partial u}{\partial y}\frac{1}{\rho^2}\frac{\partial \rho}{\partial y}\,dy = \int_0^{\delta} \mu(Y)\frac{U\alpha}{\delta}\left(1 - \frac{F(Y)}{F(Y_C)}\right)^{\alpha-1}\frac{1}{[\rho(Y)]^2}\frac{d\rho}{dY}\frac{\partial Y}{\partial y}\,dy \tag{A3.40}$$

$$= \frac{U\alpha}{\delta}\int_{Y_0}^{Y_C}\frac{\mu(Y)}{[\rho(Y)]^2}\left(1 - \frac{F(Y)}{F(Y_C)}\right)^{\alpha-1}\frac{d\rho}{dY}\,dY \tag{A3.41}$$

since $Y = Y_0$ at $y = 0$, $Y = Y_C$ at $y = \delta(x)$ and the integrand is defined in terms of $Y$. Taking the original Equation (A3.19) and substituting in Equations (A3.23), (A3.39) and (A3.41) gives

$$\frac{d}{dx}\left[\frac{U^2\alpha}{(\alpha+1)(2\alpha+1)}\delta(x)\right] = U\frac{m_w(x)}{\rho(Y_0)} + \frac{U\alpha}{\delta(x)}\frac{\mu(Y_0)}{\rho(Y_0)} - \frac{U\alpha}{\delta(x)}\int_{Y_0(x)}^{Y_C}\frac{\mu(Y)}{[\rho(Y)]^2}\left(1 - \frac{F(Y)}{F(Y_C)}\right)^{\alpha-1}\frac{d\rho}{dY}\,dY \tag{A3.42}$$

But, from Equation (A3.31),

$$\frac{m_w(x)}{\rho(Y_0)} = \frac{1}{\delta(x)\rho(Y_0)}F(Y_C) \tag{A3.43}$$

So Equation (A3.42) becomes,

$$\frac{d}{dx}\left[\frac{\alpha U^2}{(\alpha+1)(2\alpha+1)}\delta(x)\right] = \frac{U}{\delta(x)}\frac{F(Y_C)}{\rho(Y_0)} + \frac{U\alpha}{\delta(x)}\frac{\mu(Y_0)}{\rho(Y_0)} - \frac{U\alpha}{\delta(x)}\int_{Y_0(x)}^{Y_C}\frac{\mu(Y)}{[\rho(Y)]^2}\left(1 - \frac{F(Y)}{F(Y_C)}\right)^{\alpha-1}\frac{d\rho}{dY}\,dY \tag{A3.44}$$

Multiply Equation (A3.44) by

$$\frac{2(\alpha+1)(2\alpha+1)\delta}{U^2\alpha}$$

and using the chain rule

$$2\delta\frac{d}{dx}\delta = \frac{2(\alpha+1)(2\alpha+1)}{\alpha U}\left[\frac{F(Y_C)}{\rho(Y_0)} + \frac{\alpha\mu(Y_0)}{\rho(Y_0)} - \alpha\int_{Y_0(x)}^{Y_C}\frac{\mu(Y)}{[\rho(Y)]^2}\left(1 - \frac{F(Y)}{F(Y_C)}\right)^{\alpha-1}\frac{d\rho}{dY}\,dY\right] \tag{A3.45}$$

$$\frac{d}{dx}(\delta^2) = \frac{2(\alpha + 1)(2\alpha + 1)}{\alpha U}\left[\frac{F(Y_C)}{\rho(Y_0)} + \frac{\alpha\mu(Y_0)}{\rho(Y_0)} - \alpha\int_{Y_0(x)}^{Y_C}\frac{\mu(Y)}{[\rho(Y)]^2}\left(1 - \frac{F(Y)}{F(Y_C)}\right)^{\alpha-1}\frac{d\rho}{dY}dY\right] \tag{A3.46}$$

Now, the membrane water flux is given by

$$\begin{aligned} m_w(x) &= \frac{F(Y)}{\delta(x)} \\ &= \frac{1}{\delta(x)}\int_{Y_0(x)}^{Y_c}\frac{\rho(Y)D_{fw}(Y)}{Y}\,dY \end{aligned} \tag{A3.47}$$

and as

$$m_w(x) = C\pi(Y_1) \tag{A3.48}$$

then

$$C\pi(Y_1)\delta(x) \approx (Y_C - Y_0)\left\{\frac{\frac{1}{2}[\rho(Y_0) + \rho(Y_C)]\ \frac{1}{2}[D_{fw}(Y_0) + D_{fw}(Y_C)]}{\frac{1}{2}(Y_0 + Y_C)}\right\} \tag{A3.49}$$

So

$$Y_0 = Y_C - \frac{C\delta(x)\ \pi(Y_1)}{\left\{\frac{\frac{1}{2}[\rho(Y_0) + \rho(Y_C)]\ \frac{1}{2}[D_{fw}(Y_0) + D_{fw}(Y_C)]}{\frac{1}{2}(Y_0 + Y_C)}\right\}} \tag{A3.50}$$

The boundary layer thickness can be determined using the differential Equation (A3.46) and the concentration $Y_0$ at the interface between the support layer and the boundary layer can be determined with Equation (A3.50). The constant value of $D_{fw}(Y)$ over the boundary layer was assumed to be an average value given by $D_{fw}(Y) = 0.5(D_{fw}(Y_0) + D_{fw}(Y_C))$. The water flux rate through the membrane was calculated by integrating along the length of the membrane determining at each segment ($dx$) (along the $x$ direction) the boundary layer thickness [$\delta(x)$] and the concentration $Y_0$, therefore solving Equation (A3.48).

This model was found to over estimate the thickness of the boundary layer and therefore resulted in lower mass flux rates than determined experimentally.

# A4. Pascal program to solve DOC mathematical model

Program solves the DOC mathematical model to determine the mass flux rate of water across the membrane and the concentration profiles across the support layer and the fully-developed boundary layer.

| | |
|---|---|
| Procedure Calculation1 | - solves for the case with active layer facing the OA circuit, support layer facing the juice circuit and velocity boundary layer present in OA flow channel (Case 3) |
| Procedure Calculation2 | - solves for the case with active layer facing the juice circuit, support layer facing the OA circuit and velocity boundary layer present in OA flow channel (Case 1). |
| Procedure Calculation3 | - solves for the case with active layer facing the juice circuit, support layer facing the OA circuit but with no boundary layer in the OA flow channel (Case 2) |

Program written using Turbo Pascal 7 (Borland International, California, USA)

```
Program EFFECTF1 (Output);

Uses
  Crt;

{02 January 1997}
{Marie Wong}
{**Takes into account porosity, toruosity, ie effective diffusion coefficient**}
{**Takes into account density of solution and movement in z-direction**}
{Model assumes fully developed flow across channel, laminar flow}
{Program calculates total mass flux taking into account}
{active layer, support layer and boundary layers on the OA side}
{without and with support layer, with and without fully developed boundary layer}
{with concentration profiles}

{***IMPORTANT THIS VERSION ONLY FOR FRUCTOSE AT 20C***}

Const

   C      = 1.4e-9;     {membrane constant, kg/m^2/s/Pa}
   L      = 0.1545;     {length of each channel}
   w1     = 0.0301;     {equivalent channel widths in section 1&3, side 1}
   w2     = 0.01626;    {equivalent channel widths in section 2}
   w3     = 0.03916;    {equivalent channel widths in secion 1&3, side 2}
   cc1    = 2.0;
   cc2    = 17.0;       {number of channels in section 2 total two sides}
   cc3    = 2.0;
   Am     = 0.064;      {m^2, total membrane area}
   denw   = 998.2;
   ds     = 0.00015;    {150 microns, thickness of support layer}
   h      = 0.0168;     {height from membrane to solid OA wall}
   U      = 0.03;       {velocity, m/s}
   alred  = 0.023;      {reduction factor  for I}
   MWf    = 180.16;     {molecular weight of fructose}
   Mww    = 18.0;       {molecular weight of water}
   Dwo    = 5.97e-10;   {m^2/s, Do at infinite dilution for fructose at 20C}
   muo    = 0.001002;   {kg/m/s, viscosity of wate at 20C}
   phi    = 0.5;        {porosity, = epsilon in equations}
   tau    = 1.2 ;       {tortuosity, value from beaudry approx equal to ds = 500}

Type
Osmotic_Data = Record

   afac1,
   afac2,
   I,
   U,
   Yc,
   PiYc,
   PiY0,
   PiY1   : Extended;
   mf     : Integer;
   Q      : array[0..25] of Extended;
   Y0     : array[0..25] of Extended;
   Y1     : array[0..25] of Extended;
   mw     : array[0..25] of Extended;

End;

Var
   BData : Osmotic_Data;

Function Power (X,N :Extended): Extended;
var
   Result   : Extended;
   i        : Integer;
   Y        : LongInt;
Begin
   If (N=0) then
      Power := 1
   Else
      If (X=0) then
         Power := 0
      Else
      Begin
         If (Frac(N) = 0) then
         Begin
            Y := Trunc(N);
            If (Y>0) then
            Begin
               Result := 1.0;
               For i := 1 to Y Do
                  Result := X*Result;
               Power := Result;
            End
            Else
            Begin
               {N is a negative integar}
               Result := 1.0;
               For i := -1 downto Y Do
                  Result := 1/(X*Result);
               Power := Result;
            End;
         End
         Else
         Begin
            {N is a fractional number}
            if X>0 then
            Begin
               Result := exp(N*ln(X));
               Power := Result;
            End
            Else
            Begin
               Writeln('X is a negative number cannot compute');
               halt(1);
            End;
         End;
      End;
End;
```

```
Function Molef (var Y : Extended) : Extended; {mole fraction}
var
   Result,
   A       : Extended;
Begin
   A := Y*100;
   Result := (A/MWf)/((A/MWf)+((100-A)/MWw));
   Molef := Result;
End;

Function Density (Y : Extended) : Extended;
var
   Result : Extended;
Begin
   Result := 998.2 +Y*(383.0+158.0*Y); {kg/m3}
   Density:= Result;
End;

Function Viscosity (Y : Extended) : Extended;
var
   Result : Extended;
Begin
   Result := (exp(26.8*Molef(Y)))*muo;
   Viscosity := Result;       {kg/m/s}
End;

Function Pi (Y : Extended) : Extended;
var
   Result,
   S       : Extended;
Begin
   S:= Y*(2.85+5.23*Y);
   Result := (S*(43.6+S*(2.13+0.595*S)))*1e5; {Pa}
   Pi := Result;
End;

Function Dw (var Y : Extended) : Extended;
var
   Result    : Extended;
Begin
   Result := Dwo/(exp(13.0*Molef(Y)));
   Dw    := Result;
End;

Procedure Calculation1 (var BlData : Osmotic_Data);

var
   Yc,
   Y1,
   Y1min,
   Y1max,
   Y,
   q1,
   q11,
   q12,
   q13,
   mw,
   guess,
   PiY1,
   pw,
   MY1,
   MYc,
   smally,
   step,
   bracket1,
   rhoY1,
   DwY1      : Extended;
   m,
   n,
   p,
   af        : Integer;
   Exitloop  : Boolean;
   f,
   j         : Text;

Begin
   Writeln('  m     Yc      Y0          Pi(Yc)   Pi(Y0)      Q(kg/m^2/s) ');

   BlData.mf := 20;
   BlData.I  := 0.34*alred;
   m   := 1 ;
   q11 := 0; {initialising for summing up mass flows at each n}
   q12 := 0;
   q13 := 0;
   q1  := 0;
   BlData.Yc := 0;
   BlData.Y1[m] := 0;
   BlData.PiYc := 0;
   BlData.PiY1 := 0;
   BlData.Q[m] := 0;

   Write(m:3,'   ');
   Write(BlData.Yc:3:2, '   ');
   Write(BlData.Y1[m]:7:6, '   ');
   Write(BlData.PiYc:8:1, '   ');
   Write(BlData.PiY1:8:1, '    ');
   Write(BlData.Q[m]:9:8, '   ');
   Writeln('');

   Assign(f,'EFFECTF1.dat');
   Rewrite(f);
   Writeln(f,'');
   Writeln(f,'EFFECTF1.PAS');
   Writeln(f,'FDFLOW fully developed flow, with and without support layer, for fructose');
   Write(f,'New, 02/01/97        ');
   Writeln(f,'no support');
   Write(f,'C=',C:15);
   Write(f,'   mf = ',BlData.mf:2);
   Writeln(f,'   alred = ',alred:4:3, '  Dw based on Y0 only       ');
   Writeln(f,'  m     Yc       Y1          Pi(Yc)MPa  Pi(Y1)    Q(kg/m^2/s x 10e-3) ');
   Write(f,m:3,'   ');
```

```
Write(f,BlData.Yc:3:2, '   ');
Write(f,BlData.Y1[m]:7:6, '   ');
Write(f,BlData.PiYc:8:1, '   ');
Write(f,BlData.PiY1:8:1, '   ');
Write(f,BlData.Q[m]:9:8);
Writeln(f,'');
Close(f);

Assign(j,'effcpf1.dat');
Rewrite(j);
Writeln(j,'EFFCPF1.PAS, CONCENTRATION PROFILES');
Writeln('');
Close(j);

For m := 2 to BlData.mf+1 Do
Begin
   Yc    := (m-1)*0.05;
   Y1min := 0;
   Y1max := Yc;
   Y1    := 0.5*(Y1min+Y1max);
   Exitloop := False;
   While (abs(Y1min-Y1max) > 1e-12) and (Exitloop = False) do
   Begin
      MY1 := Molef(Y1);
      MYc := Molef(Yc);
      pw  := Pi(Y1);
      rhoY1 := Density(Y1);
      DwY1  := Dw(Y1);
      guess := Yc - Y1*(1 + (((C*pw*h)/(rhoY1*DwY1))*BlData.I));
      If guess = 0 then
      Begin
         Exitloop := True;
      End
      Else
         If guess<0 then
         Begin
            Y1max := Y1;
            Y1    := 0.5*(Y1min+Y1max);
         End
         Else
            If guess>0 then
            Begin
               Y1min := Y1;
               Y1    := 0.5*(Y1min+Y1max);
            End;
   End;

   mw := C*pw;
   BlData.mw[m] := mw;
   BlData.Yc    := Yc;
   BlData.Y1[m] := Y1;
   ql  := BLData.mw[m]*L;
   ql1 := ql*w1*cc1;
   ql2 := ql*w2*cc2;
   ql3 := ql*w3*cc3;
   BlData.Q[m] := ((ql1+ql2+ql3)/Am);
   BlData.PiYc := Pi(Yc);
   BlData.PiY1 := Pi(BlData.Y1[m]);

   Write(m:3,'   ');
   Write(BlData.Yc:3:2, '   ');
   Write(BlData.Y1[m]:7:6, '   ');
   Write(BlData.PiYc:8:1, '   ');
   Write(BlData.PiY1:8:1, '    ');
   Write(BlData.Q[m]:9:8, ' ');
   Writeln('');

   Assign(f, 'EFFECTF1.dat');
   Append(f);
   Write(f,m:3,'   ');
   Write(f,BlData.Yc:3:2, '   ');
   Write(f,BlData.Y1[m]:7:6, '   ');
   Write(f,(BlData.PiYc/1e6):8:1, '   ');
   Write(f,BlData.PiY1:8:1, '    ');
   Write(f,(BlData.Q[m]*1e3):9:8, '  ');
   Writeln(f,'');
   Close(f);

   If m in[3,5,8,11,15]then
   Begin
      af := 20;
      step := h/af;
      smally := 0;
      Y := BlData.Y1[m];

      Assign(j,'EFFCPF1.dat');
      Append(j);
      Writeln(j,'active and fully developed bl, no support');
      Writeln(j,'Yc    y(m)across bl    Y0     Y');
      Write(j,BlData.Yc:4:3, '   ');
      Write(j,smally:7:6,'   ');
      Write(j,BlData.Y1[m]:6:5, '  ');
      Write(j,Y:6:5);
      Writeln(j,'');
      Close(j);

      For p:= 2 to af+1 Do
      Begin
         pw := Pi(BlData.Y1[m]);
         smally := smally + step;
         bracket1 := (1+ (((C*pw*h)/(rhoY1*DwY1))*BlData.I)/h*smally);
         Y := BlData.Y1[m]*bracket1;
         Assign(j,'EFFCPF1.dat');
         Append(j);
         Write(j,BlData.Yc:4:3, '   ');
         Write(j,smally:7:6,'   ');
         Write(j,BlData.Y1[m]:6:5, '  ');
         Write(j,Y:6:5);
         Writeln(j,'');
         Close(j);
      End;
```

```
      End;
   End;
End;

Procedure Calculation2 (var BlData : Osmotic_Data);

var
   Yc,
   Y0,
   Y1,
   Y1min,
   Y1max,
   ql,
   ql1,
   ql2,
   ql3,
   mw,
   guess,
   pw1,
   pw2,
   MY0,
   MY1,
   MYc,
   Ya,
   Yb,
   step1,
   step2,
   smally1,
   smally2,
   bracket1,
   rhoY1,
   rhoY0,
   DeY1,
   DwY0        : Extended;
   m,
   n,
   p,
   af          : Integer;
   Exitloop    : Boolean;
   f,
   j           : Text;

Begin
   Writeln('  m    Yc      Y0      Y1      Pi(Yc)    Pi(Y0)   Pi(Y1)     Q(kg/m^2/s ) ');

   BlData.mf := 20;
   BlData.I  := 0.34*alred;
   m    := 1 ;
   ql1 := 0; {initialising for summing up mass flows at each n}
   ql2 := 0;
   ql3 := 0;
   ql  := 0;
   BlData.Yc := 0;
   BlData.Y0[m] := 0;
   BlData.Y1[m] := 0;
   BlData.PiYc := 0;
   BlData.PiY0 := 0;
   BlData.PiY1 := 0;
   BlData.Q[m] := 0;

   Write(m:3,' ');
   Write(BlData.Yc:3:2, ' ');
   Write(BlData.Y0[m]:7:6, ' ');
   Write(BlData.Y1[m]:7:6, ' ');
   Write(BlData.PiYc:8:1, ' ');
   Write(BlData.PiY0:8:1, '  ');
   Write(BlData.PiY1:8:1, '    ');
   Write(BlData.Q[m]:9:8);
   Writeln('');

   Assign(f,'EFFECTF1.dat');
   Append(f);
   Writeln(f,'');
   Writeln(f,'FDFLOW fully developed flow, with and without support layer, for fructose');
   Write(f,'New, 02/01/97      ');
   Writeln(f,'with support');
   Write(f,'C=',C:15);
   Write(f,'   mf = ',BlData.mf:2);
   Writeln(f,'   alred = ',alred:4:3,'            ds = ',ds:6:5);
   Writeln(f,'       Dw1 based on Y1 only,   Dw2 based on Y0 only');
   Writeln(f,'  m    Yc    Y0      Y1      Pi(Yc)MPa Pi(Y0)   Pi(Y1)   Q(kg/m^2/s x10e-3) ');
   Write(f,m:3,' ');
   Write(f,BlData.Yc:3:2, ' ');
   Write(f,BlData.Y0[m]:7:6, ' ');
   Write(f,BlData.Y1[m]:7:6, ' ');
   Write(f,BlData.PiYc:8:1, ' ');
   Write(f,BlData.PiY0:8:1, '  ');
   Write(f,BlData.PiY1:8:1, '    ');
   Write(f,BlData.Q[m]:9:8);
   Writeln(f,'');
   Close(f);

   For m := 2 to BlData.mf+1 Do
   Begin
      Yc    := (m-1)*0.05;
      Y1min := 0;
      Y1max := Yc;
      Y1    := 0.5*(Y1min+Y1max);
      Y0    := Yc;
      Exitloop := False;
      While (abs(Y1min-Y1max) > 1e-12) and (Exitloop = False) do
      Begin
         MY0 := Molef(Y0);
         MY1 := Molef(Y1);
         MYc := Molef(Yc);
         pw1   := Pi(Y1);
         rhoY1 := Density(Y1);
         DeY1  := (phi/tau)*Dw(Y1);
         Y0  := Y1*(exp((C*pw1*ds)/(rhoY1*DeY1)));
         pw2 := Pi(Y0);
         rhoY0 := Density(Y0);
```

```
        DwY0  := Dw(Y0);
        guess := Yc - (Y0*(1 + (((C*pw1*h)/(rhoY0*DwY0))*BlData.I)));
        If guess = 0 then
        Begin
           Exitloop := True;
        End
        Else
           If guess<0 then
           Begin
              Y1max := Y1;
              Y1    := 0.5*(Y1min+Y1max);
           End
           Else
              If guess>0 then
              Begin
                 Y1min := Y1;
                 Y1    := 0.5*(Y1min+Y1max);
              End;
     End;

     mw := C*pw1;
     BlData.mw[m] := mw;
     BlData.Yc    := Yc;
     BlData.Y0[m] := Y0;
     BlData.Y1[m] := Y1;
     ql  := BlData.mw[m]*L;
     ql1 := ql*w1*cc1;
     ql2 := ql*w2*cc2;
     ql3 := ql*w3*cc3;
     BlData.Q[m] := (ql1+ql2+ql3)/Am;
     BlData.PiYc := Pi(Yc);
     BlData.PiY0 := Pi(BlData.Y0[m]);
     BlData.PiY1 := Pi(BlData.Y1[m]);

     Write(m:3,' ');
     Write(BlData.Yc:3:2, ' ');
     Write(BlData.Y0[m]:7:6, ' ');
     Write(BlData.Y1[m]:7:6, ' ');
     Write(BlData.PiYc:8:1, ' ');
     Write(BlData.PiY0:8:1, '   ');
     Write(BlData.PiY1:8:1, '   ');
     Write(BlData.Q[m]:9:8);
     Writeln('');

     Assign(f, 'EFFECTF1.dat');
     Append(f);
     Write(f,m:3,' ');
     Write(f,BlData.Yc:3:2, ' ');
     Write(f,BlData.Y0[m]:7:6, ' ');
     Write(f,BlData.Y1[m]:7:6, ' ');
     Write(f,(BlData.PiYc/1e6):8:1, ' ');
     Write(f,BlData.PiY0:8:1, '   ');
     Write(f,BlData.PiY1:8:1, '   ');
     Write(f,(BlData.Q[m]*1e3):9:8);
     Writeln(f,'');
     Close(f);

     If m in[3,5,8,11,15]then
     Begin
        af := 20;
        step1 := ds/af;
        step2 := h/af;
        smally1 := 0;
        smally2 := 0;
        Ya := BlData.Y1[m];
        Yb := BlData.Y0[m];

        Assign(j,'EFFCPF1.dat');
        Append(j);
        Writeln(j,'active,support and fully developed bl');
        Writeln(j,'Yc    y(m)across s l   Y1       Ya      y(m)across bl  Y0       Yb');
        Write(j,BlData.Yc:4:3, '   ');
        Write(j,smally1:7:6,'    ');
        Write(j,BlData.Y1[m]:6:5, '  ');
        Write(j,Ya:6:5, '   ');
        Write(j,smally2:7:6, '    ');
        Write(j,BlData.Y0[m]:6:5, '  ');
        Write(j,Yb:6:5);
        Writeln(j,'');
        Close(j);

        For p:= 2 to af+1 Do
        Begin
           pw1 := Pi(BlData.Y1[m]);
           pw2 := Pi(BlData.Y0[m]);
           smally1 := smally1 + step1;
           smally2 := smally2 + step2;
           Ya := BlData.Y1[m]*(exp(C*pw1*smally1/rhoY1/DeY1));
           bracket1 := (1+ ((C*pw1*h/rhoY0/DwY0)*BlData.I)/h*smally2);
           Yb := BlData.Y0[m]*bracket1;
           Assign(j,'EFFCPF1.dat');
           Append(j);
           Write(j,BlData.Yc:4:3, '   ');
           Write(j,smally1:7:6,'    ');
           Write(j,BlData.Y1[m]:6:5, '  ');
           Write(j,Ya:6:5, '   ');
           Write(j,smally2:7:6,'    ');
           Write(j,BlData.Y0[m]:6:5,'  ');
           Write(j,Yb:6:5);
           Writeln(j,'');
           Close(j);
        End;
     End;
  End;
End;

Procedure Calculation3 (var BlData : Osmotic_Data);

var
   Yc,
   Y0,
```

```
    Y1,
    Y1min,
    Y1max,
    q1,
    q11,
    q12,
    q13,
    mw,
    guess,
    pw,
    MY0,
    MY1,
    MYc,
    smally,
    step,
    Y,
    rhoY1,
    DeY1       : Extended;
    m,
    n,
    p,
    af         : Integer;
    Exitloop   : Boolean;
    f,
    j          : Text;

Begin
   Writeln('  m     Yc       Y1       Pi(Yc)     Pi(Y1)      Q(kg/m^2/s ) ');

   BlData.mf := 20;
   m   := 1 ;
   q11 := 0; {initialising for summing up mass flows at each n}
   q12 := 0;
   q13 := 0;
   q1  := 0;
   BlData.Yc := 0;
   BlData.Y1[m] := 0;
   BlData.PiYc := 0;
   BlData.PiY1 := 0;
   BlData.Q[m] := 0;

   Write(m:3,' ');
   Write(BlData.Yc:3:2, ' ');
   Write(BlData.Y1[m]:7:6, ' ');
   Write(BlData.PiYc:8:1, ' ');
   Write(BlData.PiY1:8:1, '    ');
   Write(BlData.Q[m]:9:8);
   Writeln('');

   Assign(f,'effectf1.dat');
   Append(f);
   Writeln(f,'');
   Writeln(f,'EFFECTF1 fully developed flow, with and without support layer, for fructose');
   Write(f,'New, 02/01/97        ');
   Writeln(f,'with support, no boundary layer');
   Write(f,'C=',C:15);
   Write(f,'   mf = ',BlData.mf:2);
   Writeln(f,'   alred = ',alred:4:3,'            ds = ',ds:6:5);
   Writeln(f,'      Dw1 based on Y1 only ');
   Writeln(f,'phi = ',phi:4:3,'       tau = ',tau:4:3);
   Writeln(f,'  m     Yc     Y1      Pi(Yc)MPa Pi(Y1)   Q(kg/m^2/s x10e-3) ');
   Write(f,m:3,' ');
   Write(f,BlData.Yc:3:2, ' ');
   Write(f,BlData.Y1[m]:7:6, ' ');
   Write(f,BlData.PiYc:8:1, ' ');
   Write(f,BlData.PiY1:8:1, '    ');
   Write(f,BlData.Q[m]:9:8);
   Writeln(f,'');
   Close(f);

   For m := 2 to BlData.mf+1 Do
   Begin
      Yc    := (m-1)*0.05;
      Y1min := 0;
      Y1max := Yc;
      Y1    := 0.5*(Y1min+Y1max);
      Exitloop := False;
      While (abs(Y1min-Y1max) > 1e-12) and (Exitloop = False) do
      Begin
         MY1 := Molef(Y1);
         MYc := Molef(Yc);
         pw := Pi(Y1);
         rhoY1 := Density(Y1);
         DeY1  := (phi/tau)*Dw(Y1);
         guess := (Yc*exp(-((C*pw*ds)/(rhoY1*DeY1)))) - Y1;
         If guess = 0 then
         Begin
            Exitloop := True;
         End
         Else
            If guess<0 then
            Begin
               Y1max := Y1;
               Y1    := 0.5*(Y1min+Y1max);
            End
            Else
               If guess>0 then
               Begin
                  Y1min := Y1;
                  Y1    := 0.5*(Y1min+Y1max);
               End;
      End;

      mw := C*pw;
      BlData.mw[m] := mw;
      BlData.Yc    := Yc;
      BlData.Y1[m] := Y1;
      q1  := BlData.mw[m]*L;
      q11 := q1*w1*cc1;
      q12 := q1*w2*cc2;
      q13 := q1*w3*cc3;
```

```
      BlData.Q[m] := (q11+q12+q13)/Am;
      BlData.PiYc := Pi(Yc);
      BlData.PiY1 := Pi(BlData.Y1[m]);

      Write(m:3,' ');
      Write(BlData.Yc:3:2, ' ');
      Write(BlData.Y1[m]:7:6, ' ');
      Write(BlData.PiYc:8:1, ' ');
      Write(BlData.PiY1:8:1, '   ');
      Write(BlData.Q[m]:9:8);
      Writeln('');

      Assign(f, 'effectf1.dat');
      Append(f);
      Write(f,m:3,' ');
      Write(f,BlData.Yc:3:2, ' ');
      Write(f,BlData.Y1[m]:7:6, ' ');
      Write(f,(BlData.PiYc/1e6):8:1, ' ');
      Write(f,BlData.PiY1:8:1, '   ');
      Write(f,(BlData.Q[m]*1e3):9:8);
      Writeln(f,'');
      Close(f);

      If m in[3,5,8,11,15]then
      Begin
         af := 20;
         step := ds/af;
         smally := 0;
         Y := BlData.Y1[m];

         Assign(j,'EFFCPF1.dat');
         Append(j);
         Writeln(j,'active and support, no bl');
         Writeln(j,'Yc    y(m)across sl    Y1      Y');
         Write(j,BlData.Yc:4:3, '   ');
         Write(j,smally:7:6,'    ');
         Write(j,BlData.Y1[m]:6:5, '  ');
         Write(j,Y:6:5);
         Writeln(j,'');
         Close(j);

         For p:= 2 to af+1 Do
         Begin
            pw := Pi(BlData.Y1[m]);
            smally := smally + step;
            Y := BlData.Y1[m]*(exp(C*pw*smally/rhoY1/DeY1));
            Assign(j,'EFFCPF1.dat');
            Append(j);
            Write(j,BlData.Yc:4:3, '   ');
            Write(j,smally:7:6,'    ');
            Write(j,BlData.Y1[m]:6:5, '  ');
            Write(j,Y:6:5);
            Writeln(j,'');
            Close(j);
         End;
      End;
   End;
End;

Begin
   clrscr;
   Calculation1(BData);  {without support layer, with fully developed flow}
   Calculation2(BData);  {with support layer, with fully developed flow}
   Calculation3(BData);  {with support layer, without fully developed flow}
End.
```

# BIBLIOGRAPHY

Atkins, P.W. 1982. Physical Chemistry. 2nd ed. Oxford University Press, Oxford, England. 1095 p.

Beaudry, E.G., Lampi, K.A. and Biermann, C. 1989. Osmotek's cold process juice concentration technology. Performance review of an innovative membrane technology used for osmotic concentration of fruit juices. Report by Osmotek Inc., Oregon, USA September. 16 p.

Beaudry, E.G. and Lampi, K.A. 1990(a). Osmotic concentration of fruit juice. Flüssiges Obst. 57(10): 652-656, 663-664.

Beaudry, E.G. and Lampi, K. A. 1990(b). Membrane technology for direct-osmosis concentration of fruit juices. Food Technology. 44(6): 121.

Belfort, G. 1977. Pressure-driven membrane processes and wastewater renovation. In: Water Renovation and Reuse. Shuval, H.I. (ed.). Academic Press, New York. p. 129-189.

Belfort, G. 1984. Synthetic Membrane Processes. Fundamentals and Water Applications. Academic Press, Orlando, Florida. 552 p.

Bengtsson, E., Trägårdh, G. and Hallström, B. 1992. Concentration of apple juice aroma from evaporator condensate using pervaporation. Lebensmittel-Wissenschaft und - Technologie. 25(1): 29-34.

Bhattacharyya, D. and Williams, M.E. 1992. Reverse osmosis. Theory. In: Membrane Handbook. Winston Ho, W.S. and Sirkar, K.K. (eds.). Van Nostrand Reinhold, New York. p. 269-280.

Bird, R.B., Stewart, W.E. and Lightfoot, E.N. 1960. Transport Phenomena. John Wiley & Sons, Inc., New York. 780 p.

Bolin, H.R. and Salunkhe, D.K. 1971. Physicochemical and volatile flavor changes occurring in fruit juices during concentration and foam-mat drying. Journal of Food Science.36: 665-668.

Bourne, M.C. 1982. Food Texture and Viscosity: Concept and Measurement. Academic Press, New York. 325 p.

Canning, R.P., Hogan, P.A. Johnson, R.A. and Micheals, A.S. 1996. Osmotic distillation: A new technology for low temperature concentration in the beverage and pharmaceutical industries. Proceedings of the International Membrane Science and Technology Conference. UNESCO Centre for Membrane Science and Technology. November: 79-80.

Caro, R.F. and Salter, R.J. 1988. Membrane separation apparatus and method. United States Patent. Nov 29: 4,787,982. 12 p.

Chandrasekaran, S.K. and Judson King, C. 1972. Multicomponent diffusion and vapor-liquid equilibria of dilute organic components in aqueous sugar solutions. AIChE Journal. 18(3): 513-520.

Cheryan, M. 1992. Concentration of liquid foods by reverse osmosis. In: Handbook of Food Engineering. Heldman, D. R. and Lund, D.B. (eds.). Marcel Dekker Inc., New York. p. 393-436.

Cheryan, M. and Nichols, D.J. 1992. Modelling of membrane processes. In: Mathematical Modelling of Food Processing Operations. Thorne, S. (ed.). Elsevier Applied Science, London and New York. p. 49-98.

Cleland, A.C. 1983. Estimation of data uncertainties. Department of Biotechnology, Massey University, Palmerston North, NZ

Clesceri, L. S., Greenberg, A. E. and Rhodes Trussel, R. 1989. Standard Methods for the Examination of Water and Wastewater. 17th ed. American Public Health Association, Washington DC.

Cussler, E.L. 1984. Diffusion. Mass transfer in fluid systems. Cambridge University Press, Cambridge, England. 525 p.

Draper, N.R. and Smith, H. 1981. Applied Regression Analysis. 2nd ed. John Wiley & Sons, Inc., New York. 709 p.

Easteal, A.J. 1990. Tracer diffusion in aqueous sucrose and urea solutions. Canadian Journal of Chemistry. 68: 1611-1615.

Easteal, A.J. 1996. Personal communication. Department of Chemistry, University of Auckland, NZ

English, A.C. and Dole, M. 1950. Diffusion of sucrose in supersaturated solutions. Journal of American Chemical Society. 72: 3261-3267.

Field, R.W. 1993. Transport processes in membrane systems. In: Membranes in Bioprocessing. Theory and Applications. Howell, J.A., Sanchez, V. and Field, R.W. (eds.). Chapman & Hall, London. p. 55-112.

Flemming, H.L. and Slater, C.S. 1992. Pervaporation. Applications and economics. In: Membrane Handbook. Winston Ho, W.S. and Sirkar, K.K. (eds.). Van Nostrand Reinhold, New York. p. 132-159.

Foust, A.S., Wenzel, L. A., Clump, C.W., Maus, L. and Anderson, L.B. 1980. Principles of Unit Operations. 2nd ed. John Wiley & Sons, New York. p. 768.

Frey, D.D. and Judson King, C. 1982. Diffusion coefficients of acetates in aqueous sucrose solutions. Journal of Chemical Engineering Data. 27: 419-422.

Galeb, A.D.S. 1994. Use of ion-exchange and direct osmotic concentration technologies for processing cantaloupe juice. Ph.D. thesis, Oregon State University. 176 p.

Gladden, J.K. and Dole, M. 1953. Diffusion in supersaturated solutions. II. Glucose solutions. Journal of American Chemical Society. 75: 3900-3904.

Glasstone, S., Laidler, K.J. and Eyring, H. 1941. The Theory of Rate Processes. The Kinetics of Chemical Reactions, Viscosity, Diffusion and Electrochemical Phenomena. McGraw-Hill Book Company, Inc., New York and London. 611 p.

Gostoli, C. and Sarti, G.C. 1989. Separation of liquid mixtures by membrane distillation. Journal of Membrane Science. 41: 211-224.

Gove, P.B., 1966. Webster's Third New International Dictionary of the English Language Unabridged. G. & C. Merriam Company, Massachusetts, USA

Henrion, P.N. 1964. Diffusion in the sucrose+water system. Trans. Faraday Society. 60: 72-74.

Herron, J.R. 1995. Personal communication. Osmotek Inc., Oregon, USA

Herron, J.R.; Beaudry, E.G.; Jochums, C.E and Medina, L.E. 1994. Osmotic concentration apparatus and method for direct osmotic concentration of fruit juices. United States Patent. 5,281,430. 16 p.

Herron, J.R., Beaudry, E.G. and Lampi, K.A. 1995. Direct osmotic concentration. Report by Osmotek Inc., Corvallis, Oregon, USA

Hiss, T.G. and Cussler, E.L. 1973. Diffusion in high viscosity liquids. AIChE Journal. 19(4): 698-703.

Honda, T. and Barclay, F. 1990. The osmotic engine. In: The Membrane Alternative: Energy Implications for Industry. Report no. 21. Howell, J.A. (ed.). The Watt Committee on Energy, Elsevier Applied Science, London and New York. p. 105-129.

Howell, J.A. 1993. Design of membrane systems. In: Membranes in Bioprocessing. Theory and Applications. Howell, J.A., Sanchez, V. and Field, R.W. (eds.). Chapman & Hall, London. p. 141-202.

Incropera, F.P. and DeWitt, D.P. 1985. Fundamentals of Heat and Mass Transfer. 2nd ed. John Wiley & Sons, New York. 802 p.

James, A.M. and Lord, M.P. 1992. Macmillan's Chemical and Physical Data. Macmillan Press, London and Basingstoke.

Johnson, J.S., Dresner, L. and Kraus, K.A. 1966. Hyperfiltration (Reverse Osmosis). In: Principles of Desalination. Spiegler, K.S. (ed.). Academic Press, New York and London. p.346-441.

Johnson, R.A., Valks, R.H. and Lefebvre, M.S. 1989. Osmotic distillation - A low temperature concentration technique. Australian Journal of Biotechnology. 3(3): 206-208.

Jonsson, G. and Boesen, C. E. 1984. Polarization phenomena in membrane processes. In: Synthetic Membrane Processes. Fundamentals and Water Applications. Belfort, G. (ed.). Academic Press Inc, Orlando, Florida. p. 101-130.

Katchalsky, A. and Curran, P.F. 1967. Nonequilibrium Thermodynamics in Biophysics. Harvard University Press, Cambridge, Massachusetts. 248 p.

Kenner, C.T. and O'Brien, R. E. 1971. Analytical Separation and Determination. MacMillian Publishing, New York. p. 21-22.

Kessler, J.O. and Moody, C.D. 1976. Drinking water from sea water by forward osmosis. Desalination. 18: 297-306.

Kravath, R.E. and Davis, J.A. 1975. Desalination of sea water by direct osmosis. Desalination. 16: 151-155.

Lang, A.R.G. 1967. Osmotic coefficients and water potentials of sodium chloride solutions from 0 to 40°C. Australian Journal of Chemistry. 20: 2017-2023.

Le Friec, Y. 1994. Food Applications and Market for Direct Osmosis Concentration. Food Science and Technology Department, Oregon State University, USA 94 p.

Lee, K.L., Baker, R.W. and Lonsdale, H.K. 1981. Membranes for power generation by pressure-retarded osmosis. Journal of Membrane Science. 8: 141-171.

Lefebvre, M. S. 1988. Method of performing osmotic distillation. United States Patent. Nov 1: 4,781,837. 14 p.

Lienhard, J.H. 1987. The Heat Transfer Textbook. Prentice-Hall, Inc., Englewood Cliffs, New Jersey. 620 p.

Lobo, V.M.M. and Quaresma, J.L. 1989. Handbook of Electrolyte Solutions. Part B. Physical Science Data 41. Elsevier, Amsterdam. p. 1602-1691.

Loeb, S. 1975. Osmotic power plants. Science. 189: 654-655.

Loeb, S. 1976. Production of energy from concentrated brine by pressure-retarded osmosis. I. Preliminary technical and economic considerations. Journal of Membrane Science. 49-63.

Loeb, S. and Bloch, M.R. 1973. Countercurrent flow osmotic processes for the production of solutions having a high osmotic pressure. Desalination. 13: 207-215.

Loeb, S. and Sourirajan, S. 1962. Sea water demineralization by means of an osmotic membrane. Advance Chemical Series. 38: 117.

Loeb, S., Zelingher, N. and Bloch, M. R. 1973. The use of osmotic sink osmosis for dewatering of concentrated brines. Proceedings of 4th International Symposium on Fresh Water from the Sea. 4: 235-241.

Loeb, S., Weintraub, M. and van Hezel, J. 1975. Dewatering of Dead Sea brine by osmosis. Israel Journal of Chemistry. 14: 244-251.

Loeb, S., Honda, T. and Reali, M. 1990. Comparative mechanical efficiency of several plant configurations using a pressure-retarded osmosis energy converter. Journal of Membrane Science. 51: 323-335.

Lonsdale, H.K. 1972. Theory and practice of reverse osmosis and ultrafiltration. In: Industrial Processing with Membranes. Lacey, R.E. and Loeb, S. (ed.). Wiley-Interscience, John Wiley & Sons, Inc., New York. p. 123-178.

Lonsdale, H.K. 1982. The growth of membrane technology. Journal of Membrane Science. 10: 81-181.

Maindonald, J.H. 1992. Statistical design, analysis, and presentation issues. New Zealand Journal of Agricultural Research. 35: 121-141.

Maindonald, J. ; 1996. Personal communication. Department of Statistics, University of Newcastle, NSW, Australia.

Matsuura, T., Baxter, A.G. and Sourirajan, S. 1973. Concentration of fruit juices by reverse osmosis using porous cellulose acetate membranes. Acta Alimentaria. 2(2): 109-150.

Matsuura, T., Baxter, A.G. and Sourirajan, S. 1974. Studies on reverse osmosis for concentration of fruit juices. Journal of Food Science. 39: 704-711.

Mengual, J.I., Ortiz de Zárate, J.M., Peña, L. and Velázquez, A. 1993. Osmotic distillation through porous hydrophobic membranes. Journal of Membrane Science. 82: 129-140.

Menting, L.C., Hoogstad, B. and Thijssen, H. A. C. 1970. Diffusion coefficients of water and organic volatiles in carbohydrate-water systems. Journal of Food Technology. 5: 111-126.

Merson, R.L. and Ginnette, L.F. 1972. Reverse osmosis in the food industry. In: Industrial Processing With Membranes. Lacey, R.E. and Loeb, S. (ed.). Wiley-Interscience, John Wiley & Sons, Inc., New York. p. 191-221.

Merson, R.L. and Morgan, A.I. 1968. Juice concentration by reverse osmosis. Food Technology. 22: 97-100.

Merton, U. 1966. Transport properties of osmotic membranes. In: Desalination by Reverse Osmosis. Merton, U. (ed.). The M.I.T. Press, Massachusetts Institute of Technology, Cambridge, Massachusetts, and London, England. p. 15-54.

Milleville, H.P. 1990. Direct osmosis concentrates juices at low temperature. Food Processing. January: 70-71.

Moody, C.D. and Kessler, J.O. 1976. Forward osmosis extractors. Desalination. 18: 283-295.

Mulder, M. 1992. Basic Principles of Membrane Technology. Kluwer Academic Publishers, Dordrecht. 363 p.

Mulder, M. 1993. Nature of membranes. In: Membranes in Bioprocessing. Theory and Applications. Howell, J.A., Sanchez, V. and Field, R.W. (eds.). Chapman & Hall, London. p. 13-54

Nabetani, H., Nakajima, M., Watanabe, A., Ikeda, S., Nakao, S. and Kimura, S. 1992. Development of a new type of membrane osmometer. Journal of Chemical Engineering of Japan. 25(3): 269-274.

Norris, R.S. 1967. Selected tables of physical properties of sugar solutions. Scientific and Technical Surveys. No. 51. The British Food Manufacturing Industries Research Association. Leatherhead, Surrey, England.

Oosting, E.M., Gray, J.I. and Grulke, E.A. 1985. Correlating diffusion coefficients in concentrated carbohydrate solutions. AIChE Journal. 31(5): 773-780.

Osterle, J. F. and Feng, W. W. 1974. Self-energized osmotic desalination. The American Society of Mechanical Engineers. 74-WA(Ener- 1): 1-5.

Pancoast, H.M. and Junk, W.R. 1980. Handbook of Sugars. 2nd ed. AVI Publishing, Westport, Connecticut. 598 p.

Pepper, D. 1990. Concentration in the food and beverage industries without evaporation. In: The Membrane Alternative: Energy Implications for Industry. Report no. 21. Howell, J.A. (ed.). The Watt Committee on Energy, Elsevier Applied Science, London and New York. p. 55-58.

Perry, R.H., Green, D.W. and Maloney, J.O. 1984. Perry's Chemical Engineers' Handbook. 6th ed. International Student Edition. McGraw-Hill Book Company, New York.

Popper, K., Camirand, W.M., Nury, F. and Stanley, W.L. 1966. Dialyzer Concentrates Beverages. Food Engineering. 38(4): 102-104.

Popper, K., Merson, R. L. and Camirand, W. M. 1968. Desalination by osmosis-reverse osmosis couple. Science. 159: 1364-1365.

Porter, M.C. 1990. Ultrafiltration. In: Handbook of Industrial Membrane Technology. Porter, M.C. (ed.). Noyes Publications, Park Ridge, New Jersey. p. 136-259.

Punzi, V.L. and Muldowney, G.P. 1987. An overview of proposed solute rejection mechanisms in reverse osmosis. Reviews in Chemical Engineering. 4(1 and 2): 1-40.

Rautenbach, R. and Albrecht, R. 1989. Membrane Processes. John Wiley & Sons, Chichester, England. 459 p.

Reid, C.E. 1966. Principles of reverse osmosis. In: Desalination by Reverse Osmosis. Merton, U. (ed.). The M.I.T. Press, Massachusetts Institute of Technology, Cambridge, Massachusetts, and London, England. p. 1-14.

Reid, C.E. 1972. Principles of reverse osmosis. In: Industrial Processing with Membranes. Lacey, R.E. and Loeb, S. (eds.). Wiley-Interscience, John Wiley & Sons, Inc., New York. p. 109-122.

Reid, C.E. and Breton, E.J. 1959. Water and ion flow across cellulose acetate membranes. Applied Polymer Science. 1(2): 133.

Reid, R.C., Prausnitz, J.M. and Poling, B.E. 1987. The Properties of Gases and Liquids. 4th edition. McGraw-Hill, New York. 741 p.

Robinson, R.A. and Stokes, R.H. 1970. Electrolyte Solutions.The Measurement and Interpretation of Conductance, Chemical Potential and Diffusion in Solutions of Simple Electrolytes. 2nd ed. revised. Butterworths, London. 571 p.

Rommel, A. and Wrolstad, R.E. 1993. Composition of flavonols in red raspberry juice as influenced by cultivar, processing, and environmental factors. Journal of Agricultural and Food Chemistry. 41: 1941-1950.

Schneider, K., Hölz, W., Wollbeck, R. and Ripperger, S. 1988. Membranes and modules for transmembrane distillation. Journal of Membrane Science. 39: 25-42.

Schofield, R.W., Fane, A.G. and Fell, C.J.D. 1990. Gas and vapour transport through microporous membranes. II. Membrane distillation. Journal of Membrane Science. 53: 173-185.

Sheng, J., Johnson, R.A., Lefebvre, M.S. 1991. Mass and heat transfer mechanisms in the osmotic distillation process. Desalination. 80: 113-121.

Singh, R.P. and Heldman, D.R. 1993. Introduction to Food Engineering. 2nd ed. Academic Press, Inc., Harcourt Brace & Company, San Diego. 499 p.

Sirkar, K.K. 1992. New membrane processes under development. Other new membrane processes. In: Membrane Handbook. Winston Ho, W.S. and Sirkar, K.K. (eds.). Van Nostrand Reinhold, New York. p. 885-912.

Sourirajan, S. 1970. Reverse Osmosis. Logos Press, Eleck Books, London. 580 p.

Statistical Sciences Inc. 1995. S Plus User Manual. Version 3.3. Statistical Sciences, Division of Math Soft Inc., Seattle, Washington, USA

Staverman, A.J. 1951. The theory of measurement of osmotic pressure. 70: 344-352.

Steffe, J.F. 1992. Rheological Methods in Food Process Engineering. Freeman Press, East Lansing, Michigan. 228 p.

Stokes, R.H. 1950. The diffusion coefficients of eight uni-univalent electrolytes in aqueous solution at 25°. Journal of American Chemical Society. 72: 2243-2247.

Strathmann, H. 1981. Membrane separation processes. Journal of Membrane Science. 9: 121-189.

Strathmann, H. 1990. Synthetic membranes and their preparation. In: Handbook of Industrial Membrane Technology. Porter, M.C. (ed.). Noyes Publications, Park Ridge, New Jersey. p. 1-60.

Sudak, R.G. 1990. Reverse osmosis. In: Handbook of Industrial Membrane Technology. Porter, M. C. (ed.). Noyes Publications, Park Ridge, New Jersey. p.260-306.

Thijssen, H.A.C. 1974. Fundamentals of concentration processes. In: Advances in Preconcentration and Dehydration of Foods. Spicer, A. (ed.). Applied Science Publishers, London. p. 13-44.

Thijssen, H.A.C. and Middelberg, L.R.W.A. 1966. Fundamentals in fruit juice concentration. International Institute of Refrigeration Bulletin. Supplement 1966-3:113-130.

Thompson, D. 1991. The application of osmotic distillation for the wine industry. The Australian Grapegrower and Winemaker. 328: 11-14.

Timmermans, J. 1960. The Physico-chemical Constants of Binary Systems in Concentrated Solutions. Volume 4. Systems with inorganic + organic or inorganic compounds. Interscience Publishers, Inc., New York. 1331 p.

Toledo, R.T. 1994. Fundamentals of Food Process Engineering. 2nd ed. Chapman & Hall, New York. 602 p.

Tombs, M.P. and Peacocke, A.R. 1974. The Osmotic Pressure of Biological Macromolecules. Clarendon Press, Oxford, England. 143 p.

Tyrrell, H.J.V. and Harris, K.R. 1984. Diffusion in Liquids. Butterworths, London. 448 p.

Vennard, J.K. and Street, R.L. 1982. Elementary Fluid Mechanics. 6th ed. John Wiley & Sons, New York. 685 p.

Vitagliano, V. 1960. Determinazione dell mobilità ioniche per le soluzioni acquose di NaCl a diverse temperature. Gazzetta Chimica Italiana. 90: 1847-1858.

Vitagliano, V. and Lyons, P.A. 1956. Diffusion coefficients for aqueous solutions of sodium chloride and barium chloride. Journal of American Chemical Society. 78: 1549-1552.

Weast, R.C., Astle, M.J. and Beyer, W.H. 1984. CRC Handbook of Chemistry and Physics. 65th ed. CRC Press, Inc., Boca Raton, Florida.

Wilson, A. 1994. Reduced alcohol wines: some new technology. The Australian Grapegrower and Winemaker. 366a: 30-34.

Wolf, A.V., Brown, M.G. and Prentiss, P.G. 1984. Concentrative properties of aqueous solutions: Conversion tables. In: CRC Handbook of Chemistry and Physics. 65th ed. Weast, R.C., Astle, M.J. and Beyer, W.H. (eds). CRC Press, Inc., Boca Raton, Florida. p. D181-D226.

Wrolstad, R.E., McDaniel, M.R., Durst, R.W., Micheals, N., Lampi, K.A. and Beaudry, E.G. 1993. Composition and sensory characterization of red raspberry juice concentrated by direct-osmosis or evaporation. Journal of Food Science. 58(3): 633-637.